UNIVERSITA' DEGLI STUDI DI PARMA

Dottorato di Ricerca in Ingegneria Industriale

XXVII Ciclo

Passive Techniques for the Enhancement of Convective Heat Transfer in Duct Flow for Highly Viscous Fluids: the Effect of Wall Curvature and of Wall Corrugation

Tutor:

Chiar.ma Prof.ssa SARA RAINIERI

Chiar.mo Prof. Ing. FABIO BOZZOLI

Coordinatore:

Chiar.mo Prof. Ing. AGOSTINO GAMBAROTTA

Dottorando: Ing. LUCA CATTANI

INDEX

NOMENCLATURE

a	Thermal diffusivity	m^2/s
A_c	Cross sectional area	m^2
c_p	fluid specific heat	*J/kgK*
cov	Covariance	
div	Divergence	
$\boldsymbol{d}$	Direction of descent	
D_b	Bore diameter	*m*
D_c	Coil diameter	*m*
D_{env}	Envelope diameter	*m*
D_{ext}	Pipe external diameter	*m*
D_{int}	Pipe internal diameter	*m*
De	Dean number (eq. 1.44)	
D_H	Hydraulic diameter	*m*
e	Corrugation depth	*m*
$\mathrm{e_i}$	Specific Internal energy	*J/kg*
E	Expected value operator	
f	General function	
f_c	Friction factor for coiled tubes	
f_s	Friction factor for straight tubes	
$\boldsymbol{F}$,F_x,F_y,F_z	Mass force and its Cartesian components	*N*
F_r, F_α, F_z	Mass force components in cylindrical coordinates	*N*
$\boldsymbol{g}$	Gravity acceleration	m/s^2
Gn	Germano number (eq. 1.55)	
Gr	Grashof number (eq. 1.30)	

Gr_q	Grashof number modified (eq. 1.31)	
h	Convective heat transfer coefficient	W/m^2K
H	Helical pitch	m
$\boldsymbol{H}$	External transfer matrix	
He	Helical number	
$\boldsymbol{J}$	Sensitivity matrix	
l	Corrugation pitch	m
L_c	Length of the coiled pipe	m
$\boldsymbol{L_d}$	Derivative operator of derivation order d	
L_{si}	Length of the initial straight section	m
L_{sf}	Length of the final straight section	m
$\dot{m}$	Mass flowrate	Kg/s
$\boldsymbol{n}$	Motion direction versor	
N_s	Number of starts	
Nu	Nusselt number (eq. 1.26)	
O_f	Objective function	
p	Pressure	Pa
p_R	Reference pressure value	Pa
$\boldsymbol{P}$	Vector of unknown parameters	
Pr	Prandtl number (eq 1.25)	
q	Heat flux for surface unit	W/m^2
$\boldsymbol{q}$	Heat flux vector	W/m^2
Q	Heat power	W
q_g	Heat power generated per unit volume	W/m^3
r, α	Cylindrical coordinates on tube section	

r_c	Coil radius	m
r_p	Pipe radius	m
r_t	Torus radius	m
R_{env}	Overall heat transfer resistance between the tube wall and the surrounding environment	$m^2K\ /\ W$
R_t	Thermal resistance	$m^2K\ /\ W$
Re	Reynolds number (eq. 1.24)	
s	Wall thickness	m
S	Surface area	m^2
t	Time	s
T	Temperature	K
T_b	Bulk temperature	K
T_{env}	Environment temperature	K
T_s	Surface temperature	K
T_w	Wall temperature	K
$\boldsymbol{u}, u, v, w$	Velocity and its Cartesian components	m/s
u_r, u_α, u_z	Velocity components in cylindrical coordinates	m/s
u_f, v_f	Frequency components	m^{-1}
u_c	Cutoff frequency	m^{-1}
U	Overall heat transfer coefficient	W/m^2K
$\dot{V}$	Volumetric flowrate	m^3/s
W	Average velocity on the section	m/s
x, y	Coordinates on tube section in Cartesian system	m
$\mathbf{Y}$	Vector with measured temperature	K
$\mathbf{Y_f}$	Vector with filtered temperature	K

z	Axial coordinate	m

Greek letters

α	Angular coordinate	rad
α^*	Relative angle	rad
β	Thermal expansion coefficient	K^{-1}
γ	Conjugation coefficient in Conjugate Gradient method (eq. 2.36)	
Γ	Perimeter	m
δ	Curvature ratio	
δ_c	Curvature ratio for coiled tubes	
δ_m	Curvature ratio modified (eq. 1.52)	
ε	Uncertainty	
ε_f	Friction factor enhancement (eq. 4.5)	
ε_H	Heat transfer enhancement (eq. 4.6)	
ζ	Damping parameter in Levenberg-Marquardt method (eq. 2.31)	
η	Enhancement efficiency (eq. 4.7)	
θ	Relative temperature	K
λ	Thermal conductivity	W/mK
λ^*	Regularization Parameter in Tikhonov regularization method (eq. 2.20)	
μ	Dynamic viscosity	$Pa\ s$
ν	Cinematic viscosity	m^2/s
ξ	Search step size	
Π	Ordinary least square norm	
Π_W	Weighted least square norm	
ρ	Density	kg/m^3

σ	Standard deviation
σ^2	Variance
τ	Torsion (eq. 1.53)
ϕ	Fixed point sequence (eq. 5.11)
Φ	Dissipation function
ψ	Stream function
$\boldsymbol{\Omega}$	Diagonal matrix in Levenberg-Marquardt method (eq. 2.31)

Subscripts and superscripts

∞	Reference value
$+$	Pseudoinverse of the matrix
$\bar{}$	Average value
$\sim$	Fourier transform
e	Enhanced geometry
ext	External wall
int	Internal wall
0	Reference geometry
S	Surface
T	Transpose of the matrix
$*T$	Conjugate transpose of the matrix

Acronyms

HCW	Helically coiled tube with corrugated wall
HSW	Helically coiled tube with smooth wall
SCW	Straight tube with corrugated wall
SSW	Straight tube with smooth wall

PREFACE

The aim of this thesis was to study the heat transfer performance of coiled pipes having both smooth and corrugated wall. Wall curvature and wall corrugation represent two extensively used passive techniques for convective heat transfer enhancement.

The curvature of the tubes makes the fluid flowing inside the pipe experiencing the centrifugal force. This force gives rise to secondary flows and the phenomenon induces local maxima in the velocity distribution that locally increases the temperature gradients at the wall by then maximizing the heat transfer.

In corrugated wall tubes the most important effects are related to the macroscopic mixing of the fluid, activated by the destabilization of the flow. It leads to the early onset of the transfer mechanism associated to the transitional regime and to the interruption of the boundary layer that locally increases the temperature gradient in the proximity of the wall with consequent beneficial effects on the convective heat transfer coefficient. This issue becomes particularly important in industrial applications in which the thermal processing of high viscosity fluids is required, such as in the food, chemical, pharmaceutical and cosmetics industries. In fact, often, in these conditions, the momentum transfer mechanism is necessarily laminar and therefore the efficiency of the heat transfer apparatuses in which the fluids are conveyed is inevitably penalized.

These techniques essentially reduce the thermal resistance by increasing the heat transfer coefficient with or without the increase of the heat transfer surface. The benefits that can derive are, for instance, the reduction of the size of the heat exchanger that means costs reduction, the decrease of the temperature difference at which they work, that means a reduction of the thermal stress for the product or the increase of the heat exchanged. The techniques of increase of the heat transfer can be divided into active techniques that require a mechanical aid or electrostatic fields and passive techniques that do not require an external power.

This experimental investigation has the purpose to study the performances of these two passive technique in duct flow for highly viscous fluid in forced convection.

In the first chapter the general concepts about convection and in particular the dimensional analysis with the principal dimensionless groups that characterize the phenomenon, are introduced. Moreover the main active and passive techniques for the enhancement of the convective heat transfer, especially the wall curvature and wall corrugation, are presented.

Then in the second chapter the basics notions about the inverse heat transfer problems are introduced: some of the main solution methods are briefly described. Particular attention is given to the inverse heat conduction problem in pipes.

In chapter number three the pipe geometries under investigation and the experimental setup are presented. In the fourth chapter the first part of the investigation is described and the results are presented: the analysis is initially devoted to measure the heat transfer performance along the heated length of the coiled pipes in terms of Nusselt number circumferentially averaged along the cross section and computed at different axial position. The heat transfer enhancement effects are compared to the inevitably correlated pressure drop penalties.

Then, in order to deeply investigate the mechanisms that govern the heat transfer in coiled pipes, the convective heat transfer coefficient distribution along the cross section circumference is estimated. The asymmetrical distribution of the velocity field over the cross-section of the tube due to the centrifugal force that is experienced by the fluid, leads to a significant variation in the convective heat-transfer coefficient along the circumferential angular coordinate.

This irregular distribution may be critical in some industrial applications, such as in those that involve a thermal process of a fluid food. Therefore, to predict the overall performance of heat-transfer apparatuses that involve the use of curved tubes, it is necessary to know the local distribution of the convective heat-transfer coefficient not only along the axis of the heat-transfer section but also at the fluid-wall interface along the cross-section circumference.

Although many authors have investigated the forced convective heat transfer in coiled tubes, most of them have presented the results only in terms of the Nusselt number averaged along the wall circumference: only a few authors have studied the phenomenon locally, and most of them have adopted the numerical approach. The solution of the IHCP in the wall, starting from the temperature distribution acquired on the external wall surface, is a robust tool to estimate the local convective heat-transfer coefficient on the interior wall surface. In this thesis three different solution techniques are employed to solve the IHCP and to find the local convective heat transfer coefficient at the fluid-wall interface in smooth wall coiled tubes. In chapter five the procedures, based on Tikhonov Regularization Method (TRM), Gaussian Filter Technique (GFT) and Quadrupole method (QM) are presented, implemented and optimized for the problem under study, validated by synthetic data and compared. These solution techniques are well known but their implementation for the case under study is not deeply analysed in literature.

Then in chapter six these solution procedures are applied to experimental measurements in smooth coiled tubes in laminar flow regime in the fully developed region. Cause to the lack of knowledge about the local heat-transfer coefficient for the laminar flow regime in coiled tubes in the scientific literature, the results obtained here might be particularly useful in the validation of numerical models and in the design of coiled tubes heat exchangers aimed at the treatment of highly viscous fluids.

In chapter seven an estimation procedure, based on Gaussian Filter, is proposed and applied to experimental data for corrugated wall coiled tubes: preliminary results are obtained and discussed.

LIST OF FIGURES

LIST OF TABLES

1. INTRODUCTION

1.1 DIFFERENTIAL EQUATIONS OF CONVECTION

The differential equations that describe the heat transfer phenomenon (Bejan 1993; Incroprera and De Witt 2002) in a Newtonian fluid in motion are the continuity equation (a) that expresses the mass conservation, the Navier Stokes equations (b) that express the momentum conservation and the energy balance equation (c).

The general formulation in a Cartesian coordinate system (x,y,z) is as follows:

a)

$$\frac{D\rho}{Dt} + \rho \,\mathrm{div}\, \boldsymbol{u} = 0 \tag{1.1}$$

b)

$$\rho \frac{Du}{Dt} = F_x - \frac{\partial p}{\partial x} + \frac{\partial}{\partial x}\left[\mu\left(2\frac{\partial u}{\partial x} - \frac{2}{3}\,\mathrm{div}\,\boldsymbol{u}\right)\right] + \frac{\partial}{\partial y}\left[\mu\left(\frac{\partial u}{\partial y} + \frac{\partial v}{\partial x}\right)\right] + \frac{\partial}{\partial z}\left[\mu\left(\frac{\partial w}{\partial x} + \frac{\partial u}{\partial z}\right)\right] \tag{1.2}$$

$$\rho \frac{Dv}{Dt} = F_y - \frac{\partial p}{\partial y} + \frac{\partial}{\partial y}\left[\mu\left(2\frac{\partial v}{\partial y} - \frac{2}{3}\,\mathrm{div}\,\boldsymbol{u}\right)\right] + \frac{\partial}{\partial z}\left[\mu\left(\frac{\partial v}{\partial z} + \frac{\partial w}{\partial y}\right)\right] + \frac{\partial}{\partial x}\left[\mu\left(\frac{\partial u}{\partial y} + \frac{\partial v}{\partial x}\right)\right] \tag{1.3}$$

$$\rho \frac{Dw}{Dt} = F_z - \frac{\partial p}{\partial z} + \frac{\partial}{\partial z}\left[\mu\left(2\frac{\partial w}{\partial z} - \frac{2}{3}\,\mathrm{div}\,\boldsymbol{u}\right)\right] + \frac{\partial}{\partial x}\left[\mu\left(\frac{\partial w}{\partial x} + \frac{\partial u}{\partial z}\right)\right] + \frac{\partial}{\partial y}\left[\mu\left(\frac{\partial v}{\partial z} + \frac{\partial w}{\partial y}\right)\right] \tag{1.4}$$

c)

$$\rho \frac{De_i}{Dt} + p \,\mathrm{div}\, \boldsymbol{u} = -\mathrm{div}(\lambda \nabla T) + q_g + \mu\Phi \tag{1.5}$$

$$\text{with } \frac{D}{Dt} = \frac{\partial}{\partial t} + u\frac{\partial}{\partial x} + v\frac{\partial}{\partial y} + w\frac{\partial}{\partial z}$$

where:

- ρ is the fluid local density
- $\boldsymbol{u}$ is the velocity vector with components u, v, w along x, y, z axes.
- p is the fluid pressure
- μ is the local fluid dynamic viscosity
- λ is the fluid thermal conductivity
- q_g is the heat power generated per unit volume

- F_x,F_y,F_z are components of the mass force **F**
- Φ is the dissipation function
- e_i is the specific internal energy

The dissipation function Φ represents the rate at which kinetic energy is irreversibly converted to thermal energy due to viscous effects in the fluid and it is expressed as:

$$\Phi = 2\left[\left(\frac{\partial u}{\partial x}\right)^2 + \left(\frac{\partial v}{\partial y}\right)^2 + \left(\frac{\partial w}{\partial z}\right)^2\right] - \frac{2}{3}(\text{div}\,\boldsymbol{u})^2 + \left(\frac{\partial u}{\partial y} + \frac{\partial v}{\partial x}\right)^2 + \left(\frac{\partial v}{\partial z} + \frac{\partial w}{\partial y}\right)^2 + \left(\frac{\partial w}{\partial x} + \frac{\partial u}{\partial z}\right)^2 \quad (1.6)$$

It's also necessary to add the state equation that expresses the relation between the pressure, the density and the temperature (for instance $p - \rho RT = 0$ for a perfect gas) and the equations that define the dependence on the temperature of the viscosity and of the thermal conductivity:

$$\mu = \mu(T) \quad (1.7)$$

$$\lambda = \lambda(T) \quad (1.8)$$

The dependence on pressure of the thermophysics properties is usually not considerated.

Rewriting equation (1.5) in terms of specific enthalpy ($h_i = e_i + p/\rho$) and explicating the differential $\left(Dh_i = h_i/\partial T|_{p=cost} DT + \partial h_i/\partial p|_{T=cost} Dp\right)$ it is possible to obtain another and more usual formulation of the energy balance equation:

$$\rho c_p \frac{DT}{Dt} = \text{div}\,(\lambda \nabla T) + q_g + \beta T \frac{Dp}{Dt} + \mu\Phi \quad (1.9)$$

where:

- c_p is the fluid specific heat
- $\beta = -\frac{1}{\rho}\left(\frac{\partial \rho}{\partial T}\right)_{p=cost}$ is the thermal expansion coefficient

It is possible to simplify equations (1.1,1.2 and 1.9) by making some assumptions: if the fluid is a perfect gas $\beta = \frac{1}{T}$; if the fluid has a constant density $\text{div}\,\boldsymbol{u} = 0$ and $\beta = 0$; by neglecting the

temperature dependence of the viscosity and thermal conductivity and by considering zero the contribution of the viscous dissipation, the three equations could be written as follows:

$$\text{div}\,\boldsymbol{u} = 0 \tag{1.10}$$

$$\rho\frac{D\boldsymbol{u}}{Dt} = \boldsymbol{F} - \nabla p + \mu\nabla^2\boldsymbol{u} \tag{1.11}$$

$$\rho c_p\frac{DT}{Dt} = \lambda\nabla^2 T + q_g \tag{1.12}$$

The same equations could be written in cylindrical coordinates (r, α, z) as follows:

a)

$$\frac{\partial u_r}{\partial r} + \frac{u_r}{r} + \frac{1}{r}\frac{\partial u_\alpha}{\partial \alpha} + \frac{\partial u_z}{\partial z} = 0 \tag{1.13}$$

b)

$$\begin{aligned}\rho\left(\frac{\partial u_r}{\partial t} + u_r\frac{\partial u_r}{\partial r} + \frac{u_\alpha}{r}\frac{\partial u_r}{\partial \alpha} - \frac{{u_\alpha}^2}{r} + u_z\frac{\partial u_r}{\partial z}\right)\\ = F_r - \frac{\partial p}{\partial r} + \mu\left(\frac{\partial^2 u_r}{\partial r^2} + \frac{1}{r}\frac{\partial u_r}{\partial r} - \frac{u_r}{r^2} + \frac{1}{r^2}\frac{\partial^2 u_r}{\partial \alpha^2} - \frac{2}{r^2}\frac{\partial u_\alpha}{\partial \alpha} + \frac{\partial^2 u_r}{\partial z^2}\right)\end{aligned} \tag{1.14}$$

$$\begin{aligned}\rho\left(\frac{\partial u_\alpha}{\partial t} + u_r\frac{\partial u_\alpha}{\partial r} + \frac{u_\alpha}{r}\frac{\partial u_\alpha}{\partial \alpha} + \frac{u_r u_\alpha}{r} + u_z\frac{\partial u_\alpha}{\partial z}\right)\\ = F_\alpha - \frac{1}{r}\frac{\partial p}{\partial \alpha} + \mu\left(\frac{\partial^2 u_\alpha}{\partial r^2} + \frac{1}{r}\frac{\partial u_\alpha}{\partial r} - \frac{u_\alpha}{r^2} + \frac{1}{r^2}\frac{\partial^2 u_\alpha}{\partial \alpha^2} + \frac{2}{r^2}\frac{\partial u_r}{\partial \alpha} + \frac{\partial^2 u_\alpha}{\partial z^2}\right)\end{aligned} \tag{1.15}$$

$$\rho\left(\frac{\partial u_z}{\partial t} + u_r\frac{\partial u_z}{\partial r} + \frac{u_\alpha}{r}\frac{\partial u_z}{\partial \alpha} + u_z\frac{\partial u_z}{\partial z}\right) = F_z - \frac{\partial p}{\partial z} + \mu\left(\frac{\partial^2 u_z}{\partial r^2} + \frac{1}{r}\frac{\partial u_z}{\partial r} + \frac{1}{r^2}\frac{\partial^2 u_z}{\partial \alpha^2} + \frac{\partial^2 u_z}{\partial z^2}\right) \tag{1.16}$$

c)

$$\rho c_p\left(\frac{\partial T}{\partial t} + u_r\frac{\partial T}{\partial r} + \frac{u_\alpha}{r}\frac{\partial T}{\partial \alpha} + u_z\frac{\partial T}{\partial z}\right) = \lambda\left[\frac{1}{r}\frac{\partial}{\partial r}\left(r\frac{\partial T}{\partial r}\right) + \frac{1}{r^2}\frac{\partial^2 T}{\partial \alpha^2} + \frac{\partial^2 T}{\partial z^2}\right] + q_g \tag{1.17}$$

When the fluid motion is exclusively due to the density variations generated by the difference of temperature the phenomenon is named natural convection*;* otherwise if the cause of the motion is an external force the transfer mechanism, is called forced convection. It could occur also the existence of a double cause of the motion, one related to the effect of expansion of the fluid and the other generated by an external force: in this case it is called mixed convection.

In the case of natural convection it is necessary to take into account the dependence of the density on temperature and to add in the Navier Stokes equations the term that concern the buoyancy effects.

Considering the dependence of the density on temperature as follows:

$$\rho = \rho_{\infty}[1 - \beta(T - T_{\infty})] \tag{1.18}$$

where ρ_{∞} and T_{∞} represents the reference values. Substituting that in equation (1.11) it could be obtained:

$$\rho \frac{D\boldsymbol{u}}{Dt} = -\nabla p - \rho\beta(T - T_{\infty})\boldsymbol{g} + \mu\nabla^2\boldsymbol{u} \tag{1.19}$$

The equations (1.10,1.18 and 1.12) represents the Boussinesq approximation: the fluid is assumed incompressible except for the momentum heat transfer equation where it is considered the temperature dependence of the density.

To complete the analytical formulation of the problem it is necessary to define the boundary conditions for the dependent variables and in particular for the velocity and temperature.

For what concerns thermal boundary conditions they could be of different types (Incroprera et al. 2002):

- Constant surface temperature :

$$T(x, y, z, t) = T_s \quad \text{on the boundary surface.} \tag{1.20}$$

- Constant surface heat flux. This type of condition could be divided in two categories:

a) Finite heat flux:

$$-\lambda \frac{\partial T}{\partial \boldsymbol{n}}\Big|_S = q_S \tag{1.21}$$

b) Adiabatic or insulated surface:

$$\frac{\partial T}{\partial \boldsymbol{n}}\Big|_S = 0 \tag{1.22}$$

- Convection surface condition:

$$-\lambda \frac{\partial T}{\partial \boldsymbol{n}}\Big|_S = h[T_\infty - T_s(x,y,z,t)] \tag{1.23}$$

1.2 DIMENSIONAL ANALYSIS

The equations (1.1-1.8) constitute a system of eight equations with eight variables $u, v, w, p, \rho, T, \mu, \lambda$. Usually this system is impossible or very difficult to be solved and so it is necessary to measure the quantities of interest. In order to give a general relevance to experimental values that concern a specific measure, it is possible to adopt the dimensional analysis approach that is based on the assumption that all the physical laws are expressed with dimensionally homogeneous equations.

It could be performed by analyzing the differential equations that define the problem and eventually other relations that influence the physical phenomenon (boundary conditions for instance) and to bring them to a dimensionless form by introducing reference variables (Cocchi 1990).

A fundament of the dimensional analysis is the Buckingham theorem which states that any physical law can be expressed in terms of dimensionless parameters and that the number of these needed parameters is given by the difference between the independent variables and the fundamental physical quantities (Mass [M], Length [L], Time [T], Temperature [Θ], Amount of substance [N], Electric current [I], Luminous intensity [J]).

A necessary condition for the use of this methods it is to consider physical situation geometrically similar in order to employ the same dimensional characteristic. In the case of flow in ducts the characteristic dimension is represented by the hydraulic diameter D_h.

In this paragraph the principal dimensionless groups are going to be defined.

Reynolds Number

This dimensionless group represents the ratio between the inertial and viscous forces. It is expressed as follows:

$$Re = \frac{W\ D_h}{\nu} = \frac{\rho\ W\ D_h}{\mu} \tag{1.24}$$

where :

- W is the fluid average velocity on the duct's cross section expressed as $W = \frac{1}{A_c}\int_{A_c}(\boldsymbol{u}\cdot\boldsymbol{n})\,dA_c$
- $D_h = 4\ \frac{A_c}{\Gamma}$ with Γ =perimeter of the cross section

The Reynolds number allows to define the motion regime of the fluid and in the case of internal flow the following classification is available:

- $Re \lesssim 2300$, the flow remains laminar since the viscous forces are sufficiently high to prevent the amplification of those small noise and distortion present in each stream;
- $2300 \lesssim Re \lesssim 10000$, it is a zone of transition in which viscous effects become less important compared to the inertial forces and the flow distortions are amplified;
- $Re \gtrsim 10000$,the motion becomes chaotic and the flow regime is turbulent.

Prandtl Number

The Prandtl number expresses the ratio between the terms that represent the contribution due to the momentum transport and the one due to the energy transport respectively:

$$Pr = \frac{\nu}{a} = \frac{\mu\ c_p}{\lambda} \tag{1.25}$$

where a is the fluid thermal diffusivity.

The Prandtl number is a characteristic of the fluid and doesn't depend, as it happens for other dimensionless groups, from the regime of motion.

Nusselt Number

The Nusselt number is a dimensionless group widely used in the study of convection problems as it is the only one that contains the convection coefficient, necessary for the determination of heat exchanged by convection.

The Nusselt number is expressed as follows:

$$Nu = \frac{h\, D_h}{\lambda} \tag{1.26}$$

where the convective heat transfer coefficient h , in case of flow in confined space, is :

$$h = \frac{q}{(T_s - T_b)} \tag{1.27}$$

The bulk temperature T_b is expressed over the cross section A_c by:

$$T_b = \frac{\int_{A_c} \rho c_p T\, \boldsymbol{u} \cdot \boldsymbol{n}\, dA_c}{\int_{A_c} \rho c_p\, \boldsymbol{u} \cdot \boldsymbol{n}\, dA_c} \tag{1.28}$$

If the density and the specific heat are constant it could be written as:

$$T_b = \frac{\int_{A_c} T\, \boldsymbol{u} \cdot \boldsymbol{n}\, dA_c}{W\, A_c} \tag{1.29}$$

Grashof Number

The Grashof Number represents the ratio between the buoyancy forces and the viscous forces and it is used in cases of natural or mixed convection:

$$Gr = \frac{g\beta\Delta T {D_h}^3}{\nu^2} \tag{1.30}$$

In case of uniform heat flux at the wall it can also be employed a modified version of Grashof number called Gr_q:

$$Gr_q = Gr\, Nu = \frac{g\beta \mathrm{q} {D_h}^4}{\nu^2 \lambda} \tag{1.31}$$

Before starting to see how the principal dimensionless groups come out from the differential equations of convection it's necessary to define some dimensionless variables :

$$\boldsymbol{u}^* = \frac{\boldsymbol{u}}{W}; \qquad p^* = \frac{p}{p_R}; \qquad T^* = \frac{T - T_\infty}{T_s - T_\infty}; \qquad z^* = \frac{z}{D_h}; \qquad t^* = \frac{t\, W}{D_h}$$

where p_R is a reference values of pressure that is going to be defined later.

Also the dimensionless operator must be defined:

$$\nabla^* = D_h\,\nabla; \qquad div^* = D_h\,div; \qquad \nabla^{*2} = {D_h}^2\,\nabla^2$$

Starting from equation (1.19) and introducing the dimensionless variables it is possible to obtain:

$$W\frac{D\boldsymbol{u}^*}{Dt} = -\frac{p_R}{\rho D_h}\nabla^* p^* - T^*\boldsymbol{g}\beta(T_s - T_\infty) + \frac{W}{{D_h}^2}\frac{\mu}{\rho}\nabla^{*2}\boldsymbol{u}^* \tag{1.32}$$

Rearranging it by considering the dimensionless time t^*:

$$\frac{D\boldsymbol{u}^*}{Dt^*} = -\frac{p_R}{\rho W^2}\nabla^* p^* - \frac{\boldsymbol{g}\beta D_h(T_s - T_\infty)}{W^2}T^* + \frac{\nu}{WD_h}\nabla^{*2}\boldsymbol{u}^* \tag{1.33}$$

The dimensionless groups found in this equation are three:

- $N_1 = \frac{p_R}{\rho W^2}$
- $N_2 = \frac{\boldsymbol{g}\beta D_h(T_s - T_\infty)}{W^2}$
- $N_3 = \frac{\nu}{WD_h}$

The first dimensionless group could be compared to 1 finding in that way the value of reference pressure.

The third one represents the inverse of the Reynolds number as it is possible to see from equation (1.24). The second one assumes a physical meaning if multiplied for Re^2 assuming the following formulation:

$$\frac{N_2}{{N_3}^2} = \frac{g\beta(T_s - T_\infty){D_h}^3}{\nu^2} \tag{1.34}$$

that represents the Grashof number, as it is possible to see from equation (1.30).

Considering now the boundary condition expressed in equation (1.23), dividing both the members by the hydraulic diameter, and rearranging it, it is possible to obtain:

$$\frac{hD_h}{\lambda} = \frac{D_h}{(T_\infty - T_s)}\left(\frac{\partial T}{\partial x}\right)_s \tag{1.35}$$

The dimensionless group on the left part of the equation (1.35) is the Nusselt number as it is possible to see from equation (1.26).

Taking into account the energy balance equation (1.12), substituting the dimensionless variables and neglecting the generation term q_g it follows:

$$\frac{DT}{Dt^*} = \frac{a}{WD_h}\nabla^{*2}T^* \tag{1.36}$$

Considering the dimensional group $\frac{a}{WD_h}$ present in equation (1.36) and multiplying and dividing it for the cinematic viscosity it results:

$$\frac{a}{WD_h}\cdot\frac{\nu}{\nu} = \frac{a}{\nu}\cdot\frac{\nu}{WD_h} = (\mathrm{Pr}\cdot\mathrm{Re})^{-1} \tag{1.37}$$

In that way another important dimensionless group, the Prandtl number, is obtained.

Highly viscous fluids

The concept of viscosity is strictly correlated to the technical apparatus in which the fluid is conveyed: of course it is possible to classify the different fluids considering the value of dynamic or cinematic viscosity but the effect on fluid flow is inevitably connected to the characteristics of the heat exchanger under study. The same fluid could give rise to really high viscous effects if it flows in a determinate apparatus while it could generate moderate viscous effects if it flows in another one with a significantly higher characteristic dimension. A possible way to distinguish the technical applications respect to the fluid viscosity is to consider the Reynolds number: as much is low the working Reynolds number range as much the viscous forces are significant respect to the inertial ones. In this thesis work it was used Ethylene Glycol as working fluid in order to analyse a Reynolds number range within about 10^3. It was chosen this fluid to represents a class of industrial applications in which the momentum transfer mechanism is usually laminar and therefore the efficiency of the heat transfer apparatuses in which the fluids are conveyed is inevitably penalized. It is particularly of interest in manufacturing sectors such as in the food, chemical, pharmaceutical and cosmetics industries (Agarwal et al 2013, Webb 1994).

1.3 CONVECTIVE HEAT TRANSFER ENHANCEMENT

The heat transfer enhancement techniques definitely constitute an important research argument in the field of heat transfer.

This issue becomes particularly important in industrial applications in which the thermal processing of medium and high viscosity fluids is required, such as in the food, chemical, pharmaceutical and cosmetics industries.

In fact, often, in these conditions, the momentum transfer mechanism is necessarily laminar and therefore the efficiency of the heat transfer apparatuses in which the fluids are conveyed is inevitably penalized.

In these industrial fields, engineers have then been striving for techniques producing enhanced heat transfer coefficients, accompanied by reduced pumping power requirements. The first attempts to increase the heat transfer coefficients in a condensing steam flow were reported by J. P. Joule in his studies in 1861 (Bergles 1998): he tried different configurations of the experiment setup in order to investigate the influence of many parameters on the phenomenon. Among these, he studied the influence of the insertion of wires bent into the form of a spiral inside the refrigerating water passage between the steam tubes using the wires as water agitator. Today this research argument is attracting a renewed interest in the process industry due to the increase of the energy costs and raw materials and this is witnessed also by the huge amount of papers available within the world scientific literature of the last decades regarding heat transfer augmentation and by the growing numbers of registered patents related to heat transfer enhancement technology or devices.

These techniques essentially reduce the thermal resistance by increasing the heat transfer coefficients with or without the increase of the heat transfer surface. The benefits that can derive are, for instance, the reduction of the size of the heat exchanger that means costs reduction, the decrease of the temperature difference at which they work that means a reduction of the thermal stress for the product or the increase of the thermal power exchanged. This appears clear from the general heat transfer rate equation for a two fluid heat exchanger:

$$Q = US\Delta T \tag{1.38}$$

where U [W/m^2K] is the overall heat transfer coefficient, ΔT [K] the appropriate temperature difference and S [m^2] the heat transfer area.

The techniques of increase of the heat transfer can be divided into active techniques that require a mechanical aid or electrostatic fields and passive techniques that do not require an external power (Bergles 1998).

There are also methods that combine multiple techniques so that the gain obtained is greater than that achieved using these techniques individually: these methods are called compound techniques.

Concluding, the principal objective of the convective heat transfer enhancement techniques is to increment the convective heat transfer coefficient h and therefore the overall heat transfer coefficient U obtaining the benefits above mentioned.

In order to evaluate the performance of heat transfer and enhanced heat transfer surfaces several numbers of performance criteria have been developed (Ylmaz et al. 2001; Zimparov 2001). However it is not so easy to establish the performance of heat exchangers since it is influenced by many different factors that can be also conflicting. Among these factors there are the costs (initial and operating), the safety, the pumping power, the area reduction, the heat duty increase, the pressure losses, the compact fabrication. Taking into account these items many performance evaluation criteria have been suggested in literature for evaluating heat transfer enhancement techniques. A possible classification is furnished by (Ylmaz et al. 2011): methods that compare the surface or volume of a heat exchanger under constant heat power, flow rates and hydraulic losses; methods that compare the heat power with constant surface or volume, flow rates and hydraulic losses; methods that compare the hydraulic losses under constant surface or volume, heat power and flow rates; methods that evaluate on the basis of economical accounting; methods that evaluate on the basis of effective energy point; methods that evaluate on the basis of the second law criteria.

ACTIVE TECHNIQUES

Within this category there are mechanical actions, vibrations, electrostatic fields and injections (Bergles 1998; Webb 1994).

Mechanical aids

Among the mechanical actions used as a technique for increasing the convection heat transfer it is possible to distinguish: the fluid stirring, the surface rotation and scraping of the surfaces.

Mechanical devices promote the mixing of the liquid by mechanical means or by rotating the surfaces. Scraped surfaces are widely used for the treatment of viscous fluids in the process industry and many studies, based on experimental investigations, are present in literature. Reviews of the mostly widely used correlations are reported by Härröd (1986), Abichandani and Sarma (1987) and Skelland (1958).

Rainieri et al. (2014a) presented an investigation focused on the determination of heat transfer performance of SSHE (Scraped Surface Heat Exchangers). They analyzed both synthetic and experimental data acquired on a coaxial SSHE pilot plant, especially designed for treating highly

viscous fluid food enabling the estimation of an heat transfer correlation, expressing the Nusselt number as a function of the relevant dimensionless parameters.

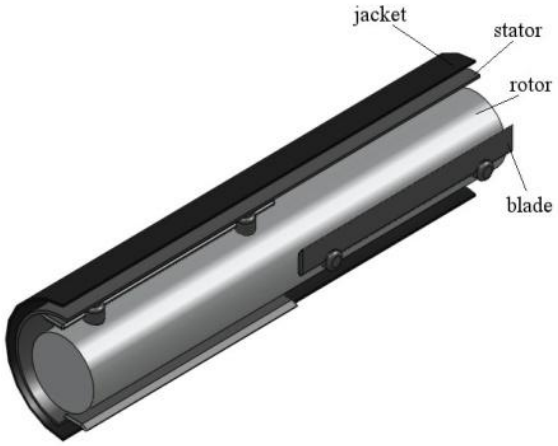

Figure 1.1: Sketch of the SSHE studied by Rainieri et al. (2014a).

A simple sketch of the apparatus used in their investigations is reported in figure 1.1.

Another kind of techniques that mechanically increase the heat transfer performance are the rotating surfaces. Rotating surfaces are commonly present in rotating electrical machines, in the rotor blades of gas turbines and in many other devices normally used in the industrial field. However rotating surfaces can be also used with the express purpose of increasing the heat transfer (Bergles 1998).

McElhincy and Prechshot (1977) performed an experimental analysis of heat transfer from steam condensing on the outside of a horizontal rotating tube through the tube wall to a laminar flow of cooling water on the inside of the tube: the overall heat-transfer coefficient and a previously developed model for the steam-side coefficient were employed to compute the coolant-film coefficient at different rotational speeds. For rotations up to 40rev/min the cooling-side coefficient was slightly improved whereas at lower rotational speeds a significant deterioration of the cooling-side coefficient was observed.

Other studies were carried out by Mori and Nakayama (1967) that investigated forced convective heat transfer in a straight pipe rotating around a parallel axis with a large angular velocity and by Miyazaki (1971) that performed an analysis of the combined free and forced convective heat transfer and fluid flow in a rotating curved circular tube for the fully developed flow with the thermal boundary condition of constant heat flux per unit length of tube.

Vibrations

The processes of heat transport can be strongly influenced by vibrations. In analyzing the relationship between the heat transfer mechanism and the presence of vibratory phenomena it is necessary to distinguish between vibrations that involve surfaces and vibrations that instead affect the fluid.

Surface Vibration

A fundamental element in the enhancement of the heat transfer is the control of fluid motion in the proximity of the wall. An efficient solution to increase heat transfer is to promote a renewal of the fluid that is near the wall. A possible way to realize it, consists in using movable walls at the location where heat transfer takes place. On the other hand wall deformation brings with itself some disadvantages, such as for example structural problems. A still nowadays important research task is the development of materials capable of accepting deformations, also for this type of applications.

The main effects expected by a periodic movement of the surfaces in contact with the fluid are fluid mixing and boundary layer disruption. In case of a single phase flow, these methods promote convection intensity in particular in regions where there would otherwise be natural convection (Leal 2013).

The easiest method to study the interaction between the heat transfer and the surface vibrations is to make the surface vibrate mechanically normally using an electrodynamics actuator.

Usually, the frequencies used are below 1000 Hz as the attempt is to achieve an adequate oscillation amplitude.

Normally, sufficiently intense vibrations lead to an increase of the heat transfer, but in certain situations, reductions of both the local and average Nusselt number have also been determined. The uncertainty of the results is to be found in the fact that there are many variables to describe both the thermal and vibratory phenomena. In particular when the vibrations are generated on the heated surface in systems with forced flows, the dispersion of the results is very wide, depending on the system under test and the intensity of the oscillation, ranging from a 300% increase of the heat transfer until a slight performance degradation.

The geometry particularly used for this type of heat transfer enhancement technique has been the horizontal heated cylinder vibrating both horizontally and vertically (Bergles 1998).

Another possible solution is the oscillation of a flexible blade constituting a piezoelectric fan that produces the motion of the surrounding fluid (Acikalin 2004). A positive element of this technique is that the piezoelectric fan could have very small dimensions permitting to reach the objective of

compactness. Normally they are employed to promote the motion of a fluid locally in a globally stagnant fluid area, increasing heat transfer in a hot spot, and so reducing local temperature.

Fluid Vibration

Sometimes it could happen that due to the large mass of the structure of the heat exchanger it is not possible or it is difficult to vibrate the surface and it is necessary to consider alternative techniques in which the vibration is transmitted directly to the fluid between the heated surfaces.

The generators used for this kind of applications are of different types ranging from flow interrupter to the piezoelectric transducer: the vibrations which are usually applied in these cases fall in a range of frequencies between 1 and 10^6 Hz.

This solution is, however, certainly much more complex than that in which the vibrations involve the surfaces, as it is much more difficult to define the vibrational variables and to describe the link between the heat transfer and vibration.

However, there are some cases in which under certain conditions the flow fields are similar and the analytical results can be applied both to the case of the surface vibration and of fluid vibration (Bergles 1998).

Some studies on the effects of sound fields on heat transfer from horizontal cylinders to air, have been carried out by Fand and Kaye (1961) and Lee and Richardson (1965). Fand and Kaye performed an experimental study showing that the heat transfer from an heated cylinder is increased by a thermoacoustic streaming. For a given temperature potential the use of sound fields at high sound pressure could enhance the convective heat transfer coefficient. Moreover they proposed an empirical equation in order to find the convective heat transfer coefficient in case of an heated horizontal cylinder in the presence of horizontal transverse sound fields.

Electrostatic fields

The electrostatic fields are applied in different ways in dielectric fluids. In general, the electrostatic fields can be addressed to generate a greater mixing of the fluid and are particularly effective in increasing the heat transfer coefficients in the case of natural convection. One possible configuration is the one of a hot wire within a concentric tube maintained at a high voltage relative to the wire. The heat transfer coefficient can be increased by several hundred percentage if a sufficient electric power is supplied.

Interesting results were obtained also for laminar flows in forced convection: an increase of 100% was seen by applying voltages of the order of magnitude of 10kV with oil as working fluid (Newton and Allen 1977).

Jet impingement

The projection of a fluid at high speed toward a surface increases the convective heat transfer coefficient, because the jet produces the breaking of the boundary layer generating a mixing of the fluid in the proximity of the surface.

Injection is used in many industrial applications as for example cooling of internal combustion engines. Their effect is to produce a significant increase of the convective heat transfer coefficient close to the stagnation region where the jets impinge on the plate. A negative element is that the heat transfer enhancement is very high near the impact zone, but it decreases rapidly away from it.

The elements that influence the convective heat transfer coefficient are in particular nozzle geometry, nozzle-to-plate distance, jet Reynolds number, heat flux, velocity profiles and turbulence intensity (Leal 2013).

Normally this technique employs multiple jets to heat or cool extensively and uniformly the surface (Oyakawa 2009). In absence of interaction between the jets, the increasing of heat transfer is comparable to the one obtained with the singular jet, only more uniformly and widely distributed over the surface: the situation is different if there are interactions between the jets and it could happen before or after the impingement on the surface. If it happens before, it can make the jet less powerful and consequently reduce the heat transfer compared to the one without interactions.

On the contrary, if the interaction happens after the impingement on the surface, it could arise a fountain flow that on one side enters the core of the closer jets reducing the heat transfer, but on the other side promotes a turbulence that increases the convective heat transfer coefficient producing global benefit effect (Weigand 2011).

Injection and Aspiration

The increase in heat transfer performance can be also achieved by injecting gas through the porous surfaces of a heat exchanger. The injection of gas produces a shaking similar to that obtained in nucleated boiling; the gains observed are very important for the laminar flow (500%) (Gose 1957).

A study to verify experimentally the hydrodynamic similarity between boiling and bubbling air from a porous media was performed by Kudirka (1965): the author analyzed the case of injection of air within porous tubes in which ethylene glycol flows and the results showed a parallelism within the two phenomena for gas-injection at low moderate bubbling rates. It was found out also an increase of convective heat transfer coefficient up to 130% compared to the one obtained in absence of gas injection.

Practical applications, however, are not very common due to the difficulty of inserting and removing the gas from the fluid. Even the suction is a technique difficult to use, especially for the

insertion of the aspiration apparatus inside the ducts, it's possible to achieve significant increases in any regime of motion of the fluid.

PASSIVE TECHNIQUES

The passive techniques for the enhancement of convective heat transfer are based on changes induced on the fluid flow through a proper conformation of the surface, such as curvature of the walls or surfaces roughness or corrugation or through the insertion of devices in the main flow directly or by means of additives (Webb 1994; Bergles 1998).

The passive techniques are of great interest for industrial applications, since they do not require any external power. Moreover it could happen to operate to an existing heat exchanger and for example it could be much easier introducing an insert instead of using an active technique. In addition the manufacturing process to realize insertion or particular conformation of the wall is quite simple and nowadays it is a consolidated technology.

Treated and Coated Surfaces

They consist in surfaces that have a slight alteration in the final part or a thin coating. These coatings can be either metallic or non-metallic and also continuous or discontinuous. They permit to significantly augment the heat transfer coefficient and are mainly used in applications that involve phenomena of boiling and condensation. An example is the use of Teflon as non-wetting coating in order to promote dropwise condensation (Webb 1994). An estimation technique of the local heat transfer coefficient, based on the solution of the 2-D inverse heat conduction problem, has been adopted by Rainieri et al. (2009) in order to investigate the effect of the surface wettability on the two-phase convective heat transfer in a dehumidifying process. The restoration of the convective heat transfer coefficient distribution on aluminum plates coated with a hydrophobic oleic film on which the dropwise condensation of the water vapor carried by a humid air turbulent stream occurs, was realised highlighting the heat transfer augmentation due to the hydrophobic surface coating.

Even if is not very common they can also be used to increase the convective heat transfer single phase.

Rough or Corrugated Surfaces

This is one of the first techniques used with the specific aim of producing an increase of the heat transfer by forced convection.

They can be produced in different configurations and they can be integrated in the wall or obtained by placing a roughness adjacent to the surface.

An integral corrugation can be obtained by using typical industrial methods such as molding, casting and welding; a certain roughness can be achieved using the inserts to create certain protuberances.

The increase of the heat transfer promoted by this technique is in part due to the fact that fin effect is generated In addition to the fact that the corrugation increases slightly the heat transfer surface, the advantages in terms of heat transfer are principally due to the creation of turbulent motions and remixing of the fluid.

In fact in corrugated wall tubes the most important effects are related to the macroscopic mixing of the fluid, activated by the destabilization of the flow which leads to the early onset of the transfer mechanism associated to the transitional regime and to the interruption of the boundary layer that locally increases the temperature gradient in the proximity of the wall with consequent beneficial effects on the convective heat transfer coefficient (Rainieri 1996 and 2002). To these heat transfer enhancement effects it is necessarily associated a pressure drop penalty which has to be accounted for (Ali 2001).

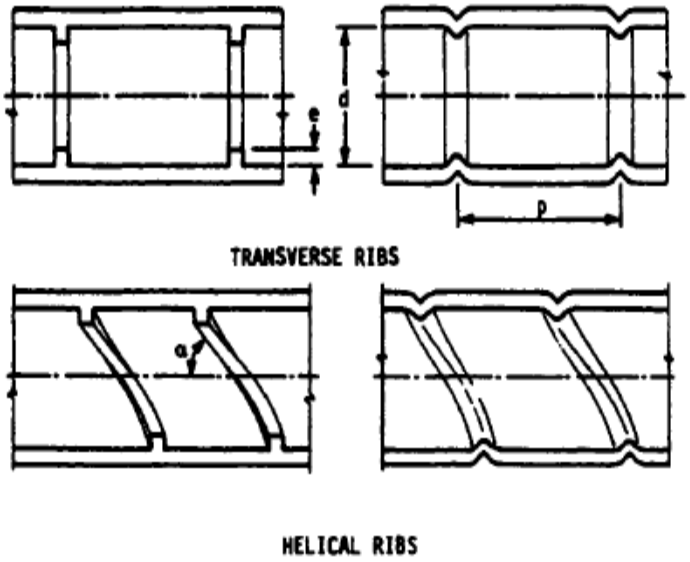

Figure 1.2: Different types of internal corrugation (Ravigururajan and Bergles 1996)

This technique is primarily used for single-phase processes. The increase of the heat transfer in the case of laminar regime obtained in this way is particularly important for applications that involve chemical and food industries, where the convective heat transfer coefficient is often confined within the intrinsic limit values of the laminar flow regime. Furthermore, compared to the insert devices

the advantage of the corrugated surfaces is to have no obstructions in the flow path, and therefore they can also be used for fluids with solid suspensions or fibers without the risk of blocks of stream (Bergles 1998).

This technique will be deeply analyzed in the following paragraphs since it is one of the topic on which this thesis is focused.

Extended Surfaces

They are more commonly known as finned surfaces and achieve a significant increase of the heat transfer surface. There is a wide use of flat fins in many heat exchangers, but recent studies have led to change its shape with the purpose of increasing the heat transfer coefficients not only by expanding the surface area, but also disturbing the flow field.

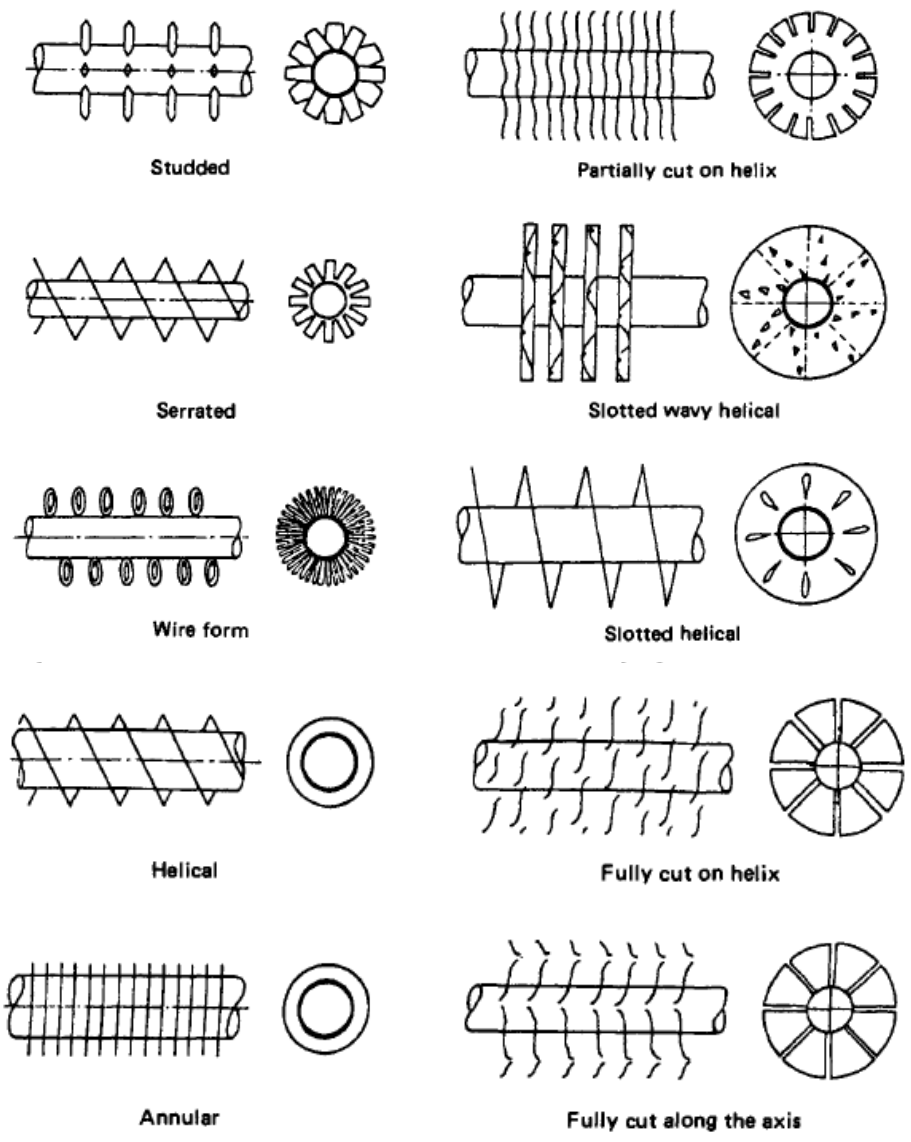

Figure 1.3: Examples of extended surfaces (Webb 1994).

In particular when there is the necessity to obtain heat exchangers with an high surface area-to-volume ratio the fins represent a very useful solution that has permitted to realize more and more compact models. Many different possible geometrical configurations could be realised, as it is possible to notice from figure 1.3.

Inserts

They are elements that are positioned in the flow passage with the aim of increasing the heat transfer rate. The principal factor of heat transfer augmentation is related to the effect of fluid blockage, partitioning of the flow and secondary flow. Within this category of passive heat transfer enhancement techniques displaced devices, twisted tapes, wire coil are present.

The insertion of these devices creates a reduction of the hydraulic diameter and that produces an enhancement of pressure and of viscous effects; it also produces an increase of flow velocity and the appearance in some situations of a significant secondary flow that promotes the mixing of the fluid obtaining in this way an augmentation of heat transfer coefficient (Dewan 2004).

Displaced enhancement devices

A large amount of inserts fall into this category of devices for the heat transfer enhancement. The heated surface is left substantially unaltered, the inserts change the fluid flow close to it increasing the transported energy. In the majority of cases the results obtained are interesting only for laminar flow regimes, as for turbulent flow the pressure losses are too high. The most used are metal grids, disks, cones, static mixers, crowns and balls.

Promvonge (2008a) verified with an experimental study the effectiveness of the use of conical rings as displaced enhancement devices: different elements were inserted in the tube under test as it is possible to see from figure 1.4. The performances of the inserts were evaluated in terms of heat transfer enhancement and friction factor. Conical rings with different diameter ratio of the ring to the tube diameter were employed and for each type three different configurations were studied (converging, diverging and converging-diverging conical rings) .

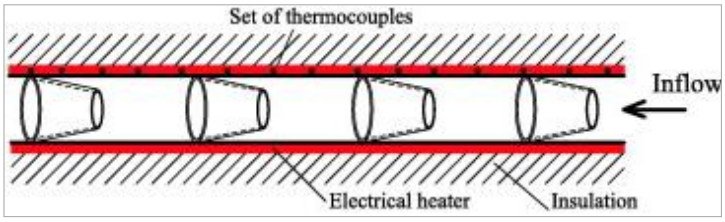

Figure 1.4: Example of diverging conical ring (Promvonge 2008a).

The experiments were performed using air as working fluid in the range $6 \cdot 10^3 < Re < 2.6 \cdot 10^4$. The results show that both the ring to tube diameter ratio and the disposition of the conical rings influence the heat transfer: moreover the author found out that the best configuration on the heat transfer point of view is the diverging one that permits to obtain an increasing of heat transfer in terms of Nusselt number of about 330%. Also the converging and the converging-diverging configuration are very effective since they reach an increasing of the Nusselt number of about 200% and 240%, respectively.

On the other hand the use of conical rings brings to a significant increase also of the friction factor.

Further studies on the same type of devices, but using cones with perforated surfaces, were made by Jadoaa (2011). The intent was to evaluate the change of the heat transfer and of the pressure losses with respect to the previous case. The results show that there were improvements both in terms of average Nusselt number and of friction factor compared to the case of non-perforated cones.

Eiamsa-ard et al.(2010) analyzed another type of displacement devices: They studied the heat transfer and friction factor characteristics of a fully developed airflow through a tube with diamond-shaped turbolators in tandem arrangements inside.

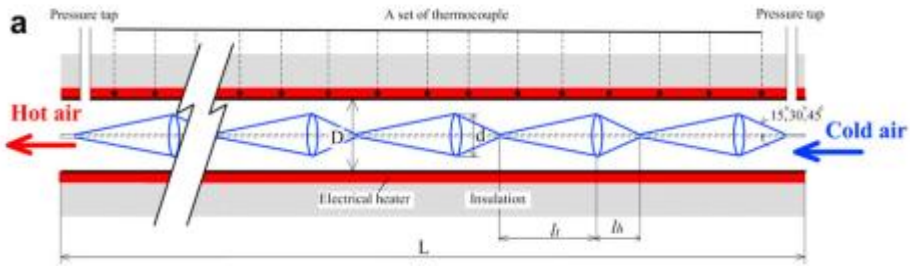

Figure 1.5: Example of diamond-shaped turbolators (Eiamsa-ard 2010).

The authors also proposed correlations for the Nusselt number and friction factor in order to evaluate the effects of using this type of devices on the heat transfer and pressure losses.

Other studies have been made by Sununu (1970) and Genetti and Priebe (1973) using the Kenics static mixer.

This type of mixer is formed by several segments of metallic ribbon wrapped 360°, each of which is rotated 90° with respect to the previous. In the experimental tests high-viscosity oil has been used: the increasing of the heat exchange is about 150%, but the friction coefficient increases by 900%.

Another type of mixer is the Sulzer mixer that has been used for more than 35 years in turbulent flow applications. Experimental studies have been performed by Van der Meer and Hoogendorn

(1978) with Sulzer mixers using silicone oils as heat transfer fluid and registering a gain of 400% of the heat transfer.

For these devices do not exist, however, equations and relationships used globally due to the many geometric variations: also the values of the Nusselt obtained depend strongly on the properties of the fluid used and the heating conditions.

Swirl flow devices

Swirl flow devices are all those devices which, by generating turbulence and/or secondary flows, increase the heat transfer coefficient.

Within this type of devices twisted-tape inserts, inlet vortex generators, wire coils and axial core inserts with a screw-type winding can be found (Webb 1994). Twisted tape has been the object of many research works that analyzed the different configuration of this type of devices studying full-length and short-length twisted tape having a constant pitch or a variable one.

Date and Singham (1972) numerically investigated heat transfer enhancement in laminar, viscous liquid flows in a tube with a uniform heat flux boundary condition. They simplify the flow conditions by considering negligible the tape thickness, but although considering the twist and fin effects device in their study.

The heat transfer enhancement in laminar, viscous liquid flows in a tube with uniform heat flux boundary conditions was also analyzed by Hong and Bergles (1976). The authors considered a laminar flow of water and Ethylene Glycol in an electrically heated metal tube with two twisted tape inserted.

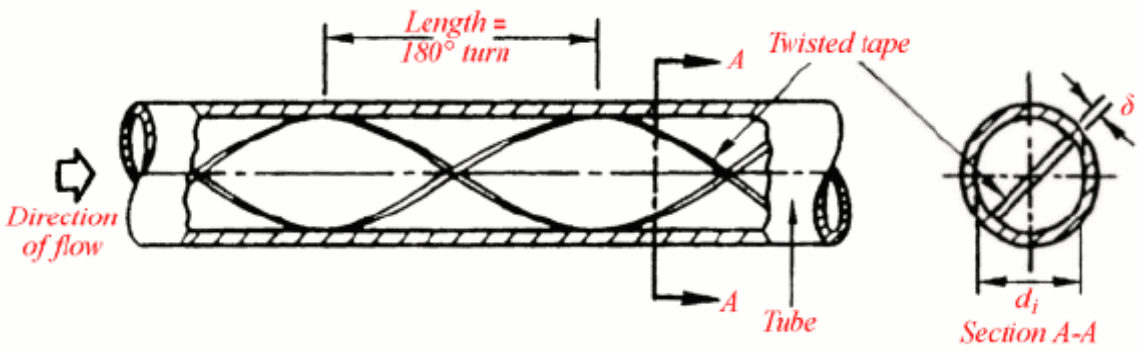

Figure 1.6: Schematic representation of a twisted tape in a pipe (Webb 1994).

The results show an increment of the heat transfer in terms of Nusselt number up to nine times the ones obtained with the empty tube.

Manglik and Bergles (1993) proposed empirical correlations for the Nusselt number and friction factor, identifying a dimensionless swirl parameter.

Wire coil inserts produces an heat transfer enhancement caused by: promotion of turbulence due to the fact that they induce separation in the flow and they act as roughness elements mixing the flow; secondary flow promotion due to the generation of an helicoidal flow at the periphery superimposed on the main axial flow; reduction of the hydraulic diameter with increasing of the average flow velocity.

Garcia et al. (2007) performed a study of the flow mechanisms in tubes with wire coils using hydrogen bubble visualization and PIV techniques. The Authors observed that at low Reynolds number ($Re < 400$), the flow in those type of tubes is similar to the flow in smooth pipes; in the Reynolds number range $400 < Re < 700$ a recirculating flow appeared in short pitch wire coils; an acceleration of the transition to turbulence that, depending on wire coil pitch, appeared in the range $700 < Re < 1000$.

Coiled Tubes

The coiled tubes are widely used passive heat transfer enhancement technique: for example they are employed in heat recovery processes, in air conditioning and refrigeration systems, in chemical reactors and food industry in general.

The effectiveness of wall curvature is due to the fact that it gives origin to the centrifugal force: this phenomenon induces local maxima in the velocity distribution that locally increases the temperature gradients at the wall by then maximizing the heat transfer (Naphon and Wongwises 2006).

This solution, which often produces a swirl or helical type flow, appears very interesting also in the conditions in which the flow persists in the laminar regime (Rainieri 2011).

This technique will be described more precisely in the following paragraphs because it represents a central topic of this study.

Additives for liquid

It is possible to distinguish different types such as solid particles and gas bubbles for single-phase flow and liquid traces for boiling systems (Webb 1994).

Solid particles for single-phase flows

Studies on the subject have been carried out by Watkins (1976) analyzing the case of suspensions of polystyrene particles in a forced laminar flow of oil determining a maximum increase of the heat transfer of 40%.

Gas bubbles for single-phase flow

Tamari and Nishikawa (1976) in their studies found out increases also of 400% of the average heat transfer coefficient value in case of air injected into water or Ethylene Glycol.

Additives for gas

Among the additives used to increase the heat transfer coefficients there are fluid droplets and solid particles that are introduced into single-phase flows both in the dilute phase (gas-solid suspension) that dense phase.

Dilute gas-solid suspensions are used as working fluids for gas turbines and nuclear reactors systems. The solid particles with a range of dimensions going from microns to millimeters are dispersed in the gas flow. These, in addition to increasing the heat capacity of the mixture, facilitate the transport of enthalpy close to the heat transfer surface.

COMPOUND TECHNIQUES

Within this category there are all the possible combination or interaction of two or more different passive or active techniques. Regarding compound techniques, it must be noted that they offer a promising tool for further enhancing the performances of thermal apparatuses, since the heat transfer coefficients are expected to be increased above any of the several techniques acting alone (Kuppan 2000): different examples are presented below.

Chen and Zhang (2003) numerically investigated the flow structure and mixed convection heat transfer in a rotating curved pipe. The Authors analyzed combined effects of rotation (coriolis force), curvature (centrifugal force) and heating/cooling (centrifugal-type buoyancy force) on the flow pattern, friction factor, temperature distribution and Nusselt number.

Usui et al. (1986) carried out a study on the heat transfer enhancement due to the combined use of internally grooved rough tube and twisted tape. From the experimental data the Authors observed a significant heat transfer increase, in particular when the grooves and the twisted tapes are rotated in opposite direction.

Another interesting article on compound technique based on corrugation wall and twisted tape inserts is represented by Zimparov (2002). The author experimentally investigated the heat transfer and the pressure drop in spirally corrugated tubes combined with five twisted-tape inserts in the Reynolds number range $4 \cdot 10^3$-$6 \cdot 10^4$. Significantly higher heat transfer coefficients and friction factor than those of the smooth tube under the same operating conditions were observed.

Promvonge (2008b) performed an experimental study on thermal augmentation in circular tube with twisted tube and wire coil turbolators: the wire coil was inside the tube and the twisted tapes were

inserted into the wire coil to create a swirl flow along the tube wall. The results, obtained for Reynolds number range from $3 \cdot 10^3$ to $1.8 \cdot 10^4$, were compared to those obtained with wire coils or twisted tapes used alone. The combined use of wire coils and twisted tapes permitted to obtain double increase respect to their use alone.

Promvonge and Eiamsa-ard (2006) experimentally investigated the heat transfer enhancement in a uniform heat flux circular tube fitted with conical nozzles and with a snail swirl generator at the inlet of the tube to provide swirling flow. Heat transfer increments of 316% over the plain tube were obtained with the combined use of the conical nozzle and snail swirl generator, bigger than those obtainable with their use alone (278% for conical nozzle and 206% for the snail).

Promvonge (2008c) in another experimental study analyzed the heat transfer augmentation obtained in a round tube with snail entry and coiled-wire inserts under uniform heat flux condition in the range $5 \cdot 10^3 < \mathrm{Re} < 2.5 \cdot 10^4$. A significant heat transfer enhancement was performed by their combined use especially at low Reynolds number.

1.4 COILED TUBES

The curvature of the tubes makes the fluid flowing inside the pipe experiencing the centrifugal force. This force gives rise to secondary flows caused by the particles of the fluid that move with different axial velocity and have the ability to increase the heat exchange. The characteristics of the single-phase heat transfer in tubes helically wound have been extensively studied by researchers both experimentally and theoretically.As already said in the previous paragraph, coiled tubes have found a lot of applications in industry since they represent a very powerful solution to passive enhance the heat transfer. This is witnessed by the great number of studies and researches on this argument that can be found in the scientific literature. As reported by Berger et al. (1983) coiled tubes have been investigated since the last years of the nineteenth century and first years of the twentieth (Thomson 1876; Grindley and Gibson 1908). An important observation was firstly made by Williams et al. (1902) about the velocity distribution inside curved pipes: they stated that the location of the maximum axial velocity is shifted toward the outer wall of the tube. In 1910 Eustice demonstrated the presence of a secondary flow by injecting colored ink inside a water flux in a pipe. A fundamental step forward in the study of curved tubes is represented by the studies performed by Dean (1927,1928). The author analyzed the fluid motion inside a toroidal pipe and mathematically described the phenomenon by considering the toroidal coordinate system (r, α, θ) in figure 1.7 where r it's the distance from the center of the cross section of the pipe, α the angle between the

radius vector and the plane of symmetry, and θ the angular distance of the cross section from the entry of the pipe:

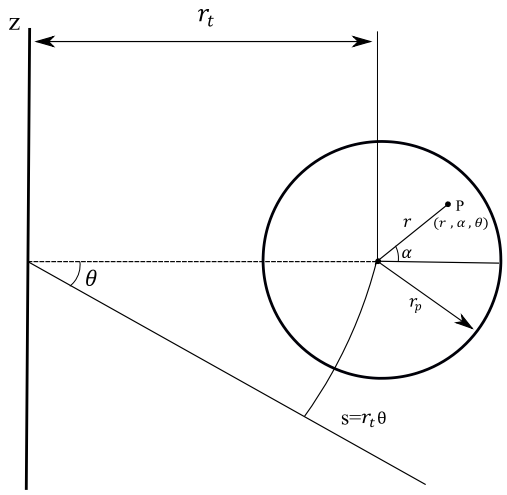

Figure 1.7: Toroidal coordinate system (Dean 1927).

By rescaling the velocities components to make the centrifugal terms of the same order of magnitude as the viscous and inertial terms, since it is the centrifugal force that drives the secondary motion, the Author rewrote the governing equation for the above toroidal coordinate system for steady flow finding out two parameters that characterize the flow in curved pipes: the Dean number and the curvature ratio. Considering the dimensionless variables $r^* = r/r_p$ and $s^* = s/r_p$, the dimensionless velocity components u_r^*, u_α^*, u_s^* obtained dividing u_r, u_α, u_s by the axial mean velocity in the pipe and the dimensionless pressure p^* obtained dividing the pressure p by the density and the square of the mean axial velocity, according to Berger et al. (1983), the momentum equations in the toroidal coordinate system becomes:

(1.39)

$$u_r{}^* \frac{\partial u_r^*}{\partial r^*} + \frac{u_\alpha^*}{r^*}\frac{\partial u_r^*}{\partial \alpha} - \frac{{u_\alpha^*}^2}{r^*} + \frac{u_s^*}{1+\delta r^* \cos\alpha}\frac{\partial u_r^*}{\partial z^*} - \frac{{u_s^*}^2 \cos\alpha}{1+\delta r^* \cos\alpha}$$

$$= -\frac{1}{\delta}\frac{\partial p^*}{\partial r^*}$$

$$-\frac{2}{De}\left[\left(\frac{1}{r^*}\frac{\partial}{\partial \alpha} - \frac{\delta \sin\alpha}{1+\delta r^* \cos\alpha}\right)\left(\frac{\partial u_\alpha^*}{\partial r^*} + \frac{u_\alpha^*}{r^*} - \frac{1}{r^*}\frac{\partial u_r^*}{\partial \alpha}\right)\right.$$

$$\left. - \frac{\delta}{(1+\delta r^* \cos\alpha)^2}\frac{\partial^2 u_r^*}{\partial {z^*}^2} + \frac{1}{1+\delta r^* \cos\alpha}\left(\frac{\partial^2 u_s^*}{\partial r^* \partial z^*} + \frac{\delta \cos\alpha}{1+\delta r^* \cos\alpha}\frac{u_s^*}{\partial z^*}\right)\right]$$

$$u_r^* \frac{\partial u_\alpha^*}{\partial r^*} + \frac{u_\alpha^*}{r^*}\frac{\partial u_\alpha^*}{\partial \alpha} + \frac{u_r^* u_\alpha^*}{r^*} + \frac{u_s^*}{1+\delta r^* \cos\alpha}\frac{\partial u_\alpha^*}{\partial z^*} + \frac{{u_s^*}^2 \sin\alpha}{1+\delta r^* \cos\alpha} \tag{1.40}$$

$$= -\frac{1}{r^*\delta}\frac{\partial p^*}{\partial \alpha}$$

$$+ \frac{2}{De}\left[\frac{\delta}{(1+\delta r^* \cos\alpha)^2}\frac{\partial^2 u_\alpha^*}{\partial {z^*}^2} - \frac{1}{1+\delta r^* \cos\alpha}\frac{1}{r^*}\frac{\partial^2 u_s^*}{\partial \alpha \partial z^*}\right.$$

$$\left. + \frac{\delta \sin\alpha}{(1+\delta r^* \cos\alpha)^2}\frac{\partial u_s^*}{\partial z^*} + \left(\frac{\partial}{\partial r^*} + \frac{\delta\cos\alpha}{1+\delta r^* \cos\alpha}\right)\left(\frac{\partial u_\alpha^*}{\partial r^*} + \frac{u_\alpha^*}{r^*} - \frac{1}{r^*}\frac{\partial u_r^*}{\partial \alpha}\right)\right]$$

$$u_r^* \frac{\partial u_s^*}{\partial r^*} + \frac{u_\alpha^*}{r^*}\frac{\partial u_s^*}{\partial \alpha} + \frac{u_r^* u_s^* \delta\cos\alpha}{1+\delta r^* \cos\alpha} + \frac{u_s^*}{1+\delta r^* \cos\alpha}\frac{\partial u_s^*}{\partial z^*} - \frac{\delta u_r^* u_s^* \sin\alpha}{1+\delta r^* \cos\alpha} \tag{1.41}$$

$$= -\frac{1}{1+\delta r^* \cos\alpha}\frac{\partial p^*}{\partial z^*}$$

$$+ \frac{2}{De}\left[\left(\frac{\partial}{\partial r^*} + \frac{1}{r^*}\right)\left(\frac{\partial u_s^*}{\partial r^*} + \frac{\delta\, u_s^* \cos\alpha}{1+\delta r^* \cos\alpha}\right) + \frac{1}{{r^*}^2}\frac{\partial^2 u_s^*}{\partial \alpha^2}\right.$$

$$- \frac{1}{r^*}\frac{\partial}{\partial \alpha}\frac{\delta\, u_s^* \sin\alpha}{1+\delta r^* \cos\alpha} - \left(\frac{\partial}{\partial r^*} + \frac{1}{r^*}\right)\frac{\delta}{1+\delta r^* \cos\alpha}\frac{\partial u_r^*}{\partial z^*}$$

$$\left. - \frac{1}{r^*}\frac{\partial}{\partial \alpha}\left(\frac{\delta}{1+\delta r^* \cos\alpha}\right)\frac{\partial u_\alpha^*}{\partial z^*}\right]$$

The boundary conditions of no slip at the pipe wall are:

$$u_r^* = u_\alpha^* = u_s^* = 0 \quad \text{at } r^* = 1 \tag{1.42}$$

The curvature ratio is expressed as :

$$\delta = r_p / r_t \tag{1.43}$$

where r_p is the radius of the pipe and r_t is the radius of the toroid.

And the Dean number is defined as follows:

$$De = Re\sqrt{\delta} \tag{1.44}$$

The Dean number could be considered as a measure of the magnitude of the secondary flow which is induced by the centrifugal force and its interaction with viscous forces. The centrifugal force make the fluid moving toward the outer wall and the viscous forces are responsible for bringing fluid elements back towards the inner wall. The parameter δ could be seen as a more specific measure of geometric effect and the extent to which the centrifugal force varies (Berger et al 1983). Considering the case of loosely coiled pipe ($\delta \ll 1$) the only dimensionless group that characterized the flow is the Dean number (Dean 1928).

Making also the assumption of fully developed flow and separating the cross sectional pressure component to the axial pressure ($p^* = p_0^*(z) + \delta p_1^*(r, \alpha, z) + \cdots$) the equations (1.39,1.40,1.41) become (Berger et al. 1983):

$$u_r^* \frac{\partial u_r^*}{\partial r^*} + \frac{u_\alpha^*}{r^*}\frac{\partial u_r^*}{\partial \alpha} - \frac{{u_\alpha^*}^2}{r^*} - {u_s^*}^2 \cos\alpha = -\frac{\partial p_1^*}{\partial r^*} - \frac{2}{De}\frac{1}{r^*}\frac{\partial}{\partial \alpha}\left(\frac{\partial u_\alpha^*}{\partial r^*} + \frac{u_\alpha^*}{r^*} - \frac{1}{r^*}\frac{\partial u_r^*}{\partial \alpha}\right) \tag{1.45}$$

$$u_r^* \frac{\partial u_\alpha^*}{\partial r^*} + \frac{u_\alpha^*}{r^*}\frac{\partial u_\alpha^*}{\partial \alpha} + \frac{u_r^* u_\alpha^*}{r^*} + {u_s^*}^2 \sin\alpha = -\frac{1}{r^*}\frac{\partial p_1^*}{\partial \alpha} + \frac{2}{De}\frac{\partial}{\partial r^*}\left(\frac{\partial u_\alpha^*}{\partial r^*} + \frac{u_\alpha^*}{r^*} - \frac{1}{r^*}\frac{\partial u_r^*}{\partial \alpha}\right) \tag{1.46}$$

$$u_r^* \frac{\partial u_s^*}{\partial r^*} + \frac{u_\alpha^*}{r^*}\frac{\partial u_s^*}{\partial \alpha} = -\frac{\partial p_0^*}{\partial z^*} + \frac{2}{De}\left[\left(\frac{\partial}{\partial r^*} + \frac{1}{r^*}\right)\frac{\partial u_s^*}{\partial r^*} + \frac{1}{{r^*}^2}\frac{\partial^2 u_s^*}{\partial \alpha^2}\right] \tag{1.47}$$

The continuity equation for fully developed flow is expressed as:

$$\frac{\partial u_r^*}{\partial r^*} + \frac{u_r^*}{r^*} + \frac{1}{r^*}\frac{\partial u_\alpha^*}{\partial \alpha} = 0 \tag{1.48}$$

By introducing a stream function for the secondary flow:

$$u_r^* = \frac{1}{r^*}\frac{\partial \psi}{\partial \alpha} \qquad u_\alpha^* = -\frac{\partial \psi}{\partial r^*} \tag{1.49}$$

from equations (1.45,1.46) it is possible to obtain:

$$\frac{2}{De}{\nabla_I}^4 \psi + \frac{1}{r^*}\left(\psi_r \frac{\partial}{\partial \alpha} - \psi_\alpha \frac{\partial}{\partial r}\right){\nabla_I}^2 \psi = -2u_s^*\left(\sin\alpha\, u_{s_r}^* + \frac{\cos\alpha}{r^*} u_{s_\alpha}^*\right) \tag{1.50}$$

where $\nabla_I{}^2 = \left(\frac{\partial^2}{\partial r^{*2}} + \frac{1}{r^*}\frac{\partial}{\partial r^*} + \frac{1}{r^{*2}}\frac{\partial^2}{\partial \alpha^2}\right)$

and from equation (1.46):

$$\nabla_I{}^2 u_s^* - \frac{De}{2}\frac{\partial p_0^*}{\partial z^*} = \frac{De}{2r^*}\left(\psi_\alpha u_{s_r}^* - \psi_r u_{s_\alpha}^*\right) \tag{1.51}$$

with boundary conditions:

$$\psi = \psi_r = u_s^* = 0 \quad \text{at } r^* = 1 \tag{1.52}$$

For small Dean number values, Dean (1927,1928) solved the problem by expanding the solution in a series in powers of the Dean number that is equivalent to perturbing the equivalent Poiseuille flow (Berger et al. 1983). In the flow a pair of counter rotating vortices, placed symmetrically with respect to the plane of symmetry appear cause to the centrifugal force that displaces the slower-moving fluid close to the wall inward and the fast-moving fluid close to the wall outward, as it is shown in figure 1.8.

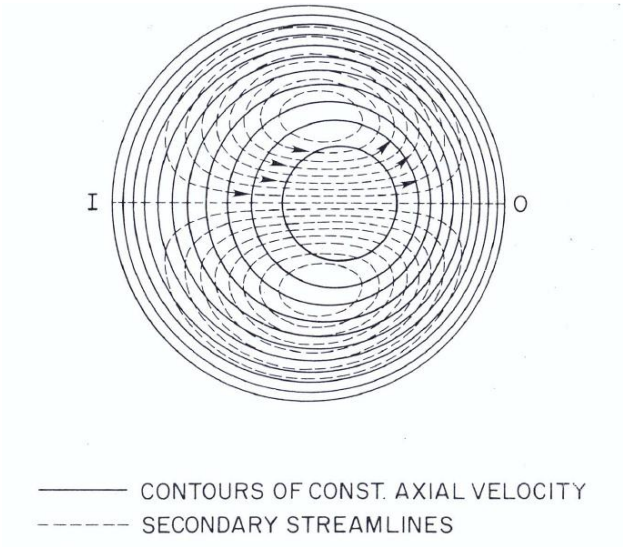

Figure 1.8: Secondary streamlines and axial-velocity contours at low Dean number. I means inner and O outer (Berger et al. 1983).

As Dean increases, the centrifugal force increases and brings to an enhancement of the circumferential velocity and therefore more fluid is pushed toward the outer bend. Consequently the boundary layers near the outer bend further make thin, while near the inner bend further thicken.

McConalogue and Srivastana (1968) analyzed the fluid motion in a curved pipe for a wide Reynolds number range (96-5000) detecting the outward movement of the location of the maximum velocity as it is shown in figure 1.9.

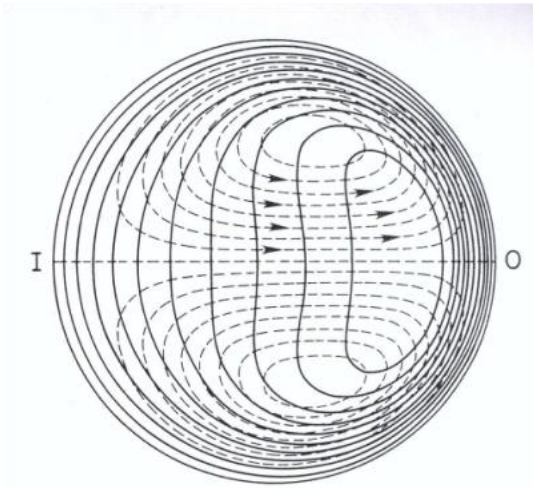

Figure 1.9: Secondary streamlines and axial-velocity contours at De=606. I means inner and O outer (McConalogue and Srivastana 1968).

The analytical formulation of the problem becomes more difficult with the introduction of helically coiled tubes. Two new parameters that characterized the flow are present (Liu et al. 1993): the torsion (1.53) and a modified curvature ratio (1.54):

$$\tau = \frac{(H/2\pi)}{{r_c}^2 + (H/2\pi)^2} \tag{1.53}$$

$$\delta_m = \frac{r_c}{{r_c}^2 + (H/2\pi)^2} \tag{1.54}$$

where r_c is the coil radius, H is the coil pitch, τ is the torsion and δ_m is the modified curvature ratio. Performing the loose-coiling analysis it is possible to find another dimensionless group that contributes to describe the fluid motion in a coiled pipe, the Germano number :

$$Gn = Re\,\tau = Re\,\frac{(H/2\pi)}{{r_c}^2 + (H/2\pi)^2} \tag{1.55}$$

The Germano number represents a measure of the ratio of the twisting forces to the viscous forces and also a measure of the torsion effect.

Truesdell and Adler (1970) stated the possibility to apply the toroidal model to coiled tube. They suggested that the numerical results that they obtained could be employed for helically coiled tubes simply substituting the curvature radius of the toroidal pipe with the helical one.

Murata et al. (1981) confirmed that resistance formula for a toroidal tube is also usable for coiled pipes by substituting curvature radius of the toroidal pipe with the helical one, but on the other side their results showed important differences in particular in the secondary flow pattern.

The effect of the torsion on the laminar convective heat transfer in an helically coiled tube were also studied by Yang et al. (1995): They created a numerical model in order to analyse the fully developed flow in coiled pipes considering a finite pitch. As boundary condition it was considered an uniform axial wall heat flux and uniform peripheral wall temperature. The results showed that heat transfer behavior in a helicoidal pipe is significantly affected by three factors: Dean number, torsion and Prandtl number. They confirmed that the secondary flow is stronger with the increasing of the Dean number and that, coupled with it, an higher temperature gradient appeared close to the outer wall. They also noticed a rotation of the temperature distribution with the changing of the torsion. Another observation was that the Nusselt number increased with the growing of Dean and Prandtl numbers but decreased with the increasing of torsion slightly for very small Pr and significantly for higher Pr.

A side effect of the wall curvature observed by some authors is the suppression of turbulent fluctuations. White (1929) detected that the flow could be maintained laminar for substantially higher Reynolds numbers than it is possible in straight pipes. Sreenivasan and Strykowski (1983) observed that when a flow through a straight tube is passed through a coiled pipe two stabilizing effects appear: in a determinate Reynolds number range the turbulent flow in straight pipes becomes laminar in coiled section and the stabilization effect persisted to a certain degree even after the flow downstream of the coil has been allowed to develop in a long straight section. Moreover in literature a complex behavior following the departure from the laminar flow regime has been described. Di Piazza and Ciofalo (2011) observed numerically in toroidal pipes a first transition to a periodic flow followed by a second transition to a quasi periodic flow and then by a transition to a chaotic flow. A much more gradual and smooth turbulence emergence process respect to the one experienced in straight pipes was confirmed also by Cioncolini and Santini (2006).

A wide review on helically coiled tubes and other curved pipes was realized by Naphon and Wongwises (2006).

Important studies on the effect that the secondary flow has on the heat transfer inside curved pipes in laminar flow regime conditions both in thermal entry region and fully developed region were performed by Dravid et al. (1971).

The authors in addiction proposed a correlation for the asymptotic Nusselt numbers in function of Dean and Prandtl numbers:

$$Nu = \left(0.65\sqrt{De} + 0.76\right)Pr^{0.175} \tag{1.56}$$

valid in the Dean number range $50 < De < 200$ and Prandtl number range $5 < Pr < 175$.

Kalb and Seader (1972) carried out a theoretical study of heat transfer in steady viscous flow in curved pipes of circular cross section for fully developed temperature and velocity fields under boundary conditions of axially uniform wall heat flux with peripherally uniform wall temperature. They investigated the phenomenon in Dean number range from 1 to 1200, Prandtl number range from 0.005 to 1600 and curvature ratio from 0.01 to 0.1. A graphical correlation is proposed for fully developed Nusselt number covering all the Dean and Prandtl numbers range.

Moreover the numerical data were analyzed by least-squares techniques to provide equations showing the effect of the Dean and Prandtl numbers on the Nusselt number, but only for a strongly limited range of Prandtl number (0.005-5):

$$Nu = 3.31\, De^{0.115}\, Pr^{0.0108} \tag{1.57}$$

valid for $20 < De < 1200$ and $0.005 < Pr < 0.05$

$$Nu = 0.913\, De^{0.476}\, Pr^{0.2} \tag{1.58}$$

valid for $80 < De < 1200$ and $0.7 < Pr < 5$.

Tarbell and Samuels (1973) solved the equations of motion and energy for flow and heat transfer in curved tubes by using the alternating direction-implicit technique. Results for the asymptotic Nusselt number were compared with those obtained by Dravid et al. (1971) and by Kalb and Seader finding a good agreement.

Patankar et al. (1974) talked over the effect of Dean number on heat transfer and friction factor in the developing and fully developed regions in helical pipes. Comparisons between the developing and fully developed velocity profiles, the wall temperature for the case of axially uniform heat flux with an isothermal periphery obtained numerically and those obtained experimentally showed good agreement.

Not only numerical studies but also experimental ones were carried out to investigate the phenomenon.

Seban and McLaughin (1963) performed an experimental analysis both for laminar and turbulent flow regimes using a oil for the laminar flow and water for the turbulent one. They also developed a correlation to determine the inner Nusselt number in function of Reynolds and Prandtl numbers. The authors observed moreover an oscillating heat transfer near the entrance region (later confirmed by Dravid et al.1971), followed by a fully developed region.

An experimental and numerical study was realized by Janssen and Hoogendoorn (1978) on convective heat transfer in coiled pipes. The analysis was performed in the Prandtl number range 10 to 500 and Reynolds number range 20 to 4000. Two different boundary conditions of uniform

peripherally averaged heat flux and of constant wall temperature were considered and the experiments were done for different tubes by varying tube diameter ratio to coil diameter from 1/100 to 1/10. They investigated heat transfer both in the thermally entry region and in the fully developed region. The authors in addition proposed correlations for average Nusselt number and the ones suggested for the fully developed region and uniform peripherally averaged heat flux boundary condition are:

$$Nu = 1.7(De^2 Pr)^{\frac{1}{6}} \tag{1.59}$$

valid for $De < 20$ and $(De^2 Pr)^{1/2} > 100$.

$$Nu = 0.9(Re^2 Pr)^{\frac{1}{6}} \tag{1.60}$$

valid for $20 < De < 100$.

$$Nu = 0.7\, Re^{0.43}\, Pr^{\frac{1}{6}}\, \delta_c{}^{0.07} \tag{1.61}$$

valid for $100 < De < 830$ and $0.01 < \delta_c < 0.083$.

The authors concluded that only for small Dean number ($De < 20$) the dimensionless group $De^2 Pr$ is characteristic for the heat transfer. For $De > 20$ the dependence of Nusselt number is not described by Dean number as instead was suggested by Dravid et al. (1971)

Also Xin and Ebadian (1997) investigated experimentally the heat transfer and the fluid motion inside helically coiled pipes both in laminar and turbulent regimes. The study was carried out using three different fluids (air, water and ethylene glycol) on five uniformly heated helical pipes with different geometrical parameters (pipe diameter and the pitch to coil diameter ratio). The authors moreover suggested a correlation for the average Nusselt number both for laminar and turbulent flow.

The one proposed for laminar regime is the following:

$$Nu = (2.153 + 0.318\, De^{0.643}) Pr^{0.177} \tag{1.62}$$

valid for 50 < De < 2000, 0.7 < Pr < 175 and pipe diameter ratio to coil diameter between 0.0267 and 0.0884 .

Prabhajan et al. (2002) carried out experiments to determine the relative advantage of helical coil versus straight tube heat exchangers for heating liquids. They utilized a particular boundary condition: instead of having constant wall heat flux or constant wall temperature they considered a

fluid-to-fluid heat exchanger. Results showed that the heat transfer coefficient depended on geometry of heat exchanger and the temperature of the water bath surrounding the heat exchanger and that the thermal performances reached with the helical coil tubes where up to 50% higher than the ones with the straight pipes.

Although many authors have experimentally investigated the forced convective heat transfer in coiled tubes, the results are usually reported only in terms of the peripherally averaged Nusselt number, whereas the local values are discussed only in few cases.

In helically coiled tubes, being the fluid temperature profile strongly asymmetrical with respect to the tube's axis, the convective heat transfer coefficient is then expected to vary significantly along the periphery of the tube's cross section. In particular it is expected that the convective heat transfer coefficient presents higher values at the outer bend side of the wall surface than at the inner bend side, due to the secondary flow pattern. The presence of an irregular heat transfer may be critical in some industrial applications, such as in those that involve a thermal process. For instance, in food pasteurisation, the irregular temperature field induced by the wall curvature could reduce the bacteria heat-killing or could locally overheat the product. Very few papers in literature (Bai et al. 1999; Seban et McLaughlin 1963, Xin and Ebadian 1997, Janssen and Hoogendoorn 1978) have presented experimental results and only two of them report the real local ones (Bai et al. 1999, Seban et McLaughlin 1963) while the others, neglecting heat conduction in the tube wall, estimate only the apparent ones (Xin and Ebadian 1997, Janssen and Hoogendoorn1978). The majority of the articles are for turbulent regime.

Bai et al. (1999) experimentally studied the turbulent heat transfer in helically coiled tubes using deionised water as the working fluid. It was heated by applying alternating current in the tube wall and, in each cross section eight thermocouples were placed on the external surface of the tube wall. The local heat-transfer distribution on the internal wall of the tube was obtained by solving the two-dimensional inverse heat conduction problem with the least-square method. As expected, they found that the local heat-transfer coefficient was not evenly distributed along the periphery of the cross section and that, in particular, at the outside surface of the coil, it was three or four times higher than that at the inside surface.

Some experimental data are discussed by Seban et McLaughlin (1963). These Authors correctly drew the attention to the difference between apparent and true local values: apparent heat transfer coefficients are obtained neglecting the circumferential heat conduction in the tube wall which means considering the average value of the convective heat flux instead of the punctual value. In terms of true heat transfer coefficient, the ratio of the outside to the inside coefficient found in this experimental campaign is about four for both the laminar flow case and the turbulent one. However,

no details about the approach adopted to estimate the local convective heat flux is given in this paper.

Both Xin and Ebadian (1997) and Janssen and Hoogendoorn (1978) conducted extensive experimental campaigns with many different fluids on a wide range of curvature ratios and Reynolds numbers. However, these Authors processed their data neglecting the circumferential heat conduction in the tube wall, and so the reported local heat-transfer coefficient distribution can be regarded as the apparent values.

Among the numerical studies it has to be noted the already cited article by Yang et al.(1995): the Authors showed that, due to torsion, the local heat-transfer coefficient, compared to the case of an ideal torus, is increased on half of the tube wall while it is decreased on the other half.

Another numerical interesting work was performed by Jayakumar et al. (2010), who numerically analysed the turbulent heat transfer in helically coiled tubes and presented the local Nusselt number at various cross sections along the curvilinear coordinate. The results showed that, on any cross section, the highest Nusselt number is on the outer side of the coil, and the lowest one is expected on the inner side. Moreover, the Authors proposed a correlation for predicting the local Nusselt number as a function of the average Nusselt number and the angular location for both the constant temperature and the constant heat-flux boundary conditions.

Any augmentation technique should be optimized in relation to the particular process (single/two phase, type of fluid, type of thermal treatment, scale of the geometry etc..) taking into account also the inevitable drawbacks (pressure drop penalties, fouling and others). For what concerns the pressure drop penalties a comprehensive review was made by Ali (2001) listing the correlations for the friction factor present in literature. Since a secondary flow is induced due to the difference in centrifugal force, the flow phenomenon in curved tubes is therefore more complex than in straight pipes (Naphon and Wongwises 2006). Many researches have been carried out about the fluid flow nature in helically coiled tubes with circular cross section. As already said one of the first was Dean (1927,1928) that proposed an analytical correlation for friction factor in a torus for small curvature ratio and Dean number lower than 20:

$$\frac{f_c}{f_s} = 1.03058\left(\frac{\mathrm{De}^2}{288}\right)^2 + 0.01195\left(\frac{\mathrm{De}^2}{288}\right)^4 \tag{1.63}$$

where f_c/f_s is the ratio between friction factor for the curved tube and the friction factor for the flow of the same fluid in a straight length of the same diameter tube.

In 1929 an empirical correlation was proposed by White valid for a larger Dean number range ($11.6 < \mathrm{De} < 2000$):

$$\frac{f_s}{f_c} = 1 - \left[1 - \left(\frac{11.6}{\mathrm{De}}\right)^{0.45}\right]^{\frac{1}{0.45}} \tag{1.64}$$

Among the most popular correlations there were surely the ones proposed by Ito (1969). The one suggested for laminar flow is the following:

$$\frac{f_c}{f_s} = \frac{21.5 \cdot De}{(1.56 + log_{10}\, De)^{5.73}} \tag{1.65}$$

valid for 13.5 < De < 2000.

Another important study was performed by Mishra and Gupta (1979) that carried out an experimental analysis on pressure losses in the laminar and turbulent region for Newtonian fluids flowing through 60 helically coiled pipes: a wide range of diameters and pitch are investigated. For the laminar flow regime the Authors proposed the following correlation for the friction factor:

$$\frac{f_c}{f_s} = 1 + 0.033(log_{10}\, He)^4 \tag{1.66}$$

valid for 1 < He < 3000 where $He = Re\left(\frac{r_p}{r_c}\right)\left[1 + \left(\frac{H}{2\pi r_c}\right)^2\right]^{1/2}$ is the Helical number.

Also Guo et al. (2001) studied frictional pressure drops of single-phase water flow in two helically coiled pipes at four different helix axial inclinations angles. The Authors found out that the helix axial angles have not a valuable effect on pressure drop. Moreover They proposed a new friction factor correlation as follows:

$$f_c = 2.552 Re^{-0.15}\left(\frac{r_p}{r_c}\right) \tag{1.67}$$

1.5 CORRUGATED WALL TUBES

The introduction of wall corrugated pipes has proven a successful method in enhancing heat transfer: the enhancement effect associated to the wall corrugation, as already said in paragraph 1.2, is due to the periodic interruption of the boundary layers development, to the increase in heat transfer area, to the generation of swirling and/or secondary flows and to the promotion of the transition to an unsteady regime. They are employed in a high number of industrial applications.

One of the first study on local and average heat and mass transfer was performed by Goldstein and Sparrow (1977) for laminar, transitional and low Reynolds number turbulent flow in a corrugated

wall channel. They found out that for laminar flow regime the transfer coefficients were only slightly bigger than those for a parallel-plate channel. Instead for Reynolds number turbulent flow the heat transfer rate is up to three times bigger than those without corrugation.

An example of corrugated passages is represented by the wavy channels that have been well investigated in literature both numerically and experimentally (Nishimura et al 1990; Wang and Vanka 1995; Niceno and Nobile 2001).

Normally they do not present heat transfer enhancement in laminar flow operating condition.

However a significant increase of the heat transfer rate is denoted with the transition to unsteady regime. This is a result of complex interactions between the core fluid and the boundary layer fluid through shear-layer self-sustained oscillations. The critical Reynolds number at which the transition to a time-dependent flow regime happens depends significantly on geometrical parameters of the pipe.

Nishimura et al. (1990) studied the flow pattern and mass transfer characteristics in symmetrical two-dimensional wavy-wall channels for low Reynolds number range (20-300). They analyzed two different wavy shape: sinusoidal and arc-shaped wall. The Authors observed that for steady flow no enhancement in mass transfer was visible but after the transition to an unsteady regime the increase was significant. The results pointed out that for the arc-shaped wall transition to the unsteady regime was obtained for a lower Reynolds number than the sinusoidal.

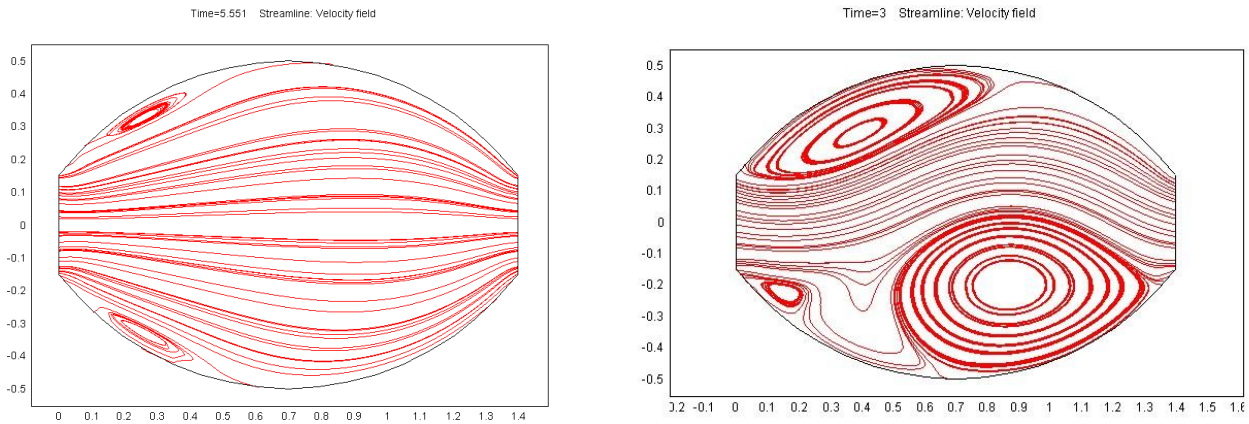

Figure 1.10: Evolution from steady to unsteady flow regime (Rainieri et al. 2005).

Guzman and Amon (1996) investigated the transition from laminar to unsteady state for converging-diverging conducts by numerical simulations in Reynolds number range from 10 to 850. They stated that the transition occurred through a sequence of intermediate state of self-sustained periodic, quasi-periodic and finally aperiodic or chaotic regime.

Wang and Vanka (1995) numerically investigated the heat transfer for flow through a periodic array of wavy passages. They observed that the flow was steady until a critical value of Reynolds number of about 180. After that, a transition appeared, characterized by a destabilization of laminar thermal boundary layers replacing the fluid close to the wall with that of the core region producing in that way a mechanism of heat and mass transfer enhancement. The average Nusselt numbers calculated for the laminar flow regime were moderate higher than those for channels without waves while heat transfer enhancement in the transitional flow regime was about 2.5 times than those for channels without waves.

The results obtained by Nishimura et al. (1990) and by Wang and Vanka (1995) were confirmed by Niceno and Nobile (2001): They numerically studied the fluid flow and heat transfer in periodic wavy channels considering two different geometrical configurations, sinusoidal and arc-shaped channels. The two tested geometries were shown to provide little or no heat transfer enhancement in steady flow regimes at lower values of Reynolds number while in unsteady regimes they reached significant heat transfer increase. Moreover, the Authors found out that both the channels had higher values of pressure drop than that of parallel-plane channel under fully developed conditions. The arc-shape channels presented both higher values of friction factor and heat transfer rate respect to the sinusoidal channels.

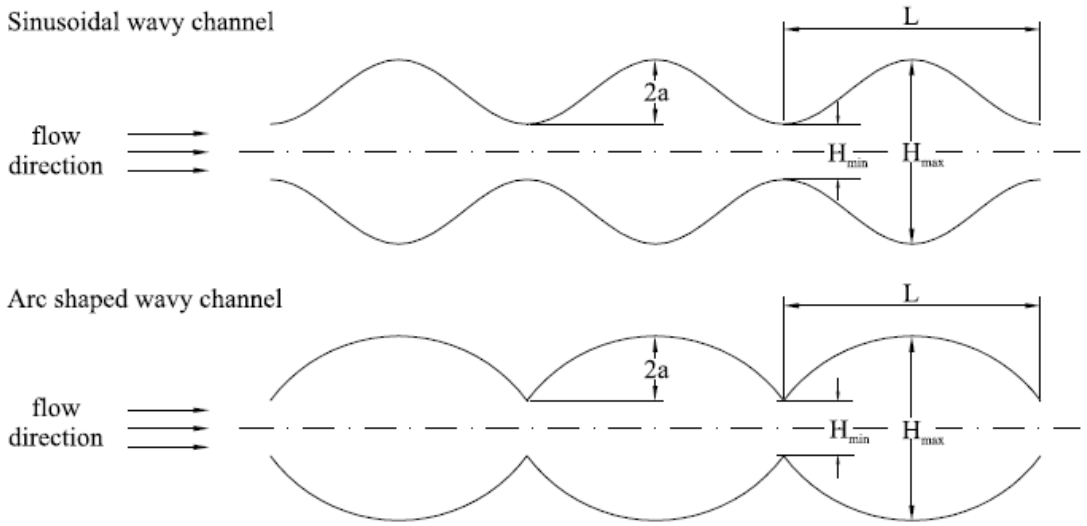

Figure 1.11: Geometrical configuration of wavy walls channels studied by Niceno and Nobile (2001).

Tubes having a transverse repeated-rib roughness with rectangular cross section have been analyzed by Webb et al. (1971). The Authors proposed some correlations of friction factor as a function of dimensionless geometric parameters and Reynolds number. Gee and Webb (1980) extended this study analyzing the effect of the helix angle.

Watkinson et al.(1975) performed a series of experiments measuring heat transfer and pressure drop in integral-fin tubes in laminar oil flow. They considered different geometries by varying the tube diameter between 12.7 and 32 mm, the number of fins from six to fifty, the shape of fins straight or spiral and the dimension of fins. The study was carried out in the Reynolds number range 50 to 3000 and Prandtl number range 180 to 250. They obtained the highest Nusselt number values for the high-spiral fin tube followed by the low-spiral fin tubes and by the straight fin ones. The enhancement of heat transfer over the smooth tube values at Re=500 is between 8 and 224% depending on geometry. They also proposed correlations for Nusselt number and friction factor and found out that the transition occurred at lower Reynolds number (250 to 1500).

The laminar flow in tubes with internal fins has also been considered by Rowley and Patankar (1984). They obtained numerical results for pressure drop and heat transfer in circular tubes with circumferential internal fins in periodic fully developed flow with the boundary condition of linearly varying wall temperature. The presence of the fins gave rise to a recirculating flow in the space between two successive fins.

Despite the recirculating flow promote the mixing of the fluid and tends to increase the heat transfer the obstacle represented by the fins caused the flow to move away from the tube wall. Consequently the presence of the fins often decreases the heat transfer coefficient rather than augmenting it for low Prandtl number fluid. The recirculation of the fluid induced by the fins enhances the heat transfer only for Prandtl number greater than 5.

Another category of corrugated tubes are those usually named spirally enhanced tubes: they can be characterized by different corrugation profile, i.e. transverse corrugation, helical corrugation with single and double helix, spirally fluted, spirally indented, spirally ribbed. The geometric parameters usually employed to describe spirally enhanced tubes are: the bore diameter D_b, the envelope diameter D_{env} that represents the maximum internal diameter (see for instance figure 1.12), the ridge depth e, the pitch l and the number of starts N_s.These tubes increase convective heat transfer by introducing swirl into flow and/or periodic disruption of the boundary layer at the tube surface due to repeated changes in the surface geometry (Srinivasan and Christensen 1992).

One of the first works on this type of tube was performed by Whithers (1980) even if in the turbulent regime. The authors proposed an empirical correlation of friction factor in terms of Reynolds number and found an heat transfer enhancement up to 2.5-3.

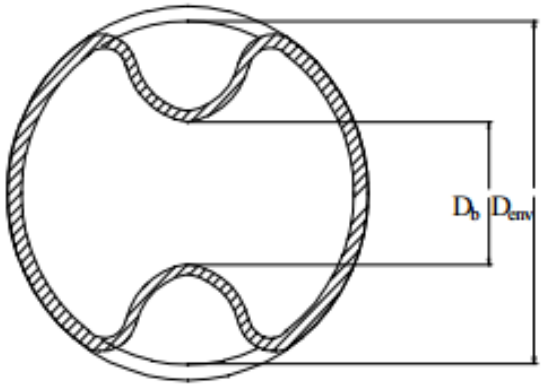

Figure 1.12: Particular of the section of the spirally enhanced tubes (Rainieri et al. 1996).

Garimella and Christensen (1995) analyzed flow mechanism and pressure drop in annuli formed by placing a spirally fluted tubes inside a smooth outer in the laminar, transition and turbulent regime. By studying the variation of friction factor as a function of Reynolds number it was shown that transition in this annuli occurs in the Reynolds number range 310 to 1000.

Garimella and Christensen (1993) also investigated the flow mechanism in annuli considering different spirally enhanced tubes: fluted, indented and ribbed. Flow patterns and transitions between flow regimes were qualitatively investigated through visualization tests. Detailed temperature profile measurements were realized on the crests and troughs of the tube surface to investigate potential circumferential, axial and spiral variations. They detected that spirally fluted tubes induce a relevant degree of swirl in the flow and that in those annuli the transition appear at significantly lower Reynolds numbers ($310 < Re < 730$) than for plain-tube annuli.

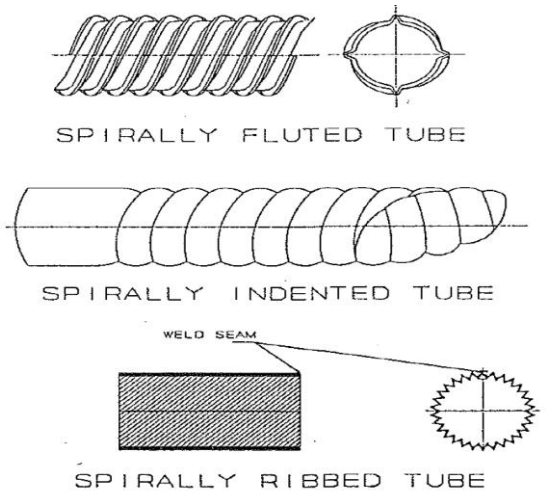

Figure 1.13: Spirally enhanced tubes studied by Garimella and Christensen (1993).

The spirally ribbed tube induced a combination of alternating swirl and axial flow but to a lower degree than the spirally fluted tube. Instead spirally indented annuli didn't produce an appreciable swirl into the flow and their main effect seemed to be to disturb the boundary layer at the inner wall. The transition in these annuli occurred at higher values of Reynolds number than in spirally flute tubes ($525 < Re < 1675$) but lower than in plain tube annuli.

The spirally fluted tube have been also the argument of an experimental study performed by Srinivasan and Christensen (1992) and focused on heat transfer and pressure drop characteristics of this type of tubes. Nusselt number in the laminar regime was found to be between 2 and 10 times the smooth tube values and the friction factor between 1.2 and 3 times the smooth tube values. From the pressure drop tests it was observed that the transition occurred in the range $300 \leq Re \leq 1000$.

The Authors moreover suggested correlations for Nusselt number as a function of Reynolds number and other relevant geometric variables both for laminar and turbulent flow.

Rainieri et al. (1996) carried out an experimental investigation of the heat transfer and pressure drop augmentation for laminar flow in spirally enhanced tubes in case of Newtonian fluid and uniform wall heat flux. The authors analyzed in their work five different geometries (see figure1.14), all falling into the generally category usually referred to as spirally enhanced tubes. The tubes have different corrugation profiles: three of them presented a single helix ridging and the others were characterized by two helical ridging that spiral along the tube in opposite direction (cross helical corrugation). The results were compared with the predictions for the smooth tube in order to point out the heat transfer enhancement and the friction factor augmentation in the laminar flow regime. The experimental data showed that for the lowest Reynolds number values considered the heat transfer coefficient is almost the same to the one typical of the smooth pipe. Instead with the Reynolds number increasing it was noticed a significant heat transfer enhancement. The critical Reynolds number at which the transition started was identified for a value between 700 and 800 for single helix corrugation and between 500 and 600 for cross-helical corrugation. They also noticed the increasing of the friction factor for corrugated tube ratio to friction factor of smooth pipe with the growing of the Reynolds number up to a value of 5.

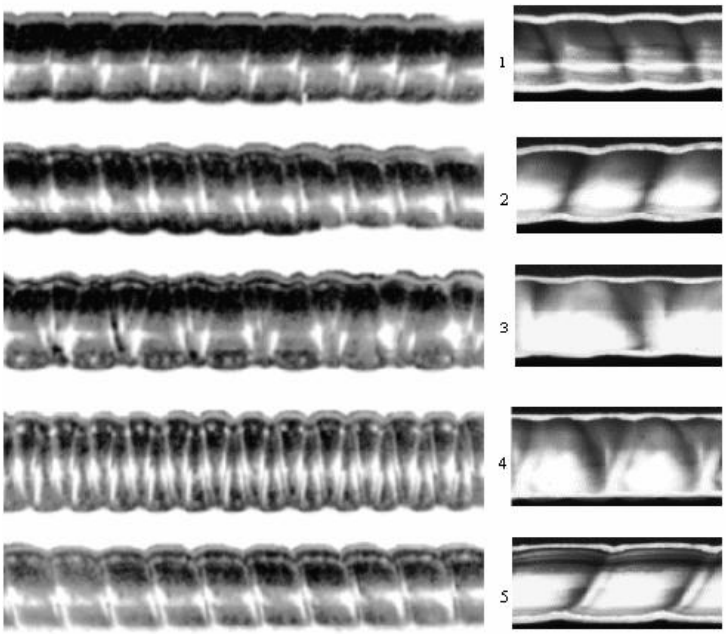

Figure 1.14: Tubes tested by Rainieri et al. (1996).

Chen et al. (2001) investigated the effect of the corrugation angles on heat transfer and hydrodynamic performance. The Results showed that the corrugation angles produce quantitative differences in heat transfer and friction losses for spirally corrugated tubes. The Authors concluded that manipulation of corrugation geometry and in particular of the angle could offer opportunities to industry to improve heat exchangers for various applications.

A recent study (Garcia et al. 2011) analyzed the effect of corrugation on heat transfer enhancement and compared it to those obtained with dimpled tubes and wire coils. Heat transfer and pressure drop experimental data in laminar, transition and turbulent regimes were used in that study. From the comparison it was found out that in pure laminar region ($Re < 200$) the heat transfer in the considered roughened tubes is very similar to that obtained in smooth tubes; for $200 < Re < 2000$ the wire coils were more advantageous and for $Re > 2000$ the use of dimpled and corrugated tubes was recommended cause of the lower pressure drop respect to wire coils for similar heat transfer coefficient levels.

1.6 COMPOUND TECHNIQUES: COILED CORRUGATED TUBES

The simultaneous use of two or more of these passive techniques has been studied to check if it is possible to obtain improvements compared to their single use.

Zachar (2010) performed an analysis of heat transfer rate in coiled-tube heat exchangers with spirally corrugated wall. As shown in figure 1.15 the outer side of the wall presented an helical corrugation that created a helical rib on the inner side of the wall in order to induce additional swirling motion to the fluid.

Different geometrical parameters of corrugation were investigated and various flow rates and temperatures were considered in order to test the impact of flow parameters on the efficiency of the heat exchanger. Numerical results were compared to existing empirical correlations for common helical tube heat exchangers: heat exchangers coils with corrugated wall presented an increase up to 80-100% respect to those with smooth wall in the Dean number range 30 to 1400. But on the other side the corrugated wall helically coiled tubes present also a pressure drop increment of 10-600%.

Moreover the Author proposed a correlation for the fully developed inner side heat transfer prediction in case of helically corrugated wall configuration expressing the peripherally averaged Nusselt number as a function of Dean and Prandtl numbers and geometrical parameters:

$$Nu = 0.5855\, De^{0.6688}\, Pr^{0.408} \left(\frac{e}{2r_p}\right)^{0.166} \left(\frac{p_c}{2r_p}\right)^{-0.192} \tag{1.68}$$

valid for $30 < De < 1400$, $3 < Pr < 30$.

Figure 1.15: Schematic geometry of the corrugated coiled tube heat exchanger considered by Zachar (2010).

It was also observed in the peripherally average Nusselt number for corrugated wall a more oscillatory behavior respect to helical smooth tube.

Helical pipes with full circumferential ribs were studied by Chang et al (2002) with reference to the design of enhanced cooling passages in the cylinder head and liner of a marine propulsive diesel engine. The flow entering the tubes was turbulent but laminar in further downstream.

A series of experiments considering also helically coiled pipes with smooth wall permitted to observe the individual and compound effects of Dean vortices and corrugation on heat transfer: the centrifugal force created circumferential heat transfer variation with better cooling performance on the outer bend. The presence of the ribs caused in addiction an increase of heat transfer 1.3 to 3 times higher respect to smooth helical tubes.

Rainieri et al.(2012) studied the forced convective heat transfer in straight and corrugated tubes having smooth and corrugated wall. The analysis was performed using highly viscous fluid: Glycerine in the Reynolds number range 5 to 13 and Ethylene Glycol in the range 150 to 1500. The authors concluded that the wall curvature enhances heat transfer at all Reynolds number considered whereas the wall corrugation only in the higher range of *Re.* Therefore the best solution was represented by smooth helical coils at low Reynolds of the range, and by corrugated helical coils at high values of the range.

2. INVERSE HEAT TRANSFER PROBLEMS

Inverse Heat Transfer Problems (IHTP) deal with estimation of unknown quantities appearing in the analysis of physical problems in thermal engineering by using temperature or flow measurements. Normally the standard heat transfer problems, usually known as Direct problems, concern the determination of the effect starting from the causes: for instance the computation of a temperature field in a body starting from the boundary heat flux conditions. Otherwise it is possible to say that inverse problems involve the estimation of the causes (boundary heat flux) from the measurement of the effect (Ozisik 2000). The word "estimation" is used talking about inverse problems because in measurements, errors are always present and they affect the accuracy of the calculation (Beck et al. 1985).

The inverse heat transfer problems are much more difficult to solve analytically than the direct problems but in the direct problem many experimental impediments could be present in measuring or producing given boundary conditions. Moreover the major difficulties in the solution of inverse heat transfer problems are connected to the fact that from the mathematical point of view they are classified as ill-posed while the direct problems are usually well-posed.

To be well-posed the solution must exist, must be unique and must be stable under small changes to the input data. The existence and the uniqueness of the solution for inverse problems is difficult to be demonstrated: it was proved just for some special cases. Moreover it is very complicate to perform the stability of the solution because, since inverse problems are very sensitive to random errors in measured data, small perturbations in the input values could originate great variations in the solution.

For a long time it was thought unsolvable every problem that didn't respect even only one of the conditions necessary for well-posedness or the results obtained from such a solution were considered meaningless or without practical importance.

However some heuristic methods of solution were developed in the '50s: an important contribution in the progression of the solution techniques of inverse problems has been furnished by the space program where, for example a typical case in which it was used the IHTP was the determination of the surface temperature for the thermal shield during reentry in the atmosphere. Later in the 60's and the 70's many methods were formalized in term of their ability to treat ill-posed unstable problems. These methods are based on the idea of reformulating the inverse problem in terms of an appropriate well-posed problem by utilizing some kind of regularization. A fundamental role in those year was played by the works of Beck, Alifanov and Tickonov.

Nowadays inverse problems are used in a great number of applications as estimation of thermophysical properties of materials (Beck and Arnold 1977), control of motion of the solid-

liquid interface during solidification (Zabaras and Ngugen 1995), estimation of inlet condition and boundary heat flux in forced convection inside pipes (Huang and Ozisik 1992), estimation of interface conductance between periodically contacting surfaces (Orlande and Ozisik 1993), estimation of heat release during friction of two solids (Alifanov 1994), estimation of local heat transfer coefficient (Bozzoli et al. 2014a), estimation of boundary shapes of the solids (Dulikravich and Martin 1996) and many others.

Inverse heat transfer problems can be classified by following different criteria like for example the nature of heat transfer problem (IHTP of conduction, convection, surface radiation, simultaneous convection and radiation or convection and radiation or conduction and convection and of phase change) or the type of causal characteristics to be estimated (IHTP of boundary condition, thermophysical properties, initial condition, source term).

Moreover IHTP can be one-, two- or three dimensional, and linear or nonlinear (Ozisik 2000).

An IHTP is a linear problem if both the heat equation and the boundary equations are linear. The linear nature in an inverse problem is a very positive aspect since it permits to eliminate the use of the iteration in the solution permitting to significantly reduce the computational cost of the calculation (Beck et al. 1985).

A common general classification of inverse problems is the distinction between parameter estimation and function estimation. The parameter estimation is characterized by: a limited number of parameters; the parameters frequently refer to a physical property, such as thermal conductivity for a specified material at a particular temperature. Otherwise in the function estimation no available information on functional form are known and thus the number of parameters that have to be determined is high. The problems are usually ill posed and could or could not be linear (Woodbury 2003).

The IHTP that it will be studied in chapters 5,6,7, is a typical inverse heat conduction problem (IHCP) that can also be classified as boundary inverse problem or function estimation inverse problem.

For the IHTP problems many different solution techniques have been developed. These methods could be classified by following different criteria: one could be the ability of the technique to treat nonlinear as well as linear problem. Other criteria might be the heat transfer equation solution method (Duhamel's theorem, finite differences, finite elements and finite control volumes, quadrupole method) and the dimensionality of the IHTP. Another possible criterion is the time domain over which measurements are used in the inverse analysis. Three different time domains could be considered: only the present time, the present time plus a few time steps and the complete time domain. The first time domain associated with a single temperature sensor allows to reach an

exact matching between the calculated and the measured temperatures. Although the significant appeal exercised it presents some complications due to the fact that it is extremely sensitive to measurements errors. In the second time domain few additional temperatures relative to few future time steps are used to improve the stability of the associated algorithms. Methods based on the first two time domains are sequential in nature. The second method permits to obtain reduced sensitivity to measurements errors and to perform much smaller time steps allowing to obtain more detailed information regarding the time variation of variables to estimate. Anyway, it is necessary to pay attention to not using time steps too smaller causing instability in the problem. The whole domain estimation procedure is also very powerful because it allows to take very small time steps permitting to estimate, with good resolution, time dependent unknown function (Beck et al. 1985). Özisik and Orlande (2000) suggested a possible classification in groups by dividing the different techniques in *Integral equation approach* (Stolz 1960, Beck 1968), *Integral transform techniques* (Sparrow et al.1964, Rouizi et al. 2013), *Series solution approach* (Burggraf 1964), *Polynomial approach* (MuIholland et al. 1975), *Hyperbolization of the heat conduction equation* (Novikov 1978), *Numerical methods such as finite differences* (D'Souza 1975), *Finite elements* (Hore et al. 1977) *and Boundary elements* (Lesnic et al. 1996), *Space marching techniques together with filtering of the noisy input data, such as in the mollification method* (Murio 1981), *Iterative filtering techniques* (Matsevityi and Multanoviskii 1986), *Steady-state techniques* (Martin and Dulikravich 1998), *Beck's sequential function specification method* (Beck 1962), *Levenberg-Marquardt method for the minimization of the least-square norm* (Levenberg 1944; Marquardt1963), *Tikhonov's regularization approach* (Tikhonov and Arsenin 1977), *Iterative regularization methods for parameter and function estimations* (Alifanov 1974).

In order to evaluate the different IHTP methods it is necessary to refer to different criteria. Beck (1979) suggested a list of possible ones:

- the method should be stable with respect to measurement errors.
- the predicted quantity should be accurate if the measured data are of high accuracy.
- temperature measurements from one or more sensors should be permitted.
- the method should have a statistical basis and permit various statistical assumptions for the measurement errors.
- the method should not require the input data to be *a priori* smoothed.
- the method should be stable for small time steps or intervals permitting to obtain an higher number of information and a better resolution of the time variation respect to those obtainable by large time steps.

- the method should not require continuous first derivatives of unknown functions. Furthermore, this method should allow functions containing significant discontinuities.
- knowledge of the precise starting time of the application of an unknown surface heat flux or source term should not be required. Also precise time at which significant changes in the unknown function occur may also be unknown.
- the method should not be restricted to any fixed number of observations.
- the method should be able to consider complex physical situations, as composite solids, temperature variable properties, moving boundaries, combined modes of heat transfer, multi-dimensional problems and irregular geometries.
- a deep experience in mathematics should not be required in order to use the method.
- the computational cost should be moderate.
- the method should permit extension to more than one unknown.
- the method should be easy to program.

Usually the solution of inverse problem is based on the minimization of an object function. Before analyzing deeply the possible solution strategies it is necessary to make some assumptions regarding the statistical description of errors. Eight assumptions that could allow some simplifications in the analysis of random errors were proposed by Beck (Beck and Arnold 1977; Beck et al. 1985):

- The errors are additive:

$$Y_i = T_i + \varepsilon_i \tag{2.1}$$

where Y_i is the measured temperature, T_i is the exact temperature and ε_i is the random error.

- The temperature errors ε_i have a zero mean:

$$E(\varepsilon_i) = 0 \tag{2.2}$$

where $E(\cdot)$ is the expected value operator. A random error is an error that varies as the measurement is repeated but its mean it's not necessary equal to zero because it could be a bias: so this assumption means that the error is considered unbiased.

- The errors present constant variance:

$$\sigma_i{}^2 = E\{[Y_i - E(Y_i)]^2\} = \sigma^2 = \text{constant} \tag{2.3}$$

- The errors associated with different measurements are not correlated. To find if two different errors ε_i and ε_j $(i \neq j)$ are correlated it is sufficient to calculate the covariance of ε_i and ε_j: if it is zero the two errors are uncorrelated.

$$cov(\varepsilon_i, \varepsilon_j) = E\{[\varepsilon_i - E(\varepsilon_i)][\varepsilon_j - E(\varepsilon_j)]\}=0 \quad (2.4)$$

- The measurement errors have a normal (Gaussian) distribution. Assuming, as valid, the assumptions (2.2), (2.3) and (2.4) the density of probability is expressed as :

$$f(\varepsilon_i) = \frac{1}{\sigma\sqrt{2\pi}} e^{\left(\frac{-\varepsilon_i{}^2}{2\sigma^2}\right)} \quad (2.5)$$

- The statistical parameters that describe the error, such as σ^2, are known
- Time, dimensions, configuration of the problem, thermal property values are errorless that means that the measurements of temperature represent the only source of random errors.
- No prior information about the variables to be estimated are available. If prior information exists, it can be employed to obtain better estimates.

If all the eight statistical assumptions are valid the objective function, O_f, that provides minimum variance estimates is the ordinary least square norm Π defined as (Özisik and Orlande 2000):

$$O_f = \Pi = (\boldsymbol{Y} - \boldsymbol{T})^T(\boldsymbol{Y} - \boldsymbol{T}) \quad (2.6)$$

where **Y** and **T** are, respectively, the vectors that contains measured and estimated temperatures and the superscript ^{T} indicates the transpose of the vector. The estimated temperatures derived from the solution of the direct problems with estimates for the unknown quantities. Let us analyze different cases that can occur:

- Time dependent study where the different measurements Y_i, read at different times $t_i, i = 1,2,3, \dots I$, of a single sensor are used as input values in the inverse heat transfer problem. In this case the transpose vector of the residuals is as follows:

$$(\boldsymbol{Y} - \boldsymbol{T})^T = (Y_1 - T_1,\ Y_2 - T_2, Y_3 - T_3, \dots, Y_I - T_I) \quad (2.7)$$

and the objective function could be expressed as:

$$O_f = (\boldsymbol{Y} - \boldsymbol{T})^T(\boldsymbol{Y} - \boldsymbol{T}) = \sum_{i=1}^{I}(Y_i - T_i)^2 \tag{2.8}$$

An equivalent expression is valid for a steady study with the different measurements Y_n, taken at the same time but at different positions by different sensors $n = 1,2,3 \dots N$:

$$O_f = (\boldsymbol{Y} - \boldsymbol{T})^T(\boldsymbol{Y} - \boldsymbol{T}) = \sum_{n=1}^{N}(Y_n - T_n)^2 \tag{2.9}$$

- A transient analysis performed with multiple sensors. The transpose vector of residuals is as follows:

$$(\boldsymbol{Y} - \boldsymbol{T})^T = \left(\vec{Y}_1 - \vec{T}_1, \vec{Y}_2 - \vec{T}_2, \vec{Y}_3 - \vec{T}_3, \dots, \vec{Y}_I - \vec{T}_I\right) \tag{2.10}$$

where for time t_i, $\left(\vec{Y}_i - \vec{T}_i\right)$ is a vector with a number of element equal to the number of sensor N:

$$\left(\vec{Y}_i - \vec{T}_i\right) = (Y_{i1} - T_{i1}, Y_{i2} - T_{i2}, Y_{i3} - T_{i3}, \dots, Y_{iN} - T_{iN}) \tag{2.11}$$

where the first subscript refers to time step *i* and the second to the sensor number. The objective function therefore could be expressed as:

$$O_f = (\boldsymbol{Y} - \boldsymbol{T})^T(\boldsymbol{Y} - \boldsymbol{T}) = \sum_{n=1}^{N}\sum_{i=1}^{I}(Y_{in} - T_{in})^2 \tag{2.12}$$

If the standard deviation values of the various measurements are not equal, the ordinary least squares method doesn't provide minimum variance estimates. This problem could be overcome by using different approaches. Some of the most important solution techniques are going to be briefly presented below.

Weighted least square norm

In this case the objective function is found by:

$$\Pi_W = (\boldsymbol{Y} - \boldsymbol{T})^T \boldsymbol{W}(\boldsymbol{Y} - \boldsymbol{T}) \tag{2.13}$$

where $\boldsymbol{W}$ is a diagonal weighting matrix that normally is considered as the inverse of the covariance matrix of the measurement errors (always considering the previous statistical assumptions as valid). In case of only one sensor and transient analysis it becomes:

$$\boldsymbol{W} = \begin{bmatrix} 1/{\sigma_1}^2 & 0 & 0 & 0 & 0 \\ 0 & 1/{\sigma_2}^2 & 0 & 0 & 0 \\ 0 & 0 & 1/{\sigma_3}^2 & 0 & 0 \\ 0 & 0 & 0 & \ddots & 0 \\ 0 & 0 & 0 & 0 & 1/{\sigma_I}^2 \end{bmatrix} \tag{2.14}$$

and Π_W in explicit form is as follows:

$$\Pi_W = \sum_{i=1}^{I} \frac{(Y_i - T_i)^2}{{\sigma_i}^2} \tag{2.15}$$

where σ_i is the standard deviation of measurement Y_i at time t_i.
In case of a steady regime study with the different measurements Y_n, taken at the same time but at different positions by different sensors $n = 1,2,3 \dots N$:

$$\Pi_W = \sum_{n=1}^{N} \frac{(Y_n - T_n)^2}{{\sigma_n}^2} \tag{2.16}$$

In case of transient analysis with multiple sensors N:

$$\Pi_W = \sum_{n=1}^{N} \sum_{i=1}^{I} \frac{(Y_{in} - T_{in})^2}{{\sigma_{in}}^2} \tag{2.17}$$

where σ_{in} is the standard deviation of measurement Y_{in} at time t_i of sensor n.
If the IHTP deals with the estimation of a limited number of parameters the use of the least square norm can be stable whereas the number of unknown is elevated the solution may present excursion and oscillation (Özisik and Orlande 2000).

Tikhonov's regularization method

An approach that allows to solve the problem of solution instability, is the Tikhonov's regularization method that add a regularization term to the least square solution. Considering the case of a restoration of a transient function *f(t)* at time $t_i,\ i = 1,2,3, \dots I$ the objective function could be written as:

$$O_f[f(t)] = \sum_{i=1}^{I}(Y_i - T_i)^2 + \lambda^* \sum_{i=1}^{I-d}(\boldsymbol{L_d} f_i)^2 \tag{2.18}$$

where $\lambda^*(> 0)$ is the regularization parameter and $\boldsymbol{L_d}$ is the derivative operator of derivation order d. Often $\boldsymbol{L_d}$ is the zero, first or second derivative operator.

In the zeroth-order regularization and whole domain procedure the objective function is as follows:

$$O_f[f(t)] = \sum_{i=1}^{I}(Y_i - T_i)^2 + \lambda^* \sum_{i=1}^{I} {f_i}^2 \tag{2.19}$$

If $\lambda^* \to 0$ the exact matching between measured and estimated temperatures is obtained, but the sum of the ${f_i}^2$ terms becomes large for small time steps; if λ^* is very large the magnitude of the f_i terms is reduced with the limit being $f_i = 0$. That means that the effect of $\lambda^* \neq 0$ is to reduce the magnitude of the f_i values.

In the whole domain first-order regularization procedure the objective function can be written as follows:

$$O_f[f(t)] = \sum_{i=1}^{I}(Y_i - T_i)^2 + \lambda^* \sum_{i=1}^{I-1}(f_{i+1} - f_i)^2 \tag{2.20}$$

Also in this case if $\lambda^* \to 0$, exact matching is reached but the inverse problem solution becomes unstable. Large λ^* values (any positive or negative value) cause f_i to be constant. Thus the magnitude of the f_i terms is not affected and for the values of $\lambda^* \neq 0$ the differences in the f_i terms are reduced.

Finally in the whole domain second order regularization procedure the objective function is:

$$O_f[f(t)] = \sum_{i=1}^{I}(Y_i - T_i)^2 + \lambda^* \sum_{i=1}^{I-2}(f_{i+2} - 2\, f_{i+1} + f_i)^2 \tag{2.21}$$

Again if $\lambda^* \to 0$, the exact matching of the temperatures is obtained whereas high λ^* values cause f_i to be a straight line. Therefore moderate values of λ^* reduce the rate of change of $f_i(t)$.

Resuming the zeroth order reduces the magnitude of f_i, the first order reduces the magnitude of changes in the f_i and the second order regularization term tends to reduce rapid oscillations in the f_i. Therefore the stability of the solution is strongly influenced by the choice of the regularization parameter: if it is too small there will be a good fitting between the measured and the estimated

temperatures but the solutions could present oscillations and instabilities; large regularisation parameter means that imposing too much regularisation on the solution prejudices the fitting of the data and the ability to obtain a great residual (Beck et al. 1985).

The importance of the choice of the regularisation parameter has been widely analysed in the literature. For a survey of the Tikhonov parameter choice rules the reader is referred to Hansen (1998). The Tikhonov regularization method could be related to damped least square methods, such the Levenberg-Marquardt method.

Levenberg-Marquardt method

This technique is a powerful iterative technique that have been applied to the solution of many inverse problems (Özisik and Orlande 2000). This method was firstly derived by Levenberg (1944) by modifying the ordinary least square norm and later also by Marquardt (1963) by using a different approach. The solution of a general inverse heat transfer problem concerning the estimation of N unknown parameters $P_j, j = 1,2,3 \dots, N$ at different time t_i, $i = 1,2,3, \dots I$, is based on the minimization of the ordinary least square norm Π:

$$\Pi(\boldsymbol{P}) = [\boldsymbol{Y} - \boldsymbol{T}(\boldsymbol{P})]^T [\boldsymbol{Y} - \boldsymbol{T}(\boldsymbol{P})] = \sum_{j=1}^{N} \left(Y_j - T_j(\boldsymbol{P})\right)^2 \tag{2.22}$$

where **P** is the vector of unknown parameters. To minimize it, it is necessary to have the derivatives of $\Pi(\boldsymbol{P})$ equal to zero:

$$\nabla\Pi(\boldsymbol{P}) = 2\left[-\frac{\partial \boldsymbol{T}^T(\boldsymbol{P})}{\partial \boldsymbol{P}}\right][\boldsymbol{Y} - \boldsymbol{T}(\boldsymbol{P})] = 0 \tag{2.23}$$

The transpose of the term $\frac{\partial \boldsymbol{T}^T(\boldsymbol{P})}{\partial \boldsymbol{P}}$ is the sensitivity matrix $\boldsymbol{J}(\boldsymbol{P})$:

$$\boldsymbol{J}(\boldsymbol{P}) = \left[\frac{\partial \boldsymbol{T}^T(\boldsymbol{P})}{\partial \boldsymbol{P}}\right]^T = \begin{bmatrix} \frac{\partial T_1}{\partial P_1} & \frac{\partial T_1}{\partial P_2} & \frac{\partial T_1}{\partial P_3} & \dots & \frac{\partial T_1}{\partial P_N} \\ \frac{\partial T_2}{\partial P_1} & \frac{\partial T_2}{\partial P_2} & \frac{\partial T_2}{\partial P_3} & \dots & \frac{\partial T_2}{\partial P_N} \\ \frac{\partial T_3}{\partial P_1} & \frac{\partial T_3}{\partial P_2} & \frac{\partial T_3}{\partial P_3} & \dots & \frac{\partial T_3}{\partial P_N} \\ \vdots & \vdots & \vdots & \dots & 0 \\ \frac{\partial T_I}{\partial P_1} & \frac{\partial T_I}{\partial P_2} & \frac{\partial T_I}{\partial P_3} & \dots & \frac{\partial T_I}{\partial P_N} \end{bmatrix} \tag{2.24}$$

The elements of the sensitivity matrix are called sensitivity coefficients $J_{i,j}$ and represent the first derivative of the estimated temperature at time t_i, with respect to the unknown parameter P_j.
The equation (2.23) therefore can be written as:

$$-2\,\boldsymbol{J}^T(\boldsymbol{P})[\boldsymbol{Y}-\boldsymbol{T}(\boldsymbol{P})]=0 \tag{2.25}$$

If the inverse problem is linear the sensitivity matrix is not a function of the unknown parameters and thus equation (2.25), according to Beck and Arnold (1977), can be solved in explicit form for the vector of the unknown parameters $\boldsymbol{P}$:

$$\boldsymbol{P}=(\boldsymbol{J}^T\boldsymbol{J})^{-1}\boldsymbol{J}^T\boldsymbol{Y} \tag{2.26}$$

The situation is more complicated in case of non linear problems where the sensitivity matrix depends on the unknown parameters vector. It was then elaborated an iterative procedure obtained by linearizing the vector of estimated temperature $\boldsymbol{T}(\boldsymbol{P})$, with a Taylor series expansion around the current solution $\boldsymbol{P^k}$ at iteration k:

$$\boldsymbol{T}(\boldsymbol{P})=\boldsymbol{T}(\boldsymbol{P}^k)+\boldsymbol{J}^k(\boldsymbol{P}-\boldsymbol{P}^k) \tag{2.27}$$

Substituting it in equation (2.25) and rearranging the resulting expression according to Beck and Arnold (1977) it is possible to obtain the iterative procedure to estimate the vector of unknown parameters $\boldsymbol{P}$:

$$\boldsymbol{P}^{k+1}=\boldsymbol{P}^k+[(\boldsymbol{J}^k)^T\boldsymbol{J}^k]^{-1}(\boldsymbol{J}^k)^T[\boldsymbol{Y}-\boldsymbol{T}(\boldsymbol{P}^k)] \tag{2.28}$$

Actually the iterative procedure based on this equation is named Gauss method. Due to the ill-posed nature of the inverse problems, oscillations in the solution can occur. A possible solution was proposed by Levenberg and Marquardt by adding a damping term to expression (2.28) in order to reduce the instabilities in the solution caused by the ill-posed nature of the inverse problems:

$$\boldsymbol{P}^{k+1}=\boldsymbol{P}^k+\left[(\boldsymbol{J}^k)^T\boldsymbol{J}^k+\zeta^k\boldsymbol{\Omega}^{\mathrm{k}}\right]^{-1}(\boldsymbol{J}^k)^T[\boldsymbol{Y}-\boldsymbol{T}(\boldsymbol{P}^k)] \tag{2.29}$$

Where ζ^k is a positive scalar called damping parameter and Ω^{k} is a diagonal matrix, often expressed as $diag[(\boldsymbol{J}^k)^T\boldsymbol{J}^k]^{-1}$ but that could be formalized also in other way: in fact different versions of Levenberg-Marquardt method are present in literature depending on the form of the diagonal matrix $\boldsymbol{\Omega}^{\mathrm{k}}$ and of the criterion of variation of the damping parameter ζ^k. After computing the sensitivity matrix $\boldsymbol{J}^k$, defining the diagonal matrix $\boldsymbol{\Omega}^{\mathrm{k}}$ and the form of variation of the damping parameter ζ^k the iterative procedure expressed by equation (2.29) can be implemented until a stopping criterion. Among the most used stopping criteria for this technique are the following:

$$\Pi(\boldsymbol{P}^{k+1}) < \varepsilon_1 \tag{2.30}$$

$$\|(\boldsymbol{J}^k)^T[\boldsymbol{Y} - \boldsymbol{T}(\boldsymbol{P}^k)]\|_2 < \varepsilon_2 \tag{2.31}$$

$$\|\boldsymbol{P}^{k+1} - \boldsymbol{P}^k\|_2 < \varepsilon_3 \tag{2.32}$$

where ε_1, ε_2 and ε_3, are user prescribed tolerances and $\|\cdot\|_2$ is the vector Euclidean norm.

Conjugate Gradient method

Another method that can be classified as an iterative regularization technique is the Conjugate Gradient method: it is used both for solving linear and non linear problems. In this iterative procedure at each iteration a suitable step size is considered along the descent direction in order to minimize the objective function. The descent direction is obtained as a linear combination of the negative gradient direction at the current iteration with the direction of descent of the previous iteration (Özisik and Orlande 2000). The iterative procedure of the Conjugate Gradient method for the solution of a general inverse heat transfer problem concerning the estimation of *N* unknown parameters $P_j, j = 1,2,3 \ldots, N$, based on the minimization of the ordinary least square norm $\Pi(\boldsymbol{P})$ is written as follows:

$$\boldsymbol{P}^{k+1} = \boldsymbol{P}^k - \xi^k \boldsymbol{d}^k \tag{2.33}$$

where ξ^k is the search step size at iteration k and $\boldsymbol{d}^k$ is the direction of descent.
The direction of descent can be expressed as follows:

$$\begin{aligned} \boldsymbol{d}^0 &= \nabla\Pi(\boldsymbol{P}^0) \\ \boldsymbol{d}^k &= \nabla\Pi(\boldsymbol{P}^k) + \gamma^k \boldsymbol{d}^{k-1} \end{aligned} \tag{2.34}$$

Different version of CGM can be found in literature depending on how the conjugation coefficient γ^k is computed. For instance in the Polak-Ribiere version it is computed as:

$$\gamma^0 = 0 \qquad k = 0$$

$$\gamma^k = \frac{\sum_{j=1}^{N}\left\{[\nabla\Pi(\boldsymbol{P}^k)]_j[\nabla\Pi(\boldsymbol{P}^k) - \nabla\Pi(\boldsymbol{P}^{k-1})]_j\right\}}{\sum_{j=1}^{N}[\nabla\Pi(\boldsymbol{P}^{k-1})]_j^2} \qquad k = 1,2,\ldots \tag{2.35}$$

while in the Fletcher-Reeves it is written as:

$$\gamma^0 = 0 \qquad k = 0$$

$$\gamma^k = \frac{\sum_{j=1}^{N}[\nabla\Pi(\boldsymbol{P}^k)]_j^2}{\sum_{j=1}^{N}[\nabla\Pi(\boldsymbol{P}^{k-1})]_j^2} \qquad k = 1,2,\ldots \tag{2.36}$$

It remains only to determine the search step size ξ^k: it is found by minimizing the ordinary least square norm $\Pi(\boldsymbol{P}^{k+1})$ at (k+1) iteration with respect to the search step size ξ^k at k iteration.

$$\min_{\xi^k}\Pi(\boldsymbol{P}^{k+1}) = \min_{\xi^k}[\boldsymbol{Y} - \boldsymbol{T}(\boldsymbol{P}^{k+1})]^T[\boldsymbol{Y} - \boldsymbol{T}(\boldsymbol{P}^{k+1})] \tag{2.37}$$

By substituting equation (2.33) in (2.37):

$$\min_{\xi^k}\Pi(\boldsymbol{P}^{k+1}) = \min_{\xi^k}[\boldsymbol{Y} - \boldsymbol{T}(\boldsymbol{P}^k - \xi^k\boldsymbol{d}^k)]^T[\boldsymbol{Y} - \boldsymbol{T}(\boldsymbol{P}^k - \xi^k\boldsymbol{d}^k)] \tag{2.38}$$

By following a standard approach (Bozzoli and Rainieri 2011; Huang et al. 2005) the temperature vector $\boldsymbol{T}(\boldsymbol{P}^k - \xi^k\boldsymbol{d}^k)$ can be linearized with Taylor series expansion. Rearranging and considering the sensitivity matrix $\boldsymbol{J^k}$, the search step size ξ^k can be written as:

$$\xi^k = \frac{\left[\boldsymbol{J^k}\boldsymbol{d}^k\right]^T[\boldsymbol{T}(\boldsymbol{P}^k) - \boldsymbol{Y}]}{[\boldsymbol{J^k}\boldsymbol{d}^k]^T[\boldsymbol{J^k}\boldsymbol{d}^k]} \tag{2.39}$$

After calculating the gradient direction $\nabla\Pi(\boldsymbol{P}^k)$, the sensitivity matrix $\boldsymbol{J^k}$, the conjugation coefficient γ^k and the search step size ξ^k, the iterative procedure expressed by equation (2.33) can be implemented until a stopping criterion: one of the most used stopping criteria for this procedure is the discrepancy principle that states that the inverse problem solution is regarded to be sufficiently accurate when the difference between the estimated and the measured temperatures is

close to the standard deviation of the measurements (Morozov 1984). An adequate choice of the stopping criterion permits to reduce the oscillations that could appear in the inverse problem solution due to its ill-posed nature.

Filtering Technique

Another solution approach that can be regarded as a regularization method is the filtering technique since it is based on computing the smoothest approximated solution consistent with available data (Orlande et al. 2011).

In fact the possibility of treating the raw input temperature data by some suitable filtering technique represents a competitive and challenging approach to handle the ill-posed nature of the IHCP, and in particular the instability of the system response with respect to random errors in the input data.

The filter permits a complete or partial suppression of the frequency components of the signal.

In real measurements the experimental errors usually are present as Gaussian noise with spectral components distributed uniformly over the entire frequency domain, while the important information is usually bandlimited, with frequency components concentrated in the low frequency range of the spectrum. A fundamental issue in the application of filter is to define how many frequencies to cut in order to overcome the ill-posed nature of the inverse problem but not to loose too much information from the signal.

Among the most used filtering techniques ideal low-pass filter is found. It passes low frequency but remove's the signal components with frequency higher than a determined cutoff frequency: its choice is really important to optimize the effect of the filter. Another common used filtering technique is the Gaussian filter whose impulse response is a Gaussian function. Since the Fourier transform of a Gaussian is again a Gaussian function, it has the effect of reducing the data high frequency components (Bozzoli et al. 2013). It's often used in enhancing the quality of images in graphic softwares. Another filter that has proved to be efficient to remove the undesired noise from experimental temperature is the Wiener filter. The success of this approach is due to the fact that the Wiener filter tailors itself to the local noise level in the signal and it performs then a better smoothing in comparison to other filtering techniques: it uses a pixel-wise adaptive filtering procedure based on statistics estimated from a local neighborhood of each data point (Rainieri et al 2004).

It is important to observe that the filtering approach to IHCPs can be considered suitable only for input signals represented by spatially and/or temporally highly resolved temperature maps, while it appears not practicable for signals represented by a limited number of input variables.

On the other hand the great advantage of the filter techniques (among the three cited above, low pass filter and Gaussian filter are particularly advantageous) is the very small computational cost compared to the other solution techniques.

TSVD: Truncated Singular Value Decomposition

The Truncated Singular Value Decomposition (TSVD) has been proved to be very powerful as regularization method of ill-posed linear least square problems (Hansen 1986).

The Singular Value Decomposition (SVD) of a matrix A (*m x n),* permits to decompose it into the three matrices U, $\mathbf{\Sigma}$ and V:

$$\mathbf{A} = \mathrm{U} \cdot \mathbf{\Sigma} \cdot \mathrm{V}^{*T} \tag{2.40}$$

Where $\mathbf{\Sigma}$ is a diagonal matrix of dimension *m x n*, the left and the right singular matrices U and V are orthogonal and of dimension *m x m* and *n x n* respectively and the superscript ^{*T} stands for the conjugate transpose of the matrix.

$$\mathbf{\Sigma} = \mathrm{diag}(\delta_1, \delta_2, \ldots \ldots \delta_n) \tag{2.41}$$

The elements δ_i of the diagonal are the singular values and are positioned in a decreasing order. The purpose of the TSVD is to force the solution to have a small norm in order to damp the contributions from the errors of the right-hand side (Hansen 1986). This is obtained by the truncation (neglection) of the solution components that correspond to the smallest singular values because they bring the largest contribution to the noise amplification in the inversion of the matrix.

Therefore the TSVD of **A** becomes:

$$\mathbf{A_t} = \mathrm{U} \cdot \mathbf{\Sigma_t} \cdot \mathrm{V}^{*T} \qquad \text{with} \quad \mathbf{\Sigma_t} = \mathrm{diag}\left(\delta_1, \delta_2, \ldots \delta_{t_p - 1}, 0, \ldots 0\right) \tag{2.42}$$

where t_p is named truncation parameter.

As said above the TSVD is used as regularization method for linear ill-posed problems: linear problems could be treated using both numerical methods as finite differences, finite elements or boundary elements and analytical methods.

Quadrupole

Among the above mentioned techniques a very effective analytical explicit method of representation of linear systems is the Quadrupole method: it can be applied to a large number of classes of linear systems and it is often used in IHCP solutions.

There are different versions of this technique, changing from the type of problem of interest but there is anyway a common based methodology. In its simpler version in heat conduction its core are 2 X 2 matrices that put in relation some transform of both temperature and heat flux on one surface of the body under analysis to the same quantities on another surface (Maillet et al. 2000). The transformation could be both in Fourier and Laplace space or a combination of the two transforms. One of its main interests is to get analytical solutions in the transformed domain.

Basically, being an analytical method, it is restricted to linear systems with simple geometries but with some assumptions these limits can be alleviated and more complicated geometries can be studied and also non-linear problems could be treated if time remains untrasformed.

In order to better comprehend how to implement this method the simple case of a medium made of a single homogeneous material is considered: it is limited by a closed surface of area S and receives heat (q_1) from outside through a portion of the surface S_1 and releases it (q_2) through another portion S_2. Considering the average temperatures T_1 and T_2 over the two portion S_1 and S_2 it is possible to write the following equations:

$$T_1 - T_2 = R_t q_1 \tag{2.43}$$

$$q_1 = q_2 \tag{2.44}$$

where R_t is the thermal resistance between S_1 and S_2.

These two equations can be easily represented following the Quadrupole formulation as:

$$\begin{bmatrix} T_1 \\ q_1 \end{bmatrix} = \begin{bmatrix} 1 & R_t \\ 0 & 1 \end{bmatrix} \begin{bmatrix} T_2 \\ q_2 \end{bmatrix} \tag{2.45}$$

2.1 INVERSE HEAT CONDUCTION PROBLEM (IHCP) IN PIPES

In order to investigate heat transfer apparatuses, it is fundamental to determine what happens on internal surfaces in terms of local surface temperatures and heat fluxes. However, it is usually infeasible to measure these quantities placing probes on the desired surface due to the size of the probes and the apparatus, the geometric inaccessibility of the surface, or because of exposure to a

hostile environment that may destroy the sensors. A successful solution to this problem can be found by monitoring the external wall surface temperature distribution and solving an Inverse Heat Conduction Problem (IHCP) to determine the unknown quantities at the internal surface.

Among the numerous possible applications of this approach, the estimation of the temperature, the heat flux, or the convective heat transfer coefficient distributions on the internal wall of a duct, using only the external wall temperature distribution, is very appealing. This application is particularly attractive because it can be employed both in the industrial applications to monitor productive processes and in the research field to investigate the heat transfer mechanisms.

Let's consider the section of a generic pipe represented in figure 2.1.

In the solid domain the energy balance equation is expressed as:

$$\rho c_p \frac{DT}{Dt} = \text{div}\,(\lambda \nabla T) + q_g \tag{2.46}$$

In case of a steady problem the term that concerns the temperature variation with time disappears. Although the solution of a steady inverse heat conduction problem could be considered as a special case of the unsteady IHCP, some care is needed in the application of standard inverse solution strategies to the steady IHCP. In fact, in the steady formulation, the negative effect of the noise is amplified by the necessity of estimating the desired information from the Laplacian of the signal and not from the first temporal derivative of the signal, as it often happens in the classical formulation of the unsteady inverse heat conduction problem (Bozzoli and Rainieri 2011).

The energy balance equation is completed by the boundary conditions on surfaces S_1 and S_2. Two common boundary conditions that are present in this type of problem are:

$$-\lambda \frac{\partial T}{\partial n}\Big|_s = -h[T(x,y,z,t) - T_\infty(t)] \tag{2.47}$$

$$-\lambda \frac{\partial T}{\partial n}\Big|_s = q(x,y,z,t) \tag{2.48}$$

where q is the local convective heat flux at the wall interface, assumed to be positive as it enters in the wall.

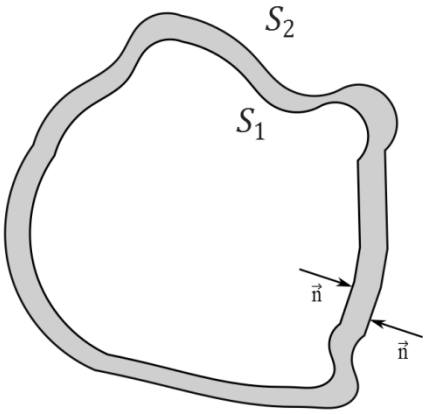

Figure 2.1: Sketch of the section of a generic pipe.

In the presence of the boundary condition reported in equation (2.47) the inverse heat conduction problem is non-linear whereas in the presence of the boundary condition shown in equation (2.48) the IHCP is linear permitting to strongly reduce the computational cost by eliminating the use of iteration. The boundary conditions could be also of different type. Some significant examples of IHCP application in pipes are reported below.

Lu et al. (2010) implemented an estimation approach based on the IHCP solution, using the conjugate gradient method, to estimate the unknown transient fluid temperatures near the inner wall in section of a pipe elbow with thermal stratification. Pseudo experimental input temperatures were considered: the temperatures obtained from the solution of the two-dimensional direct heat conduction problem using the finite element method, in fact, were employed as input data on the outer wall for the inverse heat conduction problem.

Then from the IHCP solution the fluid temperatures near the inner wall were estimated: in order to evaluate the effectiveness of the approach they were compared with the experimental fluid temperatures. The results obtained showed that the fluid temperatures near the inner wall could be estimated with accuracy.

To more deeply investigate the phenomenon and better estimate the fluctuations of the inner wall temperatures caused by the movement of the interface between the two fluids in an elbow used for mixing hot and cold fluids, the same authors (Lu et al. 2011) performed a similar study but this time solving three-dimensional problem. Again the solution approach was based on conjugate gradient method using as input data in the inverse problem the outer wall temperatures obtained from the direct problem.

Su and Hewitt (2004) estimated the time-dependent heat transfer coefficient of forced convective flow boiling over the outer surface of a heater tube solving an inverse heat conduction problem

based on Alifanov's iterative regularization method. As input data, the temperatures measured on the inner wall of the circular tube on which the flow boiling occurs, were employed. The conjugate gradient method was used to minimize a square residual functional, a sensitivity problem was solved to determine the step size in the descent direction and an adjoint problem to find the gradient of the functional.

Taler (2007) employed two different inverse solution techniques to estimate the local heat transfer coefficient on the circumference of a vertical smooth tube placed in a tube bundle with a staggered tube arrangement, starting from temperature measurements at some interior points in the body. The authors used both the Levenberg-Marquardt method and the singular value decomposition to minimize the least square norm between the measured and the computed temperatures obtaining good agreement between the results.

Mokrani et al. (2009) carried out a study to investigate the design, the construction and the instrumentation of an experimental microchannel. To analyze the wall thermal conditions inside the microchannel, being impossible to measured it directly, their estimation was performed by the solution of an inverse heat conduction in the wall based on the Gauss–Newton minimization algorithm. It compares the temperatures measured experimentally and those estimated numerically at the same positions by imposing a given convective heat transfer coefficient.

Rouizi et al. (2013) employed the Quadrupole method to retrieve the temperature and flux distributions over the internal surface of a micro-channel using temperature profiles measured at the external surface. As first step in inverse solution approach the Authors estimated mean velocity and the external heat transfer coefficient; after that the internal walls temperatures and the corresponding wall fluxes, using Fourier integral transforms of both temperatures and normal fluxes in the direction of the flow, were found starting from the external wall temperatures distributions and the external heat transfer coefficient before estimated. Then, thanks to a balance energy equation written in the Fourier domain, also the bulk temperature distribution of the flow was determined. Due to the ill-posed nature of inverse problems a small noise in the external wall temperature could bring to very significant errors in the estimated internal wall heat flux distribution. To overcome this problem, as regularization technique, the Truncated Singular Value Decomposition of the matrix linking the external temperature to the internal flux was used.

3. TUBES GEOMETRY AND EXPERIMENTAL SETUP

3.1 TUBES GEOMETRY

In the present work, both smooth and corrugated wall helically coiled stainless steel type AISI 304 tubes were tested. They were characterized by 8 coils following an helical profile along the tube's axis preceded and followed by a straight section as shown in figure 3.1.

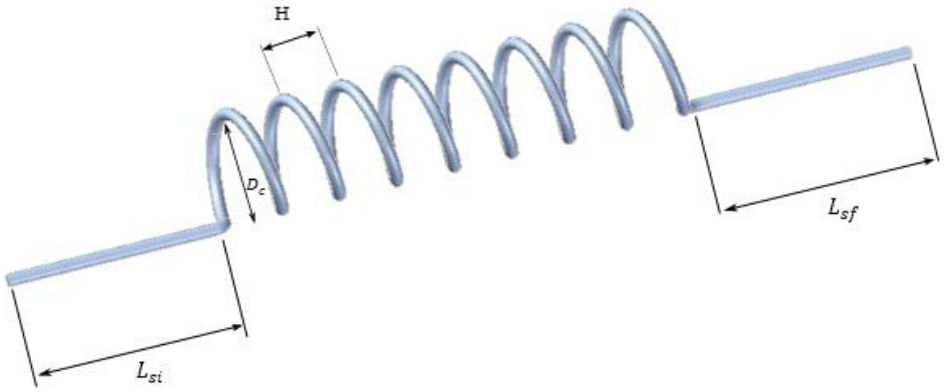

Figure 3.1: A sketch of the coiled tube configuration considered in the investigation.

The parameters used to describe the coiled pipes under test were:

1. The coil diameter D_c;
2. The Helix pitch H;
3. The length of the coiled section L_c;
4. The length of the initial straight section L_{si};
5. The length of the final straight section L_{sf};
6. The wall thickness s;
7. The internal pipe diameter D_{int}. For the corrugated wall tubes it was considered the envelope tube diameter D_{env} (for instance see figures 1.11 and 3.2).
8. The curvature ratio $\delta_c = r_p/r_c$;
9. The corrugation depth e;
10. The corrugation pitch l;

In this study three different curvature ratio values were considered, i.e. $\delta_c \cong 0.03$, 0.045 and 0.06 with helix pitch H varying between 0.1 and 0.2 m, yielding coiled section's length L in the range 5.8÷11m. The wall corrugated tubes considered in the present investigation are included in the general category usually known as spirally enhanced tubes, exemplified in figure 3.2. They present

an internal helical ridging corresponding to an external helical grooving, obtained by embossing a smooth stainless steel tube. The tubes have a wall thickness of 1 mm and an internal envelope diameter of 14 mm, while the corrugation profile have a depth *e* of 1 mm and a pitch *l* of 16 mm.

a) b)

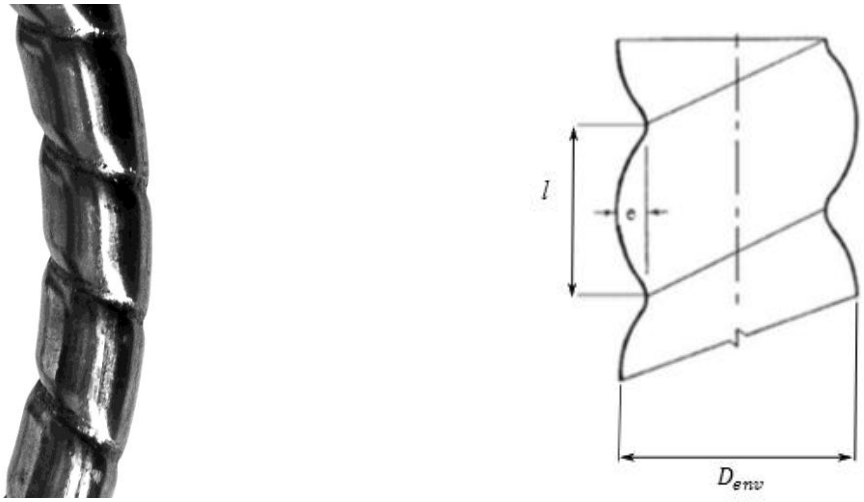

Figure 3.2: a) The corrugated wall coiled tube under test; b) Wall corrugation profile parameters.

In the present investigation six pipes, whose main geometrical parameters are summarized in tables 3.1 and 3.2, were tested. In this study the Acronyms HCW, HSW, SCW and SSW are used to refer to helically coiled tube with corrugated wall, helically coiled tube with smooth wall, straight tube with corrugated wall and straight tube with smooth wall, respectively. The values of helix pitch and coil diameter reported in tables 3.1 and 3.2 are average values.

Smooth wall helically coiled tubes

Name	D_{int} **[mm]**	s **[mm]**	D_c **[m]**	δ_c	**H [m]**	L_{si} **[m]**	L_c **[m]**	L_{sf} **[m]**
HSW060	14	1	0.237	0.059	0.103	0.66	5.88	1.65
HSW045	14	1	0.306	0.046	0.205	0.6	7.86	0.84
HSW030	14	1	0.427	0.033	0.194	0.6	10.88	0.81

Table 3.1: Geometrical parameters for smooth wall helically coiled tubes under test.

Corrugated wall helically coiled tubes

Name	D_{env} [mm]	s [mm]	D_c [m]	δ_c	H [m]	L_{si} [m]	L_c [m]	L_{sf} [m]	e [mm]	l [mm]
HCW060	14	1	0.240	0.058	0.097	0.6	6.10	1.54	1	16
HCW045	14	1	0.328	0.043	0.190	0.6	8.40	0.81	1	16
HCW030	14	1	0.430	0.033	0.182	0.6	10.92	0.83	1	16

Table 3.2: Geometrical parameters for corrugated wall helically coiled tubes under test.

Two representative figures of both the smooth wall helically coiled tubes and corrugated wall helically coiled tubes under test, are reported below.

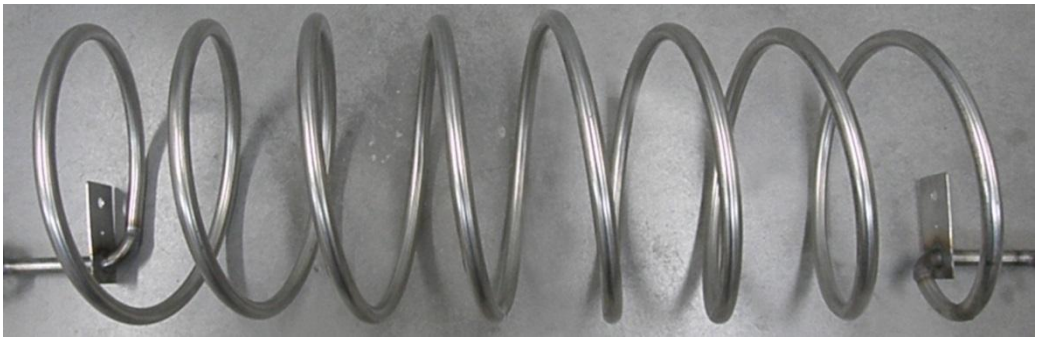

Figure 3.3: A representative smooth wall helically coiled tube under test.

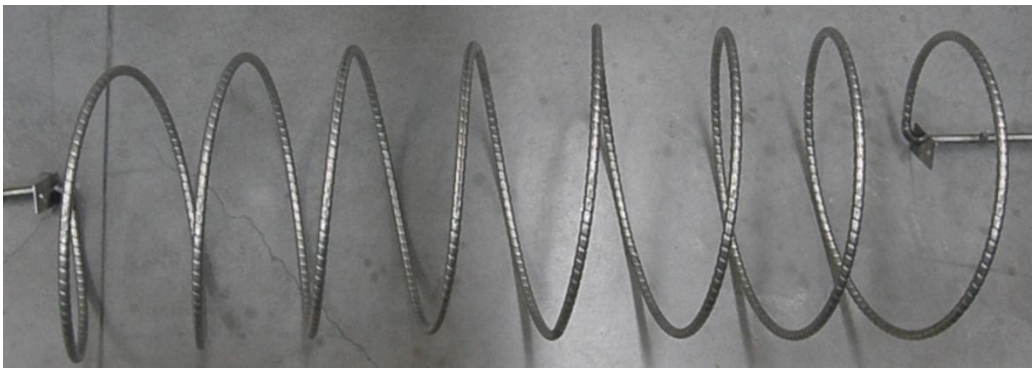

Figure 3.4: A representative corrugated wall helically coiled tube under test.

3.2 EXPERIMENTAL SETUP

The experimental apparatus, essentially composed by an hydraulic circuit coupled with an acquisition data system, was made available by the laboratory of the Industrial Engineering Department of the University of Parma.

The test sections were inserted horizontally in the loop schematically shown in figure 3.5.

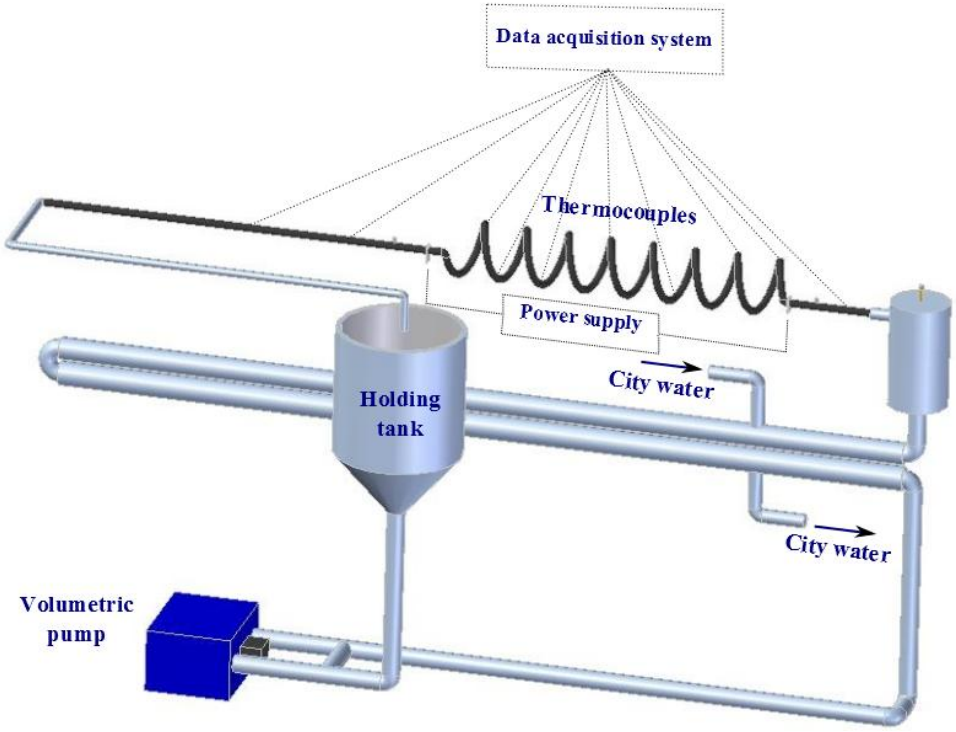

Figure 3.5: Schematic drawing of the experimental apparatus.

The fluid flowing within the circuit was heated and later cooled in order to keep the working fluid temperature constant at the inlet tube's section. The heating was performed by Joule effect in the wall while the cooling by a secondary heat exchanger, fed with city water.

Following the fluid path inside the apparatus, the principal elements of the plant are hereby described by analyzing the more important characteristics of each device.

The first component is an holding tank of 30 liters capacity and made of stainless steel: it receives the fluid coming from the heated section.

The working fluid contained in the tank is conveyed by a volumetric pump to a shell and tube counter current heat exchanger.

The pump used in this apparatus is a volumetric pump made by CSF (model A1 246300 JABSCO series). It is regulated by a mechanical reducer made by Motovario S.p.a (type TKR-10) that works in the range 40-200 rpm.

This type of pump guarantees an high stability of the flowrate value. The maximum flowrate value is determined by the characteristics of the coupling pump-mechanical reducer and it varied between 60 and 200 l/h while a secondary recirculation circuit activated through a manually operated valve permits to reduce the flowrate to values lower than 60 l/h.

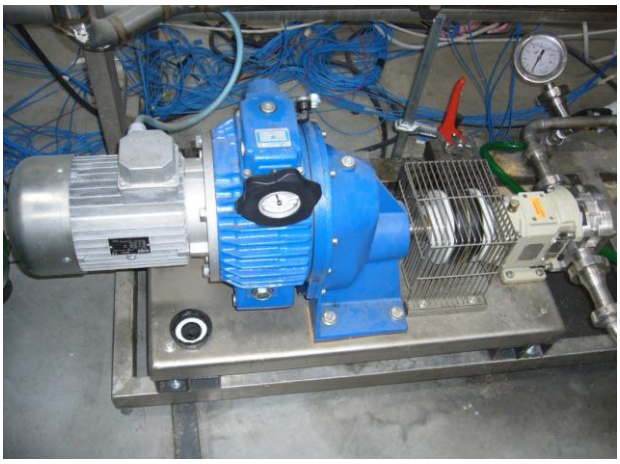

Figure 3.6: The mechanical reducer and the volumetric pump.

Figure 3.7: The recirculation circuit.

The fluid is then conveyed to the secondary heat exchanger that is fed with city water. Downstream the heat exchanger a calming section was installed in order to eliminate entrance effect. On the top of the tank a small vent valve permitted to eliminate the air that accidentally entered the circuit. The tube under test is positioned after the calming section and it is fixed to the structure by a Teflon junction: the use of a nonmetallic junction is due to the necessity to electrically insulate the rest of the circuit from the pipe. The helical section of the tube is heated, completely or just a portion by dissipating, by the Joule effect the electric current delivered by a power supply within the wall itself. This device is a model HP 6671A and it works in the range 0-8 V and 0-220 A. It is connected to the tube by means of electric cables coupled with stainless steel fins of 1 mm thickness directly welded to the tube. This setup allowed investigating the heat transfer performance of the tubes under the prescribed condition of heat generated by Joule effect in the wall. It must be noted that only if the axial and peripheral heat conduction effects within the wall can be considered negligible, the Joulean heating condition well approximates the thermal boundary condition of uniform wall heat flux at the fluid wall interface. Being wall thermal conductivity relatively low and being the wall thin, the axial heat conduction effects could be considered negligible. Regarding the peripheral heat conduction effects within the wall instead, they could be considered negligible in straight tubes, while they couldn’t be overlooked in coiled pipes, due to the secondary flow pattern. From the value of the heat power dissipated by Joule effect into the wall, the circumferentially

averaged values of the wall heat flux was derived, while for estimating its distribution along the wall periphery a different approach was needed.

Figure 3.8: Counter current heat exchanger.

The whole length of the heat transfer section was thermally insulated to minimize the heat transfer to the environment: the insulation was achieved by two layers of cellular rubber having a thickness of 9 mm and 32 mm respectively. Both the wall and the inlet and outlet fluid temperature were measured through type T thermocouples, previously calibrated and connected to a multichannel ice point reference, type KAYE K170-50C.

Regarding the wall temperature, the sensors were attached at different circumferential locations to the external tube's surface and at different axial locations along the heated section. In particular, the thermocouples were placed along the external and internal side of the coil in order to investigate the distortion over the cross section induced by the centrifugal force to the velocity and then to the temperature profile. Regarding the corrugated wall tubes the temperature probes were placed externally on the crest of the corrugation at different circumferential locations.

The inlet temperature was measured by a thermocouple probe placed on the tube's wall upstream the starting heating section. The bulk temperature at any location in the heat transfer section was calculated from the power supplied to the tube, assumed distributed uniformly per unit length over the heat transfer surface area, decreased by the heat losses through the insulation, while the outlet temperature was checked also by placing a thermocouple at the end of the heated section. The heat losses towards the environment were estimated in a preliminary calibration of the apparatus aimed to measure the overall thermal resistance between the internal tube wall and the environment. This procedure was performed as follows: in absence of fluid circulation, a known power rate was supplied to the tube wall and the wall to ambient temperature difference was measured. The value 6 m·K/W was found for the overall thermal resistance that yielded heat losses of about 1% of the supplied power. The signal coming from the ice point reference is read by high precision multimeter

(type HP 3458A) connected to a switch control unit (type HP 3488A) driven by a Personal Computer. The communication and the interaction with the temperature devices was realized by the commercial software Labview: an user friendly interface permits to activate or deactivate the different channels of acquisition data, each corresponding to a thermocouple, and to follow the temperature trend of each device both on a table and on a plot, both reported in figures 3.9.

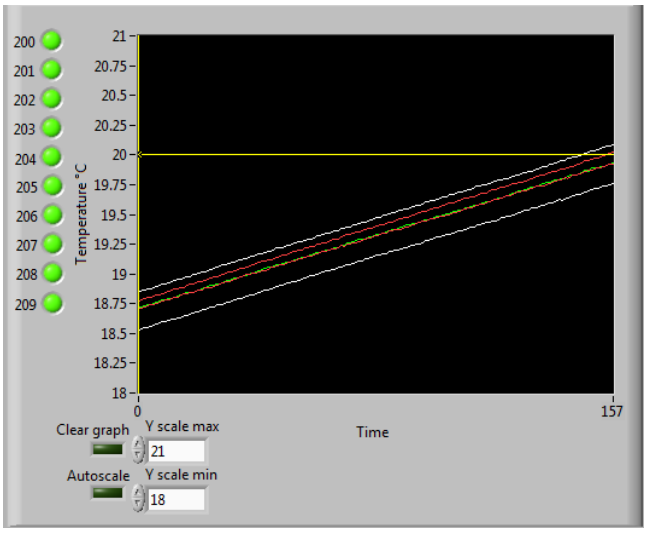

Cycle	Time, s	100	101	5
153	141	20.042602	19.976957	1
154	142	20.051237	19.984861	1
155	143	20.063897	19.997962	1
156	144	20.069641	20.007146	1
157	145	20.077690	20.009122	1

Figure 3.9: Particulars of the Labview interface.

For the tests performed to estimate the local Nusselt number along the cross section a small portion of the external tube wall was made accessible to a thermal imaging camera by removing the thermally insulating layer, and the wall portion was coated with a thin film of high emissivity paint.

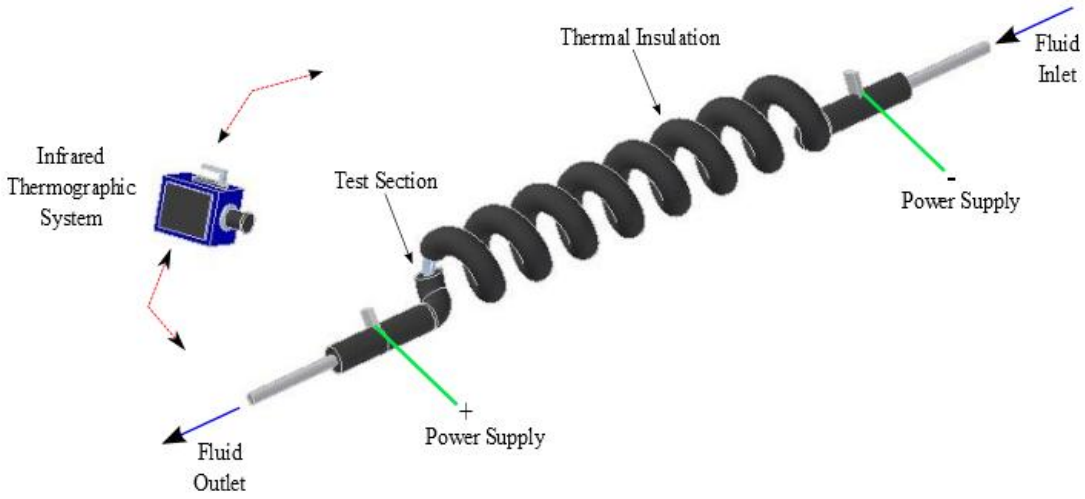

Figure 3.10: Sketch of experimental setup.

The surface temperature distribution was acquired by means of a FLIR SC7000 unit, with a 640 x 512 pixel detector array. Its thermal sensitivity, as reported by the instrument manufacturer, is 20 mK at 303 K, while its accuracy is ±1 K. A sketch of the experimental setup is reported in figure 3.10, and figure 3.11 shows the laboratory facility.

To measure the temperature distribution on the whole heat-transfer test section surface, multiples images were acquired, moving the infrared camera around the section. When using an infrared scanner, care should be taken while performing measurements if the scanned surface is not locally normal to the viewed rays due to directional emissivity of the surface.

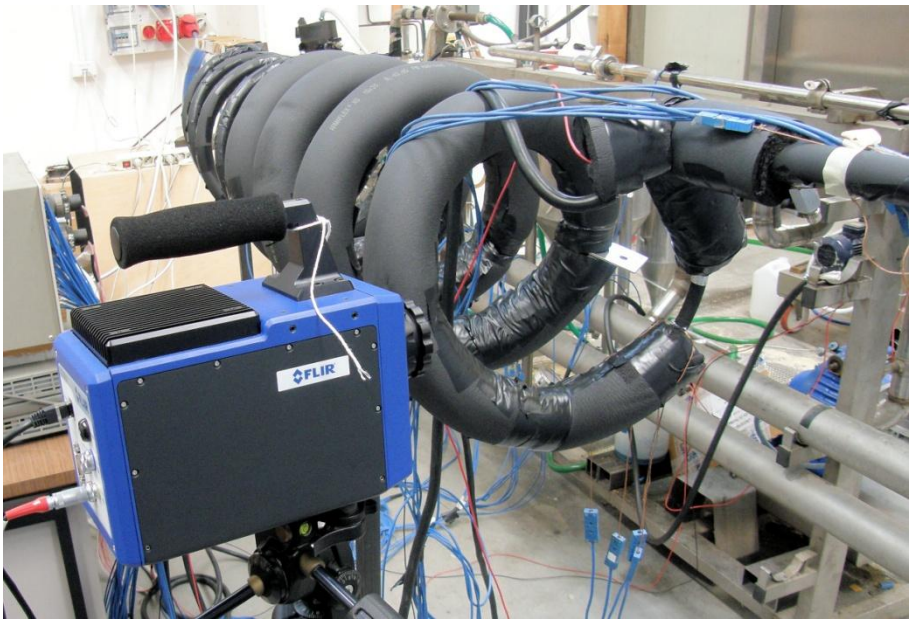

Figure 3.11: The infrared camera set-up experimental facility.

However, in the present experimental setup, the viewing angle was limited to less than ± 30°, and in this condition, the surface was considered to behaving as a diffuse grey emitter (Astarita 2012). The effective emissivity of the coating was estimated in situ by shooting a target at different known temperatures and the value 0.99 was found.

The acquired images, thanks to a position reference fixed on the tube wall (as is possible to see from figure 3.12), were conveniently cropped, processed by perspective algorithms (Cyganek 2011) and merged together in Matlab® environment to obtain continuous temperature functions on the tube wall versus the circumferential angular coordinate. Due to the infrared camera setup adopted in this investigation (e.g., the focal length and the camera position with respect to the tube test section), temperature values at 256 angular positions over the whole circumferential section were obtained.

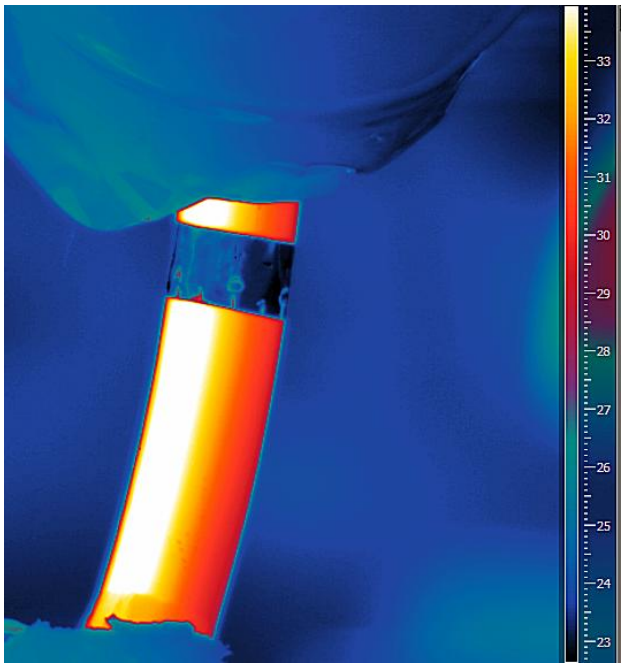

Figure 3.12: Representative infrared image of the coil wall with the particular of the position reference.

The volumetric flow rate was obtained by measuring at the outlet of the test section the time required to fill a flask whose mass was monitored by a high precision digital balance (Tamagnini). Pressure drop throughout the coiled section was measured in isothermal conditions by a U-manometer for the lower values and by a Druck-UNIK5000 differential pressure transducer for the higher values.

Ethylene Glycol was used as working fluid in the Reynolds number range 70÷1300 which, for the curvature ratio value under investigation corresponded to the Dean number range 12÷290. In the temperature range characterizing the experimental conditions the Prandtl number of the working fluid varied in the range 125÷280.

4. CIRCUMFERENTIALLY AVERAGED AND ASYMPTOTIC NUSSELT NUMBER: DATA PROCESSING AND RESULTS

4.1 DATA PROCESSING

The investigation was first devoted to measure the average heat transfer performance of the coiled pipes, by adopting the experimental setup previously described in chapter 3. The heat transfer enhancement effects were compared to the correlated pressure drop penalties: therefore the overall effectiveness of the passive techniques under study was evaluated in terms of average and asymptotic Nusselt number and average friction factor.

In the data reduction, the maximum internal diameter (the envelope diameter D_{env}) was adopted as the characteristic length: in smooth wall tube the D_{env} is equal to the D_{int}.

The performances of the different tubes were studied by varying the Reynolds number, and consequently the Dean number, which were defined in equations (1.26) and (1.44), respectively.

Under the point of view of the heat transfer, the circumferentially averaged Nusselt number along the axial coordinate *z* was calculated in the following way:

$$Nu_z = \frac{h_z \cdot D_{env}}{\lambda} \tag{4.1}$$

where the circumferentially averaged local convective heat transfer coefficient h_z is:

$$h_z = \frac{q}{(\bar{T}_w - T_b)} \tag{4.2}$$

The average wall temperature on the cross-section perimeter Γ is defined as follows:

$$\bar{T}_w = \frac{1}{\Gamma}\int_{\Gamma} T_{w,\alpha}\, d\Gamma \tag{4.3}$$

where $T_{w,\alpha}$ represents the wall local temperature. The bulk temperature is defined in equation (1.29).

The circumferentially averaged values of the wall heat flux were derived from the value of the power dissipated by Joule effect into the wall divided by the envelope cylinder surface area. The circumferentially average wall temperature $\bar{T}_w$ was estimated at different axial locations by

evaluating the arithmetic mean of the two wall temperature values measured at the outer and at the inner wall of the coil.

From the axial distributions of the heat transfer coefficient, the asymptotic Nusselt number was evaluated. In fact, for the experimental configurations here studied, the fully developed conditions were always reached in the downstream region of the heated section where, according to (Janssen and Hoogendorn 1978), the laminar boundary layers reached the asymptotic profiles. Regarding the pressure drop characteristics, the average Darcy friction factor was calculated by measuring the pressure drop along the coiled section length:

$$f_c = \frac{\Delta p}{\rho} \cdot \frac{D_{env}}{L_c} \cdot \frac{2}{W^2} \tag{4.4}$$

The performance of the enhanced geometry was suitable described by the following dimensionless quantities, the friction factor and heat transfer enhancement, defined as follows:

$$\varepsilon_f = \frac{f_e}{f_0} \tag{4.5}$$

$$\varepsilon_H = \frac{Nu_e}{Nu_0} \tag{4.6}$$

where the subscripts *e* and *0* refer to the enhanced and reference geometry respectively. The straight smooth tube was chosen as the reference geometry, by considering the analytical solution available for the thermally and hydrodynamically fully developed laminar flow problem (Shah and London 1978) in straight smooth wall tubes under the uniform wall heat flux boundary condition.

Moreover, an enhancement efficiency was evaluated:

$$\eta = \frac{\varepsilon_H}{\varepsilon_f} \tag{4.7}$$

4.2 UNCERTAINTY ANALYSIS

The uncertainty analysis was performed by using the well kwown propagation of errors procedure (Kline and McClintock 1953): it is based on the specification of the uncertainties in the various primary experimental measurements. Starting from the uncertainties of the primary measurements,

the propagation of error theory permits to estimate the uncertainty on the results obtained from a calculation based on various primary measurements (Holman 2001). Considering the result *Res* that is a function of the independent variables $x_1, x_2, x_3, \dots, x_n$:

$$Res = Res(x_1, x_2, x_3, \dots, x_n) \tag{4.8}$$

and considering $\varepsilon_1, \varepsilon_2, \dots, \varepsilon_n$ the uncertainties in the independent variables, the uncertainty in the results ε_R is given by:

$$\varepsilon_R = \left[\left(\frac{\partial Res}{\partial x_1}\varepsilon_1\right)^2 + \left(\frac{\partial Res}{\partial x_2}\varepsilon_2\right)^2 + \cdots + \left(\frac{\partial Res}{\partial x_n}\varepsilon_n\right)^2\right] \tag{4.9}$$

The uncertainties in the primary measurements are firstly analysed. For what concerns the thermocouples' signal, it is read by a high precision multimeter that has a resolution of 10nV in the range 0-100mV and an accuracy of $8 \cdot 10^{-4}$%. In the investigated conditions the electric signal was around 0.6 mV, thus having an absolute accuracy of about 0.05μV: considering that the sensibility of copper-constantan thermocouple is about 40μV/°C the accuracy correspond to 0.008°C. At this value is necessary to add the electrical noise that, at the integration time used in the acquisition, correspond to the $0.15 \cdot 10^{-4}$% of the read value plus $0.002 \cdot 10^{-4}$% of the full scale value, that means $7 \cdot 10^{-6}$ °C. These characteristics are guaranteed by the manufacturer if the measure is effectuated until 24h after the calibration and if the environmental temperature differs from the environmental temperature at the moment of the calibration of a values less than 1°C. Fluctuations of the temperature within 5°C involve an additional error of $0.15 \cdot 10^{-4}$% of the read value plus $1 \cdot 10^{-4}$% of the full scale value that means an uncertainty of 0.002 °C . Therefore it is possible to consider an overall uncertainty connected to the electric signal coming from the thermocouples of about 0.01°C. The ice point reference (model K170-50C) presents a certificate of calibration that guarantees a stability of 0.05°C.

Another factor of uncertainty is the non optimal contact between the thermocouple and the wall. Thus an overall uncertainty of 0.1°C was considered for temperature measurements.

For what concerns the volumetric flow rate, it was obtained by measuring at the outlet of the test section the time required to fill a flask whose mass was monitored by a high precision digital scale with a resolution of $0.1g$. To measure the time it was used a digital chronometer with a resolution of $0.01s$. The great part of the uncertainty in this measure comes from the reaction time of the experimenter: for this case an error of $0.1s$ was considered. An overall uncertainty of the volumetric

flowrate measurement of less than 1% could be taken into account: conservatively 1% was considered.

Talking about the average heat flux generated in the wall per unit volume, it depends on the electric power generated by the power supply and the heat exchanged with the environment. The uncertainty on the heat flux in the wall derives from the heat power dispersion from the cables and from the fin electrodes, from the effective stability of the power supply, from the correct definition of the volume and from the thermal problem of axial temperature gradients in the entry region: a conservative error of about 4% was considered.

All the fluid properties were taken from the data present in literature with the exception of the viscosity that was measured. It was measured with capillary viscometers that present a certificate of calibration that guarantees a precision of 0.4%. The functions representing the fluid properties dependence on temperature were obtained by linear interpolation. An error of about 1% was considered in all fluid properties.

Pressure drop throughout the coiled section was measured in isothermal conditions by a U-manometer for values lower than 10^4Pa and by a Druck-UNIK5000 differential pressure transducer for higher values. For the measurements performed with the U-manometer the uncertainty was estimated to be about 5% of the measured value. For what concerns the differential pressure transducer a 3% uncertainty is given by the manufacturer.

It was estimated also the uncertainty of the coil diameter since the tubes were realized mechanically and not all the coils present exactly the same diameter: it was found an uncertainty of about 2%.

It was considered the uncertainty also of the envelope diameter (internal diameter for smooth tube): even if it is difficult to estimate it, by measuring the diameter in different position for the different tubes an uncertainty of about 2% was estimated.

Resuming the following uncertainties on the input data were assumed:

T [K]	D_C [m]	ρ $[kg/m^3]$	μ $[Pa \cdot s]$	D_{env} [m]	V $[m^3]$	Q [W]	q_g $[\mathrm{W/m^3}]$	$\dot{V}$ $[m^3/s]$	Δp $[Pa]$
±0.1	±2%	±1%	±1%	±2%	±3%	±2%	±4%	±1%	3-5%

Table 4.1: The uncertainty of the main physical quantities involved in the estimation procedure

Applying the propagation of error procedure it is possible to determine the uncertainty of the principal dimensionless group used in this study.

Expressing the Re in the following form:

$$Re = \frac{4\rho\dot{V}}{\pi D_{env}\mu} \tag{4.10}$$

the uncertainty of Re could be found by:

$$\left(\frac{\varepsilon_{Re}}{Re}\right)^2 = \left(\frac{\varepsilon_{\rho}}{\rho}\right)^2 + \left(\frac{\varepsilon_{\dot{V}}}{\dot{V}}\right)^2 + \left(\frac{\varepsilon_{\mu}}{\mu}\right)^2 + \left(\frac{\varepsilon_{D_{env}}}{D_{env}}\right)^2 \tag{4.11}$$

The uncertainty on Re is estimated to be about 3%. Then the uncertainty of the Dean number is given by:

$$\left(\frac{\varepsilon_{De}}{De}\right)^2 = \left(\frac{\varepsilon_{Re}}{Re}\right)^2 + \frac{1}{2}\left[\left(\frac{\varepsilon_{D_{env}}}{D_{env}}\right)^2 + \left(\frac{\varepsilon_{D_c}}{D_c}\right)^2\right] \tag{4.12}$$

The uncertainty on De is estimated to be about 4%.

For what concerns the Nusselt number, referring to its expression in equation (1.26) the overall uncertainty could be determined by:

$$\left(\frac{\varepsilon_{Nu}}{Nu}\right)^2 = \left(\frac{\varepsilon_{q}}{q}\right)^2 + \left(\frac{\varepsilon_{\lambda}}{\lambda}\right)^2 + \left(\frac{\varepsilon_{\Delta T}}{\Delta T}\right)^2 + \left(\frac{\varepsilon_{D_{env}}}{D_{env}}\right)^2 \tag{4.13}$$

where $\Delta T = T_w - T_b$.

The bulk temperature at any location in the heat transfer section was calculated from the power supplied to the tube, assumed distributed uniformly per unit length over the heat transfer surface area, decreased by the heat losses through the insulation, while the outlet temperature was checked also by placing a thermocouple at the end of the heated section. The inlet temperature was measured by a thermocouple probe placed on the tube's wall upstream the starting heating section and an uncertainty of about 0.1K was estimated. To estimate the uncertainty on the T_b it was first estimated the error on the temperature difference between the inlet and the outlet section by referring to enthalpy balance expressed in equation (4.14):

$$T_o - T_{in} = \frac{Q}{\dot{m}c_p} \tag{4.14}$$

Thus the uncertainty could be found by:

$$\left(\frac{err_{(T_o-T_{in})}}{(T_o-T_{in})}\right)^2=\left(\frac{err_Q}{Q}\right)^2+\left(\frac{err_{\dot{m}}}{\dot{m}}\right)^2+\left(\frac{err_{c_p}}{T_{c_p}}\right)^2 \tag{4.15}$$

Considering a conservative uncertain of 1.5% on the $\dot{m}$ due to the uncertainties of the volumetric flowrate and of the density, the error on the temperature difference between inlet and outlet section is estimated to be about 2.5%. Considering an average value of 5K for the temperature difference between the inlet and the outlet section an absolute uncertainty value on (T_o-T_{in}) of about 0.1K is obtained. So, considering equation (4.16), the uncertainty on the bulk temperature obtained as the sum of the absolute error on (T_o-T_{in}) and on T_{in} is about 0.2K.

$$T_b=(T_o-T_{in})+T_{in} \tag{4.16}$$

Then the uncertainty on $\Delta T=T_w-T_b$ is about 0.3K. Eventually the uncertainty of the Nusselt number is estimated to be about 7%.

Then also the uncertainty on the friction factor was estimated, referring to equation (4.4) and using the propagation of errors as follows:

$$\left(\frac{\varepsilon_f}{f}\right)^2=\left(\frac{\varepsilon_{\Delta p}}{\Delta p}\right)^2+\left(\frac{\varepsilon_\rho}{\rho}\right)^2+\left(\frac{\varepsilon_{D_{env}}}{D_{env}}\right)^2+\left(\frac{\varepsilon_L}{L}\right)^2+2\left(\frac{\varepsilon_W}{W}\right)^2 \tag{4.17}$$

Considering an error of 1% and 2% on the length and on the average fluid velocity, respectively, the uncertainty of the friction factor was estimated to be about 5% for the measurements effectuated with the differential pressure transducer and about 6 % for the U-manometer.

4.3 RESULTS AND DISCUSSION

4.3.1 Heat Transfer

Ethylene Glycol was used as working fluid in the Reynolds number range 70÷1300 which, for the curvature ratio values under investigation corresponds to the Dean number range 12÷290. In the

temperature range characterizing the experimental conditions the Prandtl number of the working fluid varied in the range 125÷280.

In tables 4.2, 4.3, 4.4, 4.5 and 4.6 the experimental conditions of the tests performed on the tubes HSW060, HSW030, HCW060, HCW045 and HCW030 are reported.

Wall temperature distributions along the axial direction are reported for significant Re values for each tube. In each graph the temperature at the inner bend side and at the outer bend side of the coil and an average wall temperature obtained by the mean of the two values are reported.

In the calculation of the dimensionless groups (Re, Pr, De, Gr) the properties of the Glycol Ethylene were evaluated at the average bulk temperature between the inlet and outlet sections.

The circumferentially average Nusselt number distributions are reported for the different tests versus the dimensionless abscissa along the tube axis defined as:

$$z^* = \frac{z}{D_{env} \cdot Re \cdot Pr} \tag{4.18}$$

Being $Gr/Re^2 << 1$ for all the runs, the gravitational effects can be considered negligible if compared to the inertial ones.

TUBE HSW060

In Table 4.2 the experimental conditions of the tests performed on the tube HSW060 are reported.

In figures 4.1 and 4.2 the wall temperature distributions versus the dimensionless abscissa z* defined in equation (4.18), are reported for two significant Re values.

Re	Pr	$q_g\ [W/m^3]$	Gr/Re^2	De
76	226	$5.73 \cdot 10^5$	$3.37 \cdot 10^{-2}$	19
114	165	$2.26 \cdot 10^6$	$3.26 \cdot 10^{-3}$	28
124	222	$5.72 \cdot 10^5$	$2.07 \cdot 10^{-3}$	30
155	174	$2.26 \cdot 10^6$	$4.99 \cdot 10^{-3}$	38
172	230	$1.75 \cdot 10^6$	$2.59 \cdot 10^{-3}$	42
188	247	$5.74 \cdot 10^5$	$1.90 \cdot 10^{-3}$	46
232	198	$2.27 \cdot 10^6$	$3.22 \cdot 10^{-3}$	56
344	234	$5.74 \cdot 10^5$	$3.25 \cdot 10^{-3}$	84
406	239	$5.74 \cdot 10^5$	$3.78 \cdot 10^{-3}$	99
417	271	$5.75 \cdot 10^5$	$5.31 \cdot 10^{-3}$	101
426	180	$2.27 \cdot 10^6$	$4.64 \cdot 10^{-4}$	104

Re	Pr	$q_g[W/m^3]$	Gr/Re^2	De
483	236	$2.27 \cdot 10^6$	$7.59 \cdot 10^{-4}$	118
493	258	$5.74 \cdot 10^5$	$4.52 \cdot 10^{-3}$	120
523	193	$2.27 \cdot 10^6$	$2.23 \cdot 10^{-3}$	127
594	216	$2.27 \cdot 10^6$	$3.49 \cdot 10^{-3}$	144
703	228	$5.74 \cdot 10^5$	$8.80 \cdot 10^{-4}$	171
771	187	$2.27 \cdot 10^6$	$4.11 \cdot 10^{-4}$	188
772	179	$2.27 \cdot 10^6$	$1.57 \cdot 10^{-3}$	188
832	193	$2.27 \cdot 10^6$	$1.69 \cdot 10^{-4}$	202
852	185	$2.27 \cdot 10^6$	$1.33 \cdot 10^{-3}$	207
949	230	$5.74 \cdot 10^5$	$1.49 \cdot 10^{-4}$	231
982	180	$2.27 \cdot 10^6$	$1.07 \cdot 10^{-3}$	239
1001	206	$2.28 \cdot 10^6$	$3.28 \cdot 10^{-4}$	244
1128	195	$2.27 \cdot 10^6$	$2.77 \cdot 10^{-4}$	274

Table 4.2: Experimental data for tube HSW060.

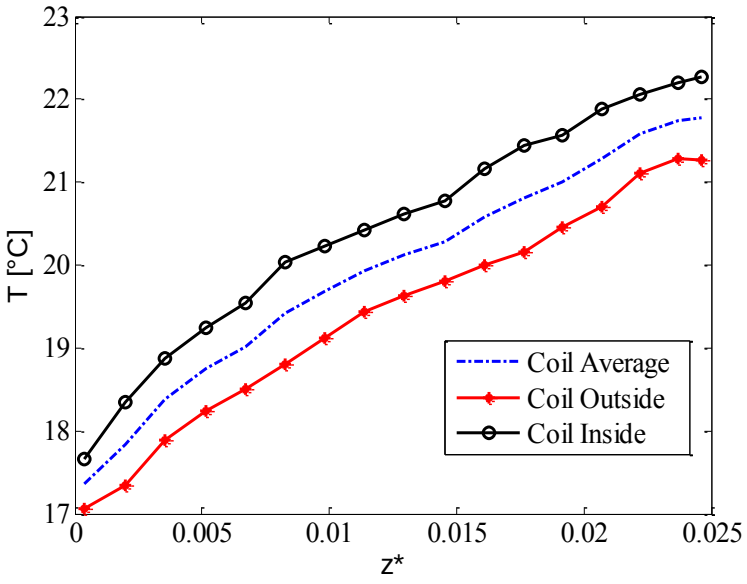

Figure 4.1: Wall temperature distribution for Re= 76 for tube HSW060.

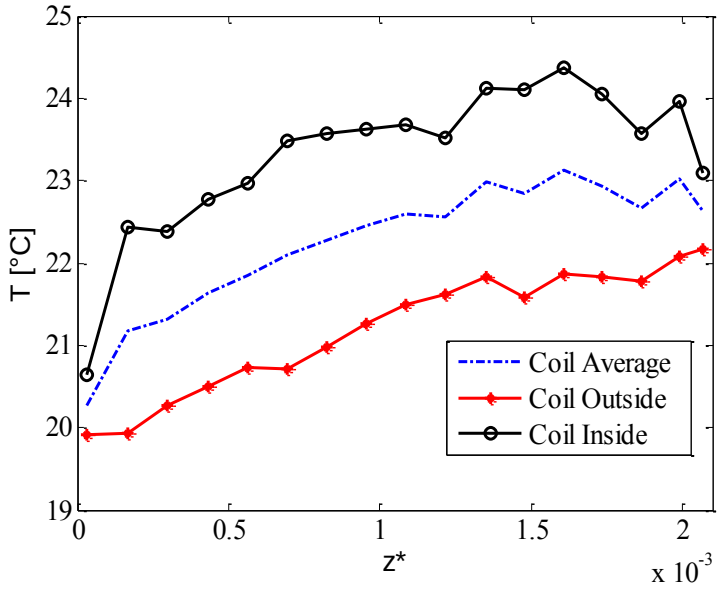

Figure 4.2: Wall temperature distribution for Re= 1001 for tube HSW060.

The Nusselt number distributions are reported in figures 4.3, 4.4 and 4.5 for the different tests versus the dimensionless abscissa z*.

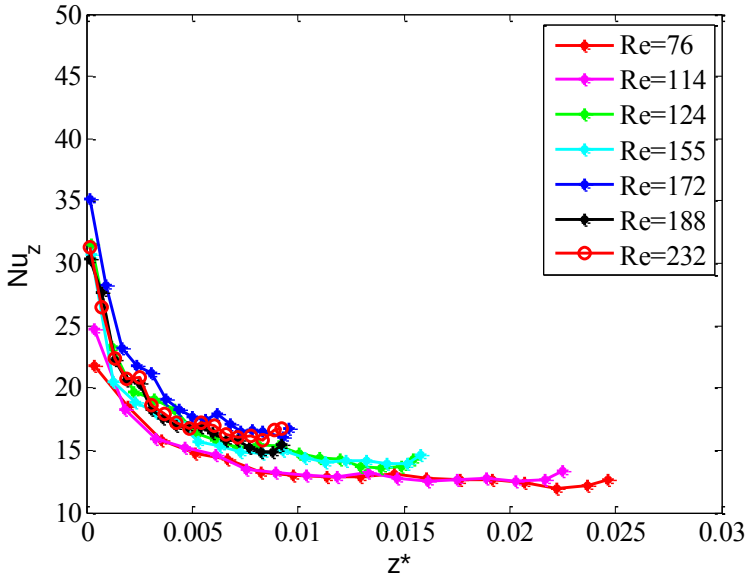

Figure 4.3: Local circumferentially averaged Nusselt number versus the dimensionless abscissa for $70 < Re < 250$ for tube HSW060.

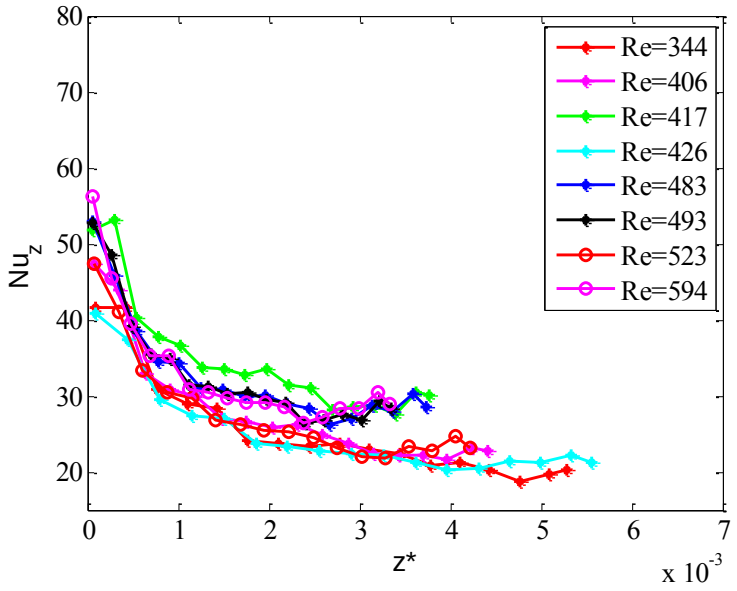

Figure 4.4: : Local circumferentially averaged Nusselt number versus the dimensionless abscissa for 340 < Re < 600 for tube HSW060.

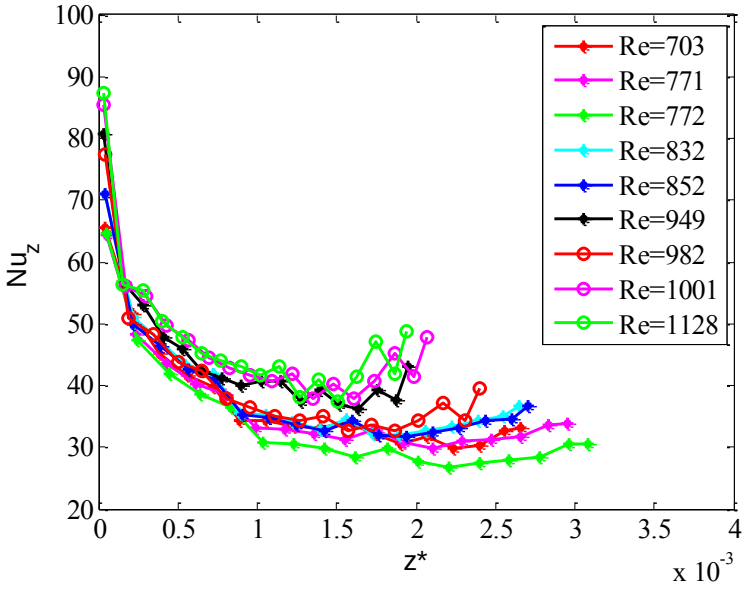

Figure 4. 5: Local circumferentially averaged Nusselt number distribution versus the dimensionless abscissa for 770 < Re < 1200 for tube HSW060.

TUBE HSW030

In Table 4.3 the experimental conditions of the tests performed on the tube HSW030 are reported.

Re	Pr	$q_g[W/m^3]$	Gr/Re^2	De
127	181	$7.17 \cdot 10^5$	$1.29 \cdot 10^{-2}$	23
144	187	$7.17 \cdot 10^5$	$9.10 \cdot 10^{-3}$	26
171	190	$7.18 \cdot 10^5$	$6.40 \cdot 10^{-3}$	31
213	192	$7.18 \cdot 10^5$	$3.80 \cdot 10^{-3}$	39
248	192	$7.18 \cdot 10^5$	$2.60 \cdot 10^{-3}$	45
287	198	$7.19 \cdot 10^5$	$1.70 \cdot 10^{-3}$	52
347	190	$7.18 \cdot 10^5$	$1.20 \cdot 10^{-3}$	63
357	205	$7.19 \cdot 10^5$	$9.11 \cdot 10^{-4}$	65
392	203	$7.19 \cdot 10^5$	$6.96 \cdot 10^{-4}$	71
415	199	$7.17 \cdot 10^5$	$7.08 \cdot 10^{-4}$	75
514	183	$7.18 \cdot 10^5$	$5.47 \cdot 10^{-4}$	93
533	160	$7.15 \cdot 10^5$	$7.24 \cdot 10^{-4}$	96
549	182	$7.18 \cdot 10^5$	$4.78 \cdot 10^{-4}$	99
597	206	$7.20 \cdot 10^5$	$2.74 \cdot 10^{-4}$	108
608	178	$7.17 \cdot 10^5$	$3.93 \cdot 10^{-4}$	110
652	205	$7.20 \cdot 10^5$	$2.31 \cdot 10^{-4}$	118
656	178	$7.17 \cdot 10^5$	$3.35 \cdot 10^{-4}$	119
660	178	$7.17 \cdot 10^5$	$3.29 \cdot 10^{-4}$	120
676	198	$7.20 \cdot 10^5$	$2.26 \cdot 10^{-4}$	122
758	201	$7.19 \cdot 10^5$	$1.58 \cdot 10^{-4}$	137
767	195	$7.20 \cdot 10^5$	$1.82 \cdot 10^{-4}$	139
784	203	$7.20 \cdot 10^5$	$1.53 \cdot 10^{-4}$	142
811	201	$7.19 \cdot 10^5$	$1.32 \cdot 10^{-4}$	147
820	202	$7.20 \cdot 10^5$	$1.38 \cdot 10^{-4}$	149
853	201	$7.19 \cdot 10^5$	$1.19 \cdot 10^{-4}$	154
883	198	$7.19 \cdot 10^5$	$1.20 \cdot 10^{-4}$	160
898	161	$7.15 \cdot 10^5$	$2.12 \cdot 10^{-4}$	163
949	161	$7.15 \cdot 10^5$	$1.84 \cdot 10^{-4}$	172
1001	164	$7.16 \cdot 10^5$	$1.56 \cdot 10^{-4}$	181
1017	170	$7.17 \cdot 10^5$	$1.26 \cdot 10^{-4}$	184
1078	164	$7.16 \cdot 10^5$	$1.20 \cdot 10^{-4}$	195
1133	168	$7.17 \cdot 10^5$	$1.08 \cdot 10^{-4}$	205
1140	165	$7.16 \cdot 10^5$	$1.01 \cdot 10^{-4}$	206
1176	151	$7.15 \cdot 10^5$	$1.21 \cdot 10^{-4}$	213
1198	155	$7.15 \cdot 10^5$	$1.05 \cdot 10^{-4}$	217

Table 4.3: Experimental data for tube HSW030

In figures 4.6 and 4.7 the wall temperature distributions versus the dimensionless abscissa z* are reported for two significant Re values.

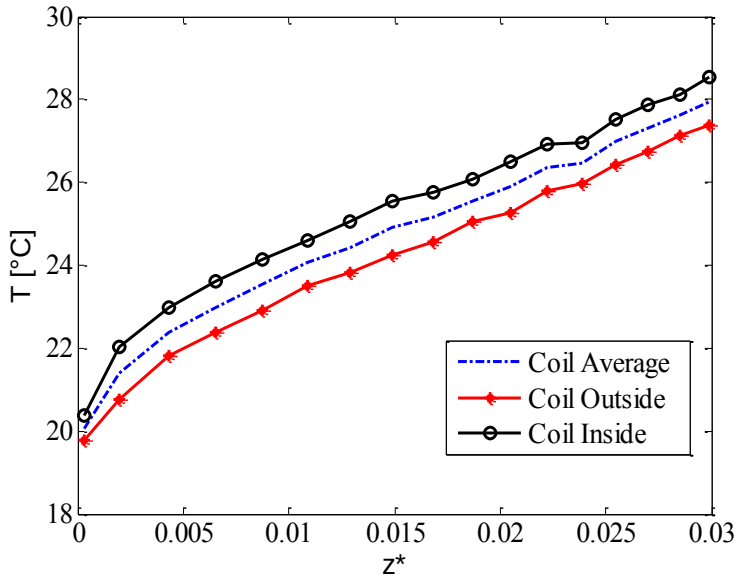

Figure 4.6: Wall temperature distribution for Re =127 for tube HSW030.

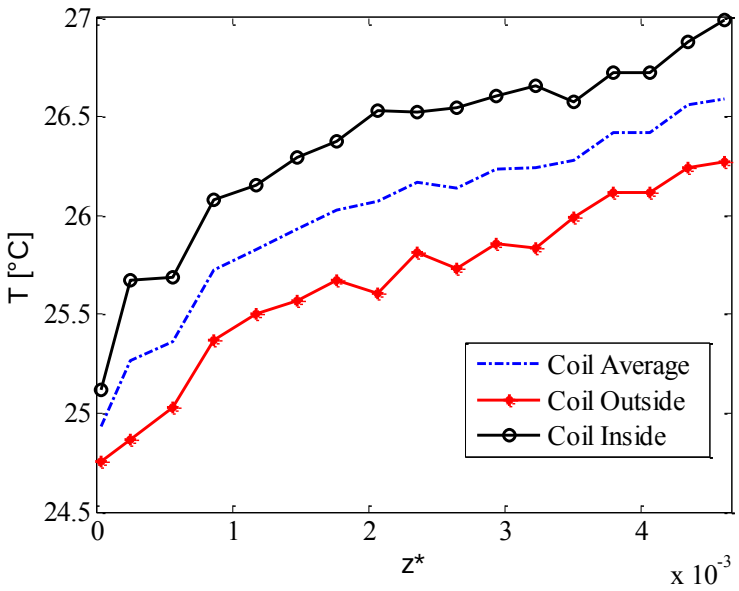

Figure 4.7: Wall temperature distribution for Re =1001 for tube HSW030.

The Nusselt number distributions are reported in figures 4.8, 4.9, 4.10 and 4.11 for the different tests versus the dimensionless abscissa z*.

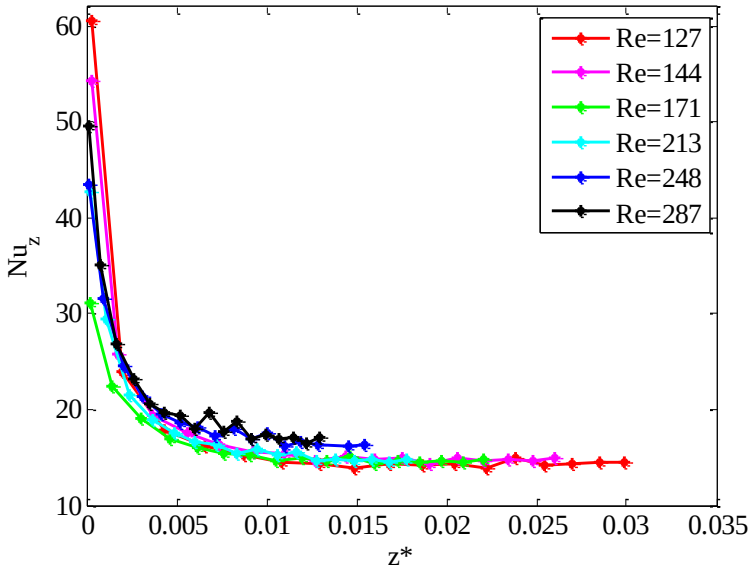

Figure 4.8: Local circumferentially averaged Nusselt number versus the dimensionless abscissa for $120 < Re < 300$ for tube HSW030.

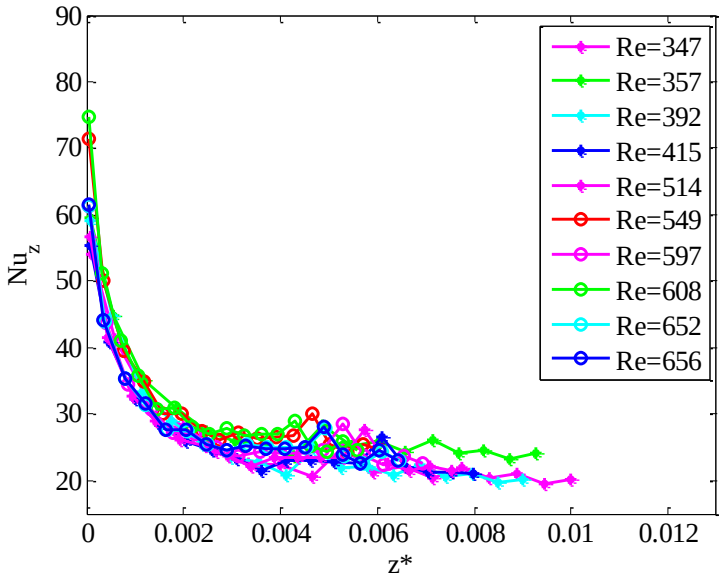

Figure 4.9: Local circumferentially averaged Nusselt number versus the dimensionless abscissa for $340 < Re < 660$ for tube HSW030.

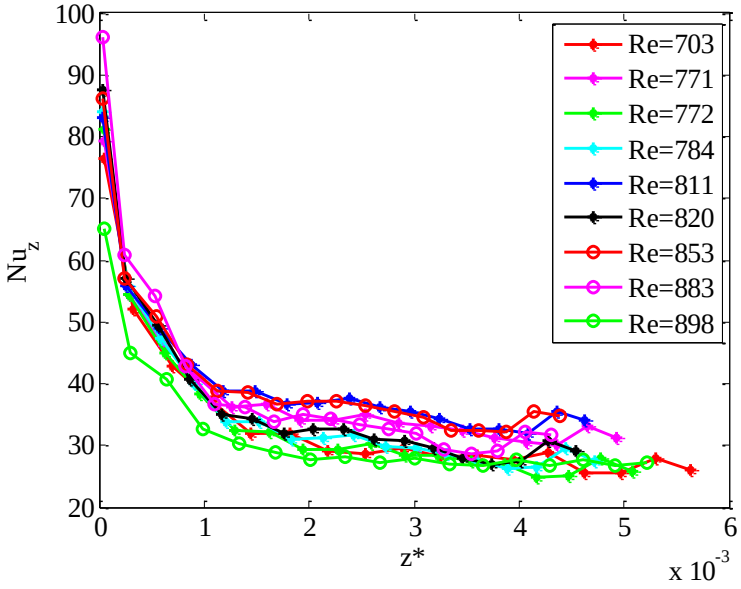

Figure 4.10: Local circumferentially averaged Nusselt number versus the dimensionless abscissa for 700 < Re < 900 for tube HSW030.

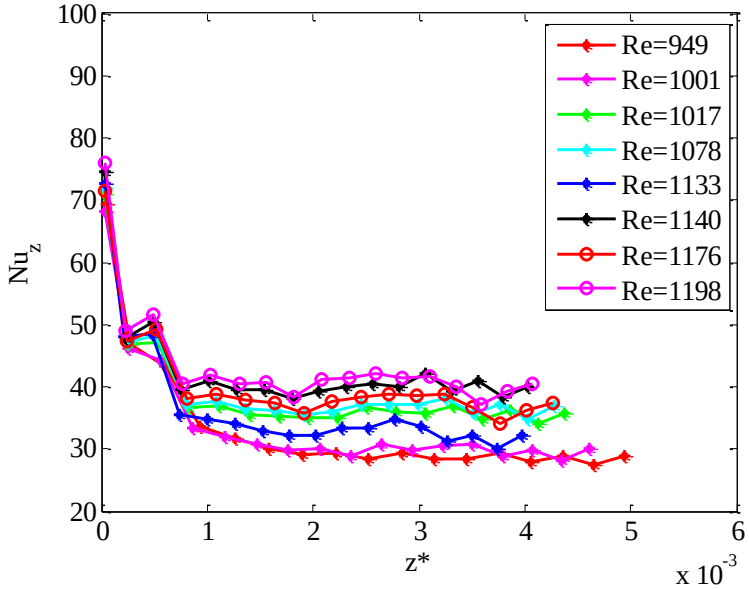

Figure 4.11: Local circumferentially averaged Nusselt number versus the dimensionless abscissa for 940 < Re < 1200 for tube HSW030.

TUBE HCW060

In Table 4.4 the experimental conditions of the tests performed on the tube HCW060 are reported.

Re	Pr	$q_g[W/m^3]$	Gr/Re^2	De
81	177	$2.17 \cdot 10^6$	$8.30 \cdot 10^{-2}$	19
126	192	$2.18 \cdot 10^6$	$2.53 \cdot 10^{-2}$	30
176	183	$2.18 \cdot 10^6$	$1.44 \cdot 10^{-2}$	43
261	207	$2.19 \cdot 10^6$	$3.60 \cdot 10^{-3}$	63
296	175	$2.18 \cdot 10^6$	$4.30 \cdot 10^{-3}$	72
352	167	$2.18 \cdot 10^6$	$3.10 \cdot 10^{-3}$	85
418	236	$2.19 \cdot 10^6$	$7.76 \cdot 10^{-4}$	101
433	175	$2.18 \cdot 10^6$	$1.50 \cdot 10^{-3}$	104
436	174	$2.19 \cdot 10^6$	$1.30 \cdot 10^{-3}$	105
509	169	$2.18 \cdot 10^6$	$9.64 \cdot 10^{-4}$	123
540	169	$2.18 \cdot 10^6$	$8.08 \cdot 10^{-4}$	130
587	172	$2.18 \cdot 10^6$	$5.93 \cdot 10^{-4}$	142
599	179	$2.19 \cdot 10^6$	$4.54 \cdot 10^{-4}$	145
612	180	$2.19 \cdot 10^6$	$4.12 \cdot 10^{-4}$	148
646	181	$2.19 \cdot 10^6$	$3.63 \cdot 10^{-4}$	156
687	171	$2.18 \cdot 10^6$	$3.17 \cdot 10^{-4}$	166
772	174	$2.19 \cdot 10^6$	$2.17 \cdot 10^{-4}$	186
826	172	$2.18 \cdot 10^6$	$1.64 \cdot 10^{-4}$	199
914	173	$2.19 \cdot 10^6$	$1.34 \cdot 10^{-4}$	221
963	162	$2.18 \cdot 10^6$	$1.31 \cdot 10^{-4}$	232
1005	162	$2.18 \cdot 10^6$	$1.12 \cdot 10^{-4}$	242
1046	164	$2.18 \cdot 10^6$	$9.70 \cdot 10^{-5}$	252
1091	169	$2.19 \cdot 10^6$	$7.79 \cdot 10^{-5}$	263

Table 4.4: Experimental data for tube HCW060.

In figures 4.12 and 4.13 the wall temperature distributions versus the dimensionless abscissa z* are reported for two significant Re values.

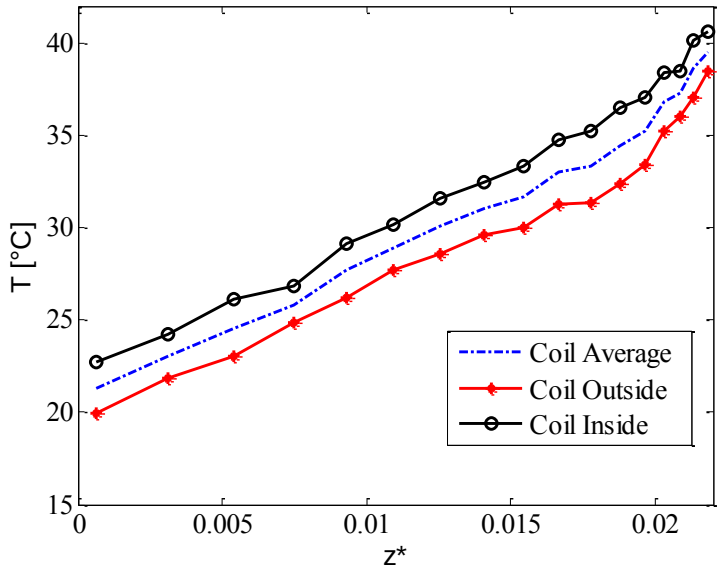

Figure 4.12: Wall temperature distribution for Re= 81 for tube HCW060.

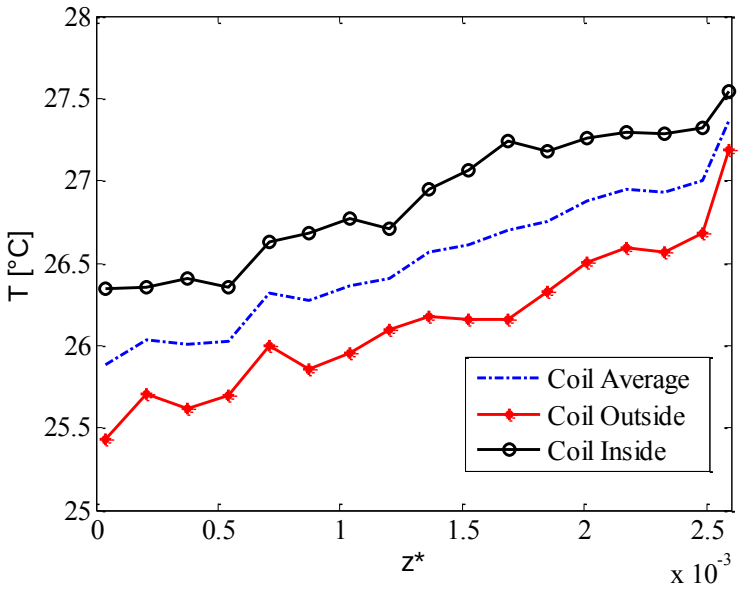

Figure 4.13: Wall temperature distribution for Re= 1005 for tube HCW060.

The Nusselt number distributions are reported in figures 4.14, 4.15 and 4.16 for the different tests versus the dimensionless abscissa z*.

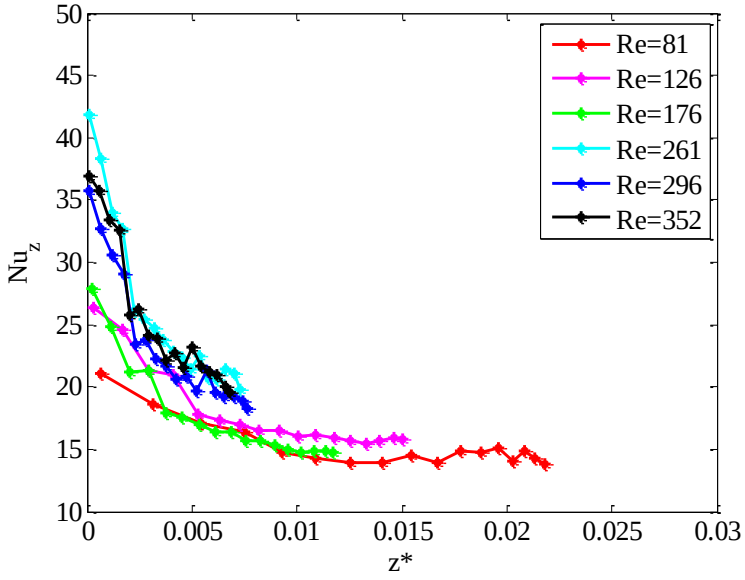

Figure 4.14: Local circumferentially averaged Nusselt number versus the dimensionless abscissa for $80 < Re < 360$ for tube HCW060.

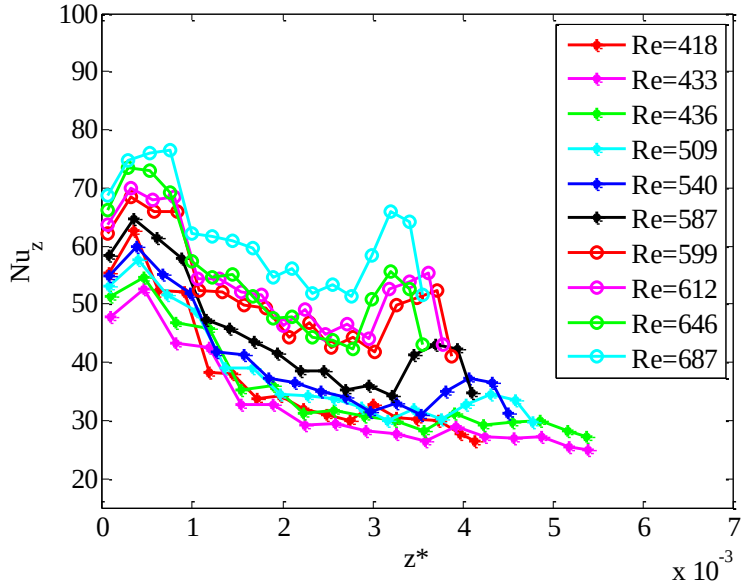

Figure 4.15: Local circumferentially averaged Nusselt number versus the dimensionless abscissa for $400 < Re < 700$ for tube HCW060.

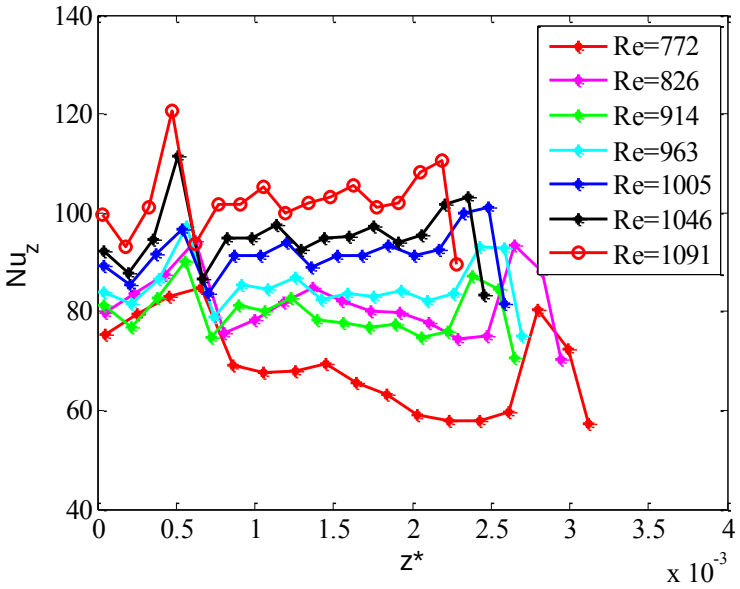

Figure 4.16: Local circumferentially averaged Nusselt number versus the dimensionless abscissa for 770 < Re < 1100 for tube HCW060.

TUBE HCW045

In Table 4.5 the experimental conditions of the tests performed on the tube HCW045 are reported.

Re	Pr	$q_g[W/m^3]$	Gr/Re^2	De
195	127	$1.16 \cdot 10^6$	$9.90 \cdot 10^{-3}$	40
205	171	$1.17 \cdot 10^6$	$4.90 \cdot 10^{-3}$	42
237	173	$1.17 \cdot 10^6$	$3.50 \cdot 10^{-3}$	49
290	175	$1.17 \cdot 10^6$	$2.20 \cdot 10^{-3}$	60
329	175	$1.17 \cdot 10^6$	$1.50 \cdot 10^{-3}$	68
370	159	$1.17 \cdot 10^6$	$1.50 \cdot 10^{-3}$	76
398	175	$1.17 \cdot 10^6$	$9.28 \cdot 10^{-4}$	82
407	169	$1.17 \cdot 10^6$	$9.67 \cdot 10^{-4}$	84
491	170	$1.17 \cdot 10^6$	$5.76 \cdot 10^{-4}$	101
499	139	$1.17 \cdot 10^6$	$9.94 \cdot 10^{-4}$	103
512	177	$1.17 \cdot 10^6$	$4.74 \cdot 10^{-4}$	106
516	147	$1.16 \cdot 10^6$	$7.16 \cdot 10^{-4}$	107
588	147	$1.16 \cdot 10^6$	$4.77 \cdot 10^{-4}$	121
630	147	$1.16 \cdot 10^6$	$3.81 \cdot 10^{-4}$	130
642	169	$1.17 \cdot 10^6$	$2.47 \cdot 10^{-4}$	133
670	147	$1.16 \cdot 10^6$	$3.08 \cdot 10^{-4}$	138
679	169	$1.17 \cdot 10^6$	$3.22 \cdot 10^{-4}$	140

Re	Pr	$q_g[W/m^3]$	Gr/Re^2	De
733	147	$1.17 \cdot 10^6$	$2.16 \cdot 10^{-4}$	151
748	157	$1.16 \cdot 10^6$	$1.73 \cdot 10^{-4}$	154
844	140	$1.16 \cdot 10^6$	$1.71 \cdot 10^{-4}$	174
864	169	$1.16 \cdot 10^6$	$9.20 \cdot 10^{-5}$	178
874	135	$1.16 \cdot 10^6$	$1.64 \cdot 10^{-4}$	181
905	128	$1.16 \cdot 10^6$	$1.75 \cdot 10^{-4}$	187
940	135	$1.16 \cdot 10^6$	$1.29 \cdot 10^{-4}$	194
971	124	$1.16 \cdot 10^6$	$1.42 \cdot 10^{-4}$	200
1002	133	$1.16 \cdot 10^6$	$1.06 \cdot 10^{-4}$	207
1008	124	$1.16 \cdot 10^6$	$1.17 \cdot 10^{-4}$	208
1059	124	$1.16 \cdot 10^6$	$9.95 \cdot 10^{-5}$	219
1132	132	$1.16 \cdot 10^6$	$7.22 \cdot 10^{-5}$	234
1197	132	$1.16 \cdot 10^6$	$6.08 \cdot 10^{-5}$	247
1253	131	$1.17 \cdot 10^6$	$5.28 \cdot 10^{-5}$	259

Table 4.5: Experimental data for tube HCW045.

In figures 4.17 and 4.18 the wall temperature distributions versus the dimensionless abscissa z* are reported for two significant Re values.

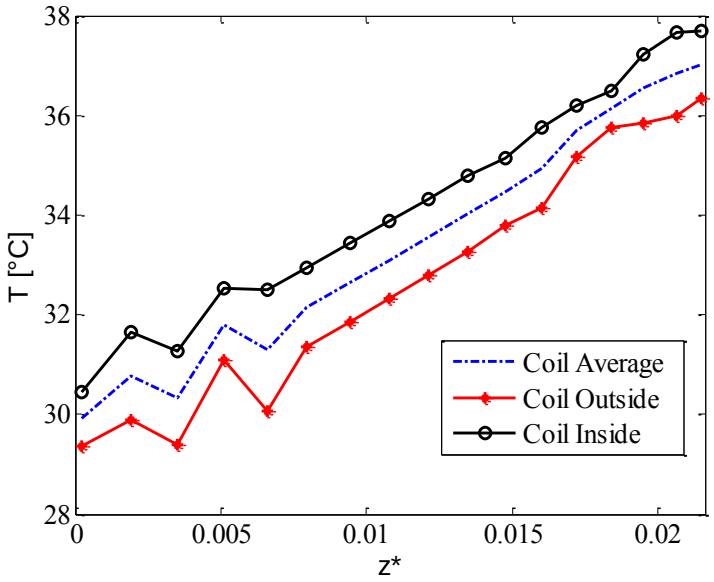

Figure 4.17: Wall temperature distribution for Re=195 for tube HCW045.

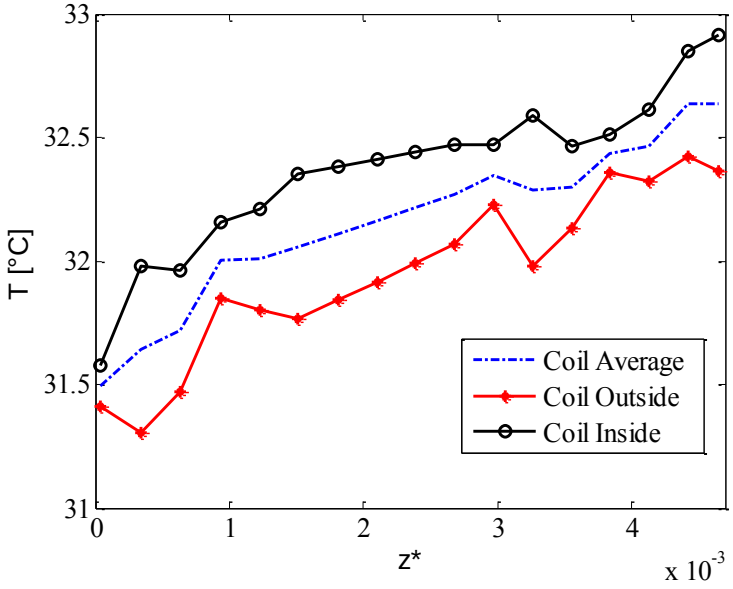

Figure 4.18: Wall temperature distribution for Re=1008 for tube HCW045.

The Nusselt number distributions are reported in figures 4.19-4.22 for the different tests versus the dimensionless abscissa z*.

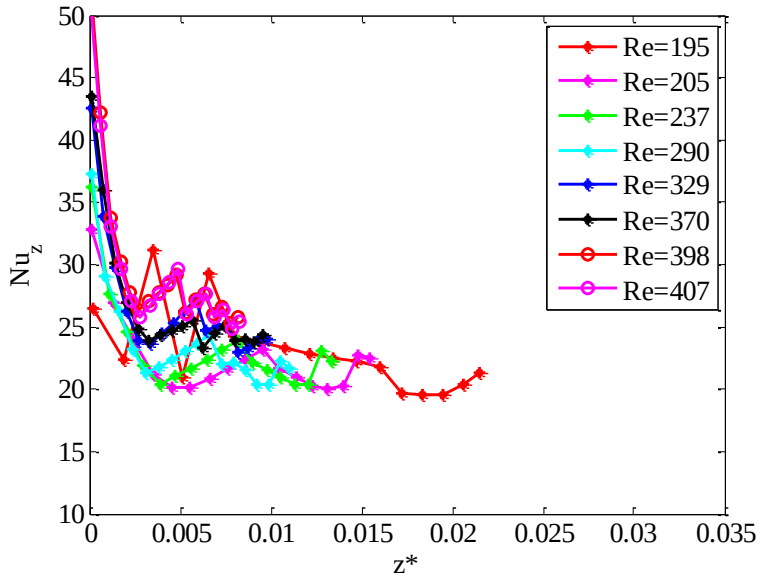

Figure 4.19: Local circumferentially averaged Nusselt number versus the dimensionless abscissa for 190 < Re < 410 for tube HCW045.

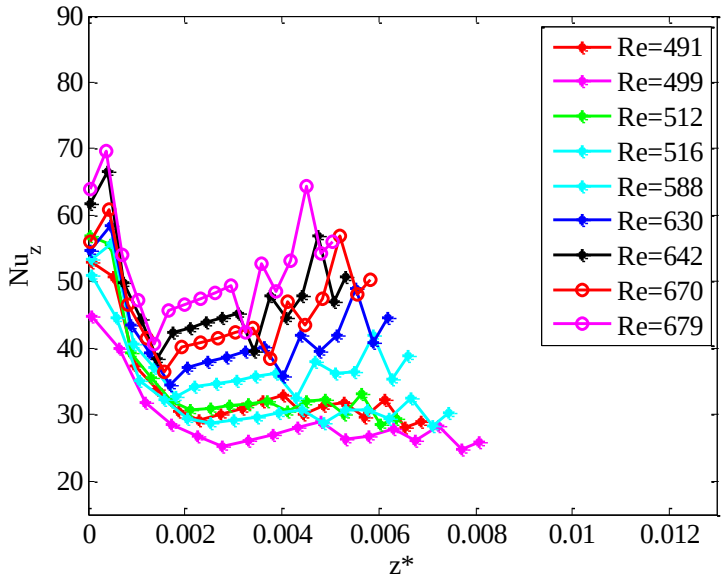

Figure 4.20: Local circumferentially averaged Nusselt number versus the dimensionless abscissa for 490 < Re < 700 for tube HCW045.

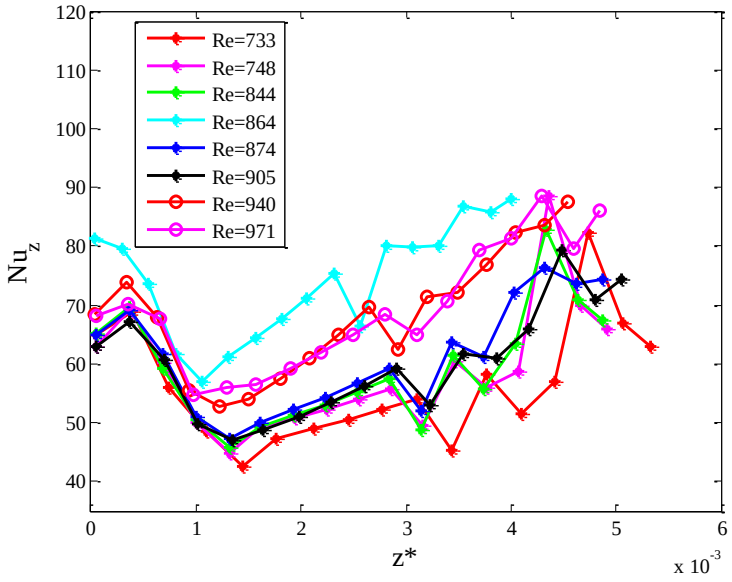

Figure 4.21: Local circumferentially averaged Nusselt number versus the dimensionless abscissa for 730 < Re < 980 for tube HCW045.

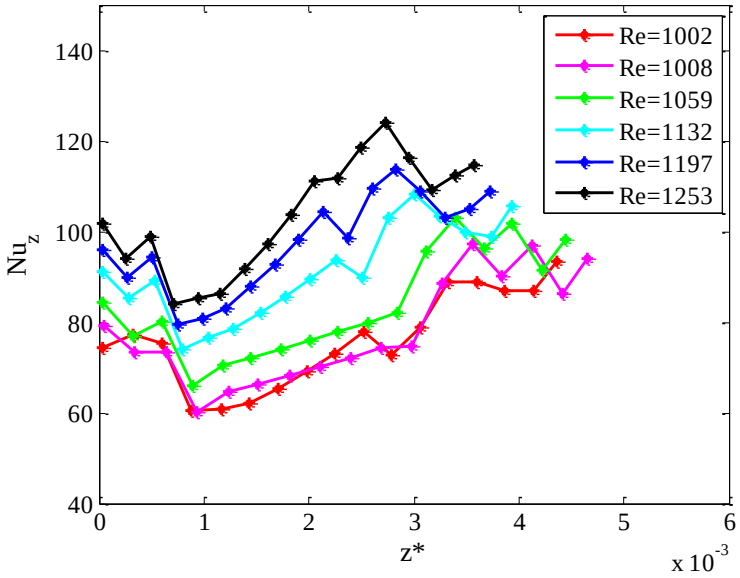

Figure 4.22: Local circumferentially averaged Nusselt number versus the dimensionless abscissa for $1000 < Re < 1260$ for tube HCW045.

TUBE HCW030

In Table 4.6 the experimental conditions of the tests performed on the tube HCW030 are reported.

Re	Pr	$q_g(W/m^3)$	Gr/Re^2	De
116	199	$6.90 \cdot 10^5$	$9.70 \cdot 10^{-3}$	21
160	188	$6.89 \cdot 10^5$	$6.30 \cdot 10^{-3}$	29
202	184	$6.88 \cdot 10^5$	$3.70 \cdot 10^{-3}$	37
240	178	$6.88 \cdot 10^5$	$2.80 \cdot 10^{-3}$	43
280	176	$6.88 \cdot 10^5$	$2.00 \cdot 10^{-3}$	51
291	192	$6.90 \cdot 10^5$	$1.30 \cdot 10^{-3}$	53
310	173	$6.88 \cdot 10^5$	$1.60 \cdot 10^{-3}$	56
321	192	$6.90 \cdot 10^5$	$1.00 \cdot 10^{-3}$	58
329	211	$6.91 \cdot 10^5$	$7.28 \cdot 10^{-4}$	59
417	187	$6.89 \cdot 10^5$	$5.46 \cdot 10^{-4}$	75
444	186	$6.89 \cdot 10^5$	$4.71 \cdot 10^{-4}$	80
509	185	$6.89 \cdot 10^5$	$3.33 \cdot 10^{-4}$	92
555	183	$6.89 \cdot 10^5$	$2.69 \cdot 10^{-4}$	100
597	181	$6.89 \cdot 10^5$	$2.23 \cdot 10^{-4}$	108
635	182	$6.89 \cdot 10^5$	$1.68 \cdot 10^{-4}$	115
674	181	$6.89 \cdot 10^5$	$1.40 \cdot 10^{-4}$	122
688	185	$6.90 \cdot 10^5$	$1.23 \cdot 10^{-4}$	124

Re	Pr	$q_g[W/m^3]$	Gr/Re^2	De
741	182	$6.89 \cdot 10^5$	$1.04 \cdot 10^{-4}$	134
762	185	$6.90 \cdot 10^5$	$9.40 \cdot 10^{-5}$	138
823	181	$6.90 \cdot 10^5$	$7.47 \cdot 10^{-5}$	149
856	179	$6.90 \cdot 10^5$	$6.64 \cdot 10^{-5}$	154
939	175	$6.90 \cdot 10^5$	$5.43 \cdot 10^{-5}$	170

Table 4.6: Experimental data for tube HCW030.

In figures 4.23 and 4.24 the wall temperature distributions versus the dimensionless abscissa z* are reported for two significant Re values.

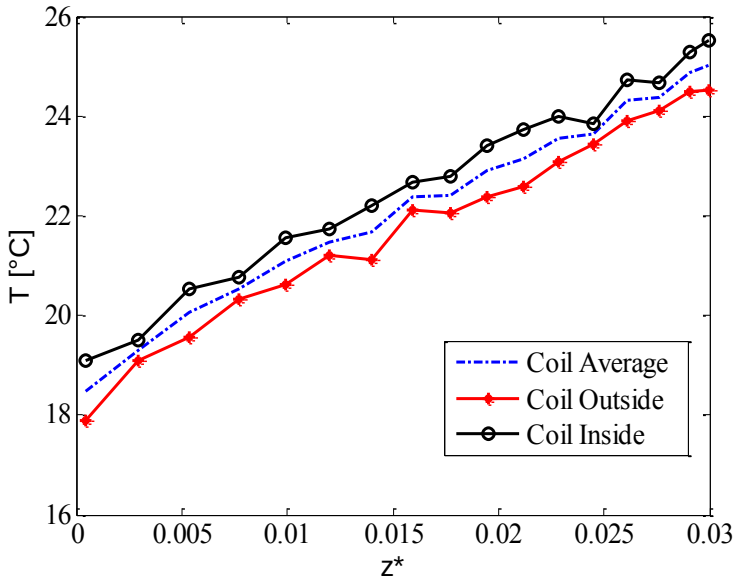

Figure 4.23: Wall temperature distribution for Re=116 for tube HCW030.

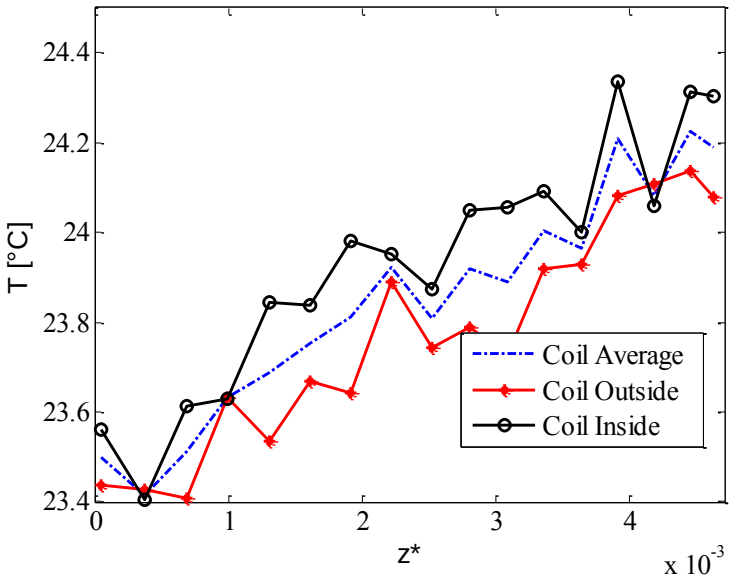

Figure 4.24: Wall temperature distribution for Re=939 for tube HCW030.

The Nusselt number distributions are reported in figures 4.25, 4.26 and 4.27 for the different tests versus the dimensionless abscissa z*.

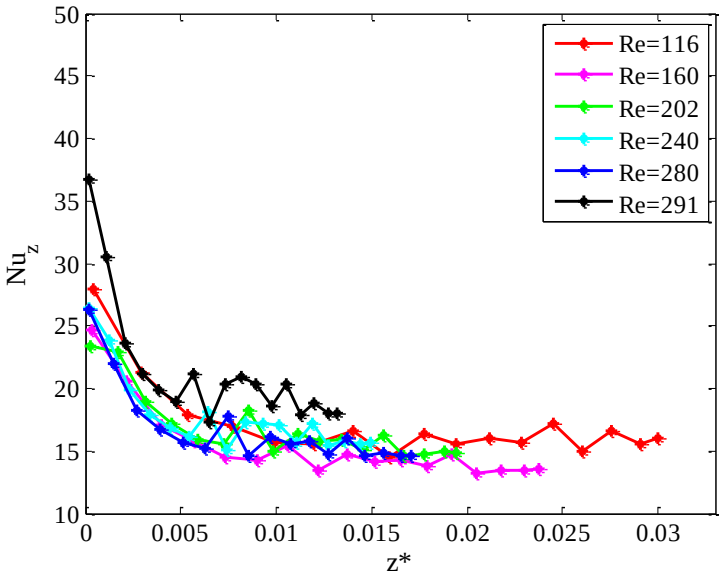

Figure 4.25: Local circumferentially averaged Nusselt number versus the dimensionless abscissa for 100 < Re < 300 for tube HCW030.

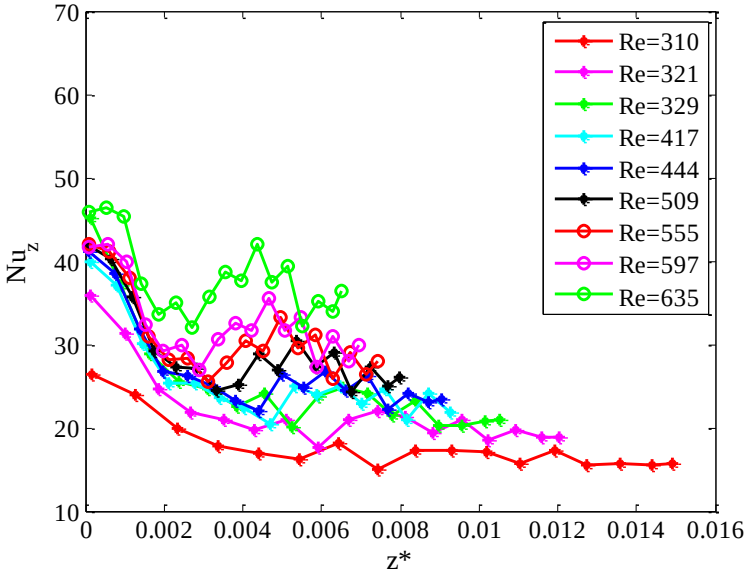

Figure 4.26: Local circumferentially averaged Nusselt number versus the dimensionless abscissa for 300 < Re < 640 for tube HCW030.

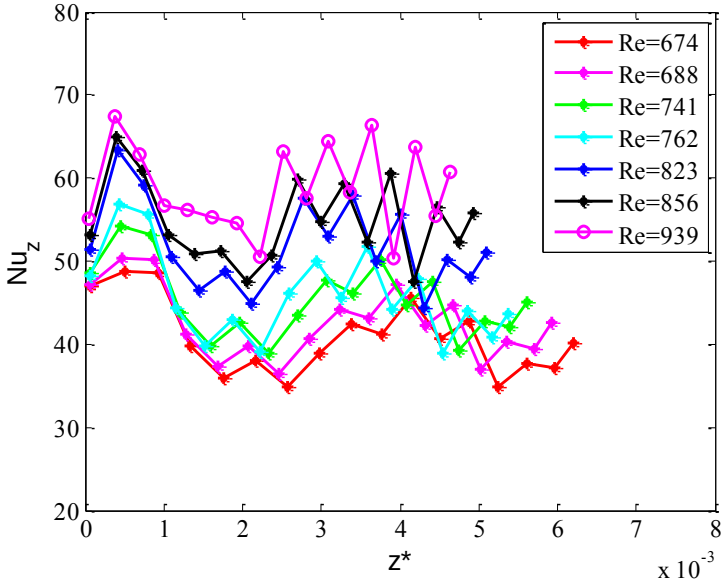

Figure 4.27: Local circumferentially averaged Nusselt number versus the dimensionless abscissa for 670 < Re < 940 for tube HCW030.

Discussion

From the wall temperature distributions reported in the figures (4.1, 4.2, 4.6, 4.7, 4.12, 4.13, 4.17, 4.18, 4.23 and 4.24) it is possible to see that as the fluid enters the coiled section it starts to be affected by the centrifugal force due to the curvature of the tube. Therefore the fluid is removing more heat from the wall at the outer bend side where the axial velocity is expected to be maximum: indeed the outer bend side is colder than the inner. This effect is more evident for the tube with $\delta_c \cong 0.06$ with respect to the tube with $\delta_c \cong 0.03$.

The distortion in the wall temperature distribution along the perimeter confirmed the presence of a secondary flow, induced by the centrifugal force, and its magnitude was enhanced by increasing the Reynolds number. In addition it could be noted that in the wall temperature of the corrugated tubes a distribution more irregular is present, characterized by sudden peaks that could be, for high Re, the consequence of an earlier departure from the steady regime caused by the corrugation.

The Nusselt number distributions for representative Reynolds number values are reported in figures 4.28-4.31 for both the smooth wall and the corrugated wall pipes for the two case $\delta_c \cong 0.03$ and $\delta_c \cong 0.06$ versus the dimensionless curvilinear abscissa.

In the same figures the analytical solution holding for the thermal entry problem in straight smooth wall tube and the empirical correlation by Janssen and Hoogendoorn (1978) holding for helical coiled smooth wall tubes under uniform heat flux boundary condition, are reported too. As

expected, as a consequence of the fluid mixing due to the centrifugally induced secondary flow, the local Nusselt number, circumferentially averaged, reaches values higher than the ones obtained in a straight pipe for both the smooth and corrugated wall helically coiled tubes.

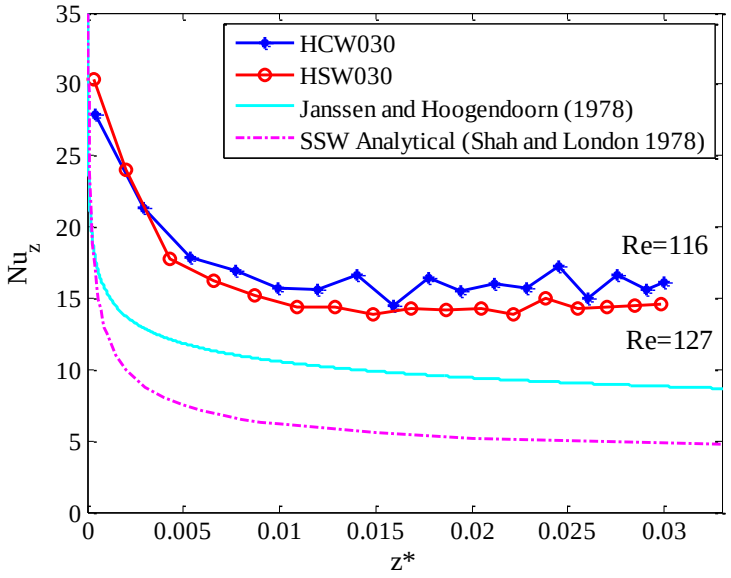

Figure 4.28: Local Nusselt number for the tubes with $\delta_c \cong 0.03$ and comparison with the analytical solution for the straight smooth wall tube under uniform heat flux boundary condition and with the correlation by Janssen and Hoogendorn (1978) (correlation of Janssen and Hoogendorn evaluated at Re=127).

The data for the smooth wall tubes are underpredicted by the empirical correlation suggested by Janssen and Hoogendorn (1978) for low Reynolds number values, while the agreement improves with the progression of the Reynolds number.

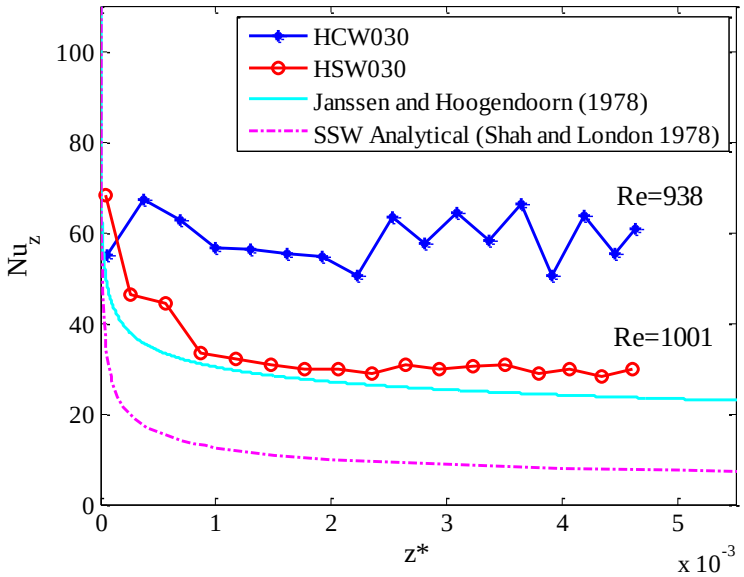

Figure 4.29: Local Nusselt number for the tubes with $\delta_c \cong 0.03$ and comparison with the analytical solution for the straight smooth wall tube under uniform heat flux boundary condition and with the correlation by Janssen and Hoogendorn (1978) - (correlation of Janssen and Hoogendorn evaluated at Re=1001).

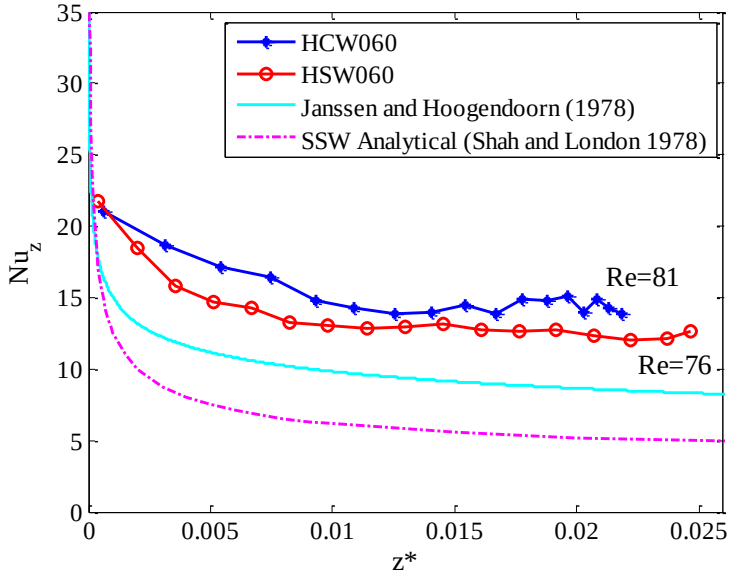

Figure 4.30: Local Nusselt number for the tubes with $\delta_c \cong 0.06$ and comparison with the analytical solution for the straight smooth wall tube under uniform heat flux boundary condition and with the correlation by Janssen andHoogendorn (1978) - (correlation of Janssen and Hoogendorn evaluated at Re=76).

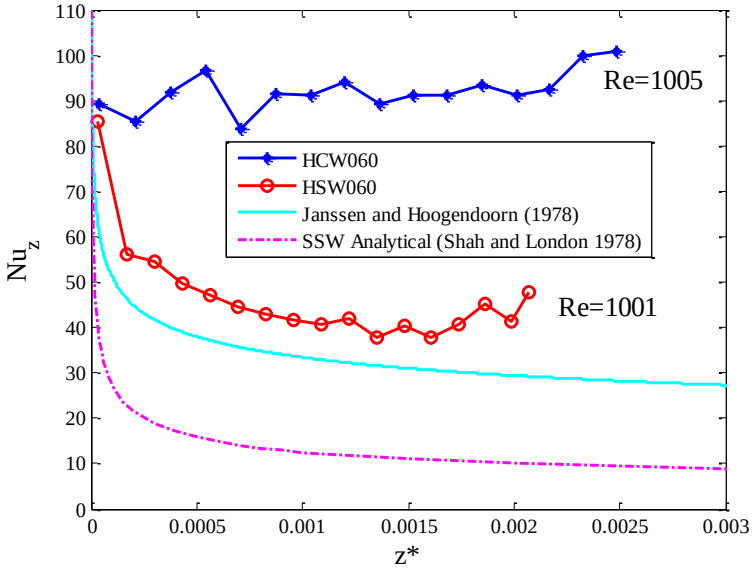

Figure 4.31: Local Nusselt number for the tubes with $\delta_c \cong 0.06$ and comparison with the analytical solution for the straight smooth wall tube under uniform heat flux boundary condition and with the correlation by Janssen and Hoogendorn (1978) - (correlation of Janssen and Hoogendorn evaluated at Re=1001).

For what concerns the effect of the wall corrugation, the data show that it is almost negligible for low Reynolds number values, whereas the increase over the smooth wall behaviour augments importantly with the progression of the Reynolds number and of the curvature ratio. This behaviour could be interpreted as a consequence of a departure from the steady laminar flow induced by the

wall corrugation as it happens in straight wall corrugated tubes (Nishimura et al. 1990; Garimella and Christensen 1993) .

With the aim to better compare the intensity of the two concurrent effects, the asymptotic Nusselt number is reported in figures 4.32 and 4.33 versus the Reynolds and the Dean number respectively. Here, in the calculation of the dimensionless groups (Re, Pr, De) the properties of the Glycol Ethylene were evaluated at the local bulk temperature. The values reported in these graphs for Nusselt, Reynolds, Dean and Prandtl numbers were obtained as average of the last values in the fully developed region.

In figure 4.32 the correlation suggested by Janssen and Hoogendorn (1978) holding for smooth coils, evaluated for $\delta_c = 0.06$ and Pr=182 is reported too. The data confirm that for low Dean and Reynolds number values the wall corrugation effect is almost negligible and the enhancement over the smooth straight tube behavior has to be ascribed to the wall curvature effect. For higher Dean and Reynolds number values the wall corrugation effect becomes to prevail producing an important enhancement of the convective heat transfer mechanism. In addition the results show that, for the corrugation profile considered in this thesis work, the departure from the smooth wall behavior occurs for Reynolds number values in the range 500-600, depending from the curvature ratio. These thresholds values are much lower than the ones expected for the smooth wall helically coiled tubes (Cioncolini and Santini 2006; Di Piazza and Ciofalo 2011).

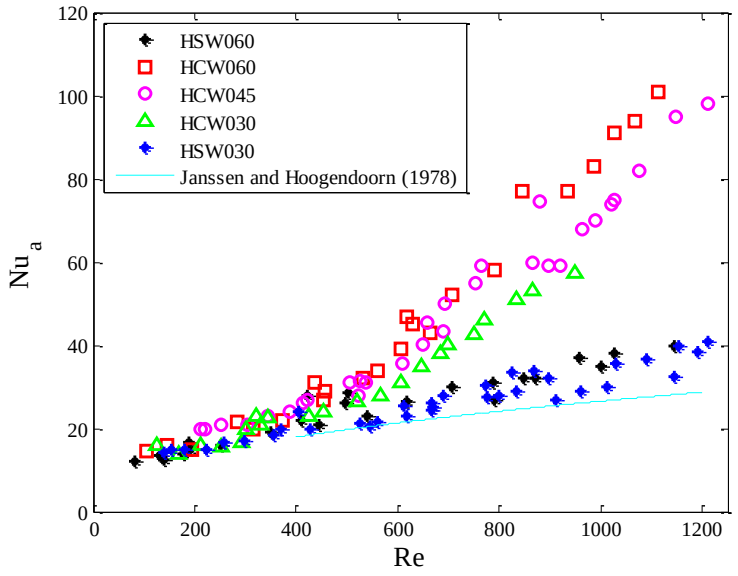

Figure 4.32: Asymptotic Nusselt number versus *Re* for the helically coiled tubes under test and comparison with the correlation proposed by Janssen and Hoogendoorn (1978) for the helically coiled smooth wall tube evaluated at δ_c=0.06.

In addition the data show that this critical condition is appropriately described by the Dean number

and that the critical value can be identified in the range between 110 and 130. This behavior is consistent with the results available for straight spirally enhanced tubes characterized by similar corrugation profile for which a critical Reynolds number in the range 300-1000 was reported (Srinivasan and Christensen 1992; Garimella and Christensen 1993; Rainieri et al. 1996).

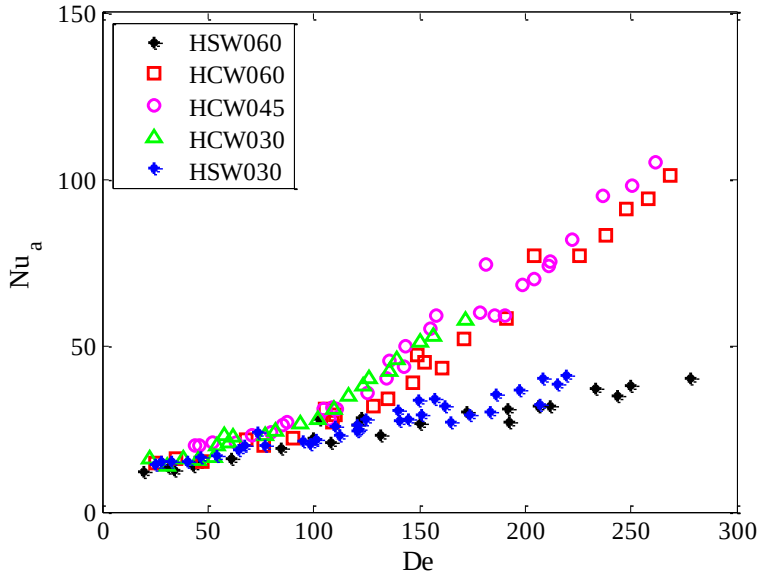

Figure 4.33: Asymptotic Nusselt number versus the *De* for the helically coiled tubes under test.

The experimental data were correlated by considering a dependence of the asymptotic Nusselt number on the Reynolds number, curvature ratio and Prandtl number for the helically coiled both smooth and corrugated wall tubes. For Nusselt, Reynolds, Dean and Prandtl numbers asymptotic values obtained as average values in the fully developed region were considered.

The data were processed by adopting the multiple linear regression tool within the Matlab® environment under the assumption of a power-law dependence of *Nu* on *Re*, *Pr* and *De*.

For the smooth wall geometry the following optimal correlation was found:

$$Nu = 1.63 \cdot De^{0.48} \cdot Pr^{0.09} \tag{4.19}$$

holding in the range 20<*De*<280, 160<*Pr*<280.

For the corrugated wall geometry instead, the following optimal correlation, derived by considering the data above the critical conditions, was found:

$$Nu = 0.035 \cdot De^{1.34} \cdot Pr^{0.1} \tag{4.20}$$

holding in the range 120 < *De* < 270, 125 < *Pr* < 240.

The correlation coefficient associated to equation (4.19) and equation (4.20) was found equal to 0.93 and 0.96 respectively.

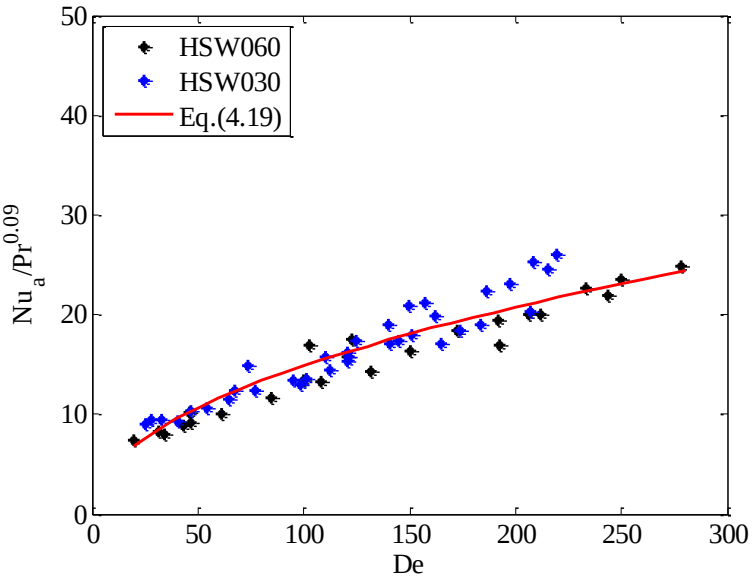

Figure 4.34: Experimental data for the smooth wall tubes and optimal correlations.

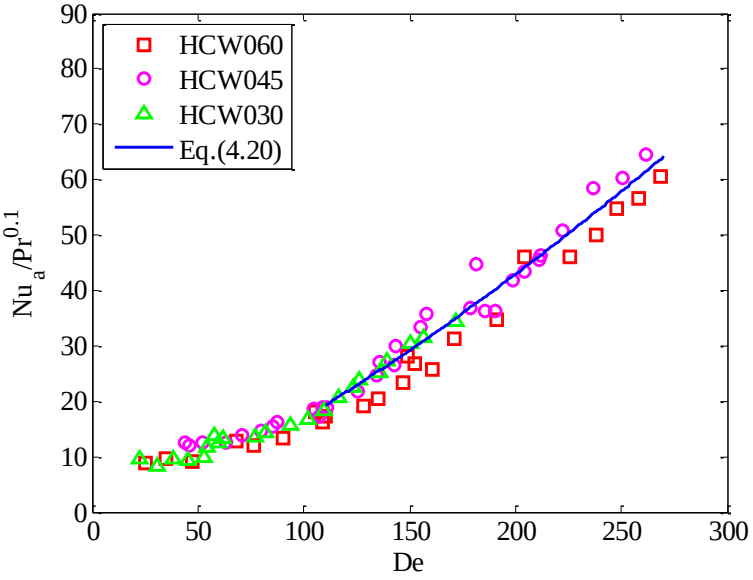

Figure 4.35: Experimental data for the corrugated wall tubes and optimal correlations.

The present data confirm the results of Zachár (2010) for what concerns the fact that for a given corrugation profile the Nusselt number is well described by the Dean number and Prandtl number. Although this, the exponents here found are different from the one numerically predicted by Zachár

(2010). The experimental data are compared to the optimal correlations for the smooth and the corrugated tubes in figures 4.34 and 4.35 respectively.

4.3.2 Pressure drop

In figure 4.36 it is reported the average Darcy friction factor for both the smooth and the corrugated wall helically coiled tube versus the Reynolds number. In the same figure the analytical solution for the laminar fully developed flow, holding for the straight smooth wall tube is reported (Shah London 1978). For the helically coiled smooth wall tube, the friction factor values are close to the expectations for the straight section for Reynolds number values lower than about 500 while for higher Reynolds number values, the curvature effect on the pressure drop is still small, but not negligible. For what concerns the helically coiled corrugated wall tube, the friction factor values are higher than the ones of the smooth coiled section and the enhancement augments with the Dean number. The data confirm the above formulated hypothesis that the wall corrugation acts in enhancing the onset of an enhanced unsteady flow regime where pressure drop is augmented over the smooth wall behavior.

This behavior is close to the phenomenon observed by Rainieri et al. (1996) for spirally corrugated straight tubes.

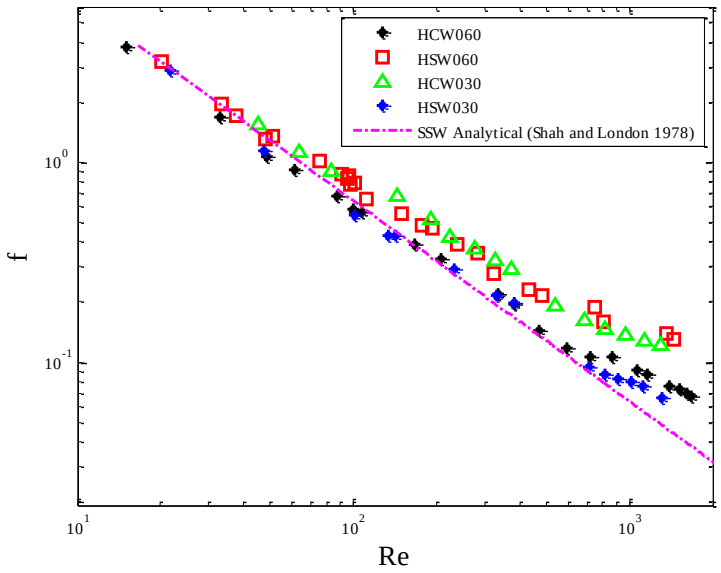

Figure 4.36: Darcy friction factor versus Reynolds number for the tubes under test and comparison with the analytical solution holding for the straight smooth wall tube.

4.3.3 Enhancement

In order to better quantify the enhancement of the helically coiled tubes over a common reference geometry the friction factor and the heat transfer enhancement defined by equations (4.5, 4.6) were evaluated. The behavior of ε_H and ε_f is reported in figures 4.37 and 4.38 versus the Dean number and the Reynolds number respectively .

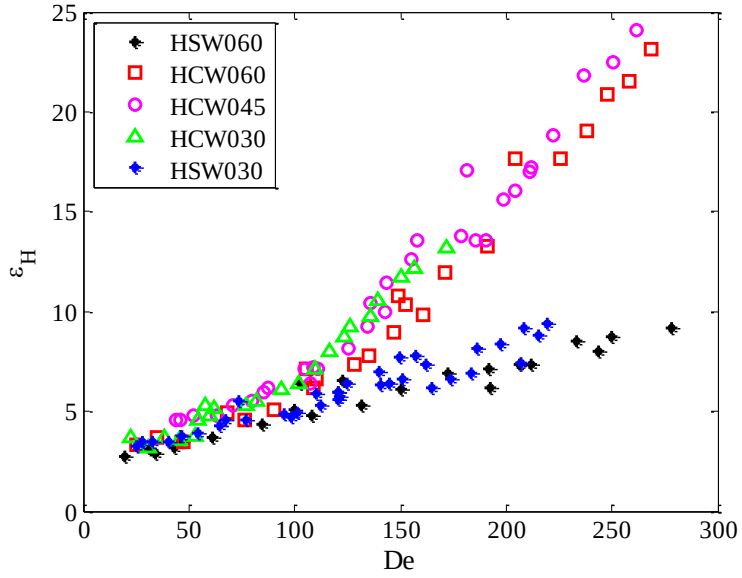

Figure 4.37: Heat transfer enhancement versus the Dean number for the tubes under test.

The results confirm that both wall curvature and wall corrugation produce an additional convective transport mechanism that enhances both the heat transfer and the pressure drop when compared to that in a straight smooth tube.

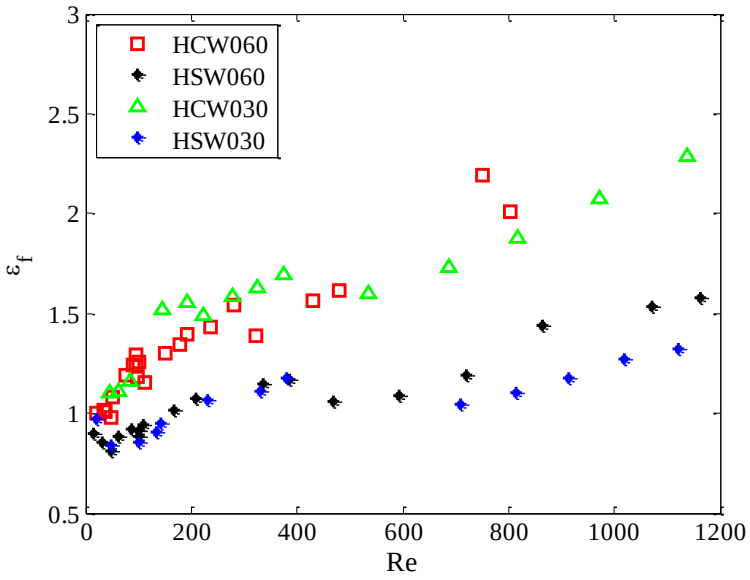

Figure 4.38: Friction factor enhancement versus the Reynolds number for the tubes under test.

The effect of the wall curvature alone brings heat transfer augmentation in the range 2÷10 against pressure drop penalties increase in the range 1÷1.5, while for the helical coiled wall corrugated tubes an heat transfer enhancement up to 25 was registered against a maximum friction factor augmentation of 2.5.

The same conclusion is remarked by the plot of figure 4.39 in which the enhancement efficiency $\eta = \frac{\varepsilon_H}{\varepsilon_f}$ is reported versus the Reynolds number for both the smooth and wall corrugated tubes with $\delta_c \cong 0.06$.

The data confirm that, above the critical condition, the wall corrugation, as superimposed to the wall curvature, brings an additional heat transfer enhancement that is combined with a modest expense of the additional pressure-losses. These results suggest that the compound use of wall curvature and wall corrugation can provide an interesting solution in the design of helical-coil heat exchangers. In fact, when helical coiled tubes are used, although significant benefits are expected in terms of heat transfer performance due to secondary flow pattern that arises due to the centrifugal force, a significant delay of the transition to the turbulent regime inevitably occurs. Moreover the negative effect due to the smoothing of turbulence emergence was found to match, or even to overcome, the increasing effect due to the triggering of the secondary flows (Cioncolini and Santini 2006). The use of corrugated wall tubes can compensate for this drawback, by promoting an early transition to the unstable/transitional flow regime that activates an heat transfer enhancement amplifying the one brought by the wall curvature.

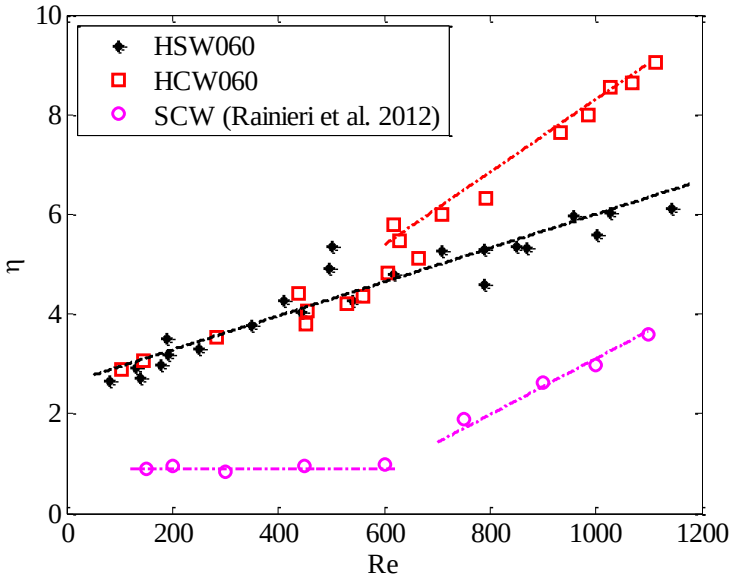

Figure 4.39: Enhancement efficiency versus the Reynolds number for the smooth and wall corrugated tubes with $\delta_c \cong 0.06$ and comparison with the straight wall corrugated behavior (Rainieri et al 2012a, 50 < Pr < 150).

In figure 4.39 the data regarding the straight corrugated wall behaviour (with the same corrugation profile), derived from (Rainieri 1996), are reported, too. The results show that the concurrent use of the two passive heat transfer augmentation techniques (wall curvature compounded with wall corrugation) is particularly effective if compared to the performance achievable through their separate use.

5. LOCAL NUSSELT NUMBER IN SMOOTH WALL TUBES: ESTIMATION PROCEDURE AND NUMERICAL VALIDATION

In order to better understand the mechanisms that govern the heat transfer in coiled pipes, the convective heat transfer coefficient distribution along the cross section circumference represents a primary information.

The effectiveness of wall curvature, as already discussed in chapters 1 and 4, occurs because it gives origin to the centrifugal force in the fluid: this phenomenon induces local maxima in the velocity distribution that locally increases the temperature gradient at the wall maximising the heat transfer. The asymmetrical distribution of the velocity field over the cross-section of the tube leads to a significant variation in the convective heat-transfer coefficient along the circumferential angular coordinate: it presents higher values at the outer bend side of the wall surface than at the inner bend side (Bai et al.1999; Jayakumar et al. 2010).

This irregular distribution may be critical in some industrial applications, such as in those that involve a thermal process. For instance, in food pasteurisation, the irregular temperature field induced by the wall curvature could reduce the bacteria heat-killing or could locally overheat the product. Therefore, to predict the overall performance of heat-transfer apparatuses that involve the use of curved tubes, it is necessary to know the local distribution of the convective heat-transfer coefficient not only along the axis of the heat-transfer section but also at the fluid-wall interface along the cross-section circumference.

Although many authors have investigated the forced convective heat transfer in coiled tubes, most of them have presented the results only in terms of the Nusselt number averaged along the wall circumference: only a few authors have studied the phenomenon locally, and most of them have adopted the numerical approach (see paragraph 1.4).

The solution of the IHCP in the wall, starting from the temperature distribution acquired on the external wall surface, is a robust tool to estimate the local convective heat-transfer coefficient on the interior wall surface. In this thesis three different techniques are employed to solve the IHCP and to find the local convective heat transfer coefficient at the fluid-wall interface. In the following paragraphs the three different procedures, that are based on Tikhonov Regularization Method (TRM), Gaussian Filter Technique (GFT) and Quadrupole method (QM), are going to be presented, implemented and optimized for the problem under study, validated by synthetic data and compared.

These solution techniques are well known but their implementation for the case under study is not deeply analysed in literature.

5.1 PROBLEM DEFINITION

To evaluate the local actual value of the convective heat transfer coefficient at the fluid internal wall interface on a given cross section (as highlighted in figure 5.1), the temperature distribution is acquired on the external wall surface and then the IHCP in the wall domain is solved by considering the convective heat flux distribution on the internal wall surface to be unknown.

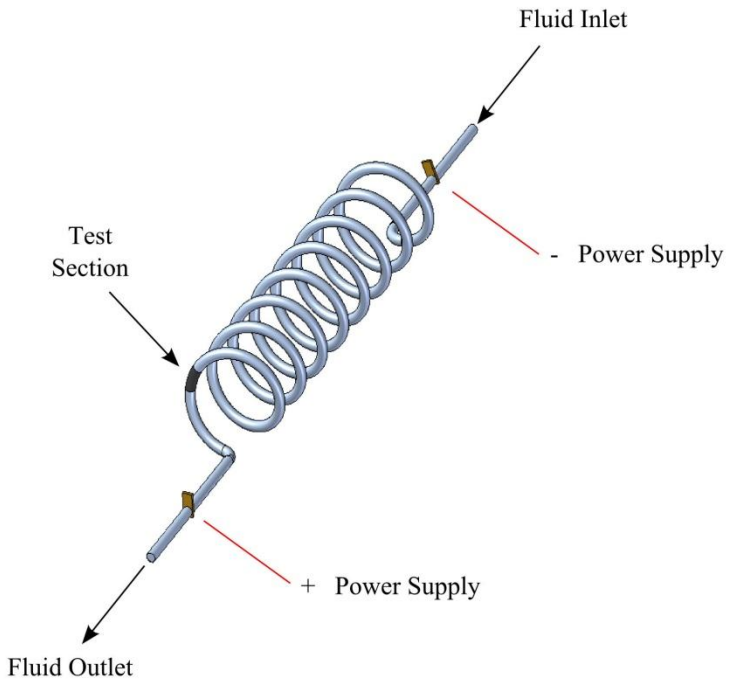

Figure 5.1: Coiled tube.

If the temperature gradient along the axis of the tube is almost negligible, the test section (sketched in figure 5.2) can be efficiently modelled as a 2-D solid domain.
In this domain the steady state energy balance equation is expressed in the form:

$$\frac{\lambda}{r}\frac{\partial}{\partial r}\left(r\frac{\partial T}{\partial r}\right)+\frac{\lambda}{r^2}\frac{\partial^2 T}{\partial \alpha^2}+q_g=0 \tag{5.1}$$

where q_g is the heat generated per unit volume and λ is the tube wall thermal conductivity. The following two boundary conditions completed the energy balance equation:

$$-\lambda\frac{\partial T}{\partial r}=\frac{(T-T_{env})}{R_{env}} \qquad \text{at } r=r_{ext} \tag{5.2}$$

that is applied on surface S_{ext} and where R_{env} is the overall heat transfer resistance between the tube wall and the surrounding environment with the temperature T_{env} ;

$$-\lambda\frac{\partial T}{\partial r} = -h_{int}\cdot(T - T_b) \qquad \text{at } r = r_{int} \tag{5.3}$$

that is applied on surface S_{int} and where T_b is the bulk fluid temperature and h_{int} is the local convective heat transfer coefficient at the fluid-internal wall interface.

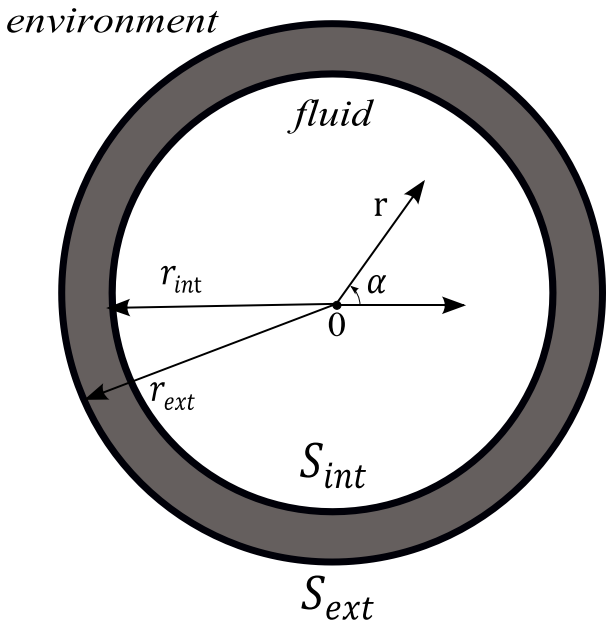

Figure 5.2: Geometrical domain with coordinate system.

5.2 TIKHONOV REGULARIZATION METHOD

It is helpful to reformulate the direct problem making explicit the local convective heat flux at the fluid-internal wall interface; under this approach the boundary condition expressed by equation (5.3) becomes:

$$-\lambda\frac{\partial T}{\partial r} = q(\alpha) \tag{5.4}$$

which is applied on surface S_{int} and where q is the local convective heat flux at the fluid-internal wall interface, assumed to be positive as it enters in the wall and to vary with the angular coordinate α.

To express the problem in the discrete domain, the convective heat flux distribution can be simplified by considering that it is described by a continuous, piecewise linear function composed of *N* sections as follows:

$$q(\alpha) = \begin{cases} b_N + \alpha \cdot \left(\dfrac{b_1 - b_N}{2\pi/N}\right), & 0 \le \alpha < \dfrac{1 \cdot 2\pi}{N} \\ b_1 + \alpha \cdot \left(\dfrac{b_2 - b_1}{2\pi/N}\right), & \dfrac{1 \cdot 2\pi}{N} \le \alpha < \dfrac{2 \cdot 2\pi}{N} \\ \cdots & \\ b_n + \alpha \cdot \left(\dfrac{b_{n+1} - b_n}{2\pi/N}\right), & \dfrac{n \cdot 2\pi}{N} \le \alpha < \dfrac{(n+1) \cdot 2\pi}{N} \\ \cdots & \\ b_{N-2} + \alpha \cdot \left(\dfrac{b_{N-1} - b_{N-2}}{2\pi/N}\right), & \dfrac{(N-2) \cdot 2\pi}{N} \le \alpha < \dfrac{(N-1) \cdot 2\pi}{N} \\ b_{N-1} + \alpha \cdot \left(\dfrac{b_N - b_{N-1}}{2\pi/N}\right), & \dfrac{(N-1) \cdot 2\pi}{N} \le \alpha < \dfrac{N \cdot 2\pi}{N} \end{cases} \tag{5.5}$$

As suggested by Beck et al. (1985) and Dennis and Dulikravich (2013), since the problem is linear with respect to the heat flux *q(α)*, it can be written in the discrete domain as follows:

$$\boldsymbol{T} = \boldsymbol{J}\boldsymbol{q} + \boldsymbol{T}_{\boldsymbol{q}=\boldsymbol{0}} \tag{5.6}$$

where **T** is the vector of the discrete temperature data at the external coil surface, **q** is the heat flux vector at the fluid-internal wall interface, $\mathbf{T_{q=0}}$ is a constant term and **J** is the sensitivity matrix.
The heat-flux vector **q** is a column vector composed by b_1, b_2, ... b_N values.
The sensitivity matrix **J** values were calculated using the two-point difference approach:

$$J_{i,j} = \frac{T_i\left(q_1\,, q_2\,, \ldots, q_j + \Delta q\,, \ldots, q_N\right) - T_i\left(q_1\,, q_2\,, \ldots, q_j\,, \ldots, q_N\right)}{\Delta q} \tag{5.7}$$

where T_i is the temperature value at the hypothetical *i* sensor position obtained by solving equations (5.1,5.2,5.4) and imposing an internal heat flux distribution as defined by equation (5.5).
In an analogous way, the constant vector was determined by imposing a null heat flux:

$$\boldsymbol{T}_{\boldsymbol{q}=\boldsymbol{0},\boldsymbol{i}} = T_i\left(q_1 = 0\,, q_2 = 0\,, \ldots, q_j = 0\,, \ldots, q_N = 0\right) \tag{5.8}$$

The direct formulation of the problem is concerned with the determination of the temperature distribution on the tube external wall when the convective heat flux vector **q** is known.

In the inverse formulation considered here, **q** is instead regarded as being unknown, whereas the surface temperature is known. The temperature distribution on the external surface of the section, **T**, can be easily computed numerically, by imposing a trial convective heat flux distribution on the internal wall side **q**.

Observing equation (5.6), it must be highlighted that the constant term $\mathbf{T_{q=0}}$ and the sensitivity matrix **J** are not functions of the unknown variable **q**, and this fact confirms that the inverse heat conduction problem investigated in this work is linear.

In the inverse formulation, this computed temperature distribution **T** is forced to match the experimental temperature distribution **Y**, by tuning the convective heat-flux distribution on the internal wall side **q**. The matching of the two temperature distributions (the computed and the experimentally acquired) could be easily performed under a least square approach. However, due to the ill-posed nature of the problem, the least square solution is generally dominated by noise, and some type of regularisation is required. The Tikhonov regularisation method is adopted: this approach makes it possible to reformulate the original problem as a well-posed problem that consists of minimising the following objective function:

$$O_f(\boldsymbol{q}) = \left\|\boldsymbol{Y} - \boldsymbol{J}\boldsymbol{q} - \boldsymbol{T}_{\boldsymbol{q}=\mathbf{0}}\right\|_2^2 + \lambda^{*2}\|\boldsymbol{L}_{\boldsymbol{d}}\boldsymbol{q}\|_2^2, \quad \lambda^* > 0 \tag{5.9}$$

where $\|\cdot\|_2^2$ stands for the square of the 2-norm, λ^* is the regularisation parameter, $\mathbf{L_d}$ is the derivative operator and **T** is the distribution of the external surface temperature derived from a direct numerical solution of the problem obtained by imposing a given convective heat flux distribution on the internal wall side **q**. Often, $\mathbf{L_d}$ is the zero, first or second derivative operator: in this work the second-order derivative formulation was chosen to preserve the local variation in the heat-flux distribution (see chapter 2).

The function expressed in equation (5.9) represents a trade-off between two optimisation processes: first, the fidelity of the fit and second the smoothness or the stability of the solution. Thus, an appropriate choice of λ^* should give an optimal balance, which in turn, should lead to a reliable approximation of the wanted solution.

As said in chapter 2, choosing a large regularisation parameter means that imposing too much regularisation on the solution prejudices the fitting of the data and the ability to obtain a great residual, whereas the absence of regularisation or an insufficiently small regularisation parameter

will provide a good fitting but also a solution affected by data errors. Therefore, the choice of a proper regularisation parameter requires a good balance between the size of the residual norm and the size of the solution norm (semi norm); this is what motivated the development of the L-curve method proposed by Hansen and O'Leary (1993). This method determines the regularisation parameter by locating the 'corner' of the parametric curve in the $\boldsymbol{u}_{\lambda^*}, \boldsymbol{v}_{\lambda^*}$ plane defined by:

$$\begin{cases} \boldsymbol{u}_{\lambda^*} = log\left(\left\|\boldsymbol{Y} - \boldsymbol{Jq} - \boldsymbol{T}_{\boldsymbol{q}=\boldsymbol{0}}\right\|_2^2\right) \\ \boldsymbol{v}_{\lambda^*} = log(\|\boldsymbol{L}_{\boldsymbol{d}}\boldsymbol{q}\|_2^2) \\ \lambda^* > 0 \end{cases} \tag{5.10}$$

The reason for this choice of the regularisation parameter is that very often this curve is L-shaped, and its corner corresponds to a parameter that produces a good balance between the residual norm and the solution norm. From a computational point of view, the 'corner' is taken to be the point on the L-curve where the curvature is maximised (Hansen and O'Leary 1993). In practice, the L-curve method has proven to produce good regularisation parameters in several cases. However, locating the corner in a robust way is not always an easy task, either because sometimes the curve displays several corners or because the corner is not visible at all. A method that has been proven to circumvent the difficulties of the L-curve method on several test problems from the literature is the fixed-point method and its variants proposed by Bazán and co-workers (Bazán 2008; Bazán and Francisco 2009; Bazán and Borges 2010). The fixed-point method requires the computation of the solution seminorm and the corresponding residual norm, and it selects the parameter that minimises the product of these norms as a function of the regularisation parameter. Like the L-curve, the reason to use this algorithm is that the sought minimiser corresponds to a good balance between the size of these norms. Algorithmically, the regularisation parameter chosen by the fixed-point method is the limit value of the sequence:

$$\lambda^*_{k+1} = \phi(\lambda^*_k) = \frac{\left\|\boldsymbol{Y} - \boldsymbol{Jq} - \boldsymbol{T}_{\boldsymbol{q}=\boldsymbol{0}}\right\|_2}{\|\boldsymbol{L}_{\boldsymbol{d}}\boldsymbol{q}\|_2}, k = 0,1,2,\ldots \tag{5.11}$$

The value for the regularisation parameter can also be visually represented as a fixed-point of the curve $\phi(\lambda^*)$.

In practice, the sequence converges very quickly, and the computed regularisation parameter yields solutions with accuracy comparable to that of the L-curve method, but it is more robust and less computationally expensive (Bazán 2008; Bazán and Francisco 2009).

In this work, the regularised solution $\boldsymbol{q}_{\lambda^*}$ is computed efficiently by means of the GSVD of the matrix pair $\{\mathbf{J}, \mathbf{L_d}\}$, which simplifies enormously the implementation of the fixed-point algorithm according to Bazán (2008).

A very positive thing is that like the L-curve approach, the fixed-point method does not require *a priori* knowledge of the noise level. Instead if the noise level that affect the measurement is known it is possible to use others method for the choice of the regularization parameter.

For instancee in this work it is also used the discrepancy principle as criterion of choice in order to make more consistent the comparison with the two other IHCP solution techniques.

Once the heat-flux distribution at the fluid-wall interface compatible with the experimental temperature data has been determined through the strategy described above, the local convective heat-transfer coefficient can be easily determined, as follows:

$$h_{int}(\alpha) = \frac{-q(\alpha)}{T(r = r_{int}, \alpha) - T_b} \tag{5.12}$$

where *q(α)* is the heat flux distribution estimated under the solution approach based on the Tikhonov regularisation method with the support of fixed-point iteration techniques, T_b is the bulk-fluid temperature on the test section, calculated from the energy balance on the heated section and $T(r = r_{int}, \alpha)$ is temperature distribution on the tube internal wall efficiently estimated by numerically solving the direct problem expressed by equations (5.1, 5.2, 5.4) by imposing a convective heat flux equal to *q(α)*.

The convective heat transfer coefficient can be suitably expressed in a dimensionless form by means of the local Nusselt number, as follows:

$$Nu(\alpha) = \frac{h_{int}(\alpha) \cdot D_{int}}{\lambda} \tag{5.13}$$

where λ in this expression represents the fluid thermal conductivity, evaluated at the bulk temperature.

5.2.1 Numerical Validation

By imposing a known distribution of $h_{int}(\alpha)$ and by numerically solving the direct problem expressed by equations (5.1-5.4) within the Comsol Multiphysics® environment adopting a 2596 triangular element mesh, a synthetic temperature distribution on the external wall surface was obtained. The physical and geometrical parameters used in the numerical validation are the same of the experimental study and thus correspond to a stainless steel tube AISI 304 with an internal radius of 7 mm and an external radius of 8 mm. For the local convective heat transfer coefficient a distribution $h_{int}{}^{(J)}$ according to Jayakumar et al. (2010) and shown in figure 5.3 was adopted. This distribution, corresponding to the thermally fully developed region in a coiled tube, was derived by numerical simulations performed under the turbulent flow regime and it shows a significant variation along the curvilinear coordinate.

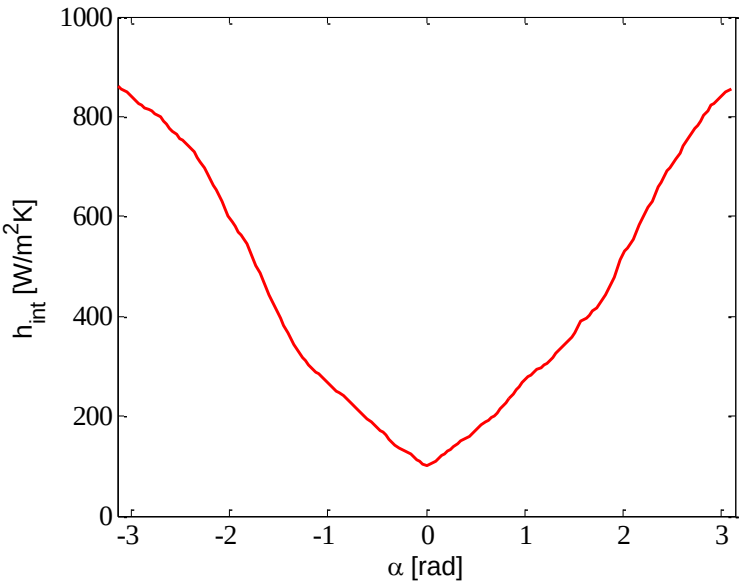

Figure 5.3: Distribution of the local convective heat transfer coefficient $h_{int}{}^{(J)}$ (Jayakumar et al. 2010).

Then the synthetic temperature distribution on the external wall surface, deliberately spoiled by random noise, was used as the input data of the inverse problem (see for instance figure 5.4). In particular, a white noise characterized by a standard deviation ranging from 0.01 K - 10 K was considered. The $h_{int}(\alpha)$ distribution found by solving IHCP was then compared to the distribution used in the direct problem to generate the synthetic temperature in order to evaluate the effectiveness of the parameter estimation procedure.

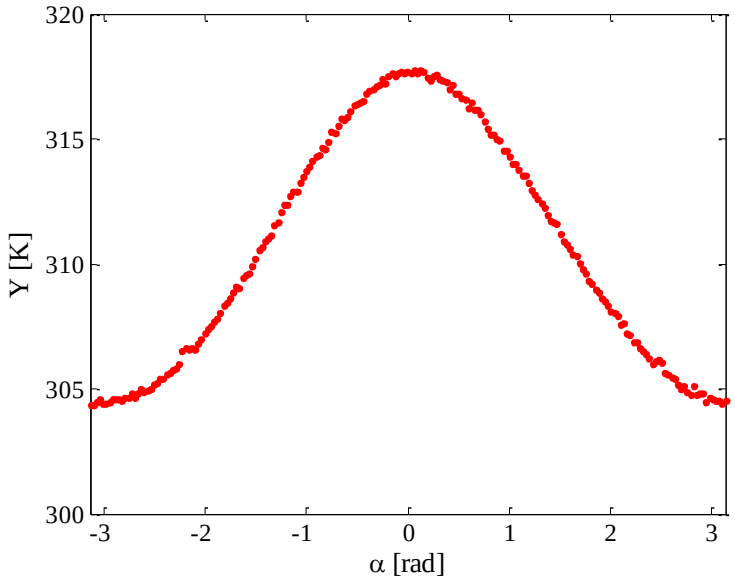

Figure 5.4: Synthetic temperature distribution on the external wall surface adopted as input data for the model validation for noise level $\sigma = 0.1K$.

In figure 5.5 the fixed point analysis for the noise level $\sigma = 0.1K$ is shown. Following the above described fixed point method, the optimal value of $\lambda^* = 1.3 \cdot 10^{-4}$ was identified. In figure 5.6 the heat transfer coefficient distribution, obtained by adopting the regularization parameter $\lambda^* = 1.3 \cdot 10^{-4}$, is reported and compared with the exact value.

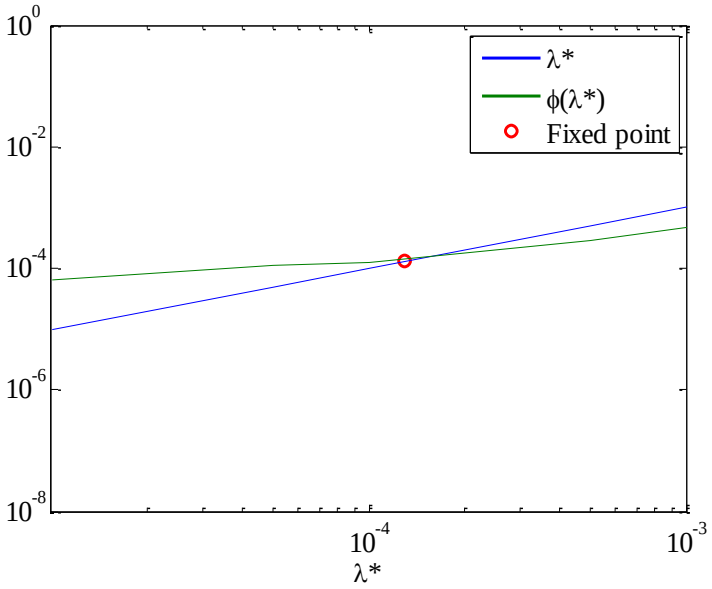

Figure 5.5: Fixed point analysis for noise level $\sigma = 0.1$K.

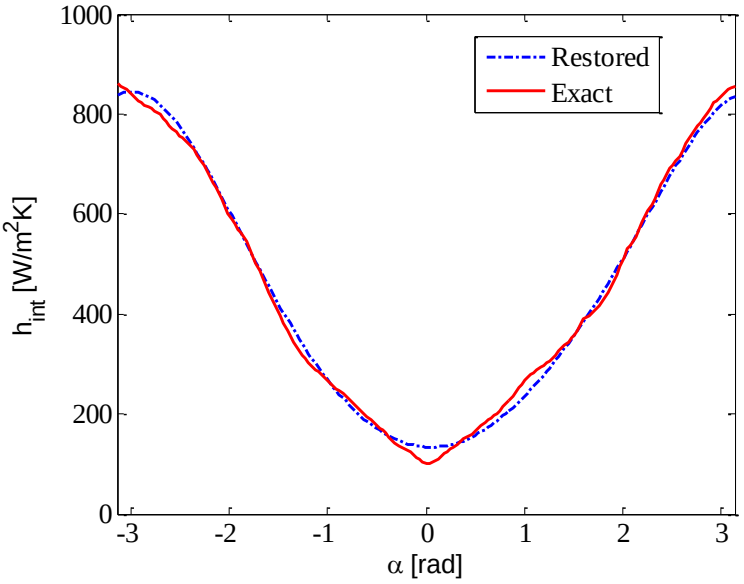

Figure 5.6: Exact and reconstructed $h_{int}{}^{(J)}$ distribution obtained by Tikhonov Regularization Method for noise level $\sigma = 0.1\ K$ and $\lambda^* = 1.3 \cdot 10^{-4}$.

The reconstructed values matches with a good approximation the original local convective heat transfer distribution by showing the effectiveness of the procedure before explained.

In figure 5.7 the restored temperature distribution resulting from minimization procedure, performed by assuming $\lambda^* = 1.3 \cdot 10^{-4}$, is reported.

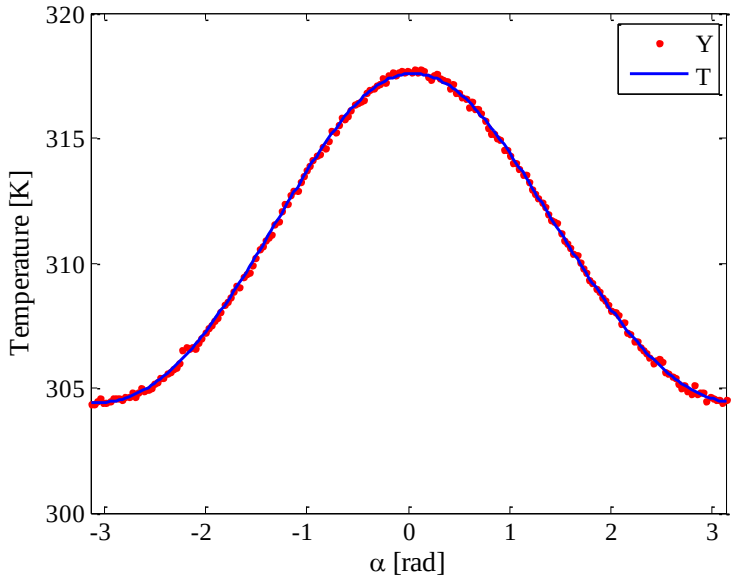

Figure 5.7: Noisy input (Y) and reconstructed (T) temperature distribution for noise level $\sigma = 0.1\ K$ and $\lambda^* = 1.3 \cdot 10^{-4}$.

The corresponding residuals between the input and the reconstructed temperature were reported in figure 5.8.

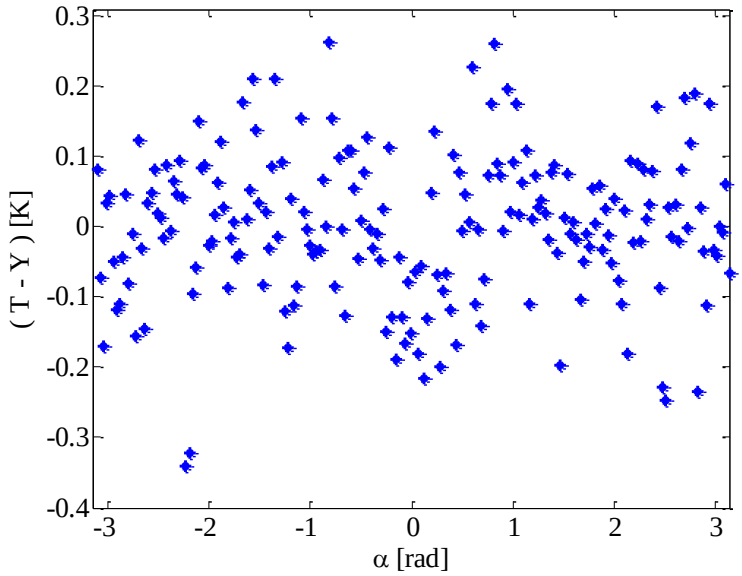

Figure 5.8: Residuals between the input (Y) and the reconstructed (T) temperature for noise level $\sigma = 0.1$K (TRM).

The random distribution of the residuals confirm the good performance of the estimation procedure: just a limited drift is notable close to $\alpha = 0$. As already said, the smoothness is controlled by the choice of the regularization parameter: if it is not the correct one and the signal to noise ratio is particularly critical, the problem's ill-posed nature could lead to an incorrect solution. For instance by considering the values of $\lambda^* = 10^{-7}$ and $\lambda^* = 10^{-1}$, that represents two generic extreme values, the local convective heat transfer coefficient obtained from minimization of the function given by equation (5.9) doesn't match the exact distribution as it is shown in figures 5.9 and 5.10.

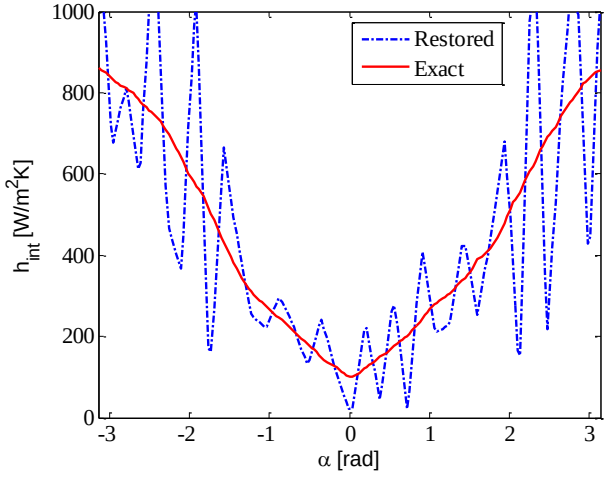

Figure 5.9: Exact and restored $h_{int}{}^{(J)}$ distribution obtained by Tikhonov Regularization Method for noise level $\sigma = 0.1$K and $\lambda^* = 10^{-7}$.

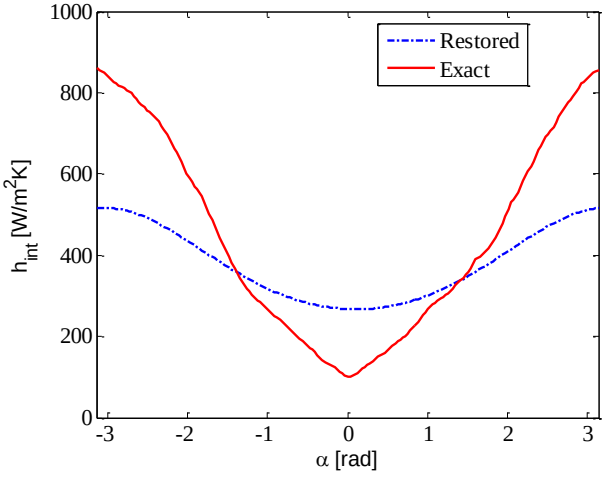

Figure 5.10: Exact and restored $h_{int}{}^{(J)}$ distribution obtained by Tichonov Regularization Method for noise level $\sigma = 0.1$K and $\lambda^* = 10^{-2}$.

In both cases ($\lambda^* = 10^{-7}$ and $\lambda^* = 10^{-2}$) the parameter estimation procedure fails by proving that the selection of the regularization parameter is a critical task within Tikhonov regularization: if it is too small the filtering of the raw signal is too weak, while if it is too large the regularized solution is over-smoothed.

In figures 5.11 and 5.12 the exact and restored convective heat transfer coefficient and the corresponding residuals between the input and the reconstructed temperature were reported for other two representative noise levels for $h_{int}{}^{(J)}$ distribution.

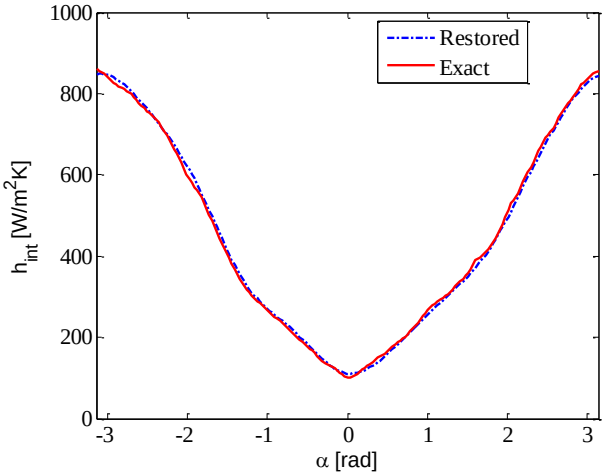

Figure 5.11a: Exact and restored $h_{int}{}^{(J)}$ distribution obtained by Tikhonov Regularization Method for noise level $\sigma = 0.01$K.

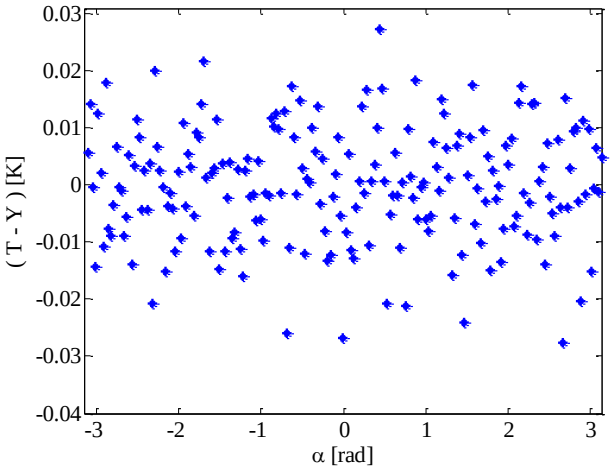

Figure 5.11b: Residuals between the input (Y) and the reconstructed (T) temperature for noise level $\sigma = 0.01$K (TRM).

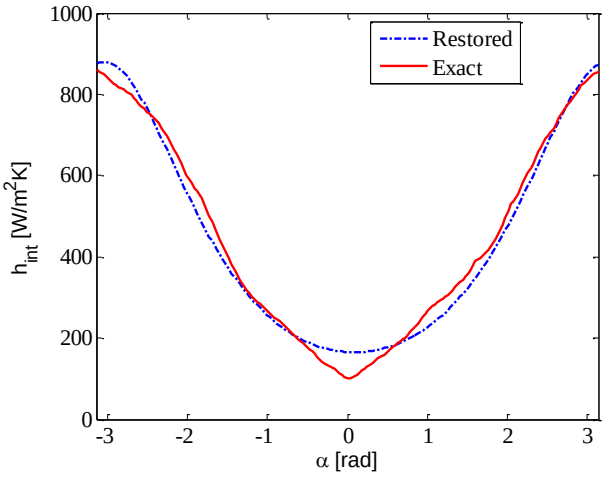

Figure 5.12a: Exact and restored $h_{int}{}^{(J)}$ distribution obtained by Tikhonov Regularization Method for noise level $\sigma = 1$K.

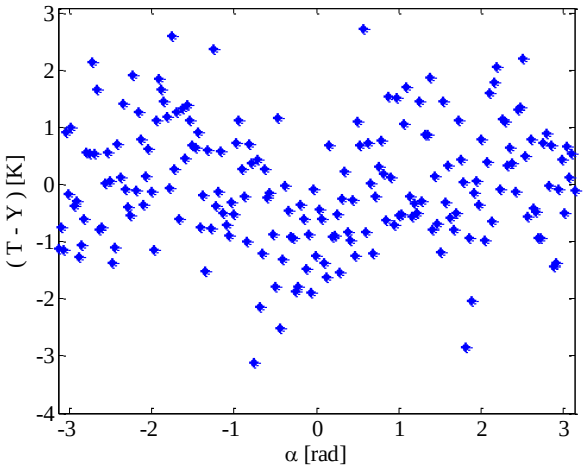

Figure 5.12b: Residuals between the input (Y) and the reconstructed (T) temperature for noise level $\sigma = 1$K (TRM).

As it is possible to see from figures 5.6-5.8, 5.11 and 5.12 the convective heat transfer coefficient reconstruction is very effective for small noise level: in particular for noise $\sigma = 0.01$K the restoration is really good and the fact that the residuals are randomly distributed confirms the excellent performance. The growing of the noise level is followed by a loose of information in particular in correspondence of the peak: if for noise $\sigma = 0.1$K it is still almost negligible, for noise $\sigma = 1$K it becomes significant. This fact is confirmed by the distribution of the residuals: they are not randomly distributed as happened for the other two levels of noise considered. It is evident in figure 5.12b a drift of the trend of the residual, once it is coming closer to $\alpha = 0$.

5.3 GAUSSIAN FILTER TECHNIQUE

In the inverse formulation considered here, h_{int} is regarded as being unknown, whereas the surface temperature is measured. A simplified numerical model of the test section (sketched in figure 5.2), formulated by assuming thin wall approximation, was considered. This assumption is fully acceptable when Biot number, defined as the convective heat transfer coefficient multiplied for the tube thickness dived for tube thermal conductivity, is smaller than 0.1 (Incoprera and De Witt 2002). Considering this assumption, the temperature on the external surface can be considered equal to the one on the internal surface:

$$T(\alpha, r) \cong T(\alpha, r_{int}) \cong T(\alpha, r_{ext}) \tag{5.14}$$

As a consequence of this assumption, the wall temperature in the test section was a function of the angular coordinate, α, only. Moreover, if the gradient of the wall heat flux along the tube axis is negligible, a further simplification to the estimation procedure is permitted:

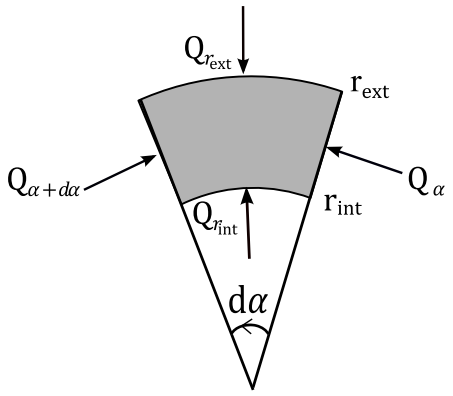

Figure 5.13: A portion of the test section.

Under this approach, with reference to the infinitesimal circular sector shown in figure 5.13, where r_{int} and r_{ext} are the inside and the outside pipe radius, respectively, and the heat is considered positive as entering, the steady state local energy balance equation becomes:

$$Q_{\alpha+d\alpha} + Q_{\alpha} + Q_{r_{int}} + Q_{r_{ext}} + Q_g = 0 \tag{5.15}$$

where:

$$Q_{\alpha} = \int_{r_{int}}^{r_{ext}} -\frac{\lambda dT}{r d\alpha} dr = -\lambda \frac{dT}{d\alpha} \cdot ln\left(\frac{r_{ext}}{r_{int}}\right) \tag{5.16}$$

$$\begin{aligned} Q_{\alpha+d\alpha} = -\left(Q_{\alpha} + \frac{dQ_{\alpha}}{d\alpha} d\alpha\right) = -\left[-\lambda \frac{dT}{d\alpha} \cdot ln\left(\frac{r_{ext}}{r_{int}}\right) + \frac{d}{d\alpha}\left(-\lambda \frac{dT}{d\alpha} \cdot ln\left(\frac{r_{ext}}{r_{int}}\right)\right) d\alpha\right] = \\ = \lambda \frac{dT}{d\alpha} \cdot ln\left(\frac{r_{ext}}{r_{int}}\right) + \lambda \cdot ln\left(\frac{r_{ext}}{r_{int}}\right) \frac{d^2T}{d\alpha^2} d\alpha \end{aligned} \tag{5.17}$$

$$Q_{r_{int}} = -h_{int}\,(T - T_b) \cdot r_{int} \cdot d\alpha \tag{5.18}$$

$$Q_{r_{ext}} = -\frac{(T - T_{env})}{R_{env}} \cdot r_{ext} \cdot d\alpha \tag{5.19}$$

$$Q_g = q_g \frac{(\pi r_{ext}^2 - \pi r_{int}^2)}{2\pi} d\alpha = \frac{q_g}{2} \cdot (r_{ext}^2 - r_{int}^2) d\alpha \tag{5.20}$$

and where T_b is the bulk temperature, R_{env} the overall heat transfer resistance between the external tube wall and the surrounding environment, whose temperature is T_{env}, q_g the heat generated per unit volume within the tube wall having thermal conductivity λ.
Substituting equations (5.16-5.20) into equation (5.15) the energy equation becomes:

$$\lambda \cdot ln\left(\frac{r_{ext}}{r_{int}}\right) \frac{d^2T}{d\alpha^2} d\alpha - h_{int}\,(T - T_b) \cdot r_{int} \cdot d\alpha - \frac{(T - T_{env})}{R_{env}} \cdot r_{ext} \cdot d\alpha + \frac{q_g}{2} \cdot (r_{ext}^2 - r_{int}^2) d\alpha = 0 \tag{5.21}$$

Therefore, the convective heat transfer coefficient on the internal wall surface is as follows:

$$h_{int} = \frac{\lambda \cdot ln\left(\frac{r_{ext}}{r_{int}}\right) \cdot \frac{d^2T}{d\alpha^2} - r_{ext} \cdot \frac{(T - T_{env})}{R_{env}} + \frac{q_g}{2} \cdot (r_{ext}^2 - r_{int}^2)}{r_{int} \cdot (T - T_b)} \tag{5.22}$$

In order to estimate the convective heat transfer coefficient from equation (5.22), it is necessary to compute the second derivative of the measured temperature distribution.

The n^{th} derivative is a linear operator that behaves as a filtering operator with a gain which amplifies the high frequency components of a given set of input data more than the low ones. In almost all practical situations regarding heat transfer, the exact signal has frequency components concentrated in the low frequency range of the spectrum, while the noise, usually being Gaussian, is uniformly distributed in the space and in the frequency domain as well (Bozzoli and Rainieri 2011). Therefore, the direct calculation of the Laplacian of the raw data is unfeasible, due to the noise that strongly affects them. An effective approach to handle the ill-posed nature of the IHCP is represented by applying to the raw input temperature data some suitable filtering technique. In order to reconstruct the second derivative of the signal, the Gaussian filter was here employed. The transfer function of the Gaussian filter in the 1-D frequency domain can be expressed as follows:

$$H(u) = e^{-(u_f)^2/2{u_c}^2} \tag{5.23}$$

where u_f is the frequency and u_c is the cutoff frequency value, as exemplified in figure 5.14.

The proper choice of the cutoff frequency is recognized as a critical issue (Bozzoli et al. 2013).

In this work, to choose the appropriate cutoff frequency, the criterion provided by the discrepancy principle, originally formulated by Morozov (1984) was adopted. According to this criterion, the solution of the inverse problem is assumed to be satisfactorily accurate when the difference between filtered, $\boldsymbol{Y_f}$, and measured, $\boldsymbol{Y}$, temperature distributions is close to the standard deviation of the raw data, σ. Consequently, the determination of the cutoff frequency was effectuated by checking the function reported below, by varying the cutoff frequency value:

$$E_d(u_c) = \frac{\left\|(\boldsymbol{Y_f} - \boldsymbol{Y})\right\|_2}{\sqrt{N}} \tag{5.24}$$

where $\|\cdot\|_2$ is the Euclidean norm and N is the size of the vector $\boldsymbol{Y}$.

The cutoff frequency was selected as the frequency at which:

$$E_d(u_c) \cong \sigma \tag{5.25}$$

In other words, the discrepancy principle tailors the filter according to the noise level, which means that the best approximation one should expect is in the order of the data random error.

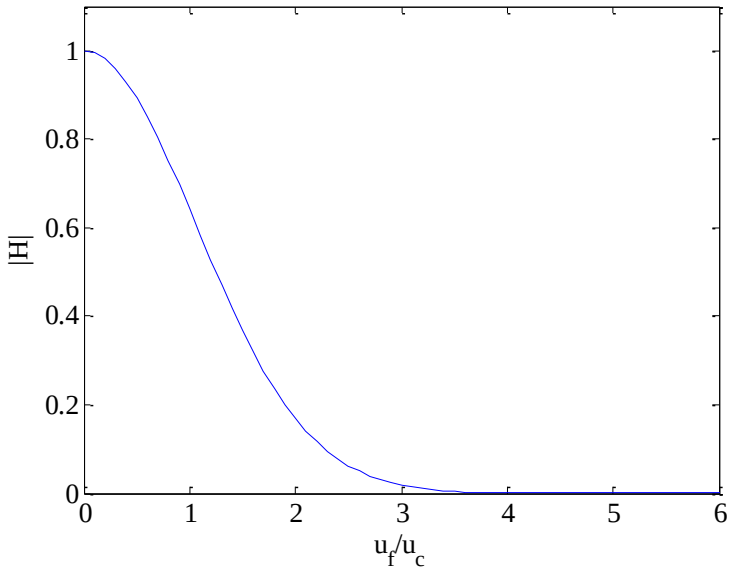

Figure 5.14: Transfer function of the Gaussian filter.

5.3.1 Numerical Validation

The same synthetic data used for the Tikhonov regularization method were employed here as input data of the inverse problem. The calculation of the Temperature laplacian is mandatory to determine heat transfer coefficient distribution as it is possible to see from equation 5.22: but without filtering, as it is shown in figure 5.26, the noise of the rough data prevent the reconstruction of the desired function.

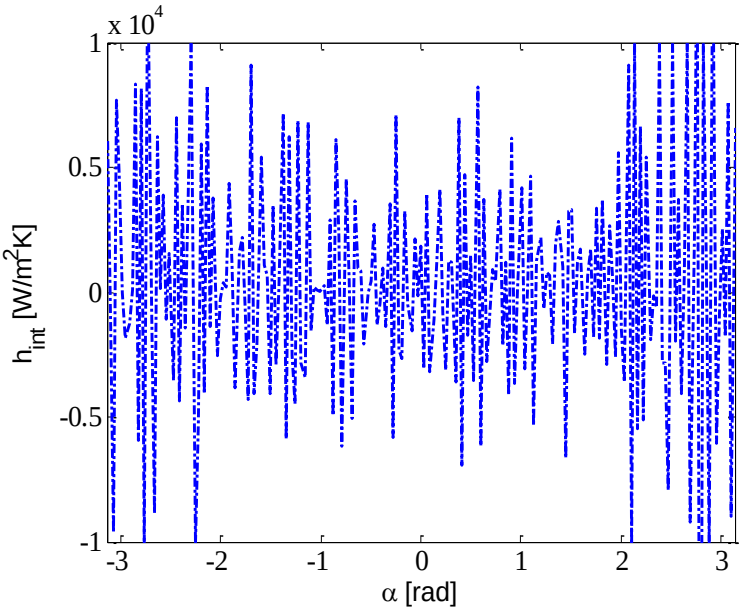

Figures 5.15: Restored $h_{int}{}^{(J)}$ distribution obtained without filtering for noise level $\sigma = 0.1$K.

Consequently it is necessary to apply a careful filtration of the measured temperature.

The interception of the curve representing E_d as a function of the cutoff frequency with the considered σ identifies the cutoff frequency as approximately $0.16\ \mathrm{rad}^{-1}$.

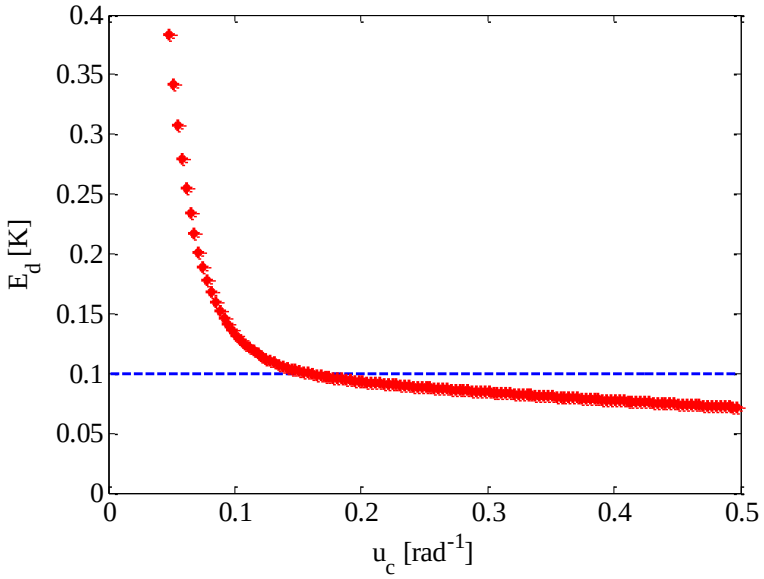

Figure 5.16: Function E_d against the cutoff frequency for noise level $\sigma = 0.1$K.

In figure 5.17 the heat transfer coefficient distribution, obtained by adopting the cutoff frequency $u_c = 0.16\ \mathrm{rad}^{-1}$, is reported and compared with the exact value.

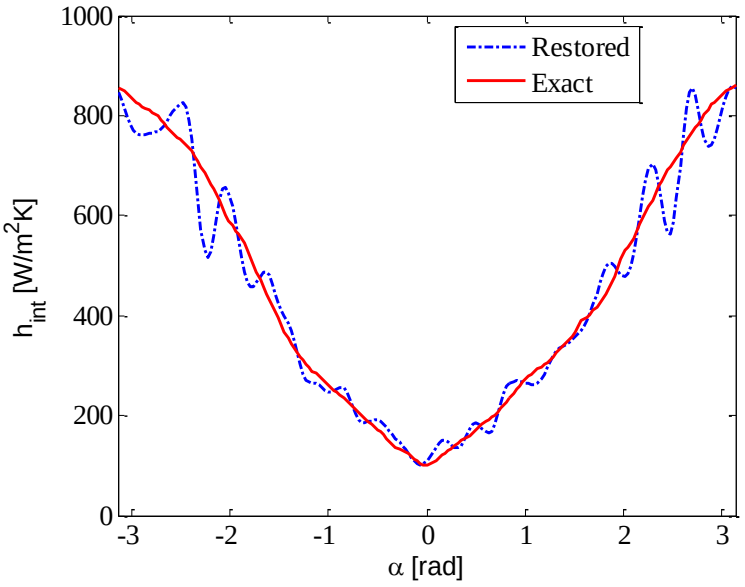

Figure 5.17: Exact and restored $h_{int}{}^{(J)}$ distribution obtained by Gaussian Filter Technique for noise level $\sigma = 0.1\ K$ and $u_c = 0.16\ \mathrm{rad}^{-1}$.

The reconstructed values matches with a satisfactorily approximation the original local convective heat transfer distribution even if the restored distribution is not as smooth as the one obtain with the previous described estimation method: the distribution trend is restored but some oscillations remain in the solution. In figure 5.18 the filtered temperature distribution performed by assuming $u_c = 0.16\ \text{rad}^{-1}$, is shown.

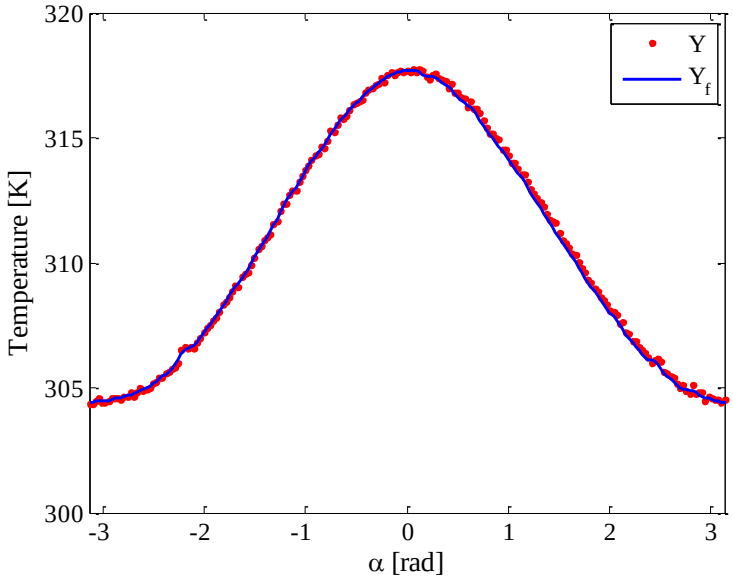

Figure 5.18: Noisy input (Y) and filtered (Y_f) temperature distribution for noise level $\sigma = 0.1\ K$ and $u_c = 0.16\ \text{rad}^{-1}$.

The corresponding residuals between the input and the filtered temperature were reported in figure 5.19.

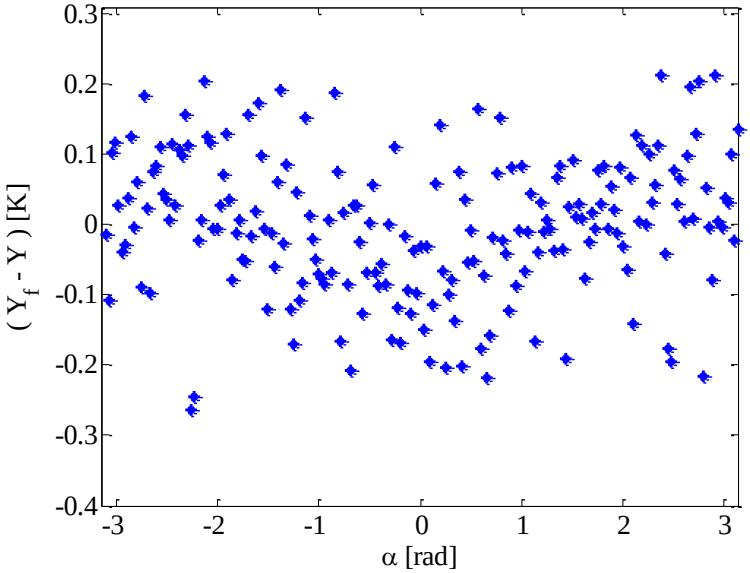

Figure 5.19: Residuals between the input (Y) and the filtered (Y_f) temperature for noise level $\sigma = 0.1$K (GFT).

The distribution of the residuals add other information to the performances of the estimation procedure presented in this paragraph: the residuals, in fact, are not exactly randomly distributed and a "v-shape" could be identified in their distribution. It highlights the fact that the GFT tends to excessively smoothen the temperature distribution, especially in correspondence of the peak.

The selection of the proper cutoff frequency is fundamental to find the correct solution as the choice of the regularization parameter λ^* was determinant for the TRM. For instance by taking into account the values of $u_c = 10^{-2}$ and $u_c = 0.35$, that represent two generic extreme values, the restored local convective heat transfer coefficient doesn't match the exact distribution, as it is shown in figures 5.20 and 5.21.

Instead of the Tikhonov estimation procedure where choosing a too large regularization parameter means to impose too much regularization, here the same effect is reached by using a too small value of cutoff frequency: this happens because if we choose a small value of u_c we are cutting more harmonics than for a higher value of cutoff frequency eliminating in this way more information. On the other hand selecting a too high value of u_c will bring to a not sufficient filtering of the signal conserving a lot of noise in the results.

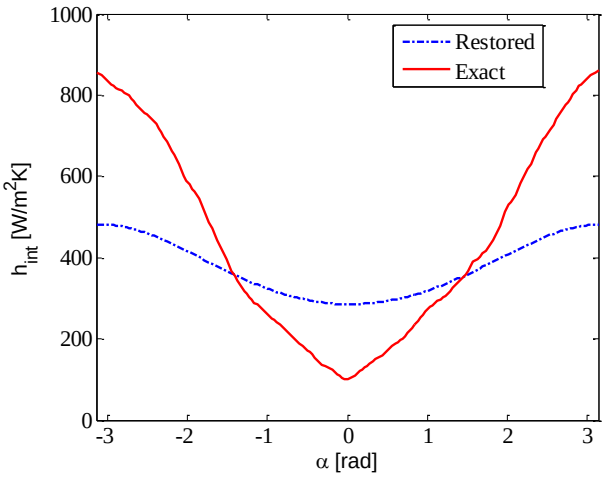

Figure 5.20: Exact and restored $h_{int}{}^{(J)}$ distribution obtained by Gaussian Filter Technique for noise level $\sigma = 0.1\ K$ and $u_c = 0.01\ \text{rad}^{-1}$.

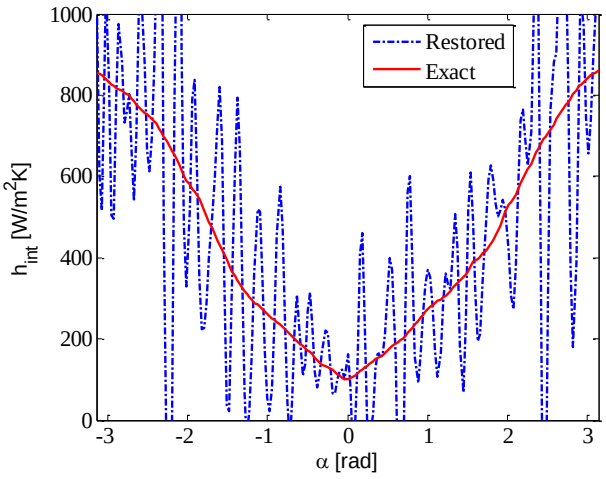

Figure 5.21: Exact and restored $h_{int}{}^{(J)}$ distribution obtained by Gaussian Filter Technique for noise level $\sigma = 0.1\ K$ and $u_c = 0.35\ \text{rad}^{-1}$.

These consideration will put the accent on the importance of a correct determination of the cutoff frequency: the estimation could be as much as possible robust but without a proper choice of u_c it is impossible to obtain a significant result.

In figures 5.22 and 5.23 the exact and restored convective heat transfer coefficient distribution and the corresponding residuals between the input and the filtered temperature were reported for other two representative noise levels for $h_{int}{}^{(J)}$ distribution.

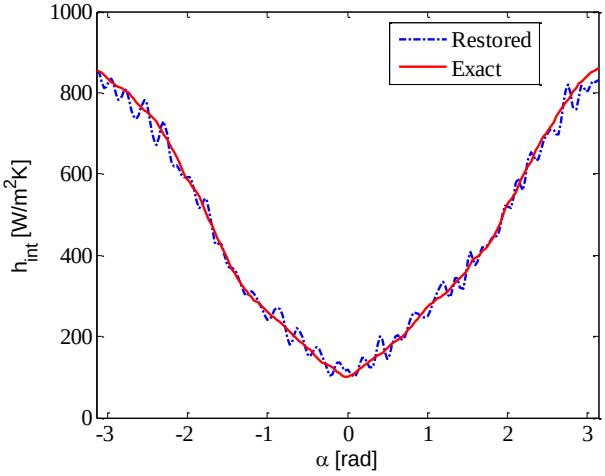

Figure 5.22a: Exact and restored $h_{int}{}^{(J)}$ distribution obtained by Gaussian Filter Technique for noise level $\sigma = 0.01$K.

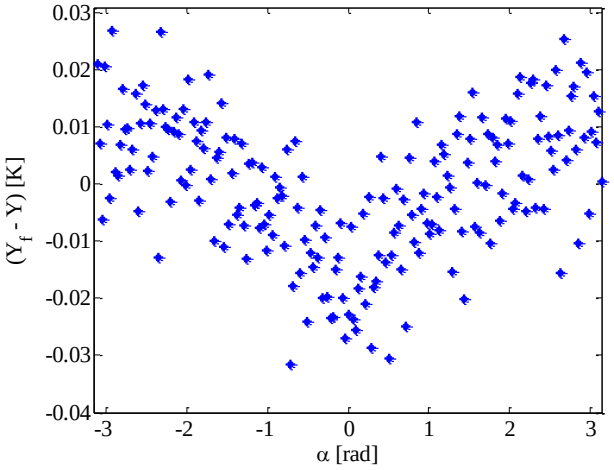

Figure 5.22b: Residuals between the input (Y) and the filtered (Y_f) temperature for noise level $\sigma = 0.01$K (GFT).

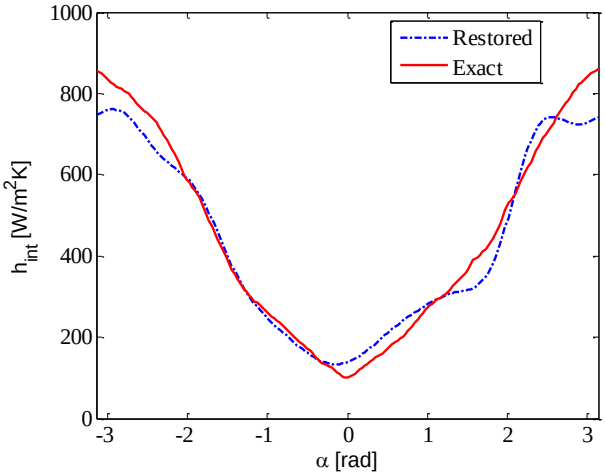

Figure 5.23a: Exact and restored $h_{int}{}^{(J)}$ distribution obtained by Gaussian Filter Technique for noise level $\sigma = 1$K.

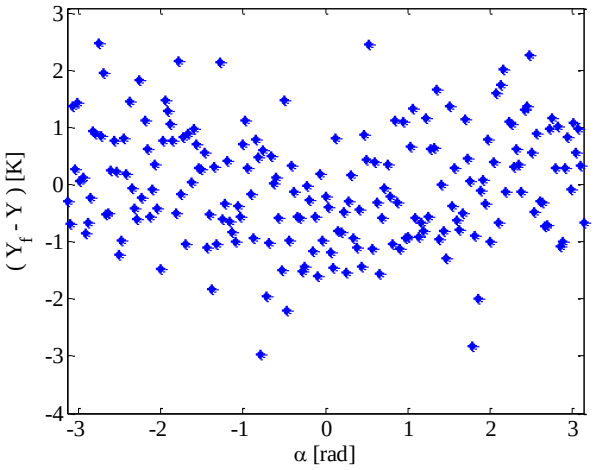

Figure 5.23b: Residuals between the input (Y) and the filtered (Y_f) temperature for noise level $\sigma = 1$K (GFT).

The results, reported in figures 5.17, 5.19, 5.22 and 5.23, underline that the Gaussian filtering technique reconstructs the convective heat transfer coefficient in an good way for small noise level while, for high noise levels, the estimation is globally correct but the reconstruction is less accurate. The residuals distributions obtained for the three different noise levels confirm that in

correspondence of the lowest value of $h_{int}{}^{(J)}$ distribution, the GFT tends to oversmooth the temperature distribution.

5.4 QUADRUPOLE METHOD

To apply the Quadrupole Method to the considered problem, the direct problem has to be formulated making explicit the local convective heat flux at the fluid-internal wall interface as it is in the boundary condition expressed by equation (5.4).

The Quadrupole method will be used here in cylindrical geometry where a Fourier transformation in the angular direction will be implemented.

However, this approach does not completely bypass all the difficulties embedded in the IHCP, in particular it does not solve the complications due to the ill-conditioned character of the problem. In order to bypass this crucial issue, the Truncated Singular Value Decomposition (TSVD) could be adopted.

5.4.1 Direct problem

The Quadrupole Method is firstly applied to the direct problem. By setting the relative temperature $\theta = T - T_{env}$ and $q(r,\alpha) = -\lambda\frac{\partial\theta}{\partial r}$, periodicity conditions can be written for both the temperature and the radial flux:

$$\theta(r,\alpha+2\pi) = \theta(r,\alpha)$$
$$q(r,\alpha+2\pi) = q(r,\alpha) \tag{5.26}$$

In order to find the solution of this problem the Fourier integral transform method is applied. Equation (5.1) is then transformed as follows:

$$\mathcal{F}\left(\frac{\partial^2\theta}{\partial r^2}\right) + \mathcal{F}\left(\frac{1}{r}\frac{\partial\theta}{\partial r}\right) + \mathcal{F}\left(\frac{1}{r^2}\frac{\partial\theta^2}{\partial\alpha^2}\right) + \mathcal{F}\left(\frac{q_g}{\lambda}\right) = 0 \tag{5.27}$$

where the Fourier and its inverse transforms are defined as:

$$\tilde{\theta}_n(r) = \mathcal{F}(\theta) = \int_{-\pi}^{\pi} \theta(r,\alpha) e^{-in\alpha}\, d\alpha \tag{5.28}$$

$$\theta(r,\alpha) = \mathcal{F}^{-1}(\theta) = \frac{1}{2\pi} \sum_{n=-\infty}^{\infty} \tilde{\theta}_n(r) e^{in\alpha} \tag{5.29}$$

with *n*, is any positive, zero or negative integer. The four terms of the above equation have been developed separately for the two cases n≠0 and n=0.

First case: n≠0

The four terms of equation (5.27) are developed separately, by integration by parts and by imposing the periodicity conditions expressed in equation (5.26), as follows:

$$\mathcal{F}\left(\frac{\partial^2\theta}{\partial r^2}\right) = \int_{-\pi}^{\pi} \frac{\partial^2\theta}{\partial r^2} e^{-in\alpha}\, d\alpha = \frac{\partial^2}{\partial r^2} \int_{-\pi}^{\pi} \theta \cdot e^{-in\alpha}\, d\alpha = \frac{d^2\tilde{\theta}_n}{dr^2} \tag{5.30}$$

$$\mathcal{F}\left(\frac{1}{r}\frac{\partial\theta}{\partial r}\right) = \int_{-\pi}^{\pi} \frac{1}{r}\frac{\partial\theta}{\partial r} e^{-in\alpha}\, d\alpha = \frac{1}{r}\frac{\partial}{\partial r} \int_{-\pi}^{\pi} \theta \cdot e^{-in\alpha}\, d\alpha = \frac{1}{r}\frac{d\tilde{\theta}_n}{dr} \tag{5.31}$$

$$\begin{aligned}
\mathcal{F}\left(\frac{1}{r^2}\frac{\partial\theta^2}{\partial\alpha^2}\right) &= \int_{-\pi}^{\pi} \frac{1}{r^2}\frac{\partial\theta^2}{\partial\alpha^2} e^{-in\alpha}\, d\alpha = \frac{1}{r^2}\left[\frac{\partial\theta}{\partial\alpha} e^{-in\alpha} - \int_{-\pi}^{\pi} (-in)\cdot\frac{\partial\theta}{\partial\alpha} e^{-in\alpha}\, d\alpha\right] \\
&= \frac{1}{r^2}\left[\frac{\partial\theta}{\partial\alpha} e^{-in\alpha} - \left(-in\theta e^{-in\alpha} - \int_{-\pi}^{\pi} i^2 n^2 \cdot \theta e^{-in\alpha}\, d\alpha\right)\right] \\
&= \frac{1}{r^2}\left[\frac{\partial\theta}{\partial\alpha} e^{-in\alpha}\Big|_{\alpha=\pi} - \frac{\partial\theta}{\partial\alpha} e^{-in\alpha}\Big|_{\alpha=-\pi} + in\theta e^{-in\alpha}\Big|_{\alpha=\pi}\right. \\
&\left. - in\theta e^{-in\alpha}\Big|_{\alpha=-\pi} - n^2\theta_n\right] \theta_n = -\frac{n^2}{r^2}\tilde{\theta}_n
\end{aligned} \tag{5.32}$$

$$\begin{aligned}
\mathcal{F}\left(\frac{q_g}{\lambda}\right) &= \int_{-\pi}^{\pi} \frac{q_g}{\lambda}\, e^{-in\alpha}\, d\alpha \\
&= -\frac{q_g}{in\lambda} \int_{-\pi}^{\pi} (-in) e^{-in\alpha}\, d\alpha = -\frac{q_g}{in\lambda}\left[e^{-in\pi} - e^{in\pi}\right] \\
&= \frac{2q_g}{in\lambda}\left[\frac{e^{in\pi} - e^{-in\pi}}{2}\right] = \frac{2q_g \sinh(in\pi)}{in\lambda} = \frac{2q_g \sin(n\pi)}{n\lambda} = 0
\end{aligned} \tag{5.33}$$

Equation (5.1) transformed in the Fourier domain becomes then:

$$\frac{d^2\tilde{\theta}_n}{dr^2}+\frac{1}{r}\frac{d\tilde{\theta}_n}{dr}-\frac{n^2}{r^2}\tilde{\theta}_n=0 \tag{5.34}$$

The general solution of equation (5.34) is given in the form:

$$\tilde{\theta}_n(r)=C_1r^n+C_2r^{-n} \tag{5.35}$$

where C_1 and C_2 are arbitrary constants.

The product of the local radial heat flux $q(r,\alpha)$ by the perimeter can also been transformed in the Fourier domain and it could be obtained from the derivation of equation (5.35) as follows:

$$\tilde{q}_n(r)=\int_{-\pi}^{\pi}q(r,\alpha)\ 2\pi r\ e^{-in\alpha}\,d\alpha\ =\int_{-\pi}^{\pi}2\pi r\left(-\lambda\frac{\partial\theta}{\partial r}\right)e^{-in\alpha}\,d\alpha\ =-2\pi r\lambda\frac{d\tilde{\theta}_n}{dr} \tag{5.36}$$

Using equation (5.35), this yields:

$$\tilde{q}_n(r)=-2\pi\lambda nC_1r^n+2\pi\lambda nC_2r^{-n} \tag{5.37}$$

From the definition of transformed temperature and transformed heat flux, given respectively by equations (5.35) and (5.37), for $r=r_{int}$ and $r=r_{ext}$ expressed as follows:

$$\begin{cases}\tilde{\theta}_n^{int}=C_1r_{int}^n+C_2r_{int}^{-n}\\ \tilde{q}_n^{int}=-2\pi\lambda nC_1r_{int}^n+2\pi\lambda nC_2r_{int}^{-n}\end{cases} \tag{5.38}$$

$$\begin{cases}\tilde{\theta}_n^{ext}=C_1r_{ext}^n+C_2r_{ext}^{-n}\\ \tilde{q}_n^{ext}=-2\pi\lambda nC_1r_{ext}^n+2\pi\lambda nC_2r_{ext}^{-n}\end{cases} \tag{5.39}$$

it is possible to obtain the expression of C_1 and C_2:

$$\begin{cases}C_1=\dfrac{\frac{\tilde{\theta}_n^{int}}{2}-\frac{\tilde{q}_n^{int}}{4\pi\lambda n}}{r_{int}^n}\\ C_2=\dfrac{\tilde{q}_n^{int}}{4\pi\lambda n}r_{int}^n+\dfrac{\tilde{\theta}_n^{int}}{2}r_{int}^n\end{cases} \tag{5.40}$$

Then substituting equation (5.40) in the equation (5.39) it is possible to obtain:

$$\begin{cases} \tilde{\theta}_n^{ext} = \dfrac{\tilde{\theta}_n^{int}}{2} \cdot \left[\left(\dfrac{r_{ext}}{r_{int}}\right)^n + \left(\dfrac{r_{int}}{r_{ext}}\right)^n\right] + \dfrac{\tilde{q}_n^{int}}{4\pi\lambda n} \cdot \left[\left(\dfrac{r_{int}}{r_{ext}}\right)^n - \left(\dfrac{r_{ext}}{r_{int}}\right)^n\right] \\ \tilde{q}_n^{ext} = \pi\lambda n\, \tilde{\theta}_n^{int} \cdot \left[\left(\dfrac{r_{int}}{r_{ext}}\right)^n - \left(\dfrac{r_{ext}}{r_{int}}\right)^n\right] + \dfrac{\tilde{q}_n^{int}}{2} \cdot \left[\left(\dfrac{r_{ext}}{r_{int}}\right)^n + \left(\dfrac{r_{int}}{r_{ext}}\right)^n\right] \end{cases} \tag{5.41}$$

Now it is possible to build a matrix that expresses the relation between columns vectors composed of transforms of temperature and local heat flux written for the two radii r_{ext} and r_{int} in the solid wall:

$$\begin{bmatrix} \tilde{\theta}_n \\ \tilde{q}_n \end{bmatrix}_{ext} = \boldsymbol{W_n} \begin{bmatrix} \tilde{\theta}_n \\ \tilde{q}_n \end{bmatrix}_{int} \tag{5.42}$$

with $\boldsymbol{W_n}$=$\begin{bmatrix} W_{n_{11}} & W_{n_{12}} \\ W_{n_{21}} & W_{n_{22}} \end{bmatrix}$ $\quad W_{n_{11}} = W_{n_{22}} = \dfrac{1}{2} \cdot \left[\left(\dfrac{r_{ext}}{r_{int}}\right)^n + \left(\dfrac{r_{int}}{r_{ext}}\right)^n\right]$

$W_{n_{12}} = \dfrac{1}{4\pi\lambda n} \cdot \left[\left(\dfrac{r_{int}}{r_{ext}}\right)^n - \left(\dfrac{r_{ext}}{r_{int}}\right)^n\right]$ $\quad W_{n_{21}} = \pi\lambda n \left[\left(\dfrac{r_{int}}{r_{ext}}\right)^n - \left(\dfrac{r_{ext}}{r_{int}}\right)^n\right]$

Boundary condition (5.2) can be transformed according to (5.36):

$$\tilde{q}_n^{ext} = \frac{2\pi r_{ext}}{R_{env}}\, \tilde{\theta}_n^{ext} \tag{5.43}$$

The column vector composed of transforms of temperature and local heat flux written for the radius r_{ext} can be rearranged as:

$$\begin{bmatrix} \tilde{\theta}_n \\ \tilde{q}_n \end{bmatrix}_{ext} = \boldsymbol{H} \begin{bmatrix} \tilde{\theta}_n \\ 0 \end{bmatrix}_{ext} \tag{5.44}$$

with $\boldsymbol{H}$=$\begin{bmatrix} 1 & 0 \\ \frac{2\pi r_{ext}}{R_{env}} & 1 \end{bmatrix}$

Thus the matrix expression in equation (5.42) can be written as:

$$\begin{bmatrix} \tilde{\theta}_n \\ 0 \end{bmatrix}_{ext} = \boldsymbol{H}^{-1}\boldsymbol{W_n} \begin{bmatrix} \tilde{\theta}_n \\ \tilde{q}_n \end{bmatrix}_{int} \tag{5.45}$$

Second case: n=0

The Fourier transform of the temperature field for the case n=0, (see equation 5.28) is given by:

$$\tilde{\theta}_0(r) = \int_{-\pi}^{\pi} \theta(r,\alpha)\, d\alpha \tag{5.46}$$

Following the same approach described above it follows:

$$F_0\left(\frac{\partial^2\theta}{\partial r^2}\right) = \int_{-\pi}^{\pi} \frac{\partial^2\theta}{\partial r^2}\, d\alpha = \frac{\partial^2}{\partial r^2}\int_{-\pi}^{\pi} \theta\, d\alpha = \frac{d^2\tilde{\theta}_0}{dr^2} \tag{5.47}$$

$$F_0\left(\frac{1}{r}\frac{\partial\theta}{\partial r}\right) = \int_{-\pi}^{\pi} \frac{1}{r}\frac{\partial\theta}{\partial r} d\alpha = \frac{1}{r}\frac{\partial}{\partial r}\int_{-\pi}^{\pi} \theta\, d\alpha = \frac{1}{r}\frac{d\tilde{\theta}_0}{dr} \tag{5.48}$$

$$F_0\left(\frac{1}{r^2}\frac{\partial\theta^2}{\partial\alpha^2}\right) = \int_{-\pi}^{\pi} \frac{1}{r^2}\frac{\partial\theta^2}{\partial\alpha^2}\, d\alpha = \frac{1}{r^2}\left[\frac{\partial\theta}{\partial\alpha}\right]_{-\pi}^{\pi} = 0 \tag{5.49}$$

$$F_0\left(\frac{q_g}{\lambda}\right) = \int_{-\pi}^{\pi} \frac{q_g}{\lambda}\, d\alpha = \frac{2\pi q_g}{\lambda} \tag{5.50}$$

Equation (5.1) transformed in the Fourier domain becomes:

$$\frac{d^2\tilde{\theta}_0}{dr^2} + \frac{1}{r}\frac{d\tilde{\theta}_0}{dr} + \frac{2\pi q_g}{\lambda} = 0 \tag{5.51}$$

whose general solution is as follows:

$$\tilde{\theta}_0(r) = C_3 \cdot ln(r) + C_4 - \frac{\pi q_g}{2\lambda} r^2 \tag{5.52}$$

The corresponding local heat flux according to (5.36) is expressed by:

$$\tilde{q}_0(r) = -2\pi r\lambda \frac{d\tilde{\theta}_0}{dr} = -2\pi\lambda C_3 + 2\pi^2 q_g r^2 \tag{5.53}$$

The constants C_3 and C_4 can be calculated like in the case n≠0 applying the definition of transformed temperature and heat flux given by equations (5.52, 5.53) for $r = r_{int}$ and $r = r_{ext}$.

$$\begin{cases} \tilde{\theta}_0^{int} = C_3 \cdot ln(r_{int}) + C_4 - \dfrac{\pi q_g}{2\lambda} r_{int}^2 \\ \\ \tilde{q}_0^{int} = -2\pi\lambda C_3 + 2\pi^2 q_g r_{int}^2 \end{cases} \tag{5.54}$$

$$\begin{cases} \tilde{\theta}_0^{ext} = C_3 \cdot ln(r_{ext}) + C_4 - \dfrac{\pi q_g}{2\lambda} r_{ext}^2 \\ \\ \tilde{q}_0^{ext} = -2\pi\lambda C_3 + 2\pi^2 q_g r_{ext}^2 \end{cases} \tag{5.55}$$

Therefore the constants C_3 and C_4 can be expressed as follows:

$$\begin{cases} C_3 = -\dfrac{1}{2\pi\lambda} \tilde{q}_0^{int} + \dfrac{\pi q_g r_{int}^2}{\lambda} \\ \\ C_4 = \tilde{\theta}_0^{int} + \dfrac{1}{2\pi\lambda} ln(r_{int})\, \tilde{q}_0^{int} + \dfrac{\pi q_g r_{int}^2}{2\lambda} - \dfrac{\pi q_g r_{int}^2 ln(r_{int})}{\lambda} \end{cases} \tag{5.56}$$

And consequently:

$$\begin{cases} \tilde{\theta}_0^{ext} = \tilde{\theta}_0^{int} + \dfrac{1}{2\pi\lambda} ln\left(\dfrac{r_{int}}{r_{ext}}\right) \tilde{q}_0^{int} + \dfrac{\pi q_g r_{int}^2}{\lambda} ln\left(\dfrac{r_{ext}}{r_{int}}\right) + \dfrac{\pi q_g (r_{int}^2 - r_{ext}^2)}{2\lambda} \\ \\ \tilde{q}_0^{ext} = \tilde{q}_0^{int} + 2\pi^2 q_g (r_{ext}^2 - r_{int}^2) \end{cases} \tag{5.57}$$

After rearrangement, the Quadrupole formulation of the problem for n=0 becomes:

$$\begin{bmatrix} \tilde{\theta}_0 \\ 0 \end{bmatrix}_{ext} = \boldsymbol{H}^{-1} \boldsymbol{W_0} \begin{bmatrix} \tilde{\theta}_0 \\ \tilde{q}_0 \end{bmatrix}_{int} + \boldsymbol{H}^{-1} \begin{bmatrix} X_0 \\ Y_0 \end{bmatrix} \tag{5.58}$$

with $\boldsymbol{W_0} = \begin{bmatrix} W_{0_{11}} & W_{0_{12}} \\ W_{0_{21}} & W_{0_{22}} \end{bmatrix}$ and:

$W_{0_{11}} = W_{0_{22}} = 1$ $\qquad$ $W_{0_{12}} = \frac{1}{2\pi\lambda} ln\left(\frac{r_{int}}{r_{ext}}\right)$ $\qquad$ $W_{0_{21}} = 0$

$X_0 = \frac{\pi q_g r_{int}^2}{\lambda} ln\left(\frac{r_{ext}}{r_{int}}\right) + \frac{\pi q_g (r_{int}^2 - r_{ext}^2)}{2\lambda}$ $\qquad$ $Y_0 = 2\pi^2 q_g (r_{ext}^2 - r_{int}^2)$

Both equations (5.45) and (5.58) show that a common quadrupolar formulation can be written for any value of *n*:

$$\begin{bmatrix}\tilde{\theta}_n\\ 0\end{bmatrix}_{ext} = \boldsymbol{H}^{-1}\boldsymbol{W_n}\begin{bmatrix}\tilde{\theta}_n\\ \tilde{q}_n\end{bmatrix}_{int} + \boldsymbol{H}^{-1}\begin{bmatrix}X_n\\ Y_n\end{bmatrix} \quad \text{where } X_n = Y_n = 0 \quad \text{if} \quad n \neq 0 \tag{5.59}$$

So, the solution of the direct problem, where $q^{int}(\alpha)$ is known and $\theta^{ext}(\alpha)$ is looked for, derives directly from equation (5.59).

Once the transformed $\tilde{\theta}$ of temperature at any radius is found, it is possible to obtain the temperature distribution $\theta(r,\alpha)$ through an inverse Fourier transform. In the practical case it is necessary to map the spatial domain on a grid characterized by a finite number (named N_α) of discrete points.

In this situation the inverse Fourier transform (5.28) can be simplified by considering a finite even number N_h of harmonics:

$$\theta(r,\alpha) \approx \frac{1}{2\pi}\sum_{-\frac{N_h}{2}+1}^{\frac{N_h}{2}} \tilde{\theta}_n(r)e^{in\alpha} \tag{5.60}$$

If one wants to retrieve the temperature for a discrete number N_α of angles α_k at the radius r_{ext}, equation (5.60) can be written under the vector/matrix form:

$$\boldsymbol{\theta}^{ext} = \boldsymbol{G}\,\tilde{\boldsymbol{\theta}}^{ext} \tag{5.61}$$

Where **G** is a matrix of dimension (N_α, N_h), $\boldsymbol{\theta}^{ext}$ is the column vector of the temperatures and $\tilde{\boldsymbol{\theta}}^{ext}$ the column vector of its harmonics of dimension (N_h):

$G_{kn} = \frac{1}{2\pi}\exp(in\alpha_k)$ for n=1 to N_h and k=1 to N_α.

5.4.2 Inverse problem

Under the inverse approach, the convective heat flux distribution on the internal side of the pipes' cross-section is assumed to be the unknown variable in equations (5.1-5.4), while the external surface temperature distribution is the input data and all the other problem's parameter are assumed to be known. According to the quadrupolar formulation for the direct problem (see equation 5.45) it follows:

$$\begin{bmatrix}\tilde{\theta}_n\\ \tilde{q}_n\end{bmatrix}_{int} = \boldsymbol{W_n}^{-1}\boldsymbol{H}\begin{bmatrix}\tilde{\theta}_n\\ 0\end{bmatrix}_{ext} \qquad \text{for n}\neq 0 \tag{5.62}$$

By considering $\boldsymbol{R_n}$ as the product of the matrices $\boldsymbol{W_n}^{-1}$ and $\boldsymbol{H}$ it follows:

$$\begin{bmatrix}\tilde{\theta}_n\\ \tilde{q}_n\end{bmatrix}_{int} = \boldsymbol{R_n}\begin{bmatrix}\tilde{\theta}_n\\ 0\end{bmatrix}_{ext} \tag{5.63}$$

For the harmonic of order zero starting from equation (5.58) it holds:

$$\begin{bmatrix}\tilde{\theta}_0\\ \tilde{q}_0\end{bmatrix}_{int} = \boldsymbol{W_0}^{-1}\left(\boldsymbol{H}\begin{bmatrix}\tilde{\theta}_0\\ 0\end{bmatrix}_{ext} - \begin{bmatrix}X_0\\ Y_0\end{bmatrix}\right) \tag{5.64}$$

Naming $\boldsymbol{R_0}$ the product of the matrices $\boldsymbol{W_0}^{-1}$ and $\boldsymbol{H}$ and $\begin{bmatrix}J_0\\ K_0\end{bmatrix}$ the result of $\boldsymbol{W_0}^{-1}\begin{bmatrix}X_0\\ Y_0\end{bmatrix}$ it follows**:**

$$\begin{bmatrix}\tilde{\theta}_0\\ \tilde{q}_0\end{bmatrix}_{int} = \boldsymbol{R_0}\begin{bmatrix}\tilde{\theta}_0\\ 0\end{bmatrix}_{ext} - \begin{bmatrix}J_0\\ K_0\end{bmatrix} \tag{5.65}$$

From the matrix expressions given in equations (5.63) and (5.65), a common quadrupolar formulation can be written for any value of *n*:

$$\begin{bmatrix}\tilde{\theta}_n\\ \tilde{q}_n\end{bmatrix}_{int} = \boldsymbol{R_n}\begin{bmatrix}\tilde{\theta}_n\\ 0\end{bmatrix}_{ext} - \begin{bmatrix}J_n\\ K_n\end{bmatrix} \qquad \text{where } J_n = K_n = 0 \quad \text{if} \quad n \neq 0 \tag{5.66}$$

and where $\boldsymbol{R_n} = \begin{bmatrix}A_n & B_n\\ C_n & D_n\end{bmatrix}$.

So, the solution of the inverse problem, where $\theta^{ext}(\alpha)$ is known and $q^{int}(\alpha)$ is looked for, derives directly from the second line of the equation (5.66).

$$\tilde{q}_n^{int} = C_n \cdot \tilde{\theta}_n^{ext} - K_n \tag{5.67}$$

As it is well known, IHCPs generally present some additional complications due to the fact that they are ill-conditioned: this entails that they show a great sensitiveness to small variations in the input data that makes unfeasible the direct inversion of equations (5.1-5.4).

The natural solution for the estimation of each harmonics $\tilde{q}_n^{int}$ of the inside flux is to get an estimation of the external temperature transform $\tilde{\theta}_n^{ext}$ using the available N_α measurements. However, a close look at equation (5.68) shows that, for large positive values of *n*, coefficient C_n can become very large and will amplify the errors in $\tilde{\theta}_n^{ext}$, making the problem severely ill posed:

$$\tilde{q}_n^{int} = C_n \cdot \tilde{\theta}_n^{ext} \approx \left(\frac{r_{ext}}{r_{int}}\right)^n \left(\pi\lambda n + \frac{1}{2}\right)\tilde{\theta}_n^{ext} \to \infty \quad if \;\; n \to \infty \tag{5.68}$$

The same is true for large negative values of *n*.

Thus it is necessary to apply a regularization procedure in order to get the highest precision in the estimation of the Fourier spectrum $\tilde{\theta}^{ext}$ of the measured surface distribution. This issue is suitably performed by means of the Truncated Singular Value Decomposition (TSVD).

This technique that has been proved to be very powerful as regularization method (Hansen 1990) has been already presented in chapter 2.

Starting from equation (5.67) and rearranging it, it is possible to obtain:

$$\tilde{\theta}_n^{ext} = \frac{1}{C_n} \cdot \tilde{q}_n^{int} + \frac{1}{C_n} \cdot K_n \tag{5. 69}$$

that represents the solution of the direct problem, where $q^{int}(\alpha)$ is known and $\theta^{ext}(\alpha)$ is looked for and it is the analogous of the one obtainable from equation (5.59).

The different C_n coefficients can be put under a diagonal matrix form $\boldsymbol{C}$ and the different harmonics $\tilde{\theta}_n^{ext}$, $\tilde{q}_n^{int}$ and K_n form are gathered in corresponding column vectors:

$$\tilde{\boldsymbol{\theta}}^{ext} = \boldsymbol{C}^{-1}\, \tilde{\boldsymbol{q}}^{int} + \boldsymbol{C}^{-1}\boldsymbol{K} \tag{5. 70}$$

where $\boldsymbol{C} = diag\left(\left[C_{-N_h/2+1} \ \dots \ C_0 \ \dots \ C_{N_h/2}\right]\right)$; $\quad \tilde{\boldsymbol{\theta}}^{ext} = \left[\tilde{\theta}^{ext}_{-N_h/2+1} \ \dots \ \tilde{\theta}^{ext}_0 \ \dots \ \tilde{\theta}^{ext}_{N_h/2}\right]^T$

$\boldsymbol{K} = \left[K_{-N_h/2+1} \ \dots \ K_0 \ \dots \ K_{N_h/2}\right]^T$; $\quad \tilde{\boldsymbol{q}}^{int} = \left[\tilde{q}^{int}_{-N_h/2+1} \ \dots \ \tilde{q}^{int}_0 \ \dots \ \tilde{q}^{int}_{N_h/2}\right]^T$

Return to the original angular space can be made using the $\boldsymbol{G}$ matrix defined in equation (5.61):

$$\boldsymbol{\theta}^{ext} = \boldsymbol{G}\, \tilde{\boldsymbol{\theta}}^{ext} = 2\pi r_{int} \boldsymbol{G}\, \boldsymbol{C}^{-1} \boldsymbol{G^{-1}} \boldsymbol{q}^{int} + \boldsymbol{G}\, \boldsymbol{C}^{-1}\boldsymbol{K} \quad \text{since } \boldsymbol{q}^{int} = \frac{1}{2\pi r_{int}} \boldsymbol{G}\, \tilde{\boldsymbol{q}}^{int} \tag{5.71}$$

So in the angular space, the discretized flux $q^{int}(\alpha)$ is the solution of the following linear equation:

$$\boldsymbol{M}\boldsymbol{q}^{int} = \boldsymbol{\theta}^{ext} - \boldsymbol{G}\, \boldsymbol{C}^{-1}\boldsymbol{K} \quad \text{where } \boldsymbol{M} = 2\pi r_{int} \boldsymbol{G}\, \boldsymbol{C}^{-1} \boldsymbol{G^{-1}} \tag{5.72}$$

Then, on matrix **M** it is possible to apply the SVD, assuming that the number N_h of harmonics that are looked for, is equal to the number N_α of angles of measurements:

$$\mathbf{M} = \mathrm{U} \cdot \boldsymbol{\Sigma} \cdot \mathrm{V}^{*T} \tag{5.73}$$

where the superscript ^{*T} stands for the conjugate transpose of the matrix.

Then it is possible to calculate the pseudoinverse $\mathbf{M}^+$ of the matrix **M** in the following way:

$$\mathbf{M}^{+} = \mathrm{V} \cdot \boldsymbol{\Sigma}^{-1} \cdot \mathrm{U}^{*T} \quad \text{where } \boldsymbol{\Sigma}^{-1} = \begin{bmatrix} 1/\delta_1 & & & & \\ & 1/\delta_2 & & 0 & \\ & & \ddots & & \\ & 0 & & \ddots & \\ & & & & 1/\delta_{N_h} \\ & & 0 & & \end{bmatrix} \tag{5.74}$$

But, as said before, it is not possible to restore the heat flux distribution by only inverting the matrix that describes the heat conduction in the wall because the noise greatly affects the starting data.
This problem could be overcome by applying the TSVD: it consists in zeroing the inverse of the smallest singular values of **M**, that is to truncate its inverse matrix. If one calls t_p the order of the first value truncated with $2 < t_p \leq N_h$, the regularized matrix becomes:

$$\mathbf{M}_{\mathbf{t}}^{+} = \mathrm{V} \cdot \boldsymbol{\Sigma}_{\mathbf{t}}^{-\mathbf{1}} \cdot \mathrm{U}^{*T} \quad \text{where } \boldsymbol{\Sigma}_{\mathbf{t}}^{-\mathbf{1}} = \begin{bmatrix} 1/\delta_1 & & & & \\ & 1/\delta_2 & & 0 & \\ & & \ddots & & \\ & 0 & & 1/\delta_{t_p-1} & \\ & & & & 0 \\ & & 0 & & \end{bmatrix} \tag{5.75}$$

After that, it's possible to find the heat flux distribution:

$$\boldsymbol{q}^{int} = \mathbf{M}_{\mathbf{t}}^{+} \cdot (\boldsymbol{\theta}^{ext} - \boldsymbol{G}\,\boldsymbol{C}^{-1}\boldsymbol{K}) \tag{5.76}$$

It is possible to do the same for the determination of θ^{int}:

$$\boldsymbol{\theta}^{int} = \mathbf{F}_{\mathbf{t}}^{+}\,(\boldsymbol{\theta}^{ext} - \mathbf{G}\,\boldsymbol{A}^{-1}\boldsymbol{J}) \qquad \text{where } \boldsymbol{F} = \mathbf{G}\,\boldsymbol{A}^{-1}\,\mathbf{G}^{-1} \tag{5.77}$$

Thus a proper choice of the truncation parameter is very important. Choosing a low value of truncation means to impose too much regularization to the solution prejudicing the fitting of the data and obtaining a great residual; a great truncation parameter will bring to a good fitting but also to a solution affected by the data errors. In the present investigation, in order to adequately choose the truncation parameter, the criterion provided by the discrepancy principle was adopted. According to this criterion (Morodzov 1984), as said in the previous paragraph, the solution of the

inverse problem is considered to be sufficiently accurate when the difference between reconstructed and input rough data is close to the standard deviation associated to the raw data itself.

Once the heat-flux distribution and the temperature distribution on the internal wall surface have been determined through the above described methodology, the local convective heat-transfer coefficient can be easily determined, according to equation (5.12).

5.4.2 Numerical Validation

The numerical validation of the above described estimation procedure was performed using as input data the synthetic temperatures already used for the Tikhonov Regularization method and for the Gaussian Filter Technique. They were obtained by solving the direct problem considering as known the convective heat transfer coefficient distribution along the circumference $h_{int}(\alpha)$.

As already said, the distribution $h_{int}{}^{(J)}$ shown in figure 5.3 was adopted. The solution of the inverse problem expressed in equation (5.67), due to its ill-posed nature, is unfeasible without a regularization procedure. In figure 5.24 the $h_{int}(\alpha)$ obtained without a regularization technique for the noise level 0.1K is reported and, as expected, the noise present in the rough data prevents from reconstructing the sought function.

Therefore, a careful regularization procedure proves to be mandatory. This issue is suitably performed by means of the TSVD. Then in order to define the truncation parameter necessary for its application the discrepancy principle was applied.

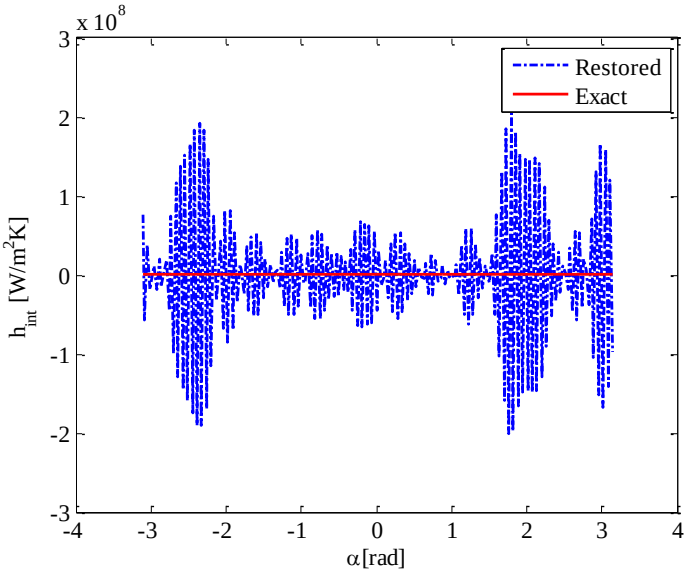

Figure 5.24: Exact and restored $h_{int}{}^{(J)}$ distribution obtained by Quadrupole Method without a regularization technique for noise level $\sigma = 0.1$K.

In figure 5.25 the trend of $E_d(t_p) = \|(T - Y)\|_2/\sqrt{N_\alpha}$ in function of the truncation parameter t_p for the noise level $\sigma = 0.1K$ is represented. The intersection of the plotted curve with the noise level σ identified the truncation parameter as approximately 8.

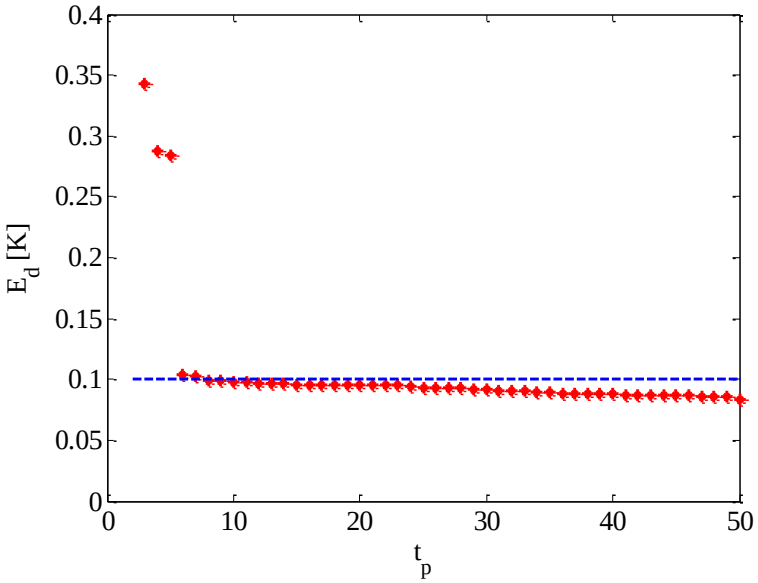

Figures 5.25: Function E_d against the truncation parameter for noise level $\sigma = 0.1$K.

In figure 5.26 the heat transfer coefficient distribution, obtained by adopting the truncation parameter t_p =8, is reported and compared with the exact value.

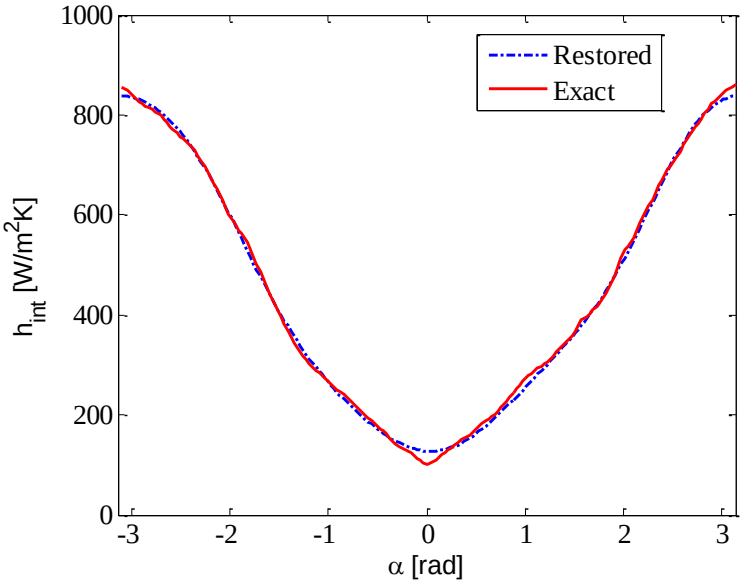

Figure 5.26: Exact and restored $h_{int}{}^{(J)}$ distribution obtained by Quadrupole Method coupled to TSVD for noise level $\sigma = 0.1\ K$ and $t_p = 8$.

The restored values match with a good approximation the original local convective heat transfer distribution by demonstrating that the procedure explained in this paragraph performs efficiently.
In figure 5.27 the restored temperature distribution obtained by the estimation procedure, applied by considering t_p =8, is reported.

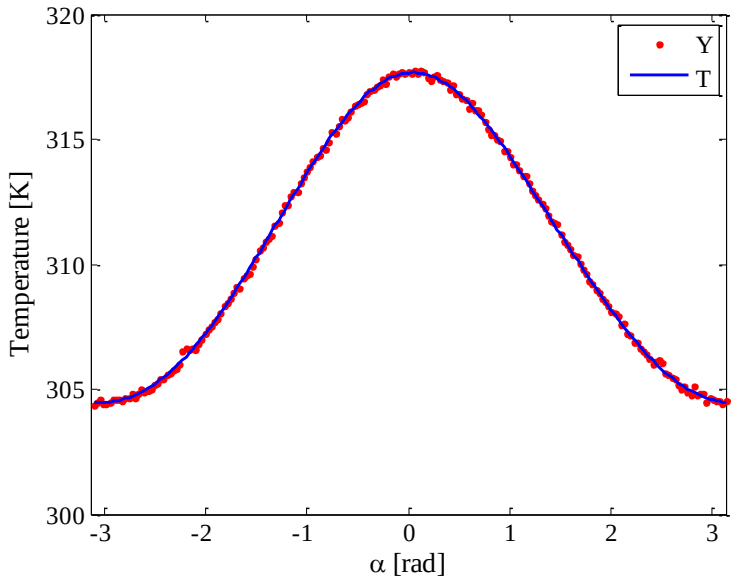

Figure 5.27: Noisy input (Y) and restored temperature (T) distribution for noise level $\sigma = 0.1\ K$ and t_p =8.

The corresponding residuals between the input and the restored temperature were reported in figure 5.28.

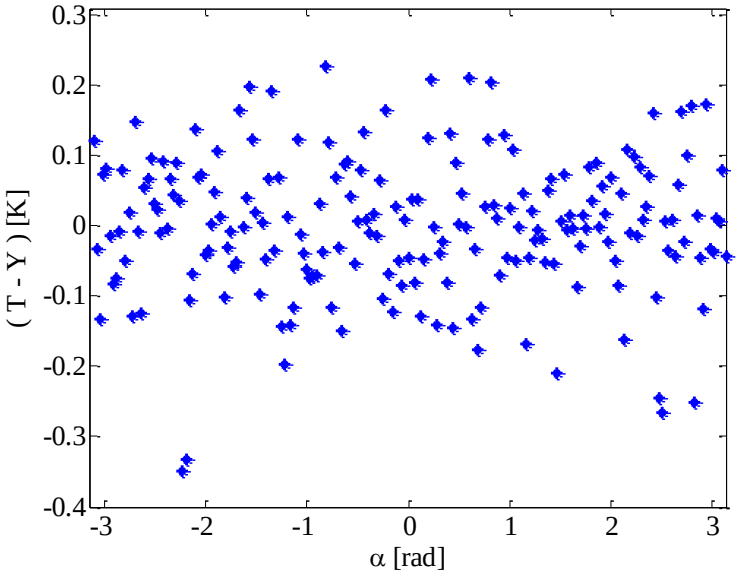

Figure 5. 28: Residuals between the input (Y) and the reconstructed (T) temperature for noise level $\sigma = 0.1$K (QM).

The effectiveness of the presented solution procedure is highlighted by the random distribution of the residuals. The choice of the truncation parameter is crucial to obtain a good restoration of the heat transfer coefficient overcoming the complications deriving from the ill-conditioned character of the inverse problem. For instance by assuming the values of $t_p = 3$ and $t_p = 30$, the local convective heat transfer coefficient estimated by applying the above described solution procedure doesn't match the exact distribution, as it is shown in figures 5.29 and 5.30.

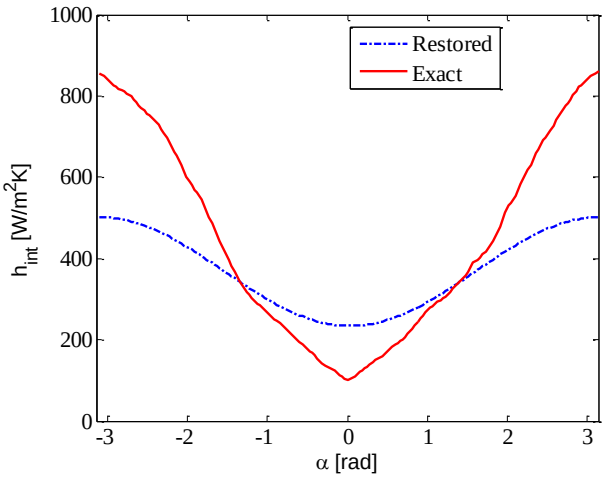

Figure 5.29: Exact and restored $h_{int}{}^{(J)}$ distribution obtained by Quadrupole Method coupled to TSVD for noise level $\sigma = 0.1$K and $t_p = 3$.

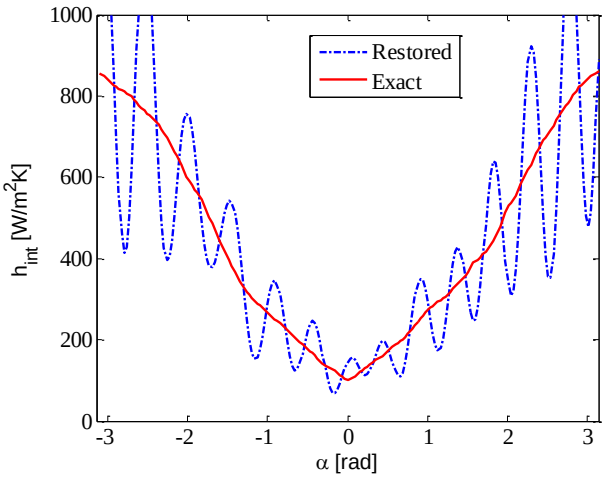

Figure 5.30: Exact and restored $h_{int}{}^{(J)}$ distribution obtained by Quadrupole Method coupled to TSVD for noise level $\sigma = 0.1$K and $t_p = 30$.

As it happens for the Gaussian filter with the cutoff frequency, choosing a too small regularization parameter means to impose too much regularization and selecting a too high value of t_p will bring to a not sufficient filtering of the signal conserving a lot of noise in the results. These considerations put the accent on the importance of a correct determination of the truncation parameter.

In figures 5.31 and 5.32 the exact and restored convective heat transfer coefficient and the corresponding residuals between the input and the reconstructed temperature were reported for 0.01K and 1K noise levels for $h_{int}{}^{(J)}$ distribution.

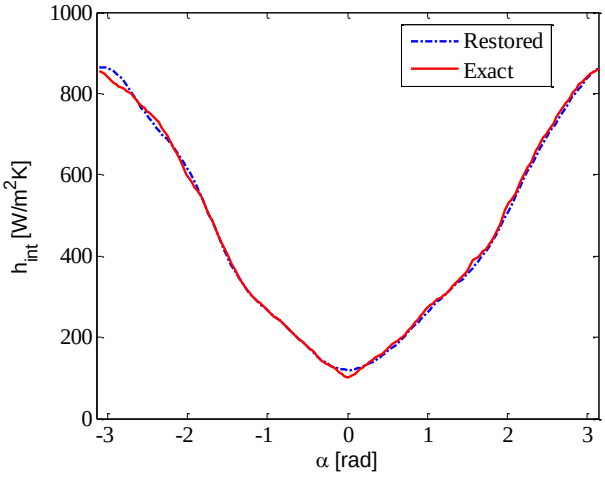

Figure 5.31a: Exact and restored $h_{int}{}^{(J)}$ distribution obtained by Quadrupole Method coupled to TSVD for noise level $\sigma = 0.01$K.

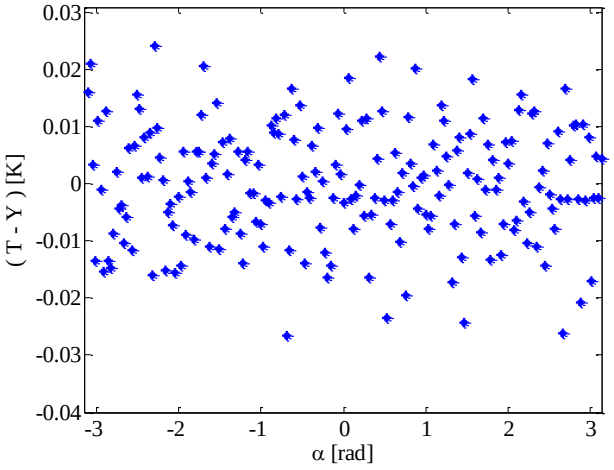

Figure 5.31b: Residuals between the input (Y) and the reconstructed (T) temperature for noise level $\sigma = 0.01$K (QM).

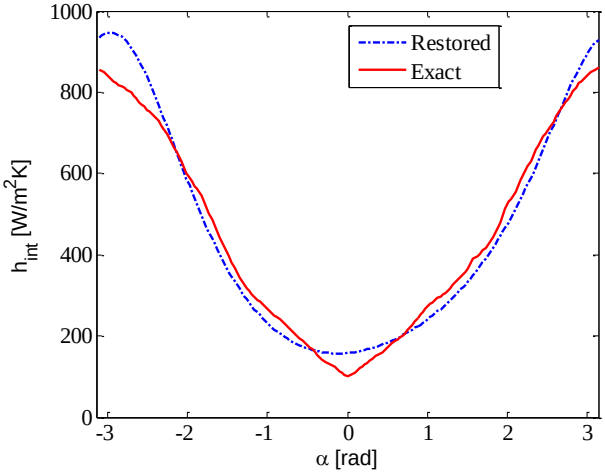

Figure 5.32a: Exact and restored $h_{int}{}^{(J)}$ distribution obtained by Quadrupole Method coupled to TSVD for noise level $\sigma = 1$K.

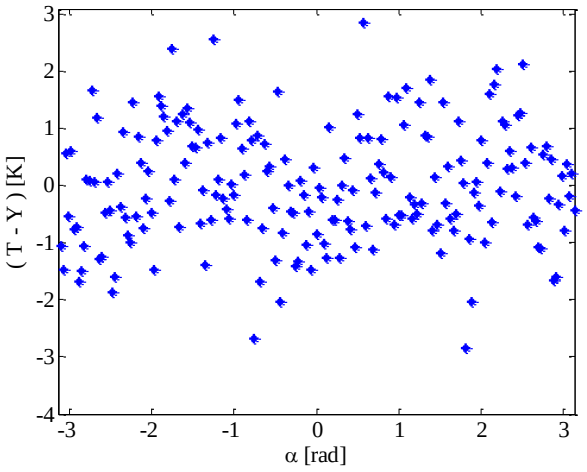

Figure 5.32b: Residuals between the input (Y) and the reconstructed (T) temperature for noise level $\sigma = 1$K (QM).

From figures 5.26, 5.28, 5.32 and 5.33 it is possible to appreciate the optimal performances of the estimation procedure presented in this paragraph, in restoring the convective heat transfer coefficient. The Reconstructed distributions match with good approximation the exact ones showing good results for all the noise levels considered. Nevertheless it has to be noticed that with the increasing of the noise level it is present a loose of information, in particular in correspondence of the peak.

5.5 NUMERICAL COMPARISON

The three different IHCP solution techniques were compared in order to better understand the powerful and effectiveness of the various methods. A very important role is executed by the choice of the regularization parameter: in order to make the comparison more consistent, the discrepancy principle was adopted for determining the proper value of the regularization parameter for all the three regularization techniques.

In figures 5.33-5.35 the convective heat transfer coefficient distributions restored by the Quadrupole Method (QM) are compared with the ones obtained by TRM (Tickonov regularization method) and GFT (Gaussian filter Technique) for the $h_{int}{}^{(J)}(\alpha)$ distribution and for three different noise levels.

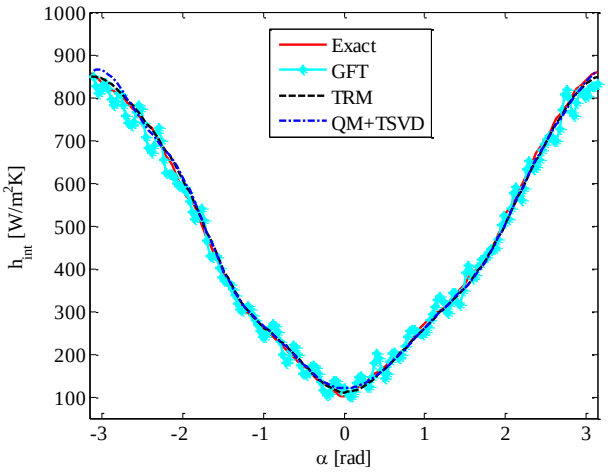

Figure 5.33a: Exact and restored $h_{int}{}^{(J)}$ distribution obtained by QM coupled to TSVD, TRM and GFT for noise level σ=0.01K.

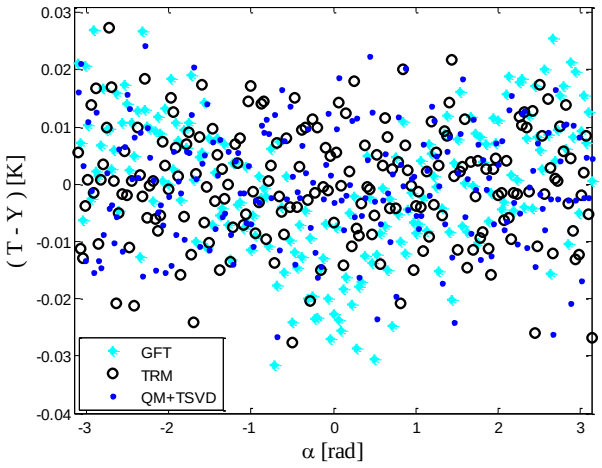

Figure 5.33b: Residuals between the input (Y) and the reconstructed (T) temperature obtained by QM coupled to TSVD, TRM and GFT for noise level $\sigma = 0.01$K.

As it is possible to see from these first pictures the TRM and QM reconstruct the convective heat transfer coefficient almost identically guaranteeing a good restoration of the original information.

Also the GFT is working good even if the reconstructed heat transfer coefficient distribution is not as smooth as the ones obtained with the other two procedures: the result obtained is not unsatisfying considering the considerably small computational cost of this procedure. The residuals between the input and the restored temperature, plotted in figure 5.33b, gives deeper insight into the performances of the three estimation procedures: the residuals produced by TRM and QM are more randomly distributed than the ones by GFT.

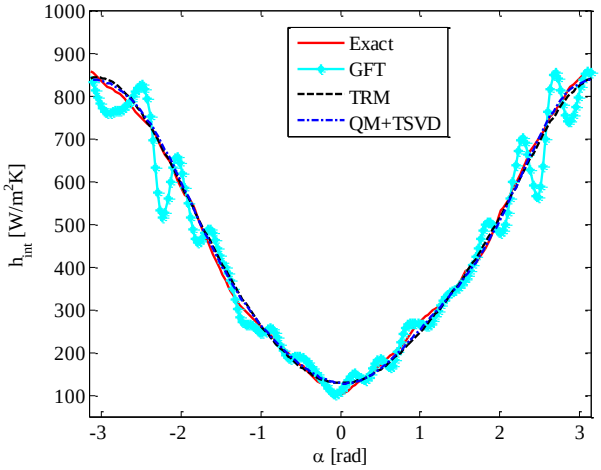

Figure 5.34a: Exact and restored $h_{int}{}^{(J)}$distribution obtained by QM coupled to TSVD, TRM and GFT for noise level $\sigma = 0.1$K.

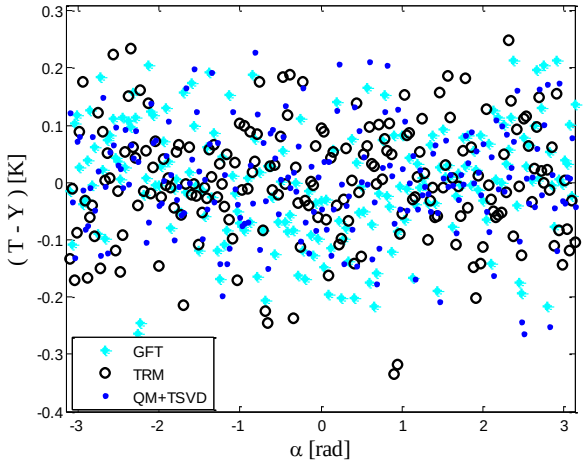

Figure 5. 34b: Residuals between the input (Y) and the reconstructed (T) temperature obtained by QM coupled to TSVD, TRM and GFT for noise level $\sigma = 0.1$K.

This observation suggests that, even if no great differences are present in terms of estimated local convective heat transfer coefficient, TRM and QM works slightly better than GFT that tends to excessively smoothen the temperature distribution.

For higher noise levels the TRM and QM continue to obtain a good restoration of the convective heat transfer coefficient distribution, also if it is notable a progressive higher loose of information in correspondence of the peak, while filter technique is encountering more difficulties. Also for the GFT the estimation is globally correct but not as accurate as the other two.

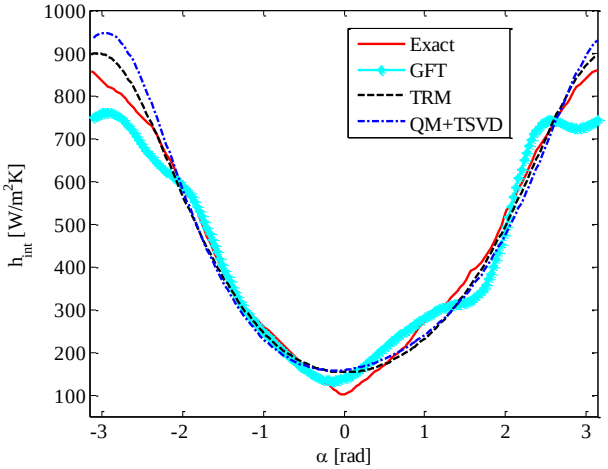

Figure 5.35a: Exact and restored $h_{int}{}^{(J)}$ distribution obtained by QM coupled to TSVD, TRM and GFT for noise level $\sigma = 1$K.

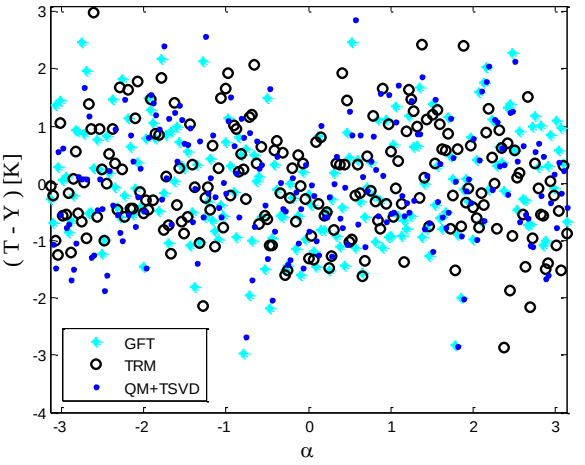

Fig 5.35b: Residuals between the input (Y) and the reconstructed (T) temperature obtained by QM coupled to TSVD, TRM and GFT for noise level $\sigma = 1$K.

The residuals distributions obtained for the two higher noise levels confirm that close to the lowest value of $h_{int}{}^{(J)}$ distribution, the GFT tends to oversmooth the temperature distribution. Also for TRM and QM start to be notable a drift of the residuals distribution for the two higher noise levels, but anyway they continue to be more randomly distributed than the filter.

In order to quantify the effectiveness of the three approaches at different signal to noise ratio values a residual analysis was performed by plotting the estimation error, defined as follows:

$$E_c = \frac{\|(h_{int})_{restored} - (h_{int})_{exact}\|_2^2}{\|(h_{int})_{exact}\|_2^2} \tag{5.78}$$

versus the standard deviation present in the input data.

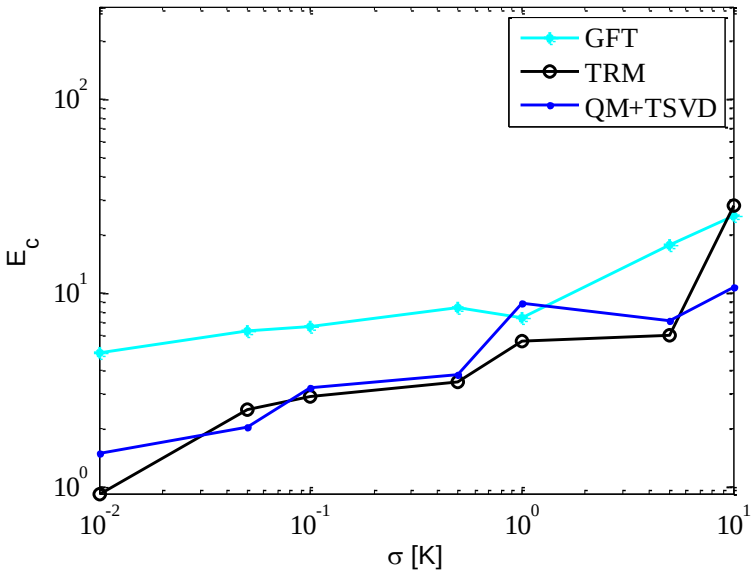

Figure 5.36: Estimation error on $h_{int}{}^{(J)}$ for QM coupled to TSVD, TRM and GFT at different noise level.

A general consideration is that for the problem here investigated, the QM and TRM performs better than the GFT if the noise is lower than 1 K while, for higher noise values, their efficiency is almost comparable, with, depending on the cases, one of the three techniques performing better than the others.

Referring to the evaluation criteria for IHTP methods proposed by Beck (1979) and already presented in chapter 2, some observations might be done. All the three methods are stable with respect to measurement errors, presenting an higher efficiency for small errors and an increasing estimation error with higher noise levels in the measurements; the predicted quantity is more accurate for the TRM and QM as it is possible to see from figure 5.36. On the other hand the great advantage of the GFT, derives from the fact that it is quite easy to be implemented and therefore it

doesn’t require a great experience in mathematics. The other two methods are more complex to be performed: it has to be said that in QM, when the quadrupole matrix in the wall is written, it is quite rapid performing changes in input data, while it requires more time and attention for the TRM. In addiction the computational cost of the GFT is significantly lower than the other two, where the TRM is probably the heaviest. A very positive element of the TRM, if the selection of the regularization parameter is effectuated with the fixed point method, is the absence of the necessity of a priori knowledge of the noise level.

6. LOCAL NUSSELT NUMBER IN SMOOTH WALL COILED TUBES: EXPERIMENTAL STUDY.

To experimentally evaluate the local actual value of the convective heat transfer coefficient at the fluid internal wall interface on a given cross section, the temperature distribution is acquired on the external wall surface by means of an infrared camera FLIR SC7000 and then the IHCP in the wall domain is solved by considering the convective heat transfer flux distribution on the internal wall surface to be unknown. A small portion of the external tube wall was made accessible to the thermal imaging camera by removing the thermally insulating layer, and the wall portion was coated with a thin film of high emissivity paint and then multiples images were acquired, moving the infrared camera around the section. More details about the experimental setup were presented in chapter 3.

The acquired images, thanks to a position reference fixed on the tube wall were conveniently cropped, processed by perspective algorithms (Cyganek 2011) and merged together in Matlab® environment to obtain continuous temperature functions on the tube wall versus the circumferential angular coordinate. Due to the infrared camera set-up adopted in this work (e.g., the focal length and the camera position with respect to the tube test section), temperature values at 256 angular positions over the whole circumferential section were obtained.

The experimental analysis was performed on the tubes HSW045 and HSW030 (for geometrical parameters see chapter 3) using Glycol Ethylene to study the Reynolds number range 100-1100 in order to investigate the convective heat transfer phenomenon in coiled tubes in the laminar flow regime.

In the temperature range characterising the experimental conditions, the Prandtl number of the working fluid varied in the range of 160-230.

In order to analyse the fully developed flow the test section was taken as far as possible from the inlet section, in the region of the heated section where, according to Janssen and Hoogendoorn (1978), the laminar boundary layers reached the asymptotic profiles. The heat flux provided to the fluid was selected in order to make negligible, for the fluid velocity values here investigated, the buoyancy forces compared to inertial ones. This condition makes the results obtained for this particular section representative of the thermally fully developed region.

The overall heat-transfer resistance between the tube wall and the surrounding environment R_{env}, which was assumed to be known in the inverse problem considered here, was taken equal to 0.2 m^2K/W, which is a representative value for natural convection in air compounded with radiative heat transfer with the environment. The wall thermal conductivity λ was certified by the manufacturer equal to 15 W/mK; the heat generated by the Joule effect in the wall q_g was calculated by the ratio of the power supplied and the volume of the tube wall.

Once the temperature distribution is acquired, the heat transfer coefficient distribution is estimated by the procedures discussed in the paragraphs 5.2-5.4, i.e, Tichonov Regularization Method, Gaussian Filter Technique and Quadrupole Method.

6.1 EXPERIMENTAL VALIDATION OF IHCP SOLUTION TECHNIQUES

The three estimation procedures before described were applied to the experimental case for a representative Reynolds number value; the restored distributions of the convective heat transfer coefficients were compared to the each others to assess the performance of the three techniques.
A representative temperature map acquired by the infrared camera is reported in figure 6.1 for the tube HSW045 under the experimental conditions of *Re* = 558 and *Pr* = 182. The data clearly reveal that the temperature distribution exhibits a significant variation along the circumference, and the temperature gradient is almost negligible along the axis of the tube. This observation confirms that adopting the 2-D numerical model (described in paragraph 5.1) for this type of problem is appropriate.

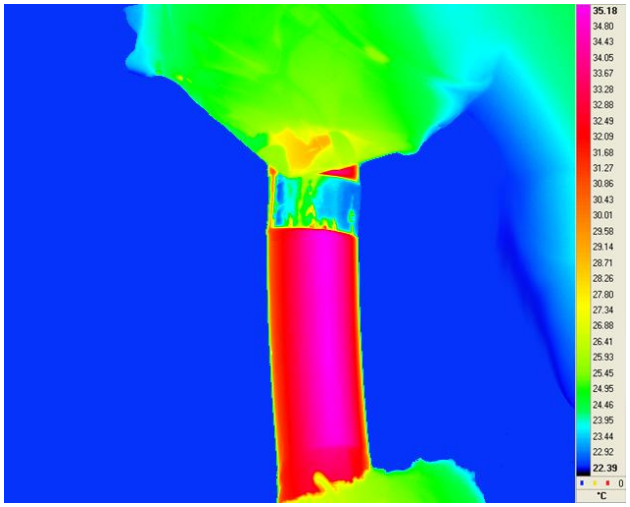

Figure 6.1: Representative infrared image of the coil wall (HSW045 *Re* = 558, *Pr* = 182).

In figures 6.2a-6.2e others infrared images of the coil wall along the circumference for the same measurement set (*Re* = 558, *Pr* = 182) are shown.

a)

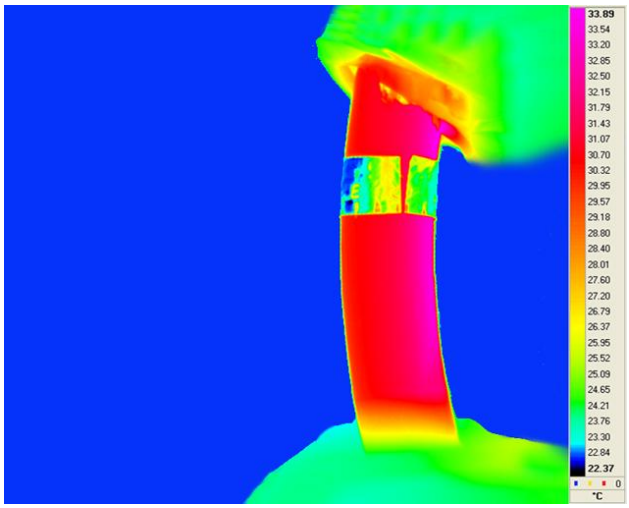

b)

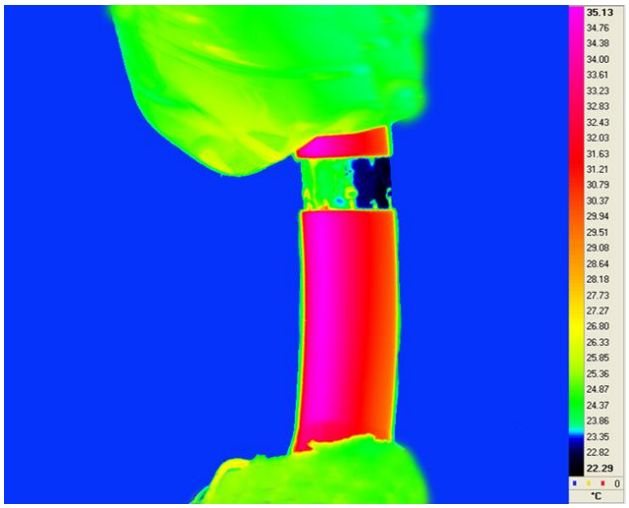

c)

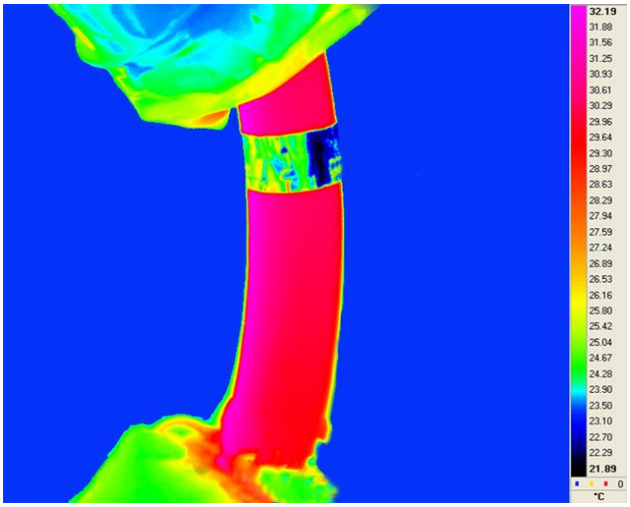

d)

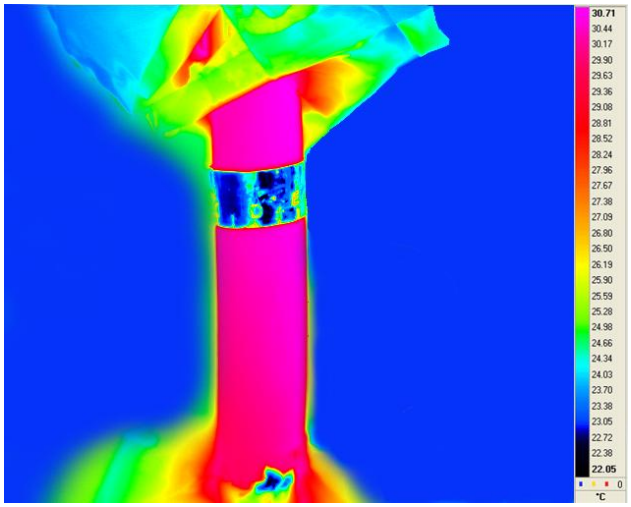

e)

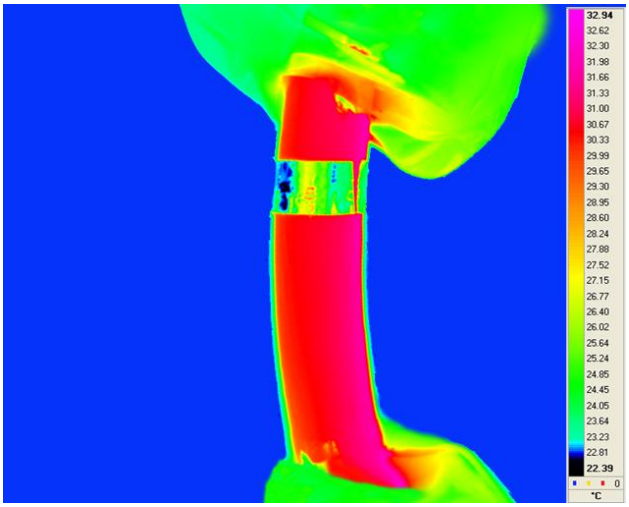

Figure 6.2a-e: Infrared images of the coil wall along the circumference (HSW045 *Re* = 558, *Pr* = 182).

In this analysis a relative angular coordinate α^*, whose origin was taken at the angular location where the wall temperature reaches its maximum, was considered. It was done to compensate the shifting effect of the torsion and thus better locally compare the Nusselt number distributions estimated for the various *Re* values. More details about the shifting effect are given in the following. The temperature distribution over the whole wall circumference, corresponding to figures 6.1 and 6.2, is reported in figure 6.3, versus the relative angular coordinate α^*.

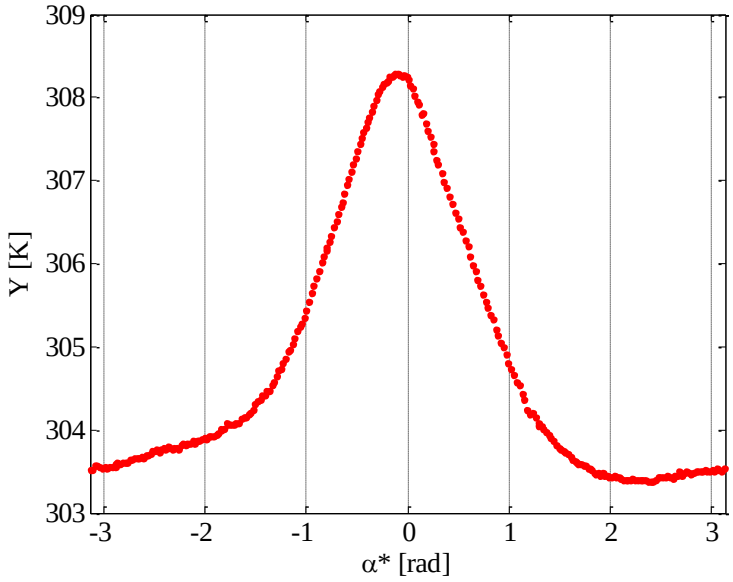

Figure 6.3: Temperature distribution on the coil external wall (HSW045 *Re* = 558, *Pr* = 182).

Tikhonov Regularization Method

To express the direct problem in the discrete domain, the convective heat-flux distribution was simplified here by considering the function expressed by equation (5.5) with *N* equal to 36. Adopting a point every 10 angular degrees for the convective heat flux distribution represents a good compromise between model precision and the computational cost. To calculate the $\mathbf{T_{q=0}}$ and **J** terms of equation (5.6), the numerical solution of equations (5.1-5.4) was calculated by the finite element method implemented in Comsol Multiphysics® environment with a mesh of 2596 triangular elements. As already specified in the paragraph 5.2, the technique used to choose the regularization parameter λ^* was the fixed-point method, as shown in figure 6.4. The analysis reveals that a proper λ^* value is equal to $1.17 \cdot 10^5$.

In figure 6.5, the reconstructed temperature distribution **T** for λ^* equal to $1.17 \cdot 10^{-5}$ is compared to the experimental data **Y**. Figure 6.6 shows that the residuals between the experimental and the computed temperature values present an average value equal to zero: it can be notice although an increment of noise level close to $\alpha^* = 0$ in correspondence of the peak.

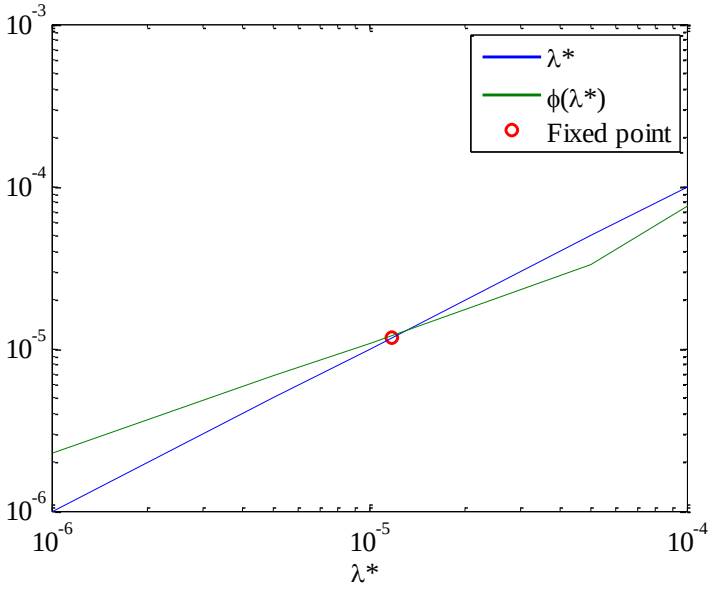

Figure 6.4: Fixed-point analysis (TRM HSW045 Re = 558, Pr = 182).

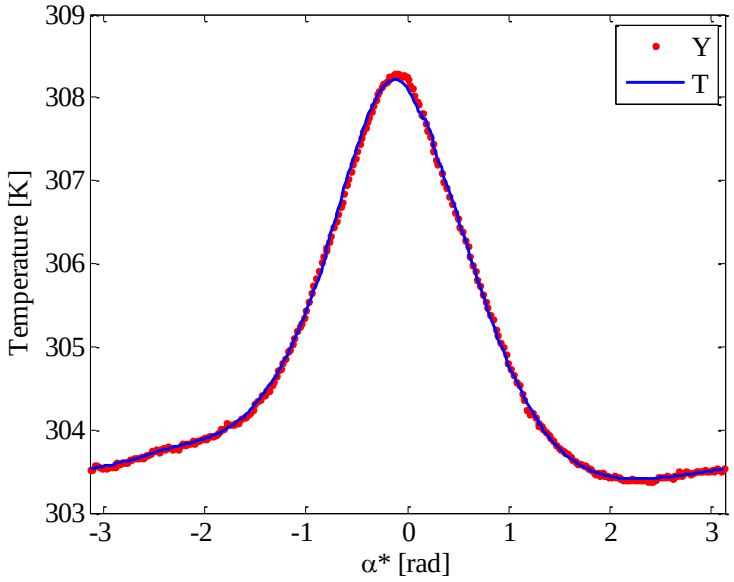

Figure 6.5: Experimental (Y) and restored (T) temperature distribution (TRM HSW045 $\lambda = 1.17 \cdot 10^5$, $Re = 558$, $Pr = 182$).

The distribution of the convective heat transfer coefficient restored by the minimisation procedure presented in paragraph 5.2 is reported in figure 6.7.

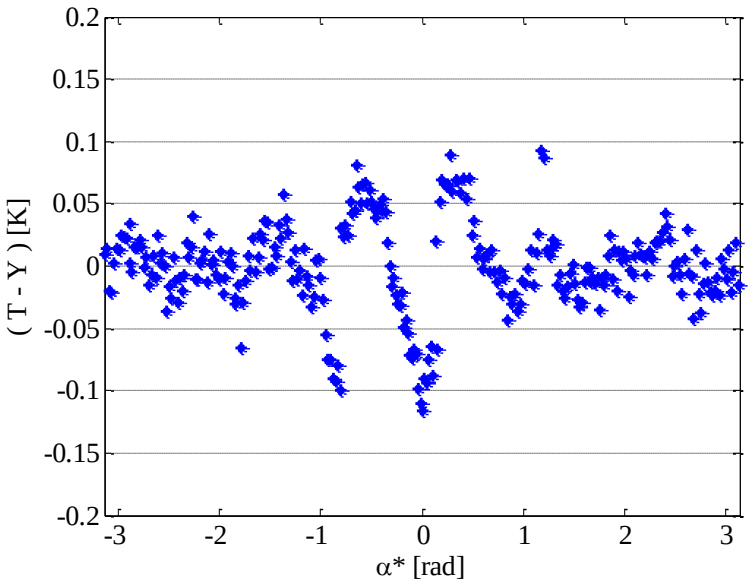

Figure 6.6: Residuals between the experimental (Y) and the reconstructed (T) temperature distribution (TRM HSW045 $\lambda = 1.17 \cdot 10^{-5}$, *Re* = 558, *Pr* = 182).

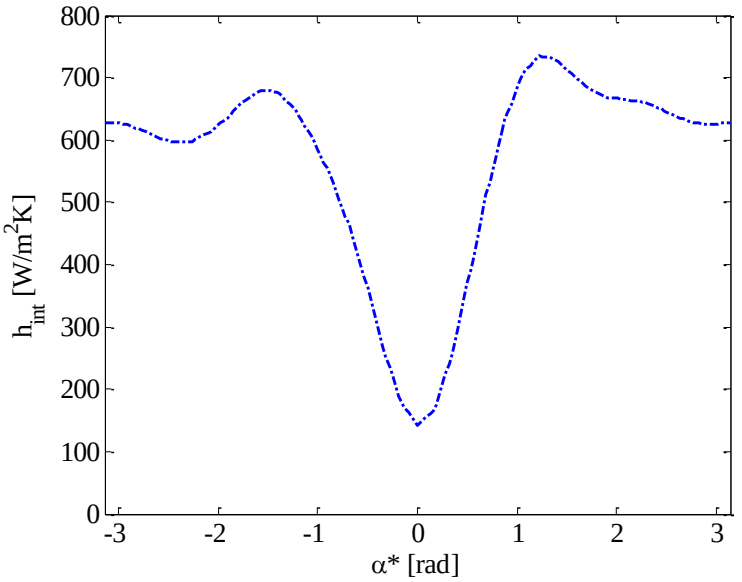

Figure 6.7. Restored convective heat-transfer coefficient distribution (TRM HSW045 $\lambda = 1.17 \cdot 10^{-5}$, *Re* = 558, *Pr* = 182).

A mesh refinement study was conducted to verify the appropriateness of the mesh size of the finite element model in relation to the inverse problem solution. Table 6.1 compares the results, reported in terms of the higher and the lower heat flux values at different mesh distributions, and it confirms that the adopted mesh ensures a satisfactory solution.

No. of elements	1298	2596	5144
$\|q_{max}\|$ (W/m^2)	6534.1	6534.1	6534.1
$\|q_{min}\|$ (W/m^2)	1843.0	1842.9	1842.9
$\|q_{max}\|/\|q_{min}\|$	3.5454	3.5456	3.5456

Table 6.1: Mesh refinement study (HSW045 Re=558).

Gaussian Filter Technique

In the application of the Gaussian filtering technique to the wall temperature distribution shown in figure 6.3, the cut-off frequency was identified using equation (5.24) considering a noise level of σ=0.04K. The noise level has been estimated by measuring the surface temperature distribution while maintaining the coil wall under isothermal conditions. The trend of E_d (see equation 5.24) versus the cut-off frequency is reported in figure 6.8.

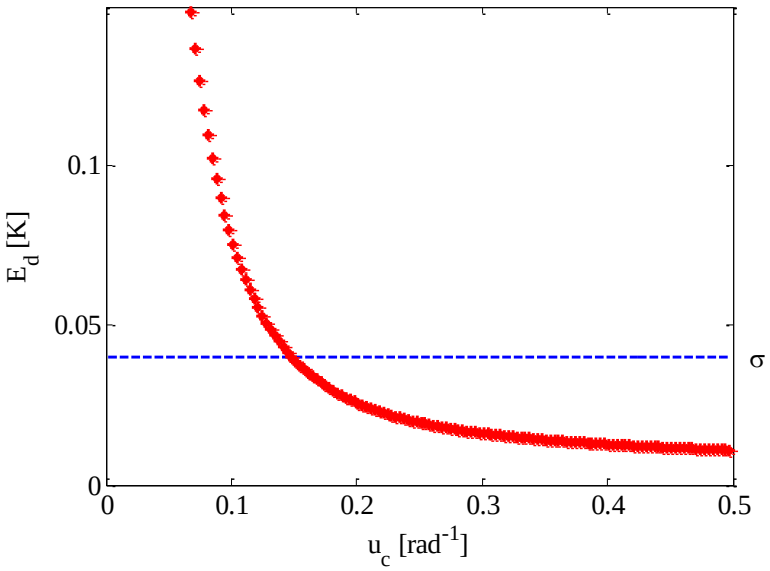

Figure 6.8. Function E_d against the cutoff frequency (GFT HSW045 , *Re* = 558, *Pr* = 182).

The intersection of the plotted curve with the assumed noise level identifies the cutoff frequency as approximately 0.15 rad^{-1}. Figures 6.9-6.11 show the reconstructed temperature distribution with the optimal cutoff frequency compared to the experimental rough data, the residuals between the experimental and filtered temperature distributions and the convective heat transfer coefficient distribution along the circumferential coordinate, which was restored from equation (5.22) after applying the filtering technique, respectively.

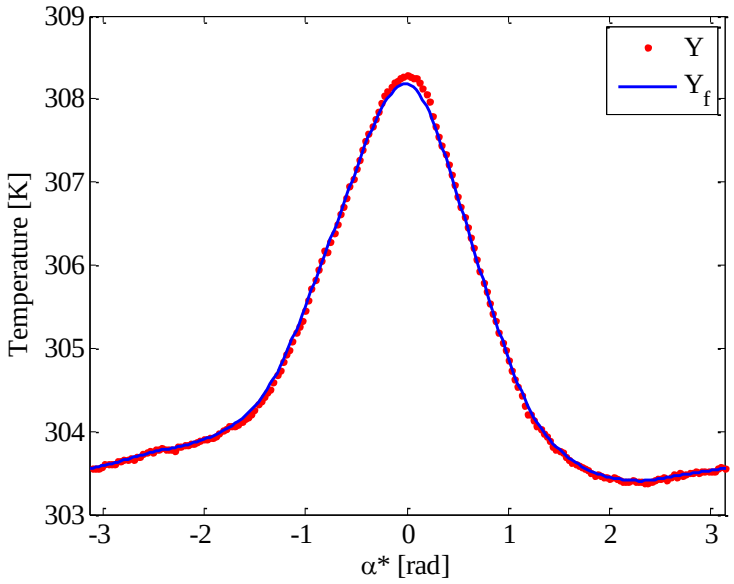

Figure 6.9: Experimental (Y) and filtered (Y_f) temperature distribution (GFT HSW045 u_c = 0.15 rad^{-1}, *Re* = 558, *Pr* = 182).

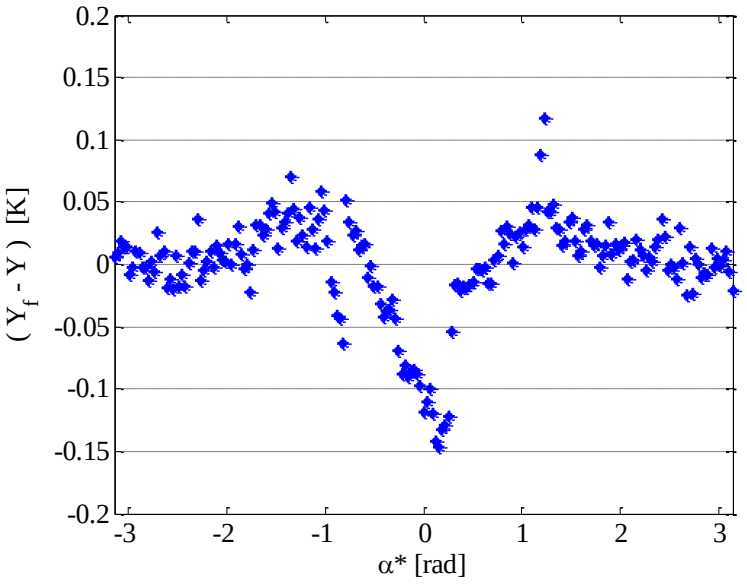

Figure 6.10: Residuals between the experimental (Y) and the filtered (Y_f) temperature distribution (GFT HSW045 u_c = 0.15 rad^{-1}, *Re* = 558, *Pr* = 182).

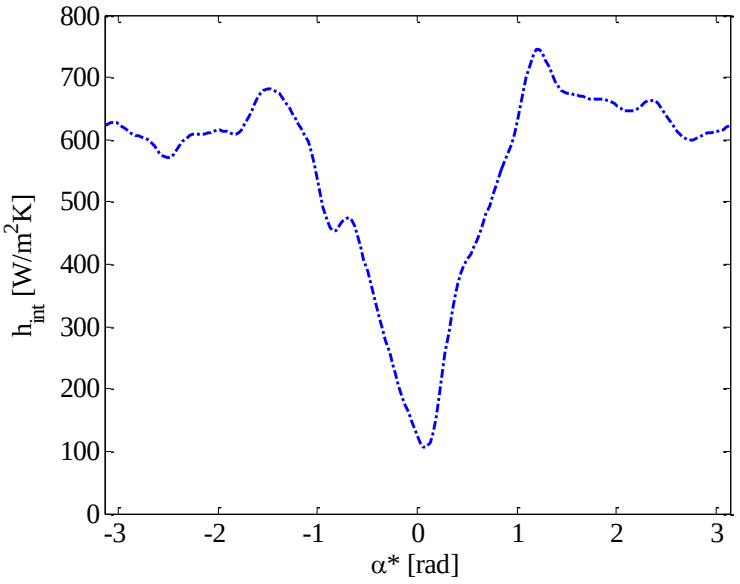

Figure 6.11. Restored convective heat-transfer coefficient distribution (GFT HSW045 u_c = 0.15 rad^{-1}, *Re* = 558, *Pr* = 182).

Quadrupole Method

In the Quadrupole formulation, described in paragraph 5.4, the truncation parameter was identified by the interception of the $E_d = \|(\boldsymbol{T} - \boldsymbol{Y})\|_2/\sqrt{N_\alpha}$ curve with the estimated noise level σ=0.04K. The trend of E_d versus the truncation parameter is reported in figure 6.12.

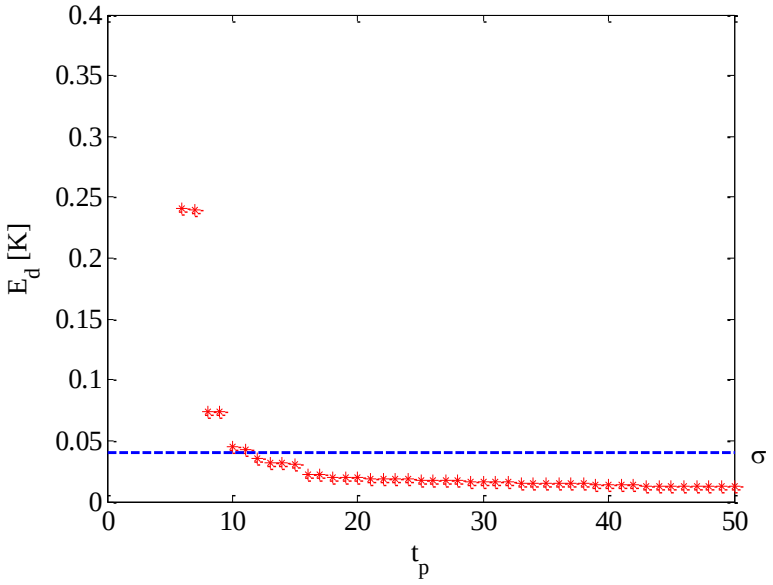

Figure 6.12. Function E_d against the truncation parameter (QM HSW045 *Re* = 558, *Pr* = 182).

From figure 6.12 the truncation parameter is individuated as about 11. In figure 6.13 the restored temperature distribution obtained by the estimation procedure, applied by considering $t_p = 11$, is shown.

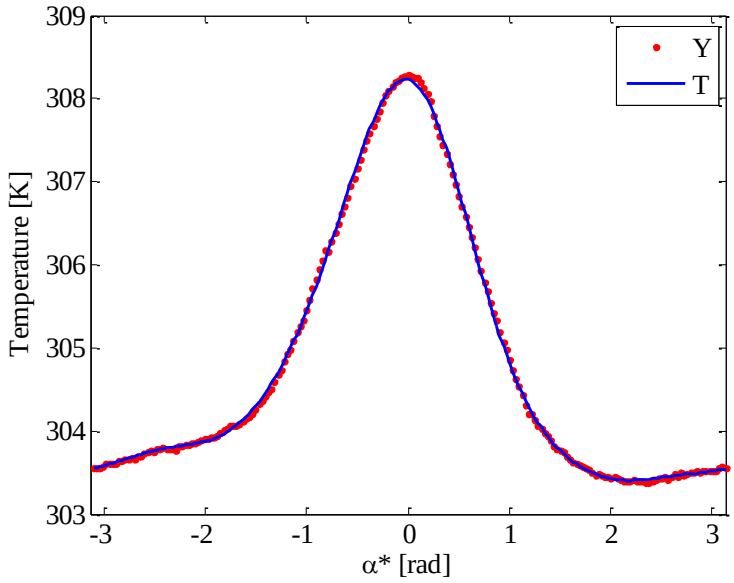

Figure 6.13: Experimental (Y) and reconstructed (T) temperature distribution (QM HSW045 $t_p = 11$, *Re* = 558, *Pr* = 182).

The corresponding residuals between the experimental and the restored temperature were reported in figure 6.14.

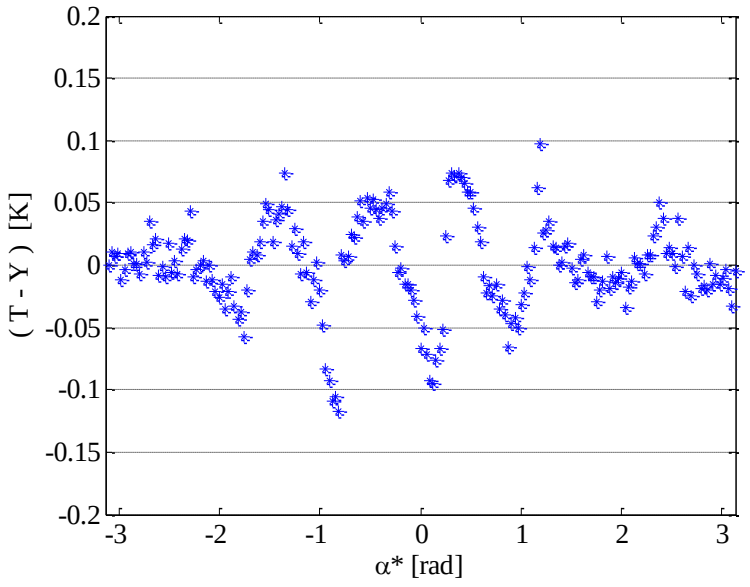

Figure 6.14: Residuals between the experimental (Y) and the reconstructed (T) temperature distribution (QM HSW045 $t_p = 11$, *Re* = 558, *Pr* = 182).

The convective heat transfer coefficient distribution, obtained by adopting the truncation parameter $t_p = 11$, is shown in figure 6.15.

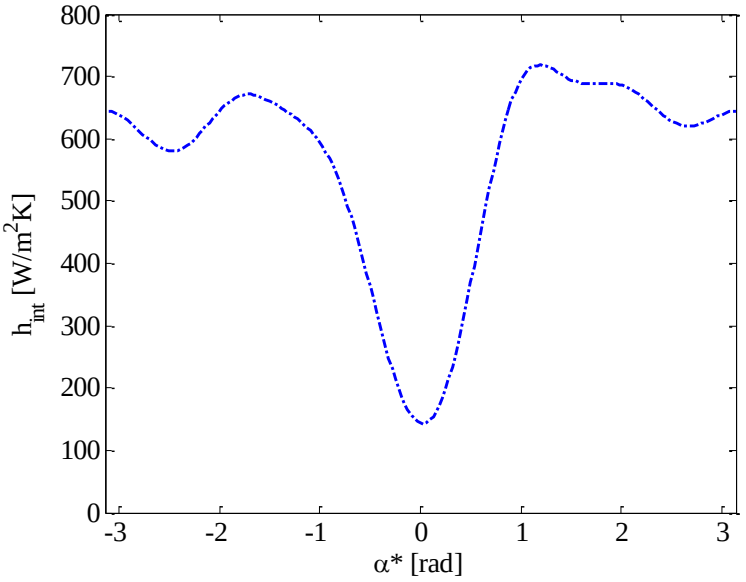

Figure 6.15. Restored convective heat-transfer coefficient distribution (QM HSW045 $t_p = 11$, *Re* = 558, *Pr* = 182).

COMPARISON

The convective heat transfer coefficient distributions restored by TRM, GFT and QM are compared in figure 6.16: the plot underlines that, for the case here investigated, the three approaches give comparable results and in particular TRM and QM perform almost equivalently.

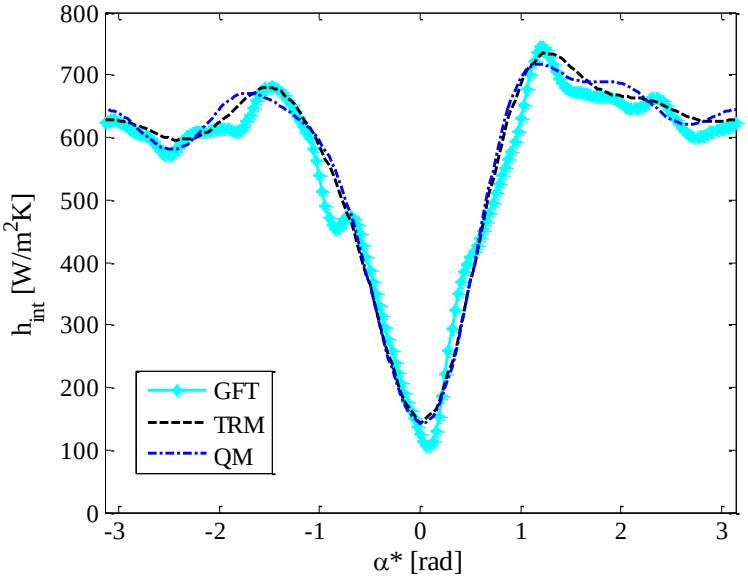

Figure 6.16: Convective heat transfer distribution obtained by QM, TRM and GFT (HSW045 *Re* = 558, *Pr* = 182).

The residuals between the restored and the experimental temperature distribution, shown in figure 6.17, add some information about the performances of the three techniques: the residuals produced by TRM and QM are more randomly distributed than the ones by GFT.

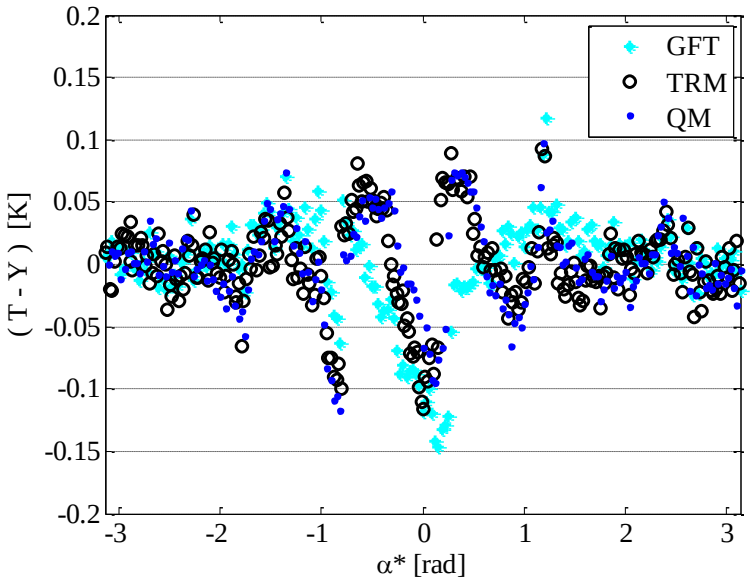

Figure 6.17: Residuals between the experimental (Y) and the reconstructed (T) temperature obtained by QM, TRM and GFT for noise level $\sigma = 1$K (HSW045 *Re* = 558, *Pr* = 182).

This fact, as already observed in the numerical validation of paragraph 5.5, suggests that TRM and GFT works slightly better than GFT that tends to smoothen the temperature distribution; it has although to be considered that the implementation of the regularization approach through Gaussian filter requires a lower computational cost if compared to TRM and QM.

Since the performances of the three different techniques, and in particular of QM and TRM, were almost equivalent the results of the experimental measurements sets are reported for only one estimation procedure: the Tikhonov regularization method. It was selected the TRM, because in addiction respect the other two techniques, the implementation with the fixed point method, makes possible to select the regularization parameter without having a priori information about the noise.

6.2 EXPERIMENTAL RESULTS

The results of experimental analysis performed on the tubes HSW045 and HSW03 are reported below.

TUBE HSW045

The experimental conditions of the tests performed on the tube HSW045 are shown in Table 6.2.

Re	De	Pr	q_g [W/m^3]	T_b [K]	$\overline{T}_w$ [K]	Gr/Re^2
135	29	172	$2.7\cdot10^6$	296.6	305.9	$3.4\cdot10^{-2}$
375	80	174	$4.8\cdot10^6$	296.4	307.1	$5.0\cdot10^{-2}$
465	100	163	$4.8\cdot10^6$	298.0	306.5	$2.9\cdot10^{-2}$
558	119	182	$4.8\cdot10^6$	295.2	304.7	$1.8\cdot10^{-3}$
665	142	185	$4.8\cdot10^6$	294.7	303.4	$1.1\cdot10^{-3}$
703	150	187	$4.8\cdot10^6$	294.5	302.4	$9.1\cdot10^{-4}$
904	194	189	$4.8\cdot10^6$	294.1	300.3	$4.2\cdot10^{-4}$
1006	215	190	$4.8\cdot10^6$	293.9	299.5	$3.0\cdot10^{-4}$
1060	227	196	$4.8\cdot10^6$	293.1	299.0	$2.7\cdot10^{-4}$
1098	235	175	$4.8\cdot10^6$	296.2	300.3	$2.2\cdot10^{-4}$

Table 6.2: Experimental conditions for tube HSW045.

In figure 6.18, in order to underline the effect of torsion induced by the coil pitch, the Nusselt number distribution for three different Dean numbers is reported versus the angular coordinate α where the angular coordinate origin was taken at the inner side of the coil. The torsion effect creates a rotation force that affects the flow pattern. Consequentially, it makes the distribution of the Nusselt number non-symmetrical, as already observed by Yang et al. (1995): the heat-transfer rate is increased on half of the tube wall compared to that on the other half.

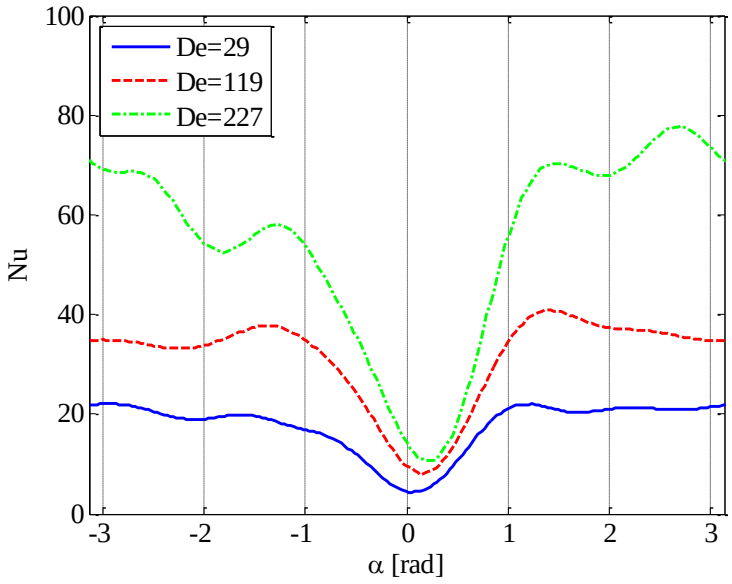

Figure 6.18: Restored Nusselt number distribution for three representative Dean number values for HSW045.

Moreover, as the Dean number increases, the location of the minimum Nusselt number shifts slightly from zero to higher angular coordinate values: the minimum is at approximately α=0.02 rad for *De* equal to 29, and it is at α=0.15 rad for *De* equal to 227.

The heat transfer coefficient distributions for each test of table 6.1 are reported in figures 6.19-6.27 versus the relative angular coordinate α^*. The distribution were reported with the 95% confidence interval: more details about the uncertainty analysis will be given in the next paragraph.

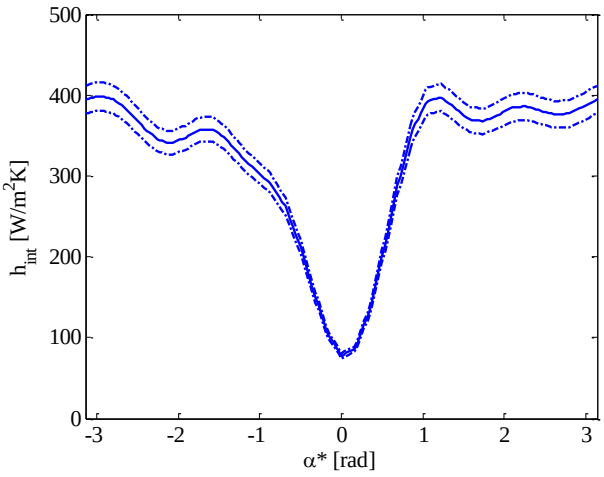

Figure 6.19: Restored convective heat-transfer coefficient distribution with 95% confidence interval (HSW045 *Re* =135).

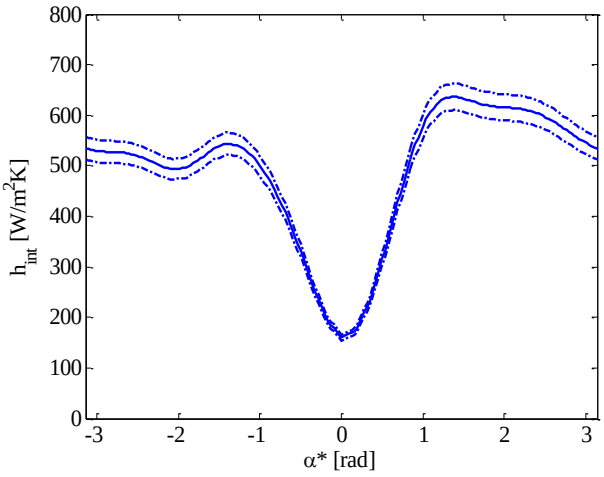

Figure 6.20: Restored convective heat-transfer coefficient distribution with 95% confidence interval (HSW045 *Re* =375).

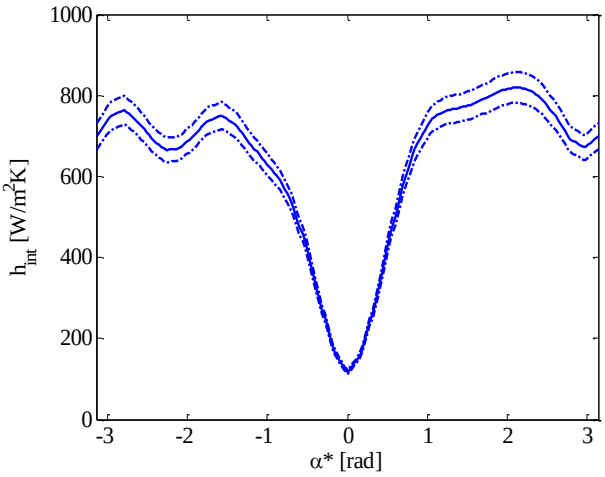

Figure 6.21: Restored convective heat-transfer coefficient distribution with 95% confidence interval (HSW045 *Re* =465).

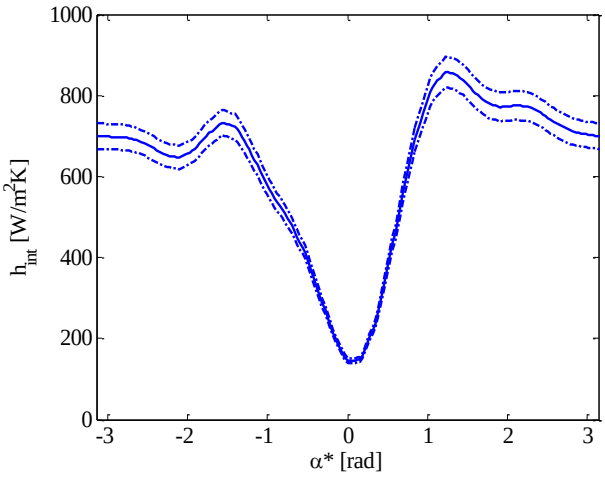

Figure 6.22: Restored convective heat-transfer coefficient distribution with 95% confidence interval (HSW045 *Re* =665).

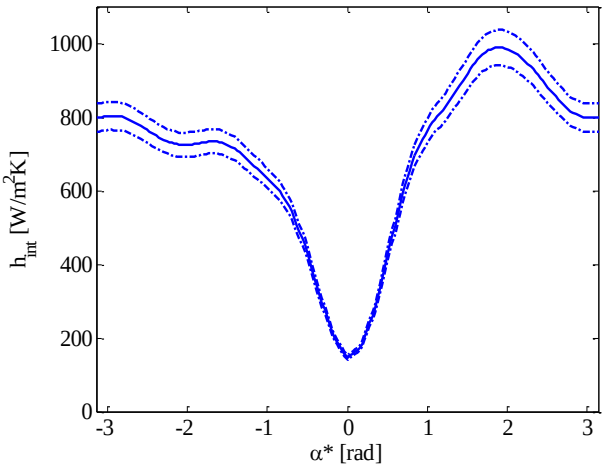

Figure 6.23: Restored convective heat-transfer coefficient distribution with 95% confidence interval (HSW045 *Re* =703).

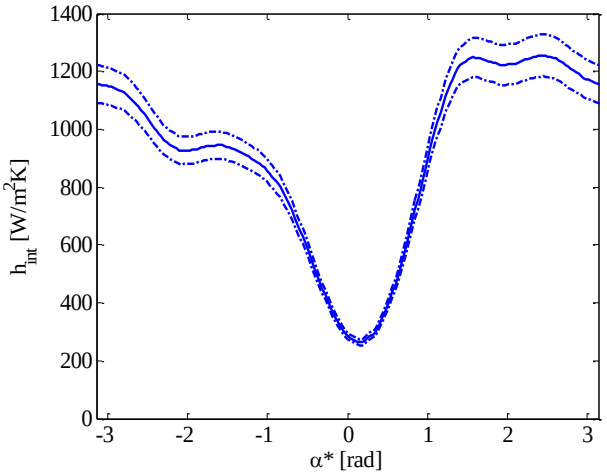

Figure 6.24: Restored convective heat-transfer coefficient distribution with 95% confidence interval (HSW045 *Re* =904).

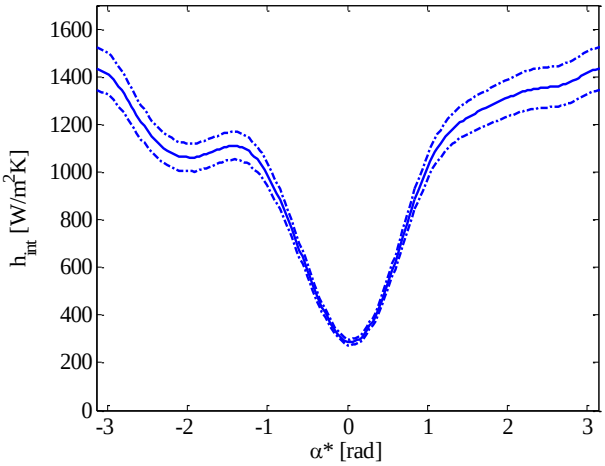

Figure 6.25: Restored convective heat-transfer coefficient distribution with 95% confidence interval (HSW045 *Re* =1006).

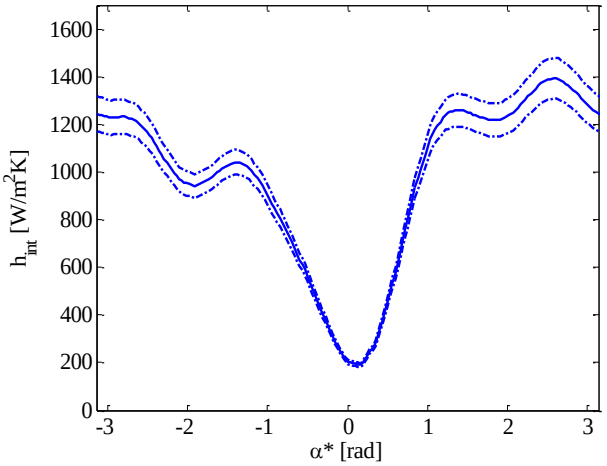

Figure 6.26: Restored convective heat-transfer coefficient distribution with 95% confidence interval (HSW045 *Re* =1060).

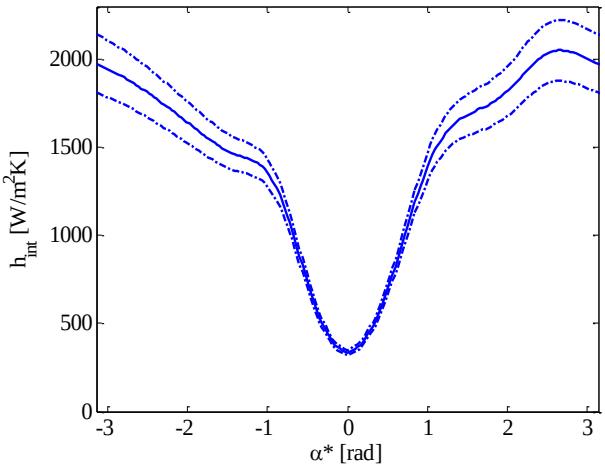

Figure 6.27: Restored convective heat-transfer coefficient distribution with 95% confidence interval (HSW045 *Re* =1098).

In order to compare the Nusselt number distribution of the various tests performed at different Reynolds numbers and thus at different Dean numbers, the Nu/Nu_{max} ratio was determined, as shown in figure 6.28: by accounting for the experimental uncertainty, it can be stated that this ratio is almost independent from the Dean number. A similar observation was made by Jayakumar et al. (2010) for turbulent heat transfer in helical pipes.

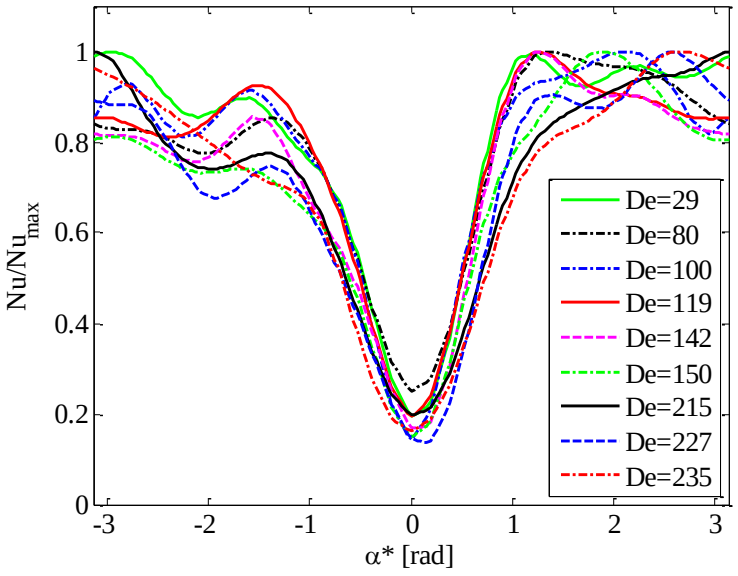

Figure 6.28: Normalised local Nusselt number for various Dean numbers for HSW045.

Moreover, the data show that, at the outside surface of the coil, the Nusselt number is approximately five times the one at the inside surface. The data confirms the observations made by Bai et al. (1999), Seban and McLaughlin (1963) and Jayakumar et al. (2010). The pattern is

particularly steep and Nu/Nu_{max} is above 0.8 for approximately 75% of the circumference. Figure 6.29 reports the best fit of the experimental distributions reported in figure 6.28, along the curvilinear coordinate with the 95% confidence interval and the correlations found by Yang et al. (1995).

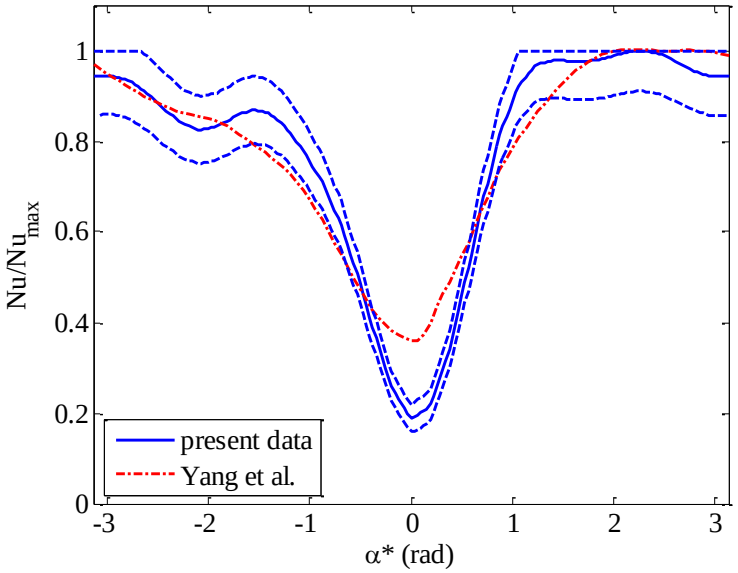

Figure 6.29: Normalised local Nusselt number for HSW045 and comparison with the data by Yang et al. (1995).

The data by Yang et al. (1995) mainly match the distribution obtained here, although some discrepancies are registered, especially close to the inner bend side of the coil. This may be because Yang et al. (1995) derived their data for a coiled tube with a torsion value similar to the one of the tube investigated here but for a fluid with a Prandtl number equal to 5.

TUBE HSW030

The experimental conditions of the tests performed on the tube HSW030 are reported in table 6.3.

Re	De	Pr	q_g [W/m^3]	T_b [K]	$\overline{T}_w$ [K]	Gr/Re^2
116	21	178	$2.59 \cdot 10^{6}$	295.7	304.18	$3.92 \cdot 10^{-2}$
187	34	223	$1.75 \cdot 10^{6}$	290.8	295.15	$4.90 \cdot 10^{-3}$
273	49	212	$2.60 \cdot 10^{6}$	291.8	297.84	$3.59 \cdot 10^{-3}$
386	70	217	$2.60 \cdot 10^{6}$	291.3	296.01	$1.32 \cdot 10^{-3}$
533	96	213	$3.10 \cdot 10^{6}$	291.7	296.45	$7.31 \cdot 10^{-4}$
572	104	203	$3.63 \cdot 10^{6}$	292.5	298.98	$9.49 \cdot 10^{-4}$
637	115	203	$3.63 \cdot 10^{6}$	292.6	298.89	$7.48 \cdot 10^{-4}$

Re	De	Pr	q_g [W/m^3]	T_b [K]	$\overline{T}_w$ [K]	Gr/Re^2
659	119	199	$4.20 \cdot 10^6$	292.9	299.33	$7.37 \cdot 10^{-4}$
716	130	203	$3.63 \cdot 10^6$	292.5	298.55	$5.64 \cdot 10^{-4}$
724	131	198	$4.20 \cdot 10^6$	293.0	299.22	$6.02 \cdot 10^{-4}$
804	146	199	$4.20 \cdot 10^6$	293. 0	298.93	$4.66 \cdot 10^{-4}$
807	146	203	$3.63 \cdot 10^6$	292.6	298.30	$4.25 \cdot 10^{-4}$
902	163	198	$4.21 \cdot 10^6$	293.0	298.64	$3.51 \cdot 10^{-4}$
910	165	196	$4.21 \cdot 10^6$	293.1	298.34	$3.23 \cdot 10^{-4}$

Table 6.3: Experimental conditions for tube HSW030.

The heat transfer coefficient distributions with the corresponding 95% confidence interval for each run of Table 6.3 are reported in figures 6.30-6.43 versus the relative angular coordinate α^*.

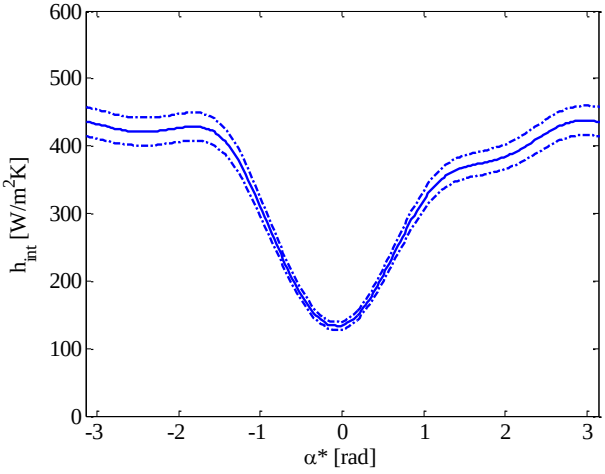

Figure 6.30: Restored convective heat-transfer coefficient distribution with 95% confidence interval (HSW030 *Re* =116).

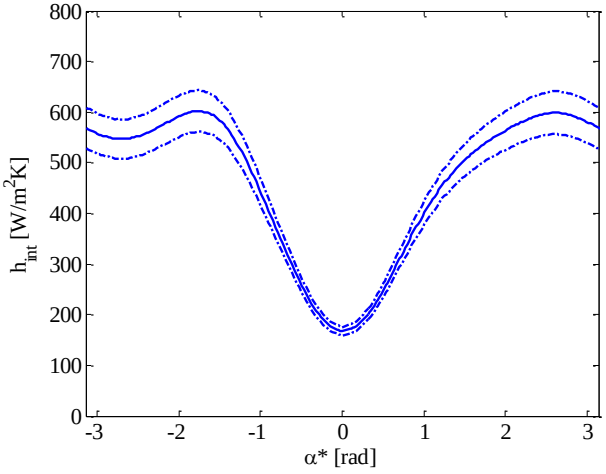

Figure 6.31: Restored convective heat-transfer coefficient distribution with 95% confidence interval (HSW030 *Re* =187).

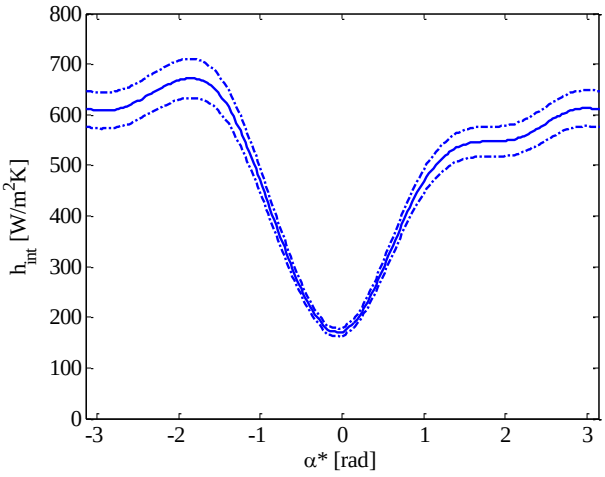

Figure 6. 32: Restored convective heat-transfer coefficient distribution with 95% confidence interval (HSW030 *Re* =273).

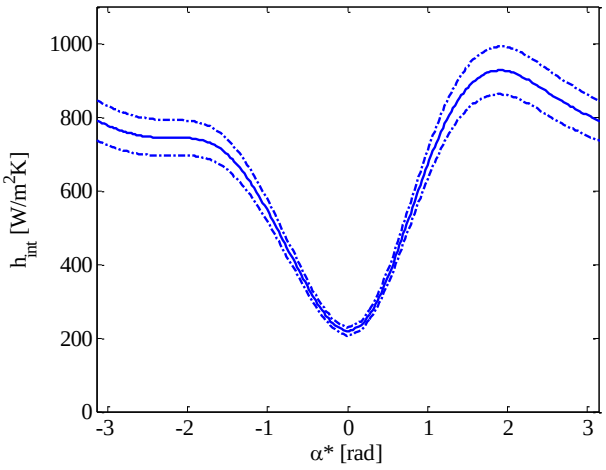

Figure 6.33: Restored convective heat-transfer coefficient distribution with 95% confidence interval (HSW030 *Re* =386).

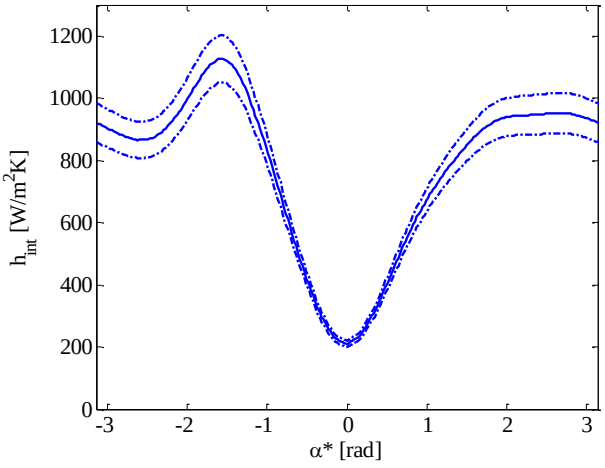

Figure 6.34: Restored convective heat-transfer coefficient distribution with 95% confidence interval (HSW030 *Re* =533).

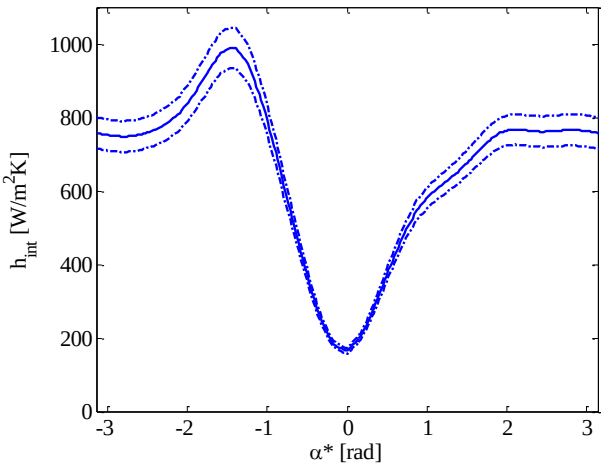

Figure 6.35: Restored convective heat-transfer coefficient distribution with 95% confidence interval (HSW030 *Re* =572).

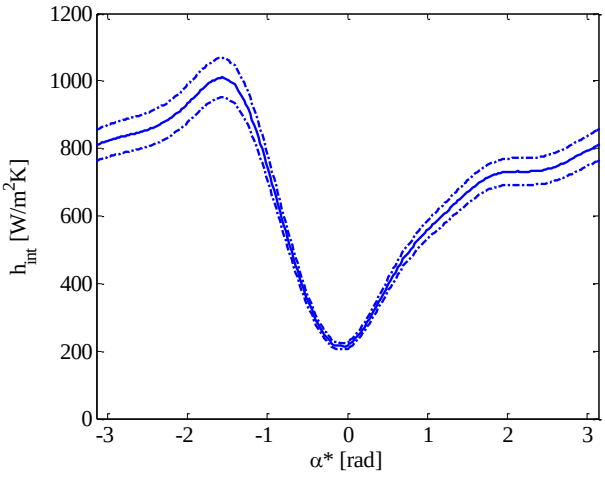

Figure 6.36: Restored convective heat-transfer coefficient distribution with 95% confidence interval (HSW030 *Re* =637).

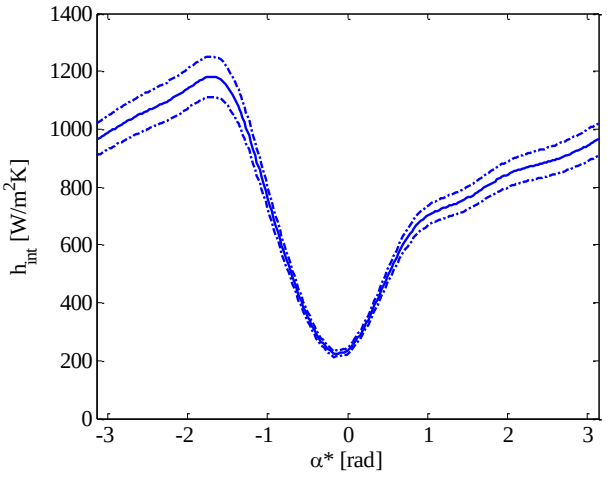

Figure 6.37: Restored convective heat-transfer coefficient distribution with 95% confidence interval (HSW030 *Re* =659).

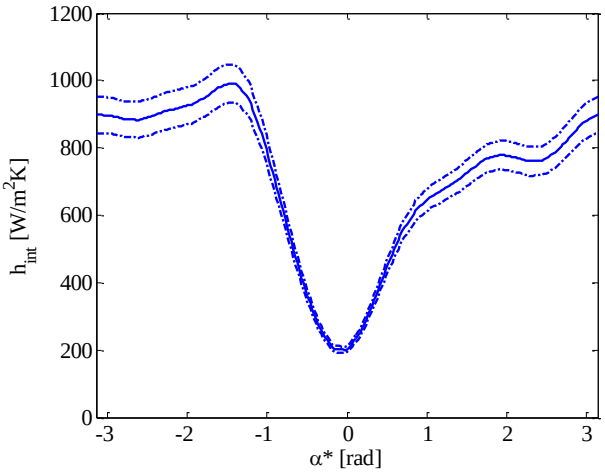

Figure 6.38: Restored convective heat-transfer coefficient distribution with 95% confidence interval (HSW030 *Re* =716).

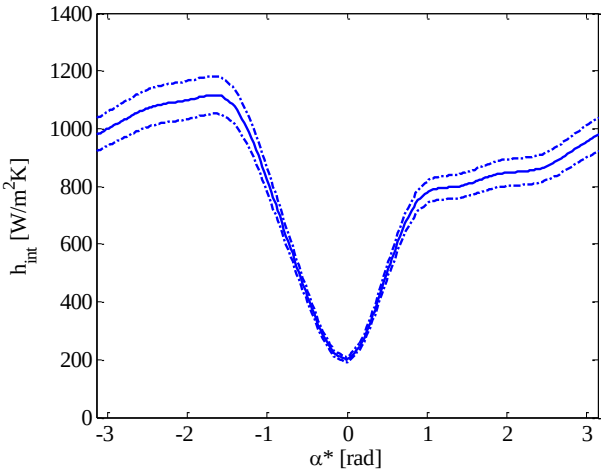

Figure 6.39: Restored convective heat-transfer coefficient distribution with 95% confidence interval (HSW030 *Re* =724).

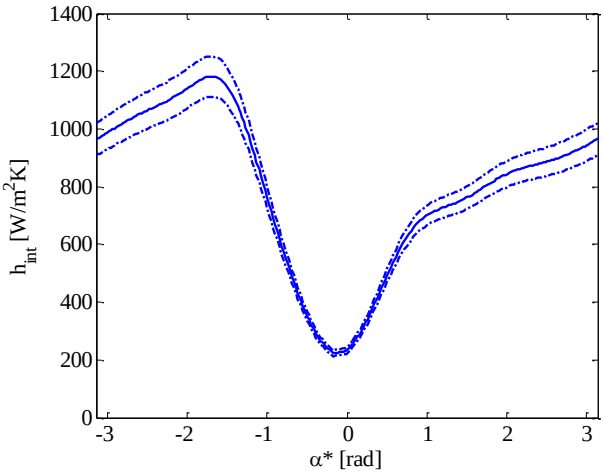

Figure 6.40: Restored convective heat-transfer coefficient distribution with 95% confidence interval (HSW030 *Re* =804).

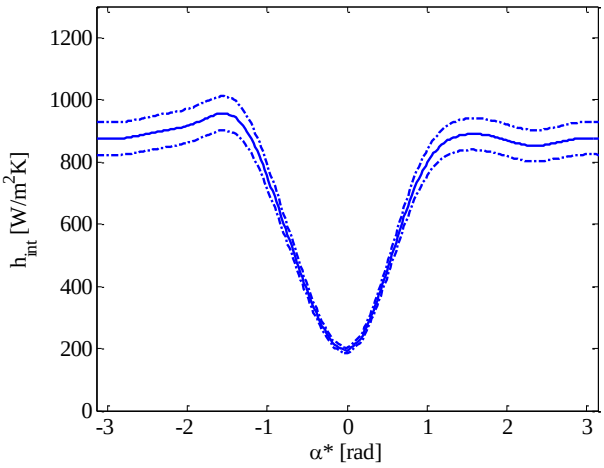

Figure 6.41: Restored convective heat-transfer coefficient distribution with 95% confidence interval (HSW030 *Re* =807).

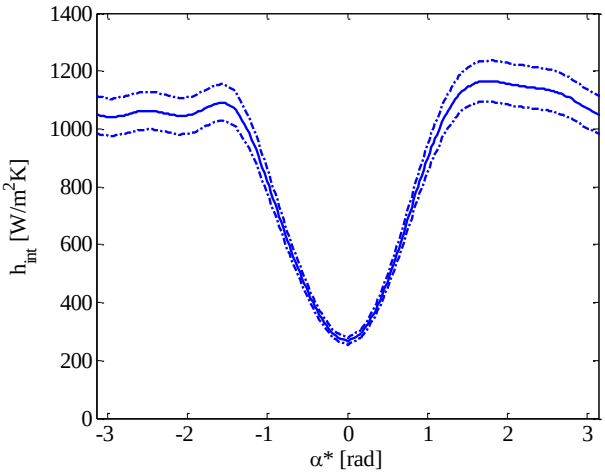

Figure 6.42: Restored convective heat-transfer coefficient distribution with 95% confidence interval (HSW030 *Re* =902).

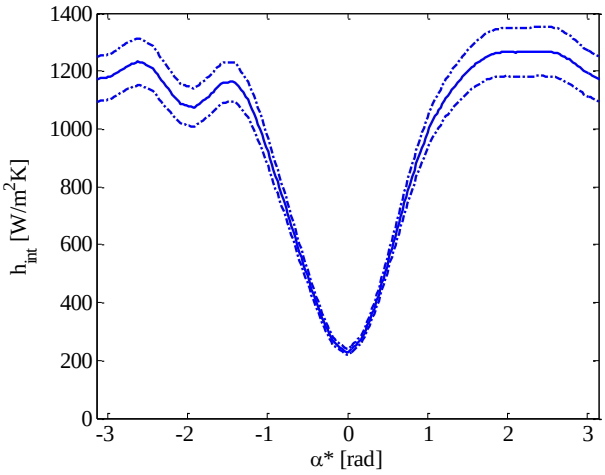

Figure 6.43: Restored convective heat-transfer coefficient distribution with 95% confidence interval (HSW030 *Re* =910).

The Nu/Nu_{max} ratio is reported in figure 6.44.

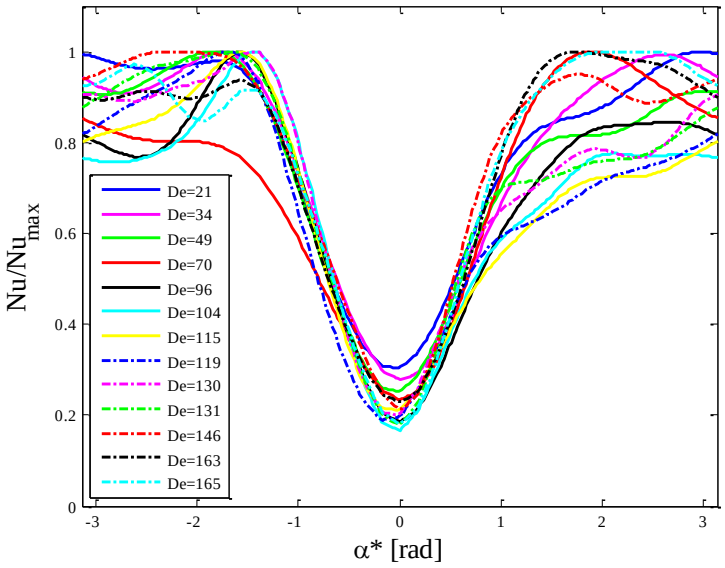

Figure 6.44: Normalised local Nusselt number for different Dean numbers for HSW030.

As already observed for the first tube under analysis there is a great variation between the Nusselt number at the outer bend side of the coil and the one at the inner bend side. Specifically the ratio between the two values is about five for almost all the tests: only the tests performed at very low Dean numbers present a ratio smaller than five. In order to compare the behaviours of the two tubes in figure 6.45 the heat transfer coefficient distributions for some significant Dean number values for both the tubes are reported.

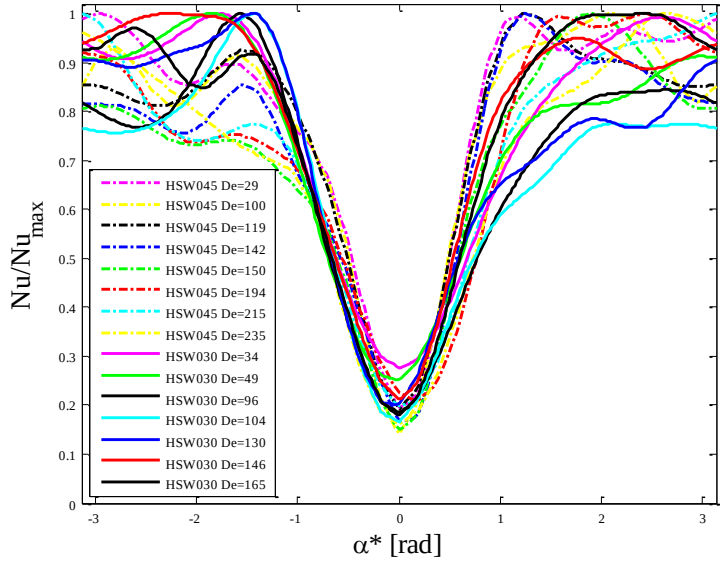

Figure 6.45: Normalised local Nusselt number for various Dean numbers. Comparison between tubes HSW045 and HSW030.

For both the tubes the pattern is particularly steep and considering the uncertainty is almost equivalent for every test. Although it has to be noticed that in tube HSW03 for low Dean number values the Nu_{min}/Nu_{max} ratio in correspondence of $\alpha^* = 0$, is higher than 0.2 and decrease with the increasing of the De reaching approximately the value of 0.2 for Dean number values higher than 70. Figure 6.46 reports the best fit of the experimental distributions shown in figure 6.44, along the relative angular coordinate α* with the 95% confidence interval and the correlations proposed by Yang et al. (1995).

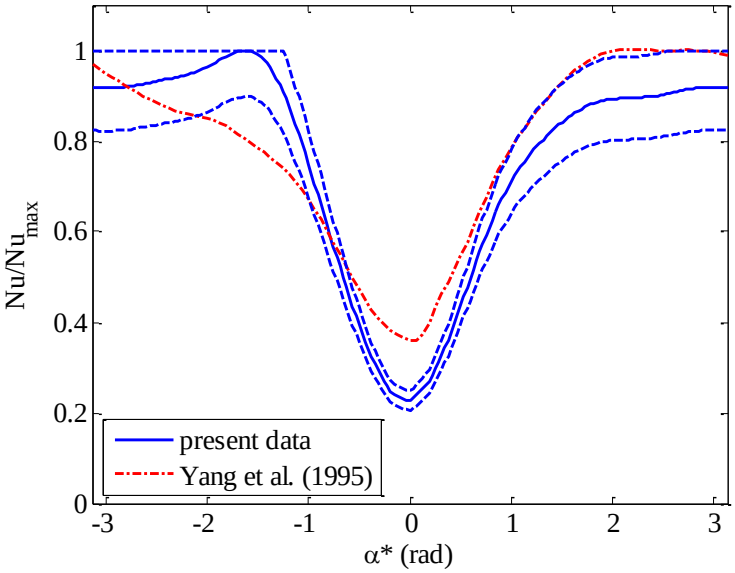

Figure 7.46: Normalised local Nusselt number and comparison with the data by Yang et al. (1995) for the tube HSW030.

Also for this tube the data by Yang et al. (1995) mainly match the distribution obtained here, even if some differences are present, especially close to the inner bend side of the coil.

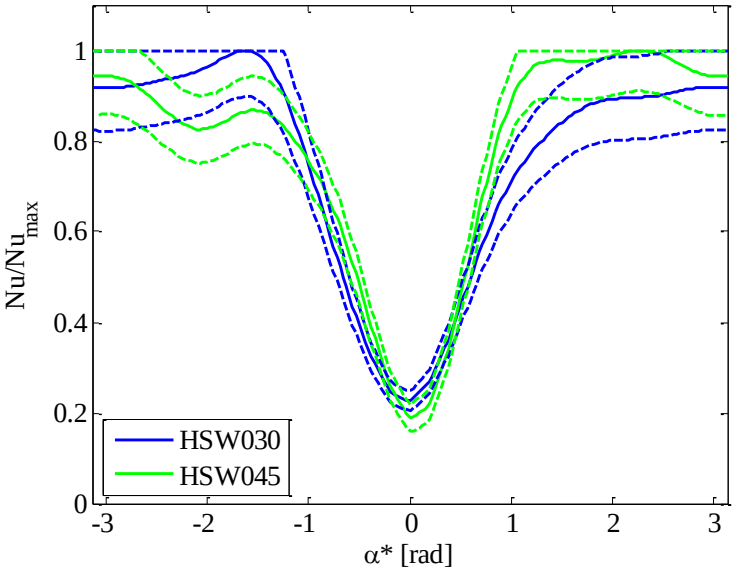

Figure 6.47: Normalised local Nusselt number for HSW045 and HSW030.

In figure 6.47 the best fit of the experimental distributions for both tube HSW045 and HSW030 is shown. By accounting for the experimental uncertainty, it can be stated that the shape of the two ratio distribution is almost the same.

The best fit of all the experimental distribution shown in figure 6.28 and 6.44 has been performed and reported along the curvilinear coordinate with the 95% confidence interval in figure 6.48.

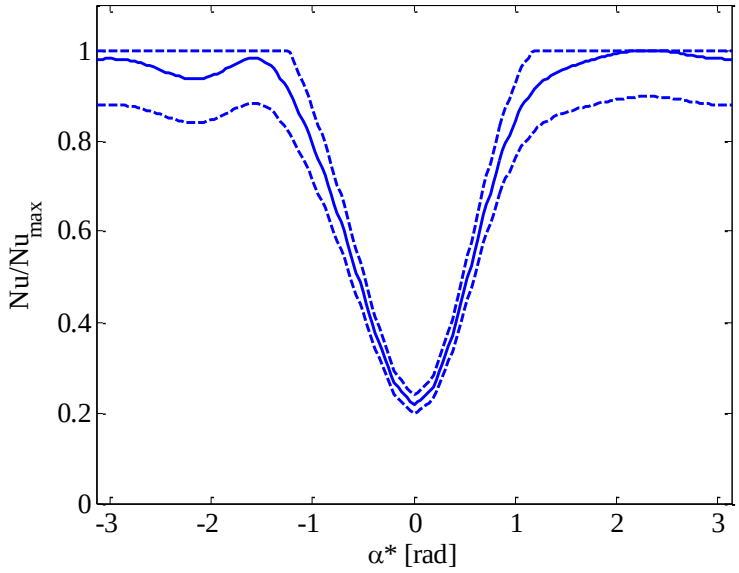

Figure 6.48: Normalised local Nusselt number for all the tests performed.

6.3 UNCERTAINTY ANALYSIS

The 95% confidence interval associated with the estimated heat flux was determined by parametric bootstrap (Orlande et al. 2011; Reinhardt et al. 2007; Blackwell and Beck 2010), adopting the Monte Carlo method. It refers to a statistical procedure for estimating mathematical solutions to certain physical problems and it has been used in science and engineering fields for a variety of applications. Monte Carlo technique is a class of computational algorithms that rely on repeated random sampling to compute results (Woodbury 2003). Monte Carlo simulation can help an experimenter to methodically investigate the uncertainty on the results associated with the uncertainty of each input variable. In fact a fundamental task of a Monte Carlo simulation is that it can give information, starting from the uncertainty on the input data, about how likely the resulting outcomes are. A random value is considered for each of the primary measurements, based on their uncertainty interval. Then the result is computed referring to these random values and for each set of input parameters a set of output parameters is found. The value of each output parameter is one

particular outcome scenario in the simulation run. These output values are detected from a number of simulation runs and eventually a statistical analysis on the values of the output parameters is performed (Raychaudhuri 2008). The 95% confidence interval associated with the estimated heat flux was computed assuming the uncertainties in the input data reported in Table 6.4.

Y (K)	**α (°)**	**λ (W/m·K)**	**T_{env} (K)**	**R_{env} (m^2·K/W)**	**q_g (W/m^3)**	**T_b (K)**
±0.1 K	±4°	±5%	±0.1 K	±50%	±4%	±0.2 K

Table 6.4: The 95% confidence interval of the main physical quantities involved in the estimation procedure.

The uncertainty on the angle was estimated considering the contributions of the uncertainty on the geometrical reference scale and its placement on the tube. The uncertainty on the tube wall thermal conductivity was given by the manufacturer and was also checked by experimental measurements. The error on the R_{env} was assumed considering the correlation present in literature. More information about the uncertainty values on the other input data are presented in paragraph 4.2.
To identify the main contributions to the uncertainty of the estimated heat flux distribution, the influence coefficient values (Holman 2001) were calculated:

$$J_{\varrho}^{Z} = \left(\frac{\partial Z}{\partial \varrho}\varepsilon_{\varrho}\right)^{2} \tag{6.1}$$

where Z is the estimated quantity and ϱ is the considered input parameter with an uncertainty equal to ε_{ϱ}. For the inverse problem investigated in this work, the analytical determination of the partial derivative present in equation (6.1) is impossible, and the adoption of a finite difference approach is needed:

$$\frac{\partial Z}{\partial \varrho} = \frac{Z(\varrho + \Delta\varrho) - Z(\varrho)}{\Delta\varrho} \tag{6.2}$$

where $\Delta\varrho$ is a small variation of the input parameter ϱ.
Tables 6.5 reports the influence-coefficient values for the main input parameters, considering the maximum and the minimum of the estimated heat flux as representative output quantities of the inverse problem solution and computed for the experimental case of tube HSW045 and Re=558. These results underline that the main contributions to the uncertainty are related to λ and q_g, and the uncertainties in R_{env} and T_{env} are almost insignificant. This means that the heat exchanged between the tube wall and the environment is negligible in comparison to that exchanged between the tube

wall and the working fluid. On the contrary, to improve the overall situation, particular attention to the accuracy of λ and q_g should be given.

	$\boldsymbol{\lambda}$	$\boldsymbol{T_{env}}$	$\boldsymbol{R_{env}}$	$\boldsymbol{q_g}$
$\boldsymbol{q_{max}}$	$J_{\lambda}^{q_{max}} = 5.3 \cdot 10^{3}\ W^2/m^4$	$J_{T_{env}}^{q_{max}} = 0.33\ W^2/m^4$	$J_{R_{env}}^{q_{max}} = 3.8 \cdot 10^{2}\ W^2/m^4$	$J_{q_g}^{q_{max}} = 4.2 \cdot 10^{4}\ W^2/m^4$
$\boldsymbol{q_{min}}$	$J_{\lambda}^{q_{min}} = 2.6 \cdot 10^{4}\ W^2/m^4$	$J_{T_{env}}^{q_{min}} = 0.33\ W^2/m^4$	$J_{R_{env}}^{q_{max}} = 8.4 \cdot 10^{2}\ W^2/m^4$	$J_{q_g}^{q_{min}} = 5.1 \cdot 10^{3}\ W^2/m^4$

Table 6.5: Influence coefficient values of λ, T_{env} , R_{env} and q_g on the maximum and the minimum of the estimated heat-flux distribution (HSW045 Re=558).

7. LOCAL NUSSELT NUMBER IN CORRUGATED WALL COILED TUBES. EXPERIMENTAL STUDY: PRELIMINARY RESULTS.

The local convective heat transfer coefficient distribution at the internal wall interface on a given cross section was experimentally investigated also for the corrugated wall coiled tubes and preliminary results were obtained. The experimental measurements procedure is the same as the one described in chapters 3 and 6 and it was performed on tube HCW045 (for geometrical parameters see chapter 3). The estimation method employed is based on a 2-D form of the procedure based on Gaussian filter technique and already presented in paragraph 5.3. In order to evaluate the local actual value of the convective heat transfer coefficient at the fluid internal wall interface, a simplified model of the test section was adopted: it is formulated by assuming that the coil portion viewed by the infrared camera can be modeled as a finite section of a circular cylindrical shell. This model introduces a negligible error since the helix diameter is significantly bigger than tube external diameter and wall corrugation doesn't significantly modify the thickness of the tube wall.

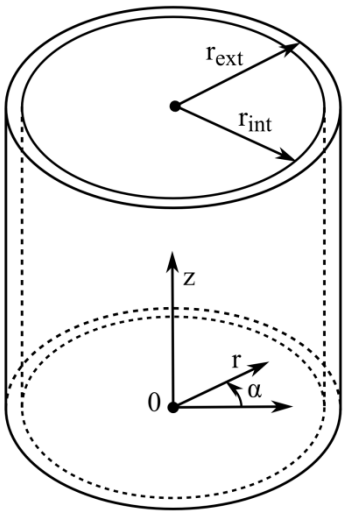

Figure 7.1: Geometrical domain with coordinate system.

By assuming the thin wall approximation:

$$T(\alpha, r, z) \cong T(\alpha, r_{int}, z) \cong T(\alpha, r_{ext}, z) \tag{7.1}$$

and with reference to the infinitesimal cylindrical sector shown in figure 7.2, the steady state local energy balance equation becomes:

$$Q_{\alpha+d\alpha} + Q_{\alpha} + Q_{r_{int}} + Q_{r_{ext}} + Q_z + Q_{z+dz} + Q_g = 0 \tag{7.2}$$

with:

$$Q_{\alpha} = \int_{r_{int}}^{r_{ext}} -\frac{\lambda \partial T}{r \partial \alpha} dr dz = -\lambda \frac{dT}{d\alpha} ln\left(\frac{r_{ext}}{r_{int}}\right) dz \tag{7.3}$$

$$\begin{aligned} Q_{\alpha+d\alpha} &= -\left(Q_{\alpha} + \frac{\partial Q_{\alpha}}{\partial \alpha} d\alpha\right) = -\left[-\lambda \frac{\partial T}{\partial \alpha} ln\left(\frac{r_{ext}}{r_{int}}\right) dz + \frac{\partial}{\partial \alpha}\left(-\lambda \frac{\partial T}{\partial \alpha} ln\left(\frac{r_{ext}}{r_{int}}\right) dz\right) d\alpha\right] = \\ &= \lambda \frac{\partial T}{\partial \alpha} ln\left(\frac{r_{ext}}{r_{int}}\right) dz + \lambda \frac{\partial^2 T}{\partial \alpha^2} ln\left(\frac{r_{ext}}{r_{int}}\right) d\alpha \, dz \end{aligned} \tag{7.4}$$

$$Q_{r_{int}} = -h_{int} \, (T - T_b) \, r_{int} \, d\alpha \, dz \tag{7.5}$$

$$Q_{r_{ext}} = -\frac{(T - T_{env})}{R_{env}} \, r_{ext} \, d\alpha \, dz \tag{7.6}$$

$$Q_z = \int_{r_{int}}^{r_{ext}} -\frac{\lambda \partial T}{\partial z} \frac{\pi r^2}{2\pi} d\alpha \, dr = -\lambda \frac{\partial T}{\partial z} \frac{(r_{ext}^2 - r_{int}^2)}{2} d\alpha \tag{7.7}$$

$$\begin{aligned} Q_{z+dz} &= -\left(Q_z + \frac{\partial Q_z}{\partial z} dz\right) = -\left[-\lambda \frac{\partial T}{\partial z} \frac{\left(r_{ext}^2 - r_{int}^2\right)}{2} d\alpha + \frac{\partial}{\partial z}\left(-\lambda \frac{\partial T}{\partial z} \frac{\left(r_{ext}^2 - r_{int}^2\right)}{2} d\alpha\right) dz\right] = \\ &= \lambda \frac{\partial T}{\partial z} \frac{\left(r_{ext}^2 - r_{int}^2\right)}{2} d\alpha + \lambda \frac{\partial^2 T}{\partial z^2} \frac{\left(r_{ext}^2 - r_{int}^2\right)}{2} d\alpha \, dz \end{aligned} \tag{7.8}$$

$$Q_g = q_g \frac{(\pi r_{ext}^2 - \pi r_{int}^2)}{2\pi} dz \, d\alpha = \frac{q_g}{2} \cdot (r_{ext}^2 - r_{int}^2) dz \, d\alpha \tag{7.9}$$

where r_{int} and r_{ext} are the internal and the external pipe radius, respectively, R_{env} is the overall heat transfer resistance between the tube wall and the surrounding environment with the temperature T_{env}, q_g is the heat generated per unit volume within the tube wall having thermal conductivity λ and T_b is the fluid local bulk temperature.

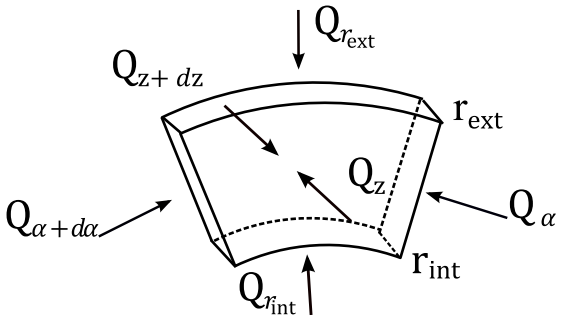

Figure 7.2: A portion of the test section.

Substituting equations (7.3-7.9) into equation (7.2) the energy equation becomes:

$$\lambda \cdot \ln\left(\frac{r_{ext}}{r_{int}}\right) \cdot \frac{\partial^2 T}{\partial \alpha^2} - h_{int} \cdot r_{int} \cdot (T - T_b) - \frac{r_{ext}}{R_{env}} \cdot (T - T_{env}) + \frac{\lambda}{2} \cdot (r_{ext}^2 - r_{int}^2) \cdot \frac{\partial^2 T}{\partial z^2} + \frac{q_g}{2} \cdot (r_{ext}^2 - r_{int}^2) = 0 \quad (7.10)$$

Eventually, the convective heat transfer coefficient on the internal wall surface follows as:

$$h_{int} = \frac{\lambda \cdot \ln\left(\frac{r_{ext}}{r_{int}}\right) \cdot \frac{\partial^2 T}{\partial \alpha^2} - \frac{r_{ext}}{R_{env}} \cdot (T - T_{env}) + \frac{\lambda}{2} \cdot \left(r_{ext}^2 - r_{int}^2\right) \cdot \frac{\partial^2 T}{\partial z^2} + \frac{q_g}{2} \cdot \left(r_{ext}^2 - r_{int}^2\right)}{r_{int} \cdot (T - T_b)} \quad (7.11)$$

This equation, if applied to discrete noisy data, gives unreliable results due to the peculiarities of the second derivative operator which is very sensitive to small perturbations in the input data due to the well-known destructive effect of the noise in IHCPs (see chapter 2). A convenient way to overcome these difficulties is found in filtering out the unwanted noise from the raw temperature data in order to make feasible the direct calculation of its Laplacian.

A Gaussian filter 2-D formulation was employed and the transfer function in the frequency domain, of this kind of filter can be expressed as follows:

$$H(u, v) = e^{-(u_f^2 + v_f^2)/2u_c^2}, \quad (7.12)$$

where u_c is the cutoff frequency. Since in real application the optimal cutoff frequency value for each kind of filter is not known a priori, a criterion to choose must be selected in order to make the regularization procedure successful. As it was described in paragraph 5.3, in the present analysis the criterion provided by the discrepancy principle (Morozov 1984), was adopted. According to this principle, the inverse problem solution is regarded to be sufficiently accurate when the difference between measured temperatures $\mathbf{Y}$ and filtered ones $\mathbf{Y}_f$ is close to the standard deviation of the raw measurements. The cutoff frequency was determined as the frequency at which the condition expressed in equation (7.13) is satisfied:

$$\frac{\|\mathbf{Y}_f - \mathbf{Y}\|_2}{\sqrt{N \cdot M}} = \sigma \quad (7.13)$$

where $\|\cdot\|_2$ stands for the 2-norm of a matrix, $N \cdot M$ is the size of the matrix $\boldsymbol{Y}$ and σ is the standard deviation of the measurement noise.

The estimation procedure was applied to two representative Dean number values, 25 and 202 i.e. in two conditions in which, according to chapter 4 and to Rainieri et al. (2012), the effect of the corrugation was expected to be significantly different.

In order to identify the position of the corrugation in the section under test, the representation in the visible spectrum of the unwrapped image of the coil external surface is reported in figure 7.3. In this

figure the position of the corrugation is highlighted and the adopted axes are indicated: the angular coordinate origin was taken at the inner side of the coil.

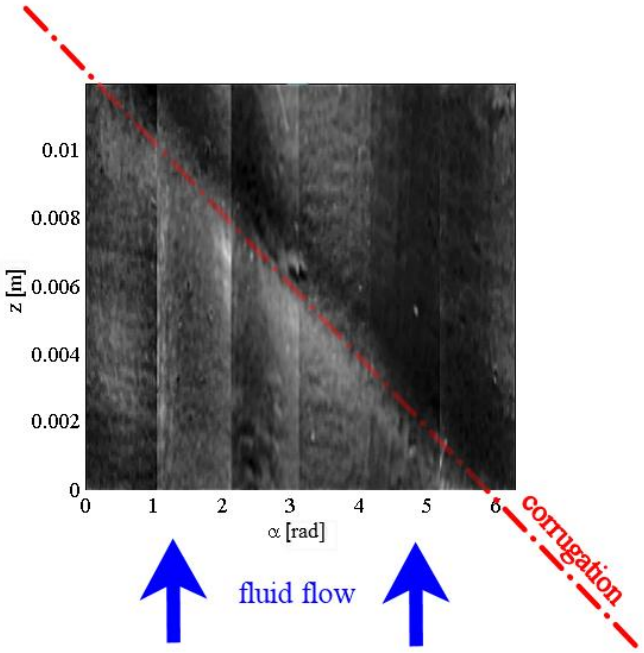

Figure 7.3: Unwrapped image of the coil external surface regarding the section under test.

In this chapter the plots are reported versus the angular coordinate taken from 0 to 2π to better describe and comprehend the effect of the corrugation in all its extension.

Figures 7.4 shows the wall temperature distributions for the two flow conditions; the data show that for *De*=25 the temperature distribution exhibits a significant variation along the circumference and that the temperature gradient is almost negligible along the axis of the tube, as it was observed for coiled tubes with smooth wall. On the contrary, for *De*=202, the temperature gradient along the tube axis, induced by the effect of the wall corrugation of the boundary layers, cannot be neglected.

The maps of the convective heat flux restored by applying the filtering procedure is reported in figure 7.5 while in figure 7.6 the $h_{int}/h_{int,max}$ ratio distributions for the two Dean numbers at different *z* positions are reported and compared to the smooth wall coiled tube behavior.

The data confirm that for low *De* value the wall curvature effect prevails and the presence of the corrugation does not notably impact on the convective heat-transfer coefficient distributions, which are comparable to the one observed for coiled tubes with smooth wall. In particular at the outside surface of the coil, h_{int} is approximately five times that at the inside surface as it was for smooth coiled tubes.

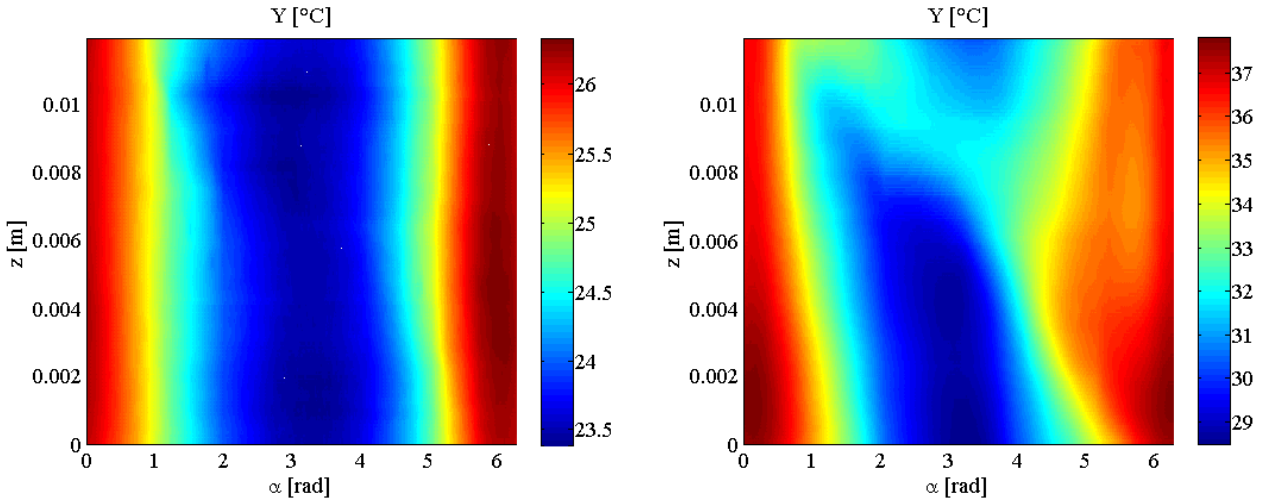

a) b)

Figure 7.4: Infrared temperature maps for *De*=25 (a) and *De*=202 (b).

For higher *De* value instead, the wall corrugation influences the fluid flow and it brings a further heat transfer enhancement. For *De*=202 the convective heat-transfer coefficient distribution is strongly irregular and it shows a local maximum close to the pitch of the corrugation and local minimum downstream of the corrugation: this distribution highlights the presence of flow instabilities.

a) b)

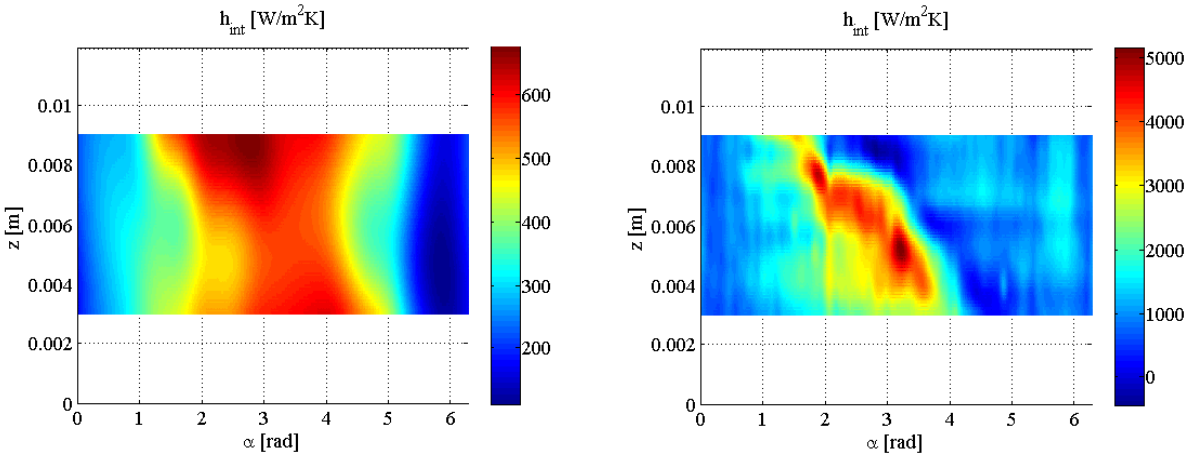

Figure 7.5: Restored convective heat-transfer coefficient distribution for *De*=25 (a) and *De*=202 (b).

a) b)

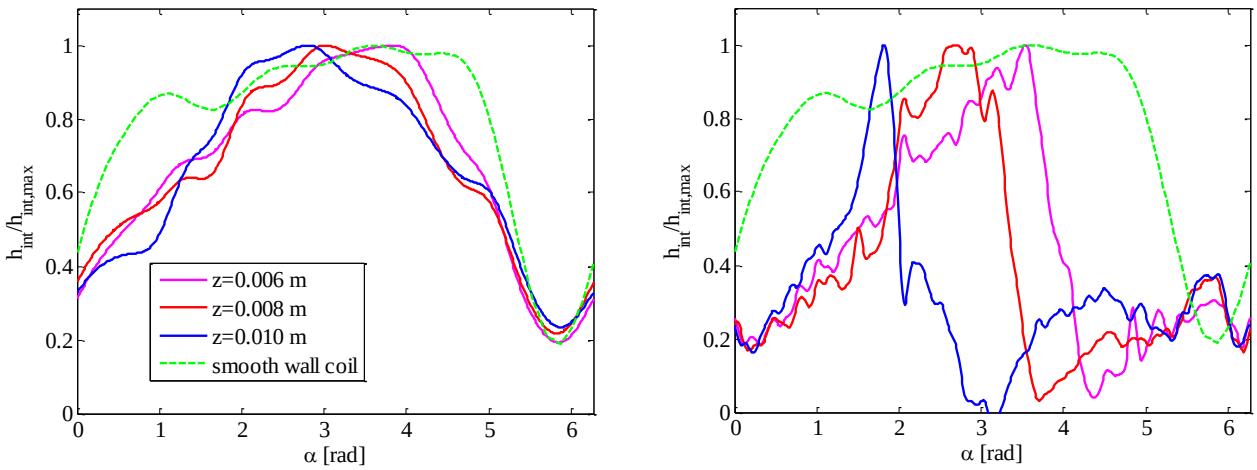

Figure 7.6: Normalized local convective heat transfer coefficient for *De*=25 (a), *De*=202 (b) and comparison with the data for smooth wall coils (HSW045 best fit 29< De < 235).

CONCLUSIONS

The aim of this thesis was to study the heat transfer enhancement achievable by using coiled pipes having both smooth and corrugated wall.

The investigation was firstly devoted to measure the heat transfer performance along the heated length of the coiled pipes in terms of Nusselt number circumferentially averaged along the cross section and computed at different axial position. The heat transfer enhancement effects were compared to the correlated pressure drop penalties. Ethylene Glycol was used as working fluid in the Reynolds number range 70÷1300 which, for the curvature ratio values under investigation corresponded to the Dean number range 12÷290. In the temperature range characterizing the experimental conditions the Prandtl number of the working fluid varied between 125 and 280.

As expected, as a consequence of the fluid mixing due to the centrifugally induced secondary flow, the local Nusselt number, circumferentially averaged, reached values higher than the ones obtained in a straight pipe for both the smooth and corrugated wall helically coiled tubes.

The data show that for low Dean and Reynolds number values the wall corrugation effect was almost negligible and the enhancement over the smooth straight tube behavior has to be ascribed to the wall curvature effect. For larger Dean and Reynolds number values the effect of the wall corrugation starts to prevail by augmenting the convective heat transfer mechanism significantly.

This behavior was interpreted as a consequence of an early departure from the steady laminar flow, as it is widely accepted in literature for corrugated wall straight tubes (Garcia et al. 2012, Rainieri et al. 2002). The data show also that, for the corrugation profile under test in the present investigation, the departure from the smooth wall behavior occurs for Reynolds number values in the range 500-600. Moreover the results show that this critical condition is suitably described by the Dean number and that the critical value can be identified in the range between 110 and 130. This behavior is consistent with the results available for straight spirally enhanced tubes characterized by similar corrugation profile for which a critical Reynolds number in the range 300-1000 was reported (Srinivasan and Christensen 1992;Garimella and Christensen 1993; Rainieri et al. 1996).

For what concerns the pressure drops in the helically coiled smooth wall tube, the friction factor values were close to the expectations for the straight section for Reynolds number values lower than about 500 while for greater Reynolds number values, the effect is still small, but not negligible. For the helically coiled corrugated wall tube, the friction factor values are higher than the ones of the smooth coiled section and the augmentation increases with the Dean number.

In order to better quantify the enhancement of the helically coiled tubes over a common reference geometry the friction factor and the heat transfer enhancement respect to the smooth straight tube solution were computed. The effect of the wall curvature alone brings heat transfer enhancement in

the range 2÷10 against pressure drop penalties augmentation in the range 1÷1.5, while for the helical coiled wall corrugated tubes an heat transfer augmentation up to 25 was registered against a maximum friction factor increase of 2.5.

These outcomes suggest that the compound use of wall curvature and wall corrugation can offer an interesting solution in the design of helical-coil heat exchangers. In fact, when helical coiled tubes are used, although significant benefits are expected in terms of heat transfer performance due to secondary flow pattern that arises due to the centrifugal force, a significant delay of the transition to the turbulent regime inevitably occurs. Moreover the negative effect due to the smoothing of turbulence emergence was found to match, or even to overcome, the increasing effect due to the triggering of the secondary flows (Cioncolini and Santini 2006; Di piazza and Ciofalo 2011). The use of corrugated wall tubes can compensate for this drawback, by promoting an early transition to the unstable/transitional flow regime that activates an heat transfer enhancement amplifying the one brought by the wall curvature. This aspect makes wall corrugated coils a suitable tool to increase the overall thermal performance of the apparatuses employed in industrial applications where highly viscous fluids have to be thermally treated, like in the food, chemical and pharmaceutics industries.

In the second part of this Thesis in order to better understand the mechanisms that govern the heat transfer in coiled pipes, the convective heat transfer coefficient distribution along the cross section circumference was estimated. The asymmetrical distribution of the velocity field over the cross-section of the tube due to the centrifugal force that is experienced by the fluid, leads to a significant variation in the convective heat-transfer coefficient along the circumferential angular coordinate.

The solution of the IHCP in the wall, starting from the temperature distribution acquired on the external wall surface, has been employed to estimate the local convective heat-transfer coefficient on the interior wall surface. Three different solution techniques were employed to solve the IHCP and to find the local convective heat transfer coefficient at the fluid-wall interface. The three procedures, based on Tikhonov Regularization Method (TRM), Gaussian Filter Technique (GFT) and Quadrupole method (QM) respectively, have been presented, implemented and optimized for the problem under study, validated by synthetic data and compared.

A simplified 2-D numerical model of the test section was formulated by assuming that along the axis of the tube the temperature gradient is almost negligible. A synthetic temperature distribution on the external wall surface was then obtained by imposing a given distribution of the local convective heat transfer coefficient on the internal side of the wall. The synthetic temperature distribution on the external wall surface, deliberately spoiled by random noise, was then used as the input data of the inverse problem. The TRM and QM for small noise level reconstruct the convective heat transfer coefficient almost identically guaranteeing a good restoration of the

original information. Also the GFT it's working well even if the reconstructed heat transfer coefficient distribution is not as smooth as the ones obtained with the other two procedures: the result obtained is not unsatisfying considering the significantly small computational cost of this procedure. The residuals between the input and the restored temperature, gives deeper insight into the performance of the three estimation procedures: the residuals produced by TRM and QM are more randomly distributed than the ones by GFT. This observation suggests that, even if no great differences are present in terms of estimated local convective heat transfer coefficient, TRM and QM works slightly better than GFT that tends to smoothen the temperature distribution.

For higher noise levels the TRM and QM continue to obtain a good restoration of the convective heat transfer coefficient distribution, also if it is notable a progressive higher loose of information in correspondence of the peaks: also for the GFT the estimation is globally correct but not as accurate as the other two.

Referring to the estimation error of equation (5.78) a general consideration, that could be made, is that for the problem here investigated, the QM and TRM performs better than the GFT if the noise is lower than 1K while, for higher noise values, their efficiency is almost comparable, with, depending on the cases, one of the three techniques performing better than the others.

They were then applied to experimental measurements in smooth coiled tubes in laminar fully developed region. The experimental analysis was performed on two tubes having different curvature ratio using Glycol Ethylene to study the Reynolds number range 100-1100.

In the temperature range characterising the experimental conditions, the Prandtl number of the working fluid varied in the range 160-230. The temperature distribution on the external surface of a coiled wall was acquired by means of an high precision infrared camera and it was then employed as input data in the inverse heat conduction problem in the wall. The results pointed out a very significant variation of the convective heat transfer coefficient along the boundary of the duct cross section. Indeed, in the considered range for the dimensionless parameters, at the outer bend of the coil, the Nusselt number was about five times that one at the inner bend.

The data confirm the observations made by Yang et al. (1995), Bai et al. (1999), Seban et McLaughlin (1963) and Jayakumar et al. (2010) that found out that the value of the convective heat transfer coefficient at the outer bend is significantly higher than the value at the inside surface.

In addition an estimation procedure, based on Gaussian Filter, is proposed and applied to experimental data for corrugated wall coiled tubes: preliminary results were obtained.

The estimation procedure was applied to two representative Dean number values, 25 and 202 i.e. in two conditions in which, as previously said, the effect of the corrugation was expected to be significantly different.

The temperature data show that for *De*=25 the temperature distribution exhibits a significant variation along the circumference and that the temperature gradient is almost negligible along the axis of the tube, as it was observed for coiled tubes with smooth wall. On the contrary, for *De*=202, the temperature gradient along the tube axis, induced by the effect of the wall corrugation of the boundary layers, cannot be neglected.

The maps of the convective heat flux restored by applying the filtering procedure confirm that for low *De* value the wall curvature effect prevails and the presence of the corrugation does not notably impact on the convective heat-transfer coefficient distributions, which are comparable to the one observed for coiled tubes with smooth wall. In particular at the outside surface of the coil, h_{int} is approximately five times than at the inside surface as it was for smooth coiled tubes.

For higher *De* value instead, the wall corrugation influences the fluid flow and it brings a further heat transfer enhancement. The convective heat-transfer coefficient distribution is strongly irregular and shows a local maximum close to the pitch of the corrugation and local minimum downstream of the corrugation: this distribution highlights the presence of flow instabilities. Cause to the lack of knowledge about the local heat-transfer coefficient for the laminar flow regime in coiled tubes in the scientific literature, the results obtained here might be particularly useful in the validation of numerical models and in the design of coiled tube heat exchangers aimed at the treatment of highly viscous fluids.

Some of the results reported in this thesis were also published in several recent scientific journals at international level (Rainieri et al. 2012b, Rainieri et al. 2013, Bozzoli et al. 2014a, Bozzoli et al. 2014b, Bozzoli et al. 2014c, Rainieri et al. 2014b).

BIBLIOGRAPHY

- Abichandani H., Sarma S. C., Hydrodynamics and heat transfer in liquid full scraper surface heat exchanger – a review, *Food Process Engineering*, **9** 121-141 (1987).
- Acikalin T., Wait S., Garimella S., Raman A., Experimental investigation of the thermal performance of piezoelectric fans, *Heat Transfer Eng*ineering, **25 (1)** 4–14 (2004).
- Agarwal P., Sikand A. and Shanti V., Application of heat exchangers in bioprocess industry: a review, *International Journal of Pharmacy and Pharmaceutical Sciences*, **6 (1)** (2014).
- Ali S., Pressure drop correlations for flow through regular helical coil tubes, *Fluid Dynamic Research*, **28** 295-310 (2001).
- Alifanov, 0.M., Solution of an Inverse Problem of Heat-Conduction by Iterative Methods, *Journal of Engineering Physiscs*, **26 (4)** 471-476 (1974).
- Alifanov, 0. M., Inverse Heat Transfer Problems, *Springer-Verlag*, NewYork, (1994).
- Astarita T., Carlomagno G.M., Infrared Thermography for Thermo-fluid-dynamics, *Springer*, Berlin (2012).
- Bai B., Guo L., Feng Z., Chen X., Turbulent Heat Transfer in a Horizontal Helically Coiled Tube, *Heat Transfer-Asian Research*, **28 (5)** 395-403 (1999).
- Bazán F.S.V., Fixed-point iteration in determining the Tikhonov regularization parameter, *Inverse Problems in Science and Engineering*, **24** 035001 (2008).
- Bazán F.S.V., Francisco J.B., An improved fixed-point algorithm for determining a Tikhonov regularization parameter, *Inverse Problems in Science and Engineering*, **25** 045007 (2009).
- Bazán F.S.V., Borges L.S., GKB-FP: an algorithm for large-scale discrete ill-posed problems, *Bit Numerical Mathematics*, **50 (3)** 481–507 (2010).
- Beck, J. V., Calculation of Surface Heat Flux from an Internal Temperature History, *ASME* Paper *62-HT-46*, (1962).
- Beck, J. V., Surface Heat Flux Determination Using an Integral Method, *Nuclear Engineering and Design*, **7** 170- 178 (1968).
- Beck J.V. and Arnold K.J, Parameter estimation in engineering and science, John Wiley & Sons, New York (1977).
- Bejan A., Heat Transfer, *John Wiley & Sons*, Inc New York (1993).
- Bergles A.E., Handbook of heat transfer. Chapter 11: techniques to enhance heat transfer, *McGraw-Hill* (1998).
- Berger S.A., Talbot L., Yao L.S., Flow in curved pipes, *Annual Review of Fluid Mechanics*, **15** 461-512 (1983).

- Blackwell B., Beck J.V., A technique for uncertainty analysis for inverse heat conduction problems, *International Journal of Heat and Mass Transfer*, **53(4)** 753-759 (2010).
- Bozzoli F. and Rainieri S., Comparative application of CGM and Wiener filtering techniques for the estimation of the heat flux distribution, *Inverse Problems in Science and Engineering*, **19** 551-571 (2011);
- Bozzoli F., Pagliarini G., Rainieri S., Experimental validation of the filtering technique approach applied to the restoration of the heat source field, *Experimental Thermal and Fluid Science*, **44** 858–867 (2013).
- Bozzoli F., Cattani L., Rainieri S., Pagliarini G., Estimation of local heat transfer coefficient in coiled tubes under inverse heat conduction problem approach, *Experimental Thermal and Fluid Science*, **59** 246–251 (2014a).
- Bozzoli F., Cattani L., Corradi C., Mordacci M., Rainieri S. Inverse estimation of the local heat transfer coefficient in curved tubes: a numerical validation, *Journal of Physics: Conference Series*, **501** (2014b).
- Bozzoli F., Cattani L., Rainieri S., Viloche Bazán F. S., Borges, L. S., Estimation of the local heat-transfer coefficient in the laminar flow regime in coiled tubes by the Tikhonov regularisation method, *International Journal of Heat and Mass Transfer*, ***72*** 352-361 (2014c).
- Burggraf, 0.R., An Exact Solution of the Inverse Problem in Heat Conduction Theory and Applications, *Journal of Heat Transfer*, **86C** 373-382 (1964).
- Chang S.W., Su L.M., Yang T.L., Enhanced heat transfer with full circumferential ribs in helical pipe, *Journal of Thermal Science* **11** 241-248 (2002).
- Chen X.D., Xu X.Y., Nguang S.K. and Bergles A. E., Characterization of the effect of corrugation angles on hydrodynamic and heat transfer performance of four-start spiral tube, *Journal of Heat Transfer*, **123** 1149-1158 (2001).
- Chen H., Zhang B., Fluid flow and mixed heat transfer in a rotating curved pipe, *International Journal of Thermal Sciences*, **42** 1047-1059 (2003).
- Cioncolini, L. Santini, On the laminar to turbulent flow transition in diabatic helically coiled pipe flow, *Experimental Thermal and Fluid Science*, **30** 653-661 (2006).
- Cocchi A., Termofisica per ingegneri, *Libreria editoriale petroni*, (1994).
- Cyganek B., Siebert J.P., An Introduction to 3D Computer Vision Techniques and Algorithms, *Wiley*, New York (2011).
- Date A.W. and Singham J.R., Numerical prediction of friction and heat transfer characteristics of fully developed laminar flow in tubes containing twisted tapes, *ASME Journal of Heat Transfer*, **17** (1972).

- Dean, W. R., Note on the motion of fluid in a curved pipe, *The London, Edinburgh, and Dublin Philosophical Magazine and Journal of Science*, **4** 208-223 (1927).
- Dean, W. R.., The stream-line motion of fluid in a curved pipe, *The London, Edinburgh, and Dublin Philosophical Magazine and Journal of Science*, **5** 673-695 (1928).
- Dennis B.H., Dulikravich G.S., Inverse determination of unsteady temperatures and heat fluxes on inaccessible boundaries, *Journal of Inverse and Ill-posed Problems*, **20** 791-803 (2013).
- Dewan A., Mahanta1 P., Sumithra Raju K. and Suresh Kumar P., Review of passive heat transfer augmentation techniques, *Proceedings of the Institution of Mechanical Engineers*, **218 A**: Journal of Power and Energy (2004).
- Di Piazza I. and Ciofalo M., Transition to turbulence in toroidal pipes, *Journal of Fluid Mechanics*, **687** 72-117 (2011).
- Dulikravich, G.S. and Martin, T.J., Inverse Shape and Boundary Condition Problems and Optimization in Heat Conduction, *Chapter 10 in Advances in Numerical Heat Transfer*, **1** 381-426, Minkowycz, W. J. And Sparrow, E. M. (eds.), *Taylor and Francis*, (1996).
- Dravid A.N., Smith K.A., Merrill E.W., Brain P.L.T., Effect of secondary fluid on laminar flow heat transfer in helically coiled tubes, AIChE *Journal*, **17** 1114-1122 (1971).
- D'Souza N., Numerical Solution of One-Dimensional Inverse Transient Heat Conduction by Finite Difference Method, *ASME Paper No. **75**-WA/HT-81*, (1975).
- Eiamsa-ard S., Promvonge P.,Thermal characterization of turbulent tube flows over diamond-shaped elements in tandem, *International Journal of Thermal Sciences*, **49** 1051-1062 (2010).
- Eustice J., Flow of water in curved pipes, *Proceedings of the Royal Society of London Series A*, **84** 107-118 (1910).
- Eustice J., Experiments on stream-line motion in curved pipes, *Proceedings of the Royal Society of London. Series A* **85** 119-131 (1911).
- Fand R.M., Kaye J., The influence of sound on free convection from a horizontal cylinder, *Journal* of *Heat Transfer*, **83(2)** 133-143 (1961).
- García A., Solano J.P., Vicente P.G., Viedma A., Flow pattern assessment in tubes with wire coil inserts in laminar and transition regimes, *International Journal of Heat and Fluid Flow*, **28** 516–525 (2007).
- García A., Solano J.P., Vicente P.G., Viedma A. , The influence of artificial roughness shape on heat transfer enhancement: Corrugated tubes, dimpled tubes and wire coils, *Applied Thermal Engineering* **35** 196-201 (2012).
- Garimella,S. and Christensen,R.N., Experimental investigation of fluid flow mechanisms in annuli with spirally fluted inner tubes, *ASHRAE Transactions*, **99** 1205-1216 (1993).

- Garimella,S. and Christensen,R.N., Heat Transfer and Pressure Drop Characteristics of Spirally Fluted Annuli: Part I-Hydrodynamics, *ASME Journal of Heat Transfer*, **117** 54-60 (1995).
- Gee D.L., and Webb R.L., Forced convection heat transfer in helically rib-roughened tubes, *International Journal Heat and Mass Transfer*, **23** 1127-1136 (1980).
- Genetti W.E., Priebe J.S., Heat transfer with a static mixer, *AIChE*, (1973).
- Gose E.E., Peterson E.E., Arcivos A., On the rate of heat transfer in liquids with gas injection through the boundary layer, *Journal of Applied Physic*s, **28** (1957).
- Goldstein L. and Sparrow E.M., Heat/Mass Transfer Characteristics for Flow in a Corrugated Wall Channel, *Journal of Heat Transfer*, **99(2)** 187-195 (1977).
- Grindley J.H. and Gibson A.H., On the frictional resistance to the flow of air through a pipe, *Proceedings of the Royal Society of London Series A*, **80** 114-139 (1908).
- Guo L., Feng Z., & Chen X., An experimental investigation of the frictional pressure drop of steam–water two-phase flow in helical coils, *International Journal of Heat and Mass Transfer*, **44(14)** 2601-2610 (2001).
- Guzman A.M. and Amon C.H., Dynamical flow characterization of transitional and chaotic regimes in converging-diverging channels, *Journal of Fluid Mechanics*, **321** 25-27 (1996).
- Hansen P.C., The truncated SVD as a method for regularization, *Numerical Analysis Project Manuscript NA-86-36*, (1986).
- Hansen P.C., Truncated singular value decomposition solutions to discrete illposed problems with ill-determined numerical rank, *SIAM Journal on Scientific Computing*, **11** 503–518 (1990).
- Hansen P.C., Rank-deficient and discrete ill-posed problems, *SIAM*, Philadelphia, (1998).
- Hansen P, O'Leary D, The use of the L-curve in the regularization of discrete ill-posed problems, *SIAM Journal on Scientific Computing* 1487-1503 (1993).
- Härröd M., Hydrodynamics Scraped Surface Heat Exchangers, *Food Process Engineering*, **9** 1-62 (1986).
- Hasson D., Streamline flow resistance in coils, *Res. Corresp* **1 S1** (1955).
- Holman J.P., Experimental Methods for Engineers, *McGraw-Hill*, New York, (2001).
- Hong S.W., Bergles A.E., Augmentation of laminar flow heat transfer in tubes by means of twisted-tape inserts, *Journal of Heat Transfer*, **98** 251-256 (1976).
- Hore P. S., Krutz G. W., and Schoenhals R. J., Application of the Finite Element Method to the Inverse Heat Conduction Problem, *ASME Paper NO. 77- WA/TM-4*, (1977).
- Huang C.H., Ozisik M.N., and Sawaf B., Conjugate Gradient Method for Determining Unknown Contact Conductance During Metal Casting, *International Journal of Heat and Mass Transfer*, **35** 1779-1789 (1992).

- Huang C-H. and Tsai Y-L., A transient 3-D inverse problem in imaging the time-dependent local heat transfer coefficient for plate fin, *Applied Thermal Engineering* **25** 2478-2495 (2005).
- Incoprera F.P., De Witt D.P., Fundamentals of Heat and Mass Transfer, *John Wiley & Sons*, Inc New York (2002).
- Itō, H., Laminar flow in curved pipes, *Journal of Applied Mathematics and Mechanics*, **49(11)** 653-663 (1969).
- Jadooa A.A., Experimental Investigations Heat Transfer and Pressure Drop Characteristics of Flow Through Circular Tube Fitted With Drilled Cut-Conical Rings, *Journal of Engineering and Technology*, **29** No.3 (2011).
- Janssen L.A.M., Hoogendoorn C.J., Laminar convective heat transfer in helical coiled tubes, *International Journal of Heat and Mass Transfer*, **21** 1197–1206 **(**1978).
- Jayakumar J.S., Mahajani S.M., Mandal J.C.,. Iyer K.N, Vijayan P.K., CFD analysis of single-phase flows inside helically coiled tubes, *Computers & chemical engineering*, **34** 430-446 (2010).
- Kalb C. E., Seader J. D., Heat and mass transfer phenomena for viscous flow in curved circular tubes, *International Journal of Heat and Mass Transfer*, **15** 801-817 (1992).
- Kline S.J. and McClintock, Describing Uncertainties in Single-Sample Experiments, *Mechanical Engineering*, (1953).
- Kudirka A.A., Two-phase heat transfer with gas injection through a porous boundary surface, *ASME*, paper 65-HT-47 (1965).
- Kuppan T., Heat Exchanger Design Handbook, *CRC Press*, (2000).
- Léal L., Miscevic M., Lavieille P., Amokrane M., Pigache F., Topin F., Nogarède c B., Tadrist L., An overview of heat transfer enhancement methods and new perspectives: Focus on active methods using electroactive materials, *International Journal of Heat and Mass Transfer*, **61** 505–524 (2013).
- Lee B.H., Richardson P.D., Effect of sound on heat transfer from a horizontal circular cylinder at large wavelength, *Journal of Mech*anical *Eng*ineering *Science*, **7** 127-130 (1965).
- Lesnic, D., Elliot, L. and Ingharn D. B., Application of the Boundary Element Method to Inverse Heat Conduction Problems, *International Journal of Heat and Mass Transfer*, **39** 1503-1517 (1996).
- Levenberg, K., A Method for the Solution of Certain Non-linear Problems in Least-Squares, *Quarterly of Applied Mathematics*, **2** 164-168 (1944).
- Liu S., Masliyah J. H., Axially invariant laminar flow in helical pipes with a finite pitch, *Journal of Fluid Mechanics*, **251** *315-353* (1993).

- Lu T., Liu B., Jiang P.X., Zhang Y.W., Li H., A two-dimensional inverse heat conduction problem in estimating the fluid temperature in a pipeline, *Applied Thermal Engineering*, **30** 1574-1579 (2010).
- Lu T., Liu B., Jiang P.X., Inverse estimation of the inner wall temperature fluctuations in a pipe elbow, *Applied Thermal Engineering*, **31** 1976-1982 (2011).
- Maillet D., André S., Batsale J., Degiovanni A., Moyne C., Thermal Quadrupoles: Solving the Heat Equation Through Integral Transforms, *Wiley*, (2000).
- Marquardt, D. W., An Algorithm for Least Squares Estimation of Nonlinear Parameters, *Journal of the Society for Industrial and Applied Mathematics*, **11** 431-441 (1963).
- Manglik R.M., A.E.Bergles, Heat transfer and pressure drop correlations for twisted tape inserts in isothermal tubes , *Journal of Heat Transfer*, **115** 890-896 (1993).
- Martin, T.J. and Dulikravich, G.S., Inverse Determination of Steady Convective Local Heat Transfer Coefficients, ASME *Journal of Heat Transfer*,**120** 328-334 (1998).
- Matsevityi , Y.M. and Multanoviskii, A. V., Pointwise Identification of Thermophysical Characteristics, *Journal of Engineering Physics* , **49(6)** 1392-1 397 (1986).
- McConalogue D. J., and Srivastava R.S., Motion of a fluid in a curved tube, *Proceedings of the Royal Society of London. Series A. Mathematical and Physical Sciences*, **307** 37-53 (1968).
- McElhiney J.E., Preckshot G.W., Heat transfer in the entrance length of a horizontal rotating tube, *International Journal of Heat and Mass transfer*, **20** 847–854 (1977).
- Mishra P. and Gupta S.N., Momentum transfer in curved pipes. 1. Newtonian fluids, *Industrial & Engineering Chemistry Process Design and Development*, **18(1)** 130-137 (1979).
- Miyazaki H., Combined free and forced convective heat transfer and fluid flow in a rotating curved circular tube, *International Journal of Heat and Mass transfer*, **14** 1295–1309 (1971).
- Mokrani O., Bourouga B., Castelain C., Peerhossaini H., Fluid flow and convective heat transfer in flat microchannels, *International Journal of Heat and Mass Transfer* **52** 1337–1352 (2009).
- Mori Y., Nakayama W., Forced convection heat transfer in a straight pipe rotating around a parallel axis, *International Journal of Heat and Mass transfer*, **10** 1179–1194 (1967).
- Morozov V.A., Methods for Solving Incorrectly Posed Problems, *Springer-Verlag*, New York (1984).
- MuIholland. *G.* P., Gupta, B. P., and San Martin, R. L., Inverse Problem of Heat Conduction in Composite Media, *ASME* Paper No. *75-WA/HT-**83,*** **(**1975).
- Murata S., Miyake Y., Inaba T., Ogawa H., Laminar flow in a helically coiled pipe, *Bulletin of JSME*, **24** 355-362 (1976).

- Murio, D. A., The Mollification Method and the Numerical Solution of an Inverse Heat Conduction Problem, *SIAM Journal on Scientific and Statistical Computing*, **2** 17-34 (1981).
- Naphon P., S.Wongwises, A review of flow and heat transfer characteristics in curved tubes, *Renewable and sustainable energy* reviews, **10** 463–490 (2004).
- Newton D.C., Allen P.H.G., Senftleben effect in insulating oil under uniform electric stress, *Letters in Heat and Mass Transfer*, **4** 9–16 (1977).
- Niceno B. and Nobile E., Numerical analysis of fluid flow and heat transfer in periodic wavy channels, *International journal of heat and fluid flow*, **22** 156-167 (2001).
- Nishimura T., Murakami S., Arakawa S., Kawamura Y., Flow observations and mass transfer characteristics in symmetrical wavy-walled channels at moderate Reynolds numbers for steady flow, *International Journal of Heat and Mass Transfer*, **33** 835–845 (1990).
- Novikov, N. A., Hyperbolic Equation of Thermal Conductivity: Solution of the Direct and Inverse Problems for a Semi-Infinite Bar, *Journal of engineering physics*.,**35** 1253-1257 (1978).
- Oyakawa K., Umeda A., Islam M.D., Saji N., Matsuda S., Flow structure and heat transfer of impingement jet, *Heat and Mass Transfer*, **46 (1)** 53–61 (2009).
- Orlande, H. R. B. and *Ö*zisik M.N, Inverse Problem of Estimating Interface Conductance Between Periodically Contacting Surfaces, *Journal of Thermophysics and Heat Transfer*, **7** 319-325 (1993).
- Orlande H.R.B., Fudym O., Maillet D., Cotta R.M., Thermal Measurements and Inverse Techniques, *Taylor & Francis*, New York (2011).
- *Ö*zisik M.N and Orlande H.R.B, Inverse Heat Transfer, *Taylor and Francis*, New York, (2000).
- Patankar S.V, Pratap V.S, Spalding D.B., Prediction of laminar flow and heat transfer in helically coiled pipes, *Journal of Fluid Mechanics*, **62** 539-551 (1974).
- Penney W.R., The spiralator. Initial tests and correlation, *AIChE No.16, 8th National Heat Transfer Conference* (1965).
- Prabhanjan D.G., Raghavan G.S.V., Rennie T.J., Comparison of heat transfer rates between a straight tube heat exchanger and a helically coiled heat exchanger, *International Communications in Heat and Mass Transfer*, **29** 185-191 (2002).
- Promvonge P., Eiamsa-ard S., Heat transfer in a circular tube fitted with free-spacing snail entry and conical-nozzle turbulators, *International Communications in Heat and Mass Transfer*, **34** 838–848 (2007).
- Promvonge P., Heat transfer behaviors in round tubes with conical ring inserts, *Energy Conversion and Management*, **49** 8-15 (2008).

- Promvonge P., Thermal augmentation in circular tube with twisted tape and wire coil turbulators, *Energy Conversion and Management*, **49** 2949–2955 (2008a).
- Promvonge P., Thermal enhancement in a round tube with snail entry and coiled-wire inserts, *International Communications in Heat and Mass Transfer*, **35** 623–629 (2008b).
- Rainieri S., Farina A. and Pagliarini G., Experimental investigation of heat transfer and pressure drop augmentation for laminar flow in spirally enhanced tubes, *Proceedings 2nd European Thermal-Sciences and 14th UIT National Heat Transfer Conference*, 203-209 (1996).
- Rainieri S. and Pagliarini G., Convective heat transfer to temperature dependent property fluids in the entry region of corrugated tubes, *International Journal of Heat and Mass Transfer*, **45** 4525-4536 (2002).
- Rainieri S., Bozzoli F., Pagliarini G., Wiener filtering technique applied to thermographic data reduction intended for the estimation of plate fins performance, *Experimental Thermal and Fluid Science*, **28** 179–183 (2004).
- Rainieri S., Bozzoli F., Pagliarini G., Numerical study of unsteady flow and heat transfer in a tube with arc-shaped corrugation, *Proceedings of 4th ICCHMT*, Paper No. 495 (2005).
- Rainieri S., Bozzoli F., Pagliarini G., Characterization of an uncooled infrared thermographic system suitable for the solution of the 2-D inverse heat conduction problem, *Experimental Thermal Fluid Science*, **32**(8) 1492–1498 (2008).
- Rainieri S., Bozzoli F. and Pagliarini G., Effect of a hydrophobic coating on the local heat transfer coefficient in forced convection under wet conditions, *Experimental Heat Transfer*, **22** 163-177 (2009).
- Rainieri S., Bozzoli F., Schiavi L. and Pagliarini G., Numerical analysis of convective heat transfer enhancement in swirl tubes, *International Journal of Numerical Methods for Heat and Fluid Flow*, **21 (5)** 559-571 (2011).
- Rainieri S., Bozzoli F., Pagliarini G. , Experimental investigation on the convective heat transfer in straight and coiled corrugated tubes for highly viscous fluids: Preliminary results, *International journal of heat and mass transfer*, **55** 498–504 (2012a).
- Rainieri S., Bozzoli F., Cattani L., and Pagliarini G., Experimental investigation on the convective heat transfer enhancement for highly viscous fluids in helical coiled corrugated tubes, *Journal of Physics: Conference Series*, **395** (2012b).
- Rainieri S., Bozzoli F., Cattani L., and Pagliarini G., Compound convective heat transfer enhancement in helically coiled wall corrugated tubes, *International Journal of Heat and Mass Transfer*, ***59*** 353-362 (2013).

- Rainieri S., Bozzoli F., Cattani L., Vocale P., Parameter estimation applied to the heat transfer characterization of Scraped Surface Heat Exchangers for food applications, *Journal of Food Engineering*, **125** 147–156 (2014a).
- Rainieri S., Bozzoli F., L. Cattani, Passive techniques for the enhancement of convective heat transfer in single phase duct flow, *Journal of Physics: Conference Series*, **547** (2014b).
- Ravigururajan T.S. and Bergles A.E., Development and verification of general correlations for pressure drop and heat transfer in single-phase turbulent flow in enhanced tubes, *Experimental Thermal and Fluid Science*, **13** 55–70 (1996).
- Raychaudhuri S., Introduction to Monte Carlo simulation, *Proceedings of the Winter Simulation Conference*, (2008)
- Reinhardt H.J., Hào D.H., Frohne J., Suttmeier F.T., Numerical solution of Inverse Heat Conduction Problems in two spatial dimensions, *Journal of Inverse and Ill-Posed Problems*, **15** 19-36 (2007).
- Rouizi Y., Maillet D., Jannot Y., Fluid temperature distribution inside a flat mini-channel: semi-analytical wall transfer functions and estimation from temperatures of external faces, *International Journal of Heat and Mass Transfer*, **64** 331-342 (2013).
- Rowley,G.J., and Patankar,S.V., Analysis of laminar flow and heat transfer in tubes with internal circumferential fins, *International Journal Heat and Mass Transfer*, **27** 553-560 (1984).
- Rozzi S., Massini R, Paciello G., Pagliarini G., Rainieri S., Trifirò A., Heat treatment of fluid foods in a shell and tube heat exchanger: Comparison between smooth and helically corrugated wall tubes, *Jounal of Food Engeneering*, **79 (1)** 249-254 (2007).
- Saha S.K., Dutta A., Dhal S.K., Friction and heat transfer characteristics of laminar swirl flow through a circular tube fitted with regularly spaced twisted-tape elements, *International Journal of Heat and Mass Transfer*, **44** 4211–4223 (2001).
- Seban R.A. and Mclaughin E.F., Heat transfer in tube coils with laminar and turbulent flow, *International Journal of Heat and Mass Transfer*, **6** *387-395* (1963).
- Shah R.K., London A.L., Laminar Flow Forced Convection in Ducts, *Academic Press*, (1978).
- Sparrow E. M., Haji-Sheikh A. and Lundgren T.S., The Inverse Problem in Transient Heat Conduction, *Journal of Applied Mechanics*, **86E** 369-375 (1964).
- Skelland, A.H.P., Correlation of scraped-film heat transfer in the votator, *Chemical Engineering Science*, **7** 166-175 (1958).
- Sreenivasan K.R. and Strykowski P.J., Stabilization Effects in Flow Through Helically Coiled Pipes, *Experiments in Fluids* I 31-36 (1983).

- Srinivasan P.S., Nandapurkar S.S., Holland F.A., Pressure drop and heat transfer in coils, *The Chemical Engineer*, **218** CE113-119 (1968).
- Srinivasan V. and Christensen R.N., Experimental investigation of heat transfer and pressure drop characteristics of flow through spirally fluted tubes, *Experimental Thermal and Fluid Science*, **5** 820-827 (1992).
- Stolz, *G.***,** Numerical Solutions to an Inverse Problem of Heat Conduction for Simple Shapes, *ASME Journal of Heat Transfer*, **82** 20-26 (1960).
- Su J. and Hewitt G.F., Inverse heat conduction problem of estimating time-varying heat transfer coefficient, *Numerical Heat Transfer*, **45** 777-789 (2004).
- Sununu J.H., Heat transfer with static mixer system, *Keniks Corp. Tech. Rep 1002*, (1970).
- Taler J., Determination of local heat transfer coefficient from the solution of the inverse heat conduction problem, *Forschung im Ingenieurwesen*, **71** 69-78 (2007).
- Tamari M., Nishikawa K., The stirring effect of bubbles upon the heat transfer to liquid, *Heat Transfer Jpn. Res*, **(5/2)** (1976).
- Tarbell J.M., Samuels M.R., Momentum and Heat Transfer in Helical Coils, *The Chemical Engineering Journal*, **5** 117-127 (1973).
- Thomson J., On the origin of windings of rivers in alluvial plants with remarks on the flow of water round bends of pipes, *Proceedings of the Royal Society of London Series A*, **26** 356-57 (1876).
- Tikhonov A.N. and Arsenin V.Y., Solution of Ill-Posed Problems, *Winston & Sons*, Washington, DC, (1977).
- Truesdell L.C., Adler R.J., Numerical treatment of fully developed laminar flow in helically coiled tubes, *AICHE Journal*, **16** 1010-1015 (1970).
- Usui H., Sano Y., Iwashita K., Isozaki A., Enhancement of heat transfer by a combination of an internally grooved rough tube and a twisted tape, *International Chemical Engineering* **26** 97-104 (1986).
- Van Der Meer T.H., Hoogendoorn C.J., Heat transfer coefficients for viscous fluids in a static mixer, *Chemical Engineering Science* **33** 1277-1282 (1978).
- Vashisth S., Kumar V., and Nigam K.D., A review on the potential applications of curved geometries in process industry, *Industrial & Engineering Chemistry Research*, ***47*(10)** 3291-3337 (2008).
- Wang G. V., Vanka S. P., Convective heat transfer in periodic wavy passages, *International Journal of Heat and Mass Transfer*, **38** 3219-3230 (1995).

- Watkins R.W., Robertson C.R., Acrivos A., Entrance Region Heat Transfer in Flowing Suspensions, International Journal of Heat and Mass Transfer, **19** 693–695 (1976).
- Watkinson P., Miletti D. L., Kubanek G. R., Heat transfer and pressure drop of internally finned tubes in laminar oil flow, *Proceedings of the AIChE-ASME Heat Transfer Conference, ASME*, New York, Paper No.75-HT-41 (1976).
- Webb L., Eckert E.R.G. and Goldstein R.J. Heat transfer and friction in tubes with repeated-rib roughness, *International Journal Heat and Mass Transfer*,**14** 601-617 (1971).
- Webb R.L., Principles of enhanced heat transfer, *John Wiley & Sons*, Inc New York (1994).
- Weigand, B., & Spring, S., Multiple Jet Impingement− A Review, *Heat Transfer Research*, **42(2)** (2011).
- White C.M., Streamline flow through curved pipes, *Proceedings of the Royal Society of London. Series A*, 645-663 (1929).
- Williams G.S., Hubbel C.W., Femkell G.H., Experiments at Detroit, Michigan, on the effect of curvature upon the flow of water in pipes, *Trans. ASCE*, **47** 1-196 (1902).
- Withers J.G., Tube-Side Heat Transfer and Pressure Drop for Tubes Having Helical Internal Ridging with Turbulent/Transitional Flow of Single-Phase Fluid. Part 1. Single-Helix Ridging, Heat Transfer Engineering, **2** 48-58 (1980).
- Withers J.G., Tube-Side Heat Transfer and Pressure Drop for Tubes Having Helical Internal Ridging with Turbulent/Transitional Flow of Single-Phase Fluid. Part 2. Multiple-Helix Ridging, *Heat Transfer Engineering*, **2** 43-50 (1980).
- Woodbury K.A, Inverse engineering handbook, *CRC Press*, 2003
- Xin R.C., Ebadian M.A., The effects of Prandtl numbers on local and average convective heat transfer characteristics in helical pipes, *Journal of Heat Transfer*, **119 (3)** 467-473 (1997).
- Yang G, Dong F, Ebadian M.A., Laminar forced convection in a helicoidal pipe with finite pitch, *International journal of heat and mass transfer*, **5** 853-862 (1995).
- Yilmaz M., Sara O.N., Karsli S., Performance evaluation criteria for heat exchangers based on second law analysis, *Exergy, an International Journal*, **1(4)** 278-294 (2001).
- Zabaras, N. and Ngugen, T. H., Control of the Freezing Interface Morphology in Solidification Processes in the Presence of Natural Convection, *International Journal for Numerical Methods in Engineering*, **38** 1555-1578 (1995).
- Zachàr A., Analysis of coiled-tube heat exchangers to improve heat transfer rate with spirally corrugated wall, *International journal of heat and mass transfer*, **53** 3928–3939 (2010).

- Zimparov V., Extended performance evaluation criteria for enhanced heat transfer surfaces: heat transfer through ducts with constant heat flux, *International Journal of Heat and Mass Transfer*, **44(1)** 169-180 (2001).
- Zimparov V., Enhancement of heat transfer by a combination of a single-start spirally corrugated tubes with a twisted tape, *Experimental Thermal and Fluid Science*, **25** 535-546 (2002).

ACKNOWLEDGEMENTS

First of all, I would like to thank my Supervisors Prof. Sara Rainieri and Prof. Fabio Bozzoli for the great help provided during all my Ph.D period. Many thanks also for the many opportunities of growth given: the congresses, PhD schools and abroad periods. Thanks also to Prof. Giorgio Pagliarini for his help and experience. I would like also to express my thanks to Prof. Dennis Maillet for having welcome me at the University of Lorraine and for the great support during my period there. Many thanks also to Marco, Carlo, Luca and Pamela for every working day of the last three years and also for the sincere friendship. I would like also to thank Waseem for his great help and true friendship. Finally I want to sincerely thank my parents Franca and Eugenio and Chiara for the daily enormous support and for the patience shown during my thesis writing. Thanks also to the rest of my family.